UNIVERSIDADE FEDERAL DE MINAS GERAIS
Instituto de Geociências
Programa de Pós-Graduação em Análise e Modelagem de Sistemas Ambientais

Nelson Pedro António Mateus

ASSOCIATIONS BETWEEN EXTREME CLIMATE EVENTS AND LAND-USE CHANGES IN THE DOCE RIVER BASIN, MG: climate change projections.

Belo Horizonte
2025

NELSON PEDRO ANTÓNIO MATEUS

ASSOCIATIONS BETWEEN EXTREME CLIMATE EVENTS AND LAND-USE CHANGES IN THE DOCE RIVER BASIN, MG: climate change projections.

Tese apresentada ao Programa de Pós-Graduação em Análise e Modelagem de Sistemas (PPGAMSA) Ambientais da Universidade Federal de Minas Gerais (UFMG), como requisito parcial para a obtenção do título de doutor.

Orientadoras: Profa. Dra. Úrsula Ruchkys e a Profa. Dra. Ana Paula Martins do Amaral Cunha.

Belo Horizonte

2025

M425a
2025

Mateus, Nelson Pedro António.
Associations between extreme climate events and land-use changes in the Doce River Basin, MG [manuscrito] : climate change projections / Nelson Pedro António Mateus. – 2025.
183 f., enc. il. (principalmente color.)

Orientadoras: Úrsula Ruchkys e Ana Paula Martins do Amaral Cunha.
Tese (doutorado) – Universidade Federal de Minas Gerais, Instituto de Geociências, 2025.
Bibliografia: f. 158-181.

1. Extremos climáticos – Teses. 2. Mudanças climáticas – Teses. 3. Solo – Uso – Minas Gerais – Teses. 4. Vegetação e clima – Minas Gerais – Teses. 5. Zonas climáticas – Teses. 6. Doce, Rio, Bacia (MG e ES). I. Ruchkys, Úrsula de Azevedo. II. Cunha, Ana Paula Martins do Amaral. III. Universidade Federal de Minas Gerais. Instituto de Geociências. IV. Título.

CDU: 911.2:519.6(815.1)

Ficha catalográfica elaborada por Nathalia Machado Laponez Maia – CRB-6/3002

Biblioteca “Vitória Pedersoli”, Instituto de Geociências da UFMG

UNIVERSIDADE FEDERAL DE MINAS GERAIS INSTITUTO DE GEOCIÊNCIAS COLEGIADO DE PÓS-GRADUAÇÃO EM ANÁLISE E MODELAGEM DE SISTEMAS AMBIENTAIS

FOLHA DE APROVAÇÃO

ASSOCIAÇÕES ENTRE EVENTOS EXTREMOS CLIMÁTICOS E MUDANÇAS NO USO DO SOLO NA BACIA DO RIO DOCE - MG: PROJEÇÕES DAS ALTERAÇÕES CLIMÁTICAS

NELSON PEDRO ANTÓNIO MATEUS

Tese de Doutorado defendida e aprovada, no dia vinte e oito de março de dois mil e vinte cinco , pela Banca Examinadora designada pelo Colegiado de Pós-Graduação em Análise e Modelagem de Sistemas Ambientais da Universidade Federal de Minas Gerais constituída pelos seguintes professores:

Matheus José Arruda Lyra
Universidade Federal de Alagoas

Raquel Aparecida Abrahão Costa e Oliveira
Instituto Militar de Engenharia

Sâmia Regina Garcia Calheiros
Universidade Federal de São Paulo

Vagner Braga Nunes Coelho
Universidade Federal de Minas Gerais

Adriana Monteiro da Costa
Universidade Federal de Minas Gerais

Úrsula Ruchkys de Azevedo - Orientadora
Universidade Federal de Minas Gerais

Belo Horizonte, 31 de março de 2025.

Belo Horizonte, 31 de março de 2025.

Documento assinado eletronicamente por **Ursula Ruchkys de Azevedo**, **Professor(a)**, em 01/04/2025, às 09:23, conforme horário oficial de Brasília, com fundamento no art. 5º do Decreto nº 10.543, de 13 de novembro de 2020.

Documento assinado eletronicamente por **Vagner Braga Nunes Coelho**, **Chefe de departamento**, em 01/04/2025, às 09:28, conforme horário oficial de Brasília, com fundamento no art. 5º do Decreto nº 10.543, de 13 de novembro de 2020.

Documento assinado eletronicamente por **Matheus José Arruda Lyra**, **Usuário Externo**, em 02/04/2025, às 19:24, conforme horário oficial de Brasília, com fundamento no art. 5º do Decreto nº 10.543, de 13 de novembro de 2020.

Documento assinado eletronicamente por **Sâmia Regina Garcia Calheiros**, **Usuária Externa**, em 03/04/2025, às 09:10, conforme horário oficial de Brasília, com fundamento no art. 5º do Decreto nº 10.543, de 13 de novembro de 2020.

Documento assinado eletronicamente por **Adriana Monteiro da Costa**, **Professora do Magistério Superior**, em 03/04/2025, às 10:33, conforme horário oficial de Brasília, com fundamento no art. 5º do Decreto nº 10.543, de 13 de novembro de 2020.

Documento assinado eletronicamente por **Raquel Aparecida Abrahão Costa e Oliveira**, **Usuário Externo**, em 03/04/2025, às 10:49, conforme horário oficial de Brasília, com fundamento no art. 5º do Decreto nº 10.543, de 13 de novembro de 2020.

A autenticidade deste documento pode ser conferida no site https://sei.ufmg.br/sei/controlador_externo.php?acao=documento_conferir&id_orgao_acesso_externo=0, informando o código verificador **4090658** e o código CRC **A8703C2A**.

Referência: Processo nº 23072.220220/2025-76 SEI nº 4090658

ACKNOWLEDGMENTS

To God, for granting me health and by His grace allowing me to reach this point. My sincere thanks to the Coordination for the Improvement of Higher Education Personnel (CAPES) for their support during part of the development of this doctorate. To my advisors, Prof. Dr. Úrsula Ruchkys and Prof. Dr. Ana do Amaral Cunha, I express my deep gratitude for all the knowledge shared and for their patience throughout this academic journey.

To my mother and warrior, Madalena Domingos António, who, throughout my life, never spared any effort to make my dreams come true—a true heroine! To my father, recently passed, who so wished to witness this moment but was unable to see the realization of this dream.

To my sisters, and to my friends who became like brothers—Jaime Fernando António, Anacleto Marito Diogo, and João Pedro Silva, to my wife Melissa Vital. I am grateful for your support and companionship at every stage.

Finally, I also thank all the members of the examination committee, whose dedication and contributions were essential to the completion of this work.

“Whatever your hand finds to do, do it with all your might...

Salomão

RESUMO

A Bacia do Rio Doce (BRD), no sudeste do Brasil, enfrenta crescentes pressões das mudanças climáticas e do uso da terra. Este estudo integra três investigações interligadas, com uma abordagem que articula as dinâmicas hidroclimáticas e do uso da terra, com ênfase na identificação das regiões mais vulneráveis a eventos extremos de chuva e temperatura. As etapas incluem: (i) análise da influência da ZCAS na variabilidade hidroclimática; (ii) avaliação do uso da terra em cenários futuros; e (iii) resposta da vegetação via coerência wavelet, fornecendo subsídios ao planejamento territorial da bacia. Os resultados mostraram que a ZCAS é o principal modulador da variabilidade hidroclimática na BRD. A análise evidenciou que o uso de médias espaciais da ZCAS tende a mascarar variações relevantes na distribuição das chuvas. Assim, propôs-se uma avaliação baseada em padrões geográficos distintos (Norte, Centro e Sul), permitindo identificar áreas com maior exposição a eventos extremos. Os padrões Norte e Central estão associados aos maiores acumulados de precipitação (≥ 18 mm/dia) nas regiões norte, noroeste e parte do oeste da bacia, afetando as sub-bacias dos rios Suaçuí, Santo Antônio, Caratinga e Piracicaba. Já o padrão Sul concentrou os maiores acumulados no setor meridional, com destaque para a sub-bacia do Piranga. Os padrões Norte e Central apresentaram maior ocorrência de inundações durante episódios de eventos extremos associados à ZCAS, com limiares de precipitação definidos em ≥ 43 mm/dia nas regiões Norte e Central, e ≥ 23 mm/dia no Sul. Esses limiares contribuem para o aprimoramento de sistemas de alerta precoce. A modelagem das mudanças no uso e cobertura da terra (LULC) reforçou os resultados obtidos na análise da ZCAS, ao indicar que as áreas previamente identificadas como vulneráveis, localizadas nas regiões Norte, Noroeste, Sudoeste e Sul da BRD, tendem a sofrer transformações significativas no curto (2030), médio (2050) e longo prazo (2080). As projeções do modelo LULC, combinadas com os IAMs, mostram que, no cenário RCP4.5, a cobertura de floresta nativa deve ocupar 28,76% da área da bacia até 2030, com uma redução estimada entre -0,21% e -0,52% até 2080. Simultaneamente, as áreas agrícolas tendem a se expandir de 0,31% a 0,78%. No cenário RCP8.5, prevê-se uma redução mais acentuada da floresta nativa (-4,88%) e um crescimento significativo das áreas agrícolas (+6,04%). As projeções dos modelos Eta-MIROC e Eta-CanESM2 corroboraram essas tendências, indicando aumentos de 2 °C a 3 °C na temperatura média (TG e TG90p), maior frequência de dias secos (CDD > 50 dias), intercalados com eventos de chuvas intensas mais frequentes (RX1day e RX5day), e redução da precipitação total (PRCPTOT). Nessas áreas identificadas com redução da floresta nativa e aumento da agropecuária, a vegetação está respondendo de forma mais rápida a eventos de seca, com respostas entre 2 e 4 meses (SPI_1, SPI_3 e SPI_6), do que a eventos extremos de chuva, cuja resposta ocorreu entre 8 e 16 meses. Isso sugere que, em um contexto de mudanças climáticas, os impactos da degradação podem se manifestar mais rapidamente do que os processos de recuperação da cobertura vegetal.

Palavras-chave: eventos extremos; alterações climáticas; uso do solo; resposta da vegetação; ZCAS.

ABSTRACT

The Doce River Basin (DRB), located in southeastern Brazil, is under increasing pressure from climate change and land use. This study integrates three interconnected investigations using an approach that combines hydroclimatic and land-use dynamics, with an emphasis on identifying the regions most vulnerable to extreme rainfall and temperature events. The study includes: (i) an analysis of the South Atlantic Convergence Zone (SACZ) and its influence on hydroclimatic variability; (ii) an assessment of land use under future climate scenarios; and (iii) vegetation response evaluated through wavelet coherence analysis, providing insights for territorial planning in the basin. The results showed that the SACZ is the main modulator of hydroclimatic variability in the DRB. The analysis revealed that spatial averaging of SACZ-related rainfall tends to mask important variations in precipitation distribution. Therefore, an assessment based on distinct geographic patterns (North, Central, and South) was proposed, allowing for the identification of areas with greater exposure to extreme events. The North and Central patterns were associated with the highest rainfall accumulations (≥ 18 mm/day) in the northern, northwestern, and parts of the western basin, affecting the sub-basins of the Suaçuí, Santo Antônio, Caratinga, and Piracicaba rivers. In contrast, the Southern pattern concentrated higher rainfall in the southern portion of the basin, especially in the Piranga sub-basin. The North and Central patterns showed a higher occurrence of floods during extreme events associated with the SACZ, with precipitation thresholds of ≥ 43 mm/day in the North and Central regions, and ≥ 23 mm/day in the South. These thresholds contribute to the improvement of early warning systems. Land use and land cover (LULC) modeling reinforced the SACZ analysis by showing that previously identified vulnerable areas, located in the North, Northwest, Southwest, and South of the DRB—are likely to undergo significant changes in the short (2030), medium (2050), and long term (2080). LULC projections combined with IAMs indicate that, under the RCP4.5 scenario, native forest cover will occupy 28.76% of the basin by 2030, with an estimated reduction between -0.21% and -0.52% by 2080. Simultaneously, agricultural areas are expected to expand by 0.31% to 0.78%. Under the RCP8.5 scenario, a more pronounced reduction in native forest (-4.88%) and a significant increase in agricultural areas (+6.04%) are projected. Projections from the Eta-MIROC and Eta-CanESM2 models support these trends, indicating increases of 2 °C to 3 °C in mean temperature (TG and TG90p), more frequent dry days (CDD > 50 days), interspersed with more frequent heavy rainfall events (RX1day and RX5day), and a decrease in total precipitation (PRCPTOT). In areas with reduced native forest and increased farming, vegetation is responding more quickly to drought events, with responses between 2 and 4 months (SPI_1, SPI_3, and SPI_6), compared to extreme rainfall events, where the response occurred between 8 and 16 months. This suggests that, in the context of climate change, the impacts of degradation may manifest more rapidly than the processes of vegetation recovery.

Keywords: extreme events; climate change; land use; vegetation response; SACZ.

LIST OF FIGURES

LIST OF TABLES

LIST OF ABBREVIATIONS

AB Bolivian High

ASAS South Atlantic Subtropical High (SASH)

CMIP6 Coupled Model Intercomparison Project Phase 6

CDD Consecutive Dry Days – Maximum number of consecutive days without significant precipitation

CN Northeast Trough

CWD Consecutive Wet Days – Maximum number of consecutive days with significant precipitation

DRB Doce River Basin

EVI Enhanced Vegetation Index

IAMs Integrated Assessment Models

IPCC Intergovernmental Panel on Climate Change

LULC Land Use and Land Cover

LUH2 Land-Use Harmonization version 2

NDVI Normalized Difference Vegetation Index

NIR Near-Infrared

OLR Outgoing Longwave Radiation

PRCPTOT Total Annual Precipitation – Sum of all daily precipitation throughout the year

PS/PC/PN South, Central, and North ZCAS Patterns

RCP Representative Concentration Pathways

RED Red Spectral Band

RDEP Rio Doce State Park

RX1day Maximum Daily Precipitation – Highest precipitation recorded in a single day

RX5day Maximum 5-Day Precipitation – Highest precipitation accumulated over five consecutive days

SASH South Atlantic Subtropical High – see ASAS

SSP Shared Socioeconomic Pathways

TG Mean Temperature

TG10p 10th Percentile of Mean Temperature – Represents extremely cold days

TG90p 90th Percentile of Mean Temperature – Represents extremely hot days

VCAN Cyclonic Vortex at High Levels

WTC Wavelet Coherence Analysis

ZCAS South Atlantic Convergence Zone

SUMMARY

1 CHAPTER 1: INTRODUCTION

1.1 Presentation and Contextualization

Global climate change is intrinsically linked to land use and land cover changes, impacting biogeochemical cycles and atmospheric dynamics, which intensifies extreme events such as heatwaves, droughts, and floods (DUVEILLER *et al.*, 2020; LAL *et al.*, 2019, 2021; MAHOWALD *et al.*, 2017; PIELKE *et al.*, 2002). It is estimated that about 68% of the Earth's land surface has already been impacted by human activities such as agriculture, croplands, and pastures, which currently occupy around 40% of the land surface — a proportion comparable to that occupied by native and planted forests (FOLEY *et al.*, 2005).

Agricultural practices over the past four decades have significantly boosted global grain production, which currently exceeds 2 billion tons per year (POTAPOV et al., 2022). This growth is due, in part, to a 12% increase in global agricultural area, but primarily to innovations from the "Green Revolution," such as high-yield cultivars, chemical fertilizers, pesticides, mechanization, and irrigation (BEILLOUIN *et al.*, 2022; KASTNER *et al.*, 2022; MATSON *et al.*, 1997; POTAPOV *et al.*, 2022). Over the past four decades, fertilizer use has increased by 700%, while irrigated areas have expanded by 70%. Historically, between 1700 and 2000, there was a continuous conversion of forests into agricultural land (FOLEY *et al.*, 2005).

Although the expansion of native forest conversion into agricultural areas is a global trend, the regional impacts of Land Use and Land Cover (LULC) have proven to be more significant, affecting precipitation dynamics in various regions (POTAPOV *et al.*, 2022). Initially focused on physical parameters, studies on the impacts of LULC on climate evolved during the 1970s and 1980s to include the carbon cycle and greenhouse gas emissions (CHOKKAVARAPU; MANDLA, 2019; DIRMEYER, PAUL A.; SHUKLA, J., 1994; LOVEJOY *et al.*, 2013; PONGRATZ *et al.*, 2010; WILLIAMS *et al.*, 2008). Despite the relevance of General Circulation Models (GCMs), their resolution limitations prompted the development of Regional Climate Models (RCMs) in the 1990s, enabling more detailed climate analyses (JIN *et al.*, 2010; VON STORCH *et al.*, 1993).

The development of RCMs made it possible to assess the impacts of LULC changes on temperature variations and precipitation patterns (CHOKKAVARAPU; MANDLA, 2019; GAO *et al.*, 2020; LAL *et al.*, 2021). The conversion of forests into pastures and croplands

alters the hydrological balance, modifies local rainfall patterns, and intensifies extreme events such as droughts and heavy rainfall (LAL *et al.*, 2021; LEITE-FILHO *et al.*, 2021; MARENGO *et al.*, 2009a; ZEMP *et al.*, 2017). For example, in the Amazon, deforestation has significantly altered the hydrological cycle and precipitation regimes. Evidence shows that deforestation has reduced tree transpiration by up to 13%, contributing to a 55% to 70% decline in annual precipitation. In addition, deforested regions exhibit a significant reduction in mean annual precipitation, highlighting the impacts of land-use changes in the region (BAUDENA *et al.*, 2021; HATJE *et al.*, 2017).

The impacts of deforestation on climate variables reflect both anthropogenic pressure and global climate change. For instance, in the Southeast and Midwest regions of Brazil, projections indicate an increase of 2°C to 3°C in mean temperature and a reduction in precipitation (DE OLIVEIRA *et al.*, 2023; MARENGO *et al.*, 2013). These changes are particularly concerning for areas sensitive to deforestation, such as the southern region of the country and parts of the Southeast (COSTA, F. de P. D. *et al.*, 2022; LYRA, 2018; MARENGO *et al.*, 2009b, 2013).

Climate changes influenced by LULC also affect hydrological processes and water quality, with impacts on contaminant concentrations (HU *et al.*, 2021; JALLIFFIER-VERNE *et al.*, 2015). These changes increase the occurrence of extreme weather events, such as floods and landslides, as well as water contamination by agrochemicals on a regional scale (CHEN et al., 2020; DUBREUIL et al., 2019; GAO et al., 2020; MARENGO ET AL., 1998; MARENGO et al., 2015, MARENGO et al., 2019).

1.2 Justification and Research Gap

In the Doce River Basin (DRB), which is the focus of this thesis, studies on land use have primarily focused on transitions between different land-use classes, such as changes in forest areas, planted forests, and pastures. It has been found that the expansion of pastures is associated with increases in mean and maximum annual streamflows, as well as reductions in minimum flows—a phenomenon influenced by rainfall variability. (AIRES *et al.*, 2018; COELHO, 2006; LIMA, 2016a; NEVES, 2022; SPOSITO, 2021). Camargo *et al.*, 2011 they investigated the relationship between flooding, land use and land cover, observing a 63%

increase in peak discharge during extreme rainfall events in the Piranga sub-basin. However, in urban areas, there was a 7% reduction in runoff depth and an 11% decrease in peak discharge.

From the perspective of hydroclimatic conditions in the basin, Paiva (1996), Cupolillo (2008), and De Castro Sena et al. (2020) highlighted that the spatial variability of SACZ results in significant impacts on both maximum and minimum streamflows during extreme precipitation events. These effects vary considerably across different regions of the basin, as observed by (CUPOLILLO *et al.*, 2008).

As at the global scale, studies conducted for the DRB have primarily focused on changes in mean precipitation (COELHO, 2020; LIMA, 2016a; LYRA, 2018), while placing less emphasis on extreme events at shorter time scales. This approach highlights a significant gap in the understanding of regional climate impacts. For example, Campos *et al.*, (2024), demonstrated that climate projections for the basin indicate a potential reduction of over 300 mm in mean annual precipitation by 2050. This decrease is significant, considering that annual totals range from 800 mm to 1,800 mm. In addition, projections indicate that mean annual temperature could increase by up to 2°C, based on Representative Concentration Pathway (RCP) scenarios 4.5 and 8.5.

In parallel, land use and land cover analysis for 2050 indicates that agricultural and livestock activities could occupy 68.7% of the DRB area, while forests would account for only 26.5%. However, if legal reserve areas are fully respected, native vegetation could reach 31.7% of land cover, reducing the extent of agricultural and livestock activities to 63.8% (CAMPOS *et al.*, 2024). According to Neves (2022), agricultural and livestock activities in the lower Doce River region occupied 66.48% of the territory in 2012, corresponding to 10,347.20 km². By 2019, this area had increased to 68.88%, totaling 10,721.21 km². This growth highlights the expansion of land use for agricultural purposes in the region over the analyzed period.

These scenarios highlight the need to broaden the scope of analyses to include the impacts of extreme events, which may have even more severe consequences for the socioeconomic and environmental structure of the basin. Deepening the understanding of these issues is essential for a better grasp of future challenges, especially in light of projected climate change. According to Campos et al. (2024), current projections for the DRB were developed based on the hypothetical inclusion of legal reserve areas and precipitation data, aiming to represent two contrasting land-use scenarios: one conservative and the other non-conservative. However, despite being a promising approach, it does not account for the impacts of land use under changing climate conditions, incorporating the climate guidelines outlined in the

Intergovernmental Panel on Climate Change (IPCC) reports. Moreover, the simple inclusion of legal reserve areas does not align with the Integrated Assessment Models (IAMs) approach proposed by the IPCC.

IAMs are tools that integrate disciplines such as energy, economics, atmospheric chemistry, climate, and ecology, enabling the construction of representative scenarios. (CALVIN *et al.*, 2017; FRICKO *et al.*, 2017; FUJIMORI *et al.*, 2017). Given the above, studies exploring the relationship between land-use changes and extreme climate events—such as heavy rainfall, temperature extremes, and droughts, including those associated with the SACZ—have yet to be developed for the DRB. The present research represents an advancement over previous studies, as the inclusion of IAMs in the land-use model for the DRB enables a more integrated and realistic analysis of these interactions. Furthermore, the response of vegetation to extreme events in areas under high anthropogenic pressure, particularly deforestation, remains insufficiently investigated, constituting a significant gap in the understanding of the DRB's environmental dynamics.

This thesis aims to understand the implications of forest and native vegetation conversion to other land uses on the dynamics of precipitation and temperature extremes, within the context of future climate change scenarios (RCP4.5 and RCP8.5). The research adopts an integrated approach to hydroclimatic and land-use dynamics, with an emphasis on identifying environmentally vulnerable areas in the DRB. In this context, the analyses provide support for land-use planning and management actions that are more responsive to ongoing environmental changes. To carry out the investigation, the research was structured into three main stages: **(A)** Initially, a hydroclimatic assessment of the DRB was conducted to identify the areas most affected by extreme events associated with the SACZ, the main system responsible for the basin's water supply. It was found that the spatial variability of the SACZ is directly related to the occurrence of precipitation extremes linked to flooding, allowing for the characterization and quantification of its dynamics and the identification of relevant patterns for understanding the distribution of extreme events. Additionally, precipitation thresholds were established for flood monitoring in areas under intense anthropogenic pressure—an unprecedented approach in the context of the DRB.

(B). Based on the identification of the main hydroclimatic conditions and the areas sensitive to SACZ-related extremes, the dynamics of land use and land cover were analyzed, focusing on these regions as well as adopting a broader perspective for the entire basin. The study investigated how areas vulnerable to deforestation are evolving in terms of the frequency

and intensity of extreme events, considering both current trends and future projections. This analysis was conducted under two climate scenarios: the optimistic scenario (RCP4.5) and the pessimistic scenario (RCP8.5). **(C)**. Finally, based on the history of forest loss and the identification of current and future impact areas associated with land use and land cover dynamics, the vegetation response to extreme events was investigated. The study assessed how vegetation, particularly in areas transitioning to other land uses, has responded to such events, aiming to understand the impacts on the resilience of ecosystem services. This evaluation deepens the understanding of the challenges posed by climate change and unsustainable land use, building upon the insights gained in the previous stages.

The analyses were conducted using observational and projected data on precipitation, temperature, and land use. Climate extreme indices recommended by the ETCCDI were applied, along with statistical trend detection methods such as the Mann-Kendall test and the Theil-Sen estimator. Land-use modeling was based on future LUH2 scenarios, incorporating the consideration of legal reserve areas. Finally, vegetation response was assessed using time series of the EVI index, with spectral coherence analysis (WTC) employed to identify relationships with extreme events across different temporal scales.

1.2 Hypotheses

Based on the considerations presented, this study tested the following hypotheses:

I. Land use and land cover areas exhibit distinct dynamics in hydroclimatic characteristics, with increased intensity and frequency of extreme events in the DRB. These effects are better understood by separately evaluating the spatial dynamics of the SACZ through its specific geographic patterns (South, Central, and North).

II. Under future climate change scenarios (RCP4.5 and RCP8.5), areas susceptible to deforestation intensify water deficits and reduce vegetation resilience, compromising the basin's essential ecosystem services.

III. The incorporation of Integrated Assessment Models (IAMs) into climate projections (CMIP6 - LUH2) enhances the realism of simulations and allows for a more accurate assessment of the relationship between land-use changes and extreme climate events. This approach enables the identification of critical impact areas, providing more reliable support for sustainable management strategies and mitigation of climate change effects in the DRB.

Based on the outlined hypotheses, this study aims to address the following key research questions:

I. Which regions of the DRB will be most susceptible to the impacts of extreme rainfall and drought events, considering changes in land use and land cover (LULC)?

II. How do the different spatial configurations of the SACZ — represented by the Southern (PS), Central (PC), and Northern (PN) patterns — influence streamflow regimes, water quality, and flood intensity in the DRB, and which areas are most vulnerable to these impacts during extreme precipitation events under each pattern?

III. Which areas of the Doce River Basin exhibit critical thresholds in land use change and the occurrence of extreme events, and how has vegetation responded to these changes over time?

1.3 Objectives

1.3.1 General goal

- To integrate the analysis of hydroclimatic and land-use dynamics into the territorial planning of the DRB, focusing on the identification of vulnerable areas and the proposal of adaptation strategies to extreme climate events in the context of climate change.

1.3.2 Specific goals

I. To identify the areas of the basin most affected by extreme events related to the spatial variability of the SACZ (Southern, Central, and Northern patterns).

II. To perform numerical simulations of LULC changes based on IAMs and investigate their associations with extreme climate events in vulnerable areas of the basin.

III. To investigate the vegetation response to variations in extreme climate events across different temporal scales within the basin.

1.4 THESIS STRUCTURE

The structure of this thesis follows an article-based format. The first chapter comprises the introduction, while the second consists of a literature review covering the most relevant studies on climate, climate change, land use, and extreme events conducted in the context of the basin. The third chapter outlines the general methodological framework, while Chapters 4, 5, and 6 present the published and submitted articles. Chapter 7 provides the overall conclusion of the thesis.

CHAPTER 1: GENERAL INTRODUCTION – Presentation of the research context, justification, objectives, and structure of the thesis.

CHAPTER 2: METHODOLOGICAL FRAMEWORK OF THE THESIS – Presentation of the data that supported the analyses developed in this thesis and served as the foundation for the main scientific articles.

CHAPTER 3: LITERATURE REVIEW – The literature review highlights studies on meteorological systems, extreme events, vegetation responses to these events, modeling using the Dinamica EGO platform, and territorial planning strategies in the face of climate change.

CHAPTER 4: OVERCOMING THE IMPACTS OF THE SPATIAL VARIATION OF SOUTH ATLANTIC CONVERGENCE ZONE ON RAINFALL, FLOW AND WATER QUALITY IN RIO DOCE, BRAZIL - The main water supply system of the basin was assessed by identifying the areas most affected by the spatial patterns of the SACZ in terms of rainfall dynamics, streamflows, water quality, and extreme events, with emphasis on precipitation thresholds and regions susceptible to flooding.

CHAPTER 5: ASSOCIATIONS BETWEEN CLIMATE CHANGE, LAND USE, AND EXTREME CLIMATE EVENTS - Data from IAMs were used in a land-use model to simulate climate change scenarios, exploring the associations between land-use changes and the frequency/intensity of extreme precipitation and temperature events, with a focus on the areas identified in Chapter 4 (Article 1).

CHAPTER 6: VEGETATION RESPONSE TO EXTREME EVENTS: IMPACTS IN THE DOCE RIVER BASIN - The response of vegetation to extreme climate events was assessed, with emphasis on the areas identified in Chapters 4 and 5. The analysis investigated how the basin's vegetation reacts to such conditions, particularly in deforested regions

highlighted in the climate change scenarios. The indices considered were the same as those evaluated in Article 2.

CHAPTER 7: GENERAL CONCLUSION – Synthesis of the main findings of the thesis, with emphasis on the identification of vulnerable areas based on the interaction between extreme climate patterns and land-use change. The results support territorial planning by suggesting adaptation measures grounded in hydroclimatic and land cover dynamics, contributing to sustainable management in the face of climate change.

2 CHAPTER 2: METHODOLOGICAL FRAMEWORK OF THE THESIS

The methodological framework of this research was developed in four phases to address the research questions and objectives outlined (Figure 1). Research Questions 1 and 2 are related to Specific Objectives (i) and (ii), and are addressed in Chapters 5 and 6. Question 3 is associated with Objectives (ii) and (iii), and is discussed in Chapters 6 and 7 (Figure 1).

The thesis methodology comprises two main approaches: an observational phase and a modeling phase. To assess extreme rainfall events in the DRB, the methodological analysis was divided into three parts:

I. **OBSERVATIONAL - Analysis of the impacts of extreme events in the Doce River Basin:** In this phase, the main areas of the basin affected by extreme events associated with the activity of the SACZ—the main system responsible for the rainfall regime in the region—were identified. The effects of the spatial patterns of the SACZ (Southern, Central, and Northern) were analyzed in relation to hydrometeorological variables such as precipitation, streamflow, water quality, and flood occurrence.

II. **MODELING – Selection and evaluation of climate extreme indices:** The Western, Northern, Northwestern, Southwestern, and Southern regions of the DRB were identified as the most vulnerable to extreme events associated with the SACZ. Based on an understanding of this dynamic and the precipitation amounts linked to each SACZ pattern during extreme events, the most representative climate extreme indices for the DRB were defined. Subsequently, numerical experiments were conducted in these regions (North, Northwest, South, West, and Southwest) using IAMs, with the aim of exploring the relationships between extreme events and LULC under future climate change scenarios (RCP4.5 and RCP8.5).

III. **OBSERVATIONAL – Vegetation response to extreme events in the Basin:** In the final phase of the thesis, beyond consolidating knowledge on the current and future trends of extreme climate events—as identified in the previous articles—the analysis was deepened by investigating how vegetation in the DRB responds to these events across different temporal scales. This approach enhances the understanding of climate impacts on the basin's ecosystems by integrating the findings of Articles 1 and 2, which defined the spatial patterns of the SACZ, the most susceptible areas, and the climate extreme indices. Article 3 complements these analyses by revealing the

sensitivity of vegetation to drought and precipitation extremes, considering the role of deforestation in the region's environmental resilience.

Figure 1 - Flowcharts developed in the 4 stages of the methodological path.

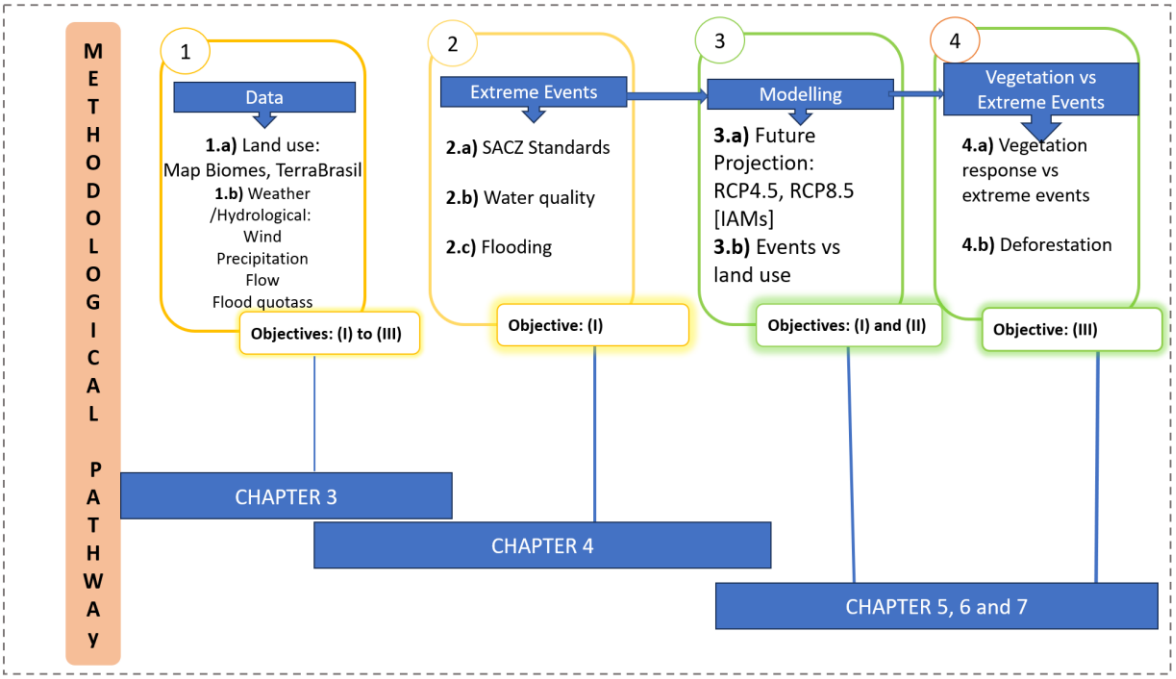

Source: elaborated by the author.

2.1 Detailed Methodological Framework

To answer Research Question 1, complement Question 2, and support Hypotheses I and II, the first article (published) was developed, in which the areas most affected by extreme precipitation events associated with different spatial patterns of the SACZ were identified. Streamflow, water quality, precipitation, and flood stage data were used to assess the effects of these events on the hydrometeorological conditions of the DRB. The entire methodological process is described in Chapter 4.

Based on these identified areas, the second article was developed to further address Question 2, answer Question 3, and support Hypotheses II and III. In this article, LULC transformations in the most vulnerable areas were modeled under different future climate scenarios (RCP 4.5 and RCP 8.5). Historical data from MapBiomas were used (SOUZA JR *et al.*, 2020) and projections from LUH2, which incorporates Integrated Assessment Models

(IAMs), in addition to climate projections from global models. The methodology is detailed in Chapter 5.

Finally, in the third article, the response of vegetation to extreme precipitation and drought events was assessed in the same areas analyzed in the previous studies, considering different temporal scales. This stage allowed for the integration and complementation of the thesis findings by addressing the role of vegetation in the face of extreme events and land-use changes, with a focus on ecosystem resilience. The methodology is presented in Chapter 6, and all datasets used in each article are detailed in Table 1.

Table 1 - Main data sources and their respective institutions.

Data	Institutions	Resolution	Article	Link
Precipitation	CHIRPS/ETA/INPE	0.05°	CHA. 4 CHA. 5	https://www.chc.ucsb.edu/data/chirps https://lattesdata.cnpq.br/dataverse/lattesdata?q=eta
Longwave Radiation	NCEP/NCAR	2.5°	CHA. 4	https://www.noaa.gov/
Land Use	MAPBIOMAS	30 m	CHA 5 e 6	https://mapbiomas.org/
Land-Use Harmonization (LUH2)		1 km	CHA. 5	https://figshare.com/articles/dataset/Global_IGBP_LULC_projection_dataset_under_eight_SSPs-RCPs/20088368/1 https://luh.umd.edu/
Precipitation/Temperature	CMIP6 /ETA	1.1°	CHA. 5 e 6	https://lattesdata.cnpq.br/dataverse/lattesdata?q=eta

Phytophysiognomy, soil types, highways, railways, protected areas, agriculture, livestock, rivers, relief, biomass, and Ottobasins.	CSR	30	CHA. 5	https://maps.csr.ufmg.br/
Agricultural Crops	IBGE	30	Cap. 5	https://www.ibge.gov.br/
Precipitation, Streamflow, and Water Levels	ANA	30	Cap.4	https://www.snirh.gov.br/hidrweb/apresentacao
Water Quality Parameters	IGAM	30	Cap.4	https://igam.mg.gov.br/
EVI	AppEARS/Earthdata	250 m	Cap.6	search.earthdata.nasa.gov/search

Source: Elaborated by the author

3 CHAPTER 3: LITERATURE REVIEW

3.1 Structure of the Literature Review

The literature review is composed of nine sections, covering topics ranging from climate change at different scales to its impacts on the DRB. It highlights analyses of meteorological systems, territorial planning in the context of climate change, extreme events in the DRB, vegetation dynamics in response to extreme events, and modeling using the Dinamica EGO platform, as detailed in Table 2.

The initial sections are dedicated to the analysis of meteorological systems and extreme events, examining the frequency, intensity, and spatial distribution of these phenomena. The reviewed literature explores the interconnections between climate change and the intensification of heavy precipitation events, droughts, and floods, with an emphasis on the implications for water resources and population safety.

Additionally, the review delves into vegetation dynamics in response to extreme events, investigating how climate change affects vegetation cover, biodiversity, and ecosystem services. Studies on the topic highlight the importance of vegetation in regulating the hydrological cycle and mitigating the impacts of climate change.

Finally, the review addresses climate change modeling using the Dinamica EGO platform. This tool enables the simulation of future scenarios and the assessment of climate change impacts at different scales, providing support for territorial planning and natural resource management. Table 2 presents a detailed overview of the reviewed studies, including their objectives, methodologies, and main findings

Table 2 - Detailing of the literature review.

Sections	Topics
3.1.2	Global Climate Change
3.1.3	Territorial Planning in the Context of Climate Change
3.1.4	Meteorological Systems Acting in the Doce River Basin
3.1.5	South Atlantic Convergence Zone (SACZ)
3.1.6	Extreme Events in the Doce River Basin
3.1.7	Land Use and Land Cover Changes in the DRB
3.1.8	Modeling with the Dinamica EGO Platform
3.1.9	Vegetation Response to Climate and Extreme Events

Source: elaborated by the author.

3.1.2 Global Climate Change

The human influence on atmospheric warming, impacting both the oceans and the land surface, is indisputable. Rapid changes in temperature and precipitation patterns are well documented. Warnings about climate change caused by human activity date back to the 1950s, and as early as the late 19th century, researchers were already considering the possibility of temperature increases due to carbon dioxide emissions. In the 1990s, climate models were developed to explain climate variability, taking into account both natural and anthropogenic contributions (IPCC, 2007, 2022; MARENGO *et al.*, 2009a, 2013).

The most recent IPCC report (2023), based on the CMIP6 framework, outlined scenarios using the Shared Socioeconomic Pathways (SSPs). The last four decades have been the warmest since 1850, with recorded warming of 1.59°C over land and 0.88°C over the oceans between 2011 and 2020.

Global temperatures have risen more rapidly since 1970 than during any other 50-year period over the past two millennia (IPCC, 2022). As indicated in the latest IPCC report (AR6), global temperatures between 2081 and 2100 are likely to be 1°C to 1.8°C higher than those of 1850–1900 under the optimistic emissions scenario (SSP2-4.5), and 3.3°C to 5.7°C higher under the pessimistic scenario (SSP5-8.5). As a result, an increase in the frequency and intensity of extreme heat and rainfall events is expected, along with longer-lasting heatwaves across much of the globe (IPCC, 2007, 2022). Recent studies emphasize the urgency for governments and society to adopt strategies to mitigate the social and economic impacts of climate change on the hydroclimatic dimension, including streamflow and precipitation (KLAAS *et al.*, 2020; TUNDISI, 2008).

The Coupled Model Intercomparison Project (CMIP), coordinated by the World Climate Research Programme (WCRP), has significantly contributed to the understanding of climate variability at both national and international levels. This is achieved through general circulation models, whose results are published in the IPCC reports (FINDELL *et al.*, 2023).

Box 1 - Climate change and scenarios

Climate change refers to significant and long-lasting alterations in global climate patterns, including changes in temperature, precipitation, winds, and storm patterns, occurring over a period of time typically measured in decades or longer (IPCC, 2022, MARENGO, 2007). Future climate change scenarios are plausible representations of future greenhouse gas (GHG) emissions based on a set of coherent and physically consistent assumptions about the driving factors, such as:

Demographics (e.g., population growth and urbanization);

Socioeconomic development (e.g., economic growth and consumption patterns);

Technological change (e.g., advances in renewable energy and energy efficiency).

These scenarios provide projections of atmospheric GHG concentrations, which are used as the basis for modeling future climate changes. They account for the complex interactions between human activities and the climate system, including feedbacks between emissions, atmospheric concentrations, and climate change

3.1.3 Planning in the Face of Climate Change

Global climate change exerts a significant influence on urban settlements, with an expected increase in the frequency of extreme rainfall events capable of causing floods and landslides in various regions of the world (FINDELL *et al.*, 2023). Reducing vulnerability and strengthening resilience to the impacts of climate change require the regulation of urban land use and occupation. In this context, climate-oriented territorial planning strategies are associated with the development of mechanisms aimed at protecting the most vulnerable populations from risks related to extreme climate events, such as floods, sea-level rise, landslides, heatwaves, flash floods, droughts, and dry spells (TEIXEIRA; PESSOA, 2021).

Box 2 - Territorial planning in the face of climate change

Territorial planning in the face of climate change is a strategic approach aimed at integrating climate variables into land-use planning and territorial management. Its central goal is to reduce the vulnerability of human communities and ecosystems, promoting socio-environmental resilience and sustainability within the context of global climate transformations (FERREIRA et al., 2023; WAMSLER et al., 2012).

Territorial planning for climate change involves: Identifying areas vulnerable to climate risks such as droughts, floods, and heatwaves; Implementing adaptive strategies such as green infrastructure (ecological corridors, parks, retention zones); Guiding urban growth toward less susceptible areas and avoiding risk zones; Promoting resilient construction and encouraging sustainable land-use practices; Integrating climate and environmental data into public policies, considering future scenario projections (CRESPO et al., 2023).

Brazil has shown increasing efforts in formulating public policies aimed at enhancing urban resilience to climate change. The National Policy on Climate Change (Federal Law 12.187/2009) and the National Policy on Civil Protection and Defense (Federal Law 12.608/2012) represent important milestones in this regard, as they establish guidelines for the creation of information and urban disaster monitoring systems, with an emphasis on intergovernmental coordination and social participation.

However, the effective implementation of these policies faces significant challenges. The literature points to a technocratic tendency in territorial planning, which often overlooks the specific characteristics and needs of the affected communities (CRESPO *et al.*, 2023; FERREIRA *et al.*, 2023; TEIXEIRA; PESSOA, 2021; WAMSLER *et al.*, 2013). This approach, characterized by institutional disconnection and fragmented information, undermines the ability of cities to respond effectively to climate impacts.

To overcome these weaknesses, it is imperative to integrate climate and environmental information into territorial planning. Studies such as those by Marengo *et al.*, 2009b, PBMC, 2014 (2014) and the reports of the IPCC (2022, 2023) highlight the need for an interdisciplinary approach that combines knowledge from various fields to formulate effective public policies. Overcoming technocratic planning and promoting the integration of diverse knowledge are therefore crucial for developing adaptation and mitigation strategies that consider the specificities of territories and the needs of vulnerable populations, thereby ensuring urban resilience in the context of climate change.

3.1.4 Meteorological Systems Acting in the DRB

Rivers, as part of extensive watershed systems, play a crucial role in Brazil. The main basins — Amazon, Tocantins, Plata, and São Francisco — cover about 80% of the national territory. These regions are influenced by various climate scales, ranging from micro to macroscale (CUARTAS *et al.*, 2022).

Studies highlight the influence of climate change on temperature extremes, resulting in anomalous meteorological systems that affect streamflow and precipitation in various Brazilian basins (RODRIGUES *et al.*, 2019). A notable example occurred in the Southeast region between 2013 and 2014, when the combined action of an atmospheric blocking pattern and an anomalous high-pressure system inhibited not only the formation SACZ but also upward atmospheric motion. This atmospheric blocking suppressed convection and the formation of rain clouds, resulting in a severe drought. The impacts were widespread, with significant losses in agricultural production—especially in coffee and soybean crops—and serious challenges in water supply, leading to rationing in several regions. (CUSTÓDIO, 2015; MARENGO *et al.*, 2015).

Meteorological systems are the main drivers of the hydroclimatic dynamics in the DRB. Copolillo (2008) identified the most relevant systems influencing rainfall dynamics in the basin, including the Upper-Level Cyclonic Vortex (ULCV), the Northeast Trough (NT), the Bolivian High (BA), and the South Atlantic Subtropical High (SASH). The BA contributes to moisture transport in the western portion of the basin, favoring precipitation—a process essential for water supply. In contrast, the influence of the SASH and ULCV in the central part of the basin contributes to an irregular spatial and temporal distribution of rainfall (Figure 2).

Box 3 - Definition of Meteorological System.

A meteorological system is an organized disturbance in the atmosphere, characterized by the dynamic interaction of various atmospheric elements and, crucially, the influence of oceanic components. These systems vary significantly in spatial and temporal scale, as well as in intensity, and may either move or remain relatively stationary, influencing atmospheric conditions and, on larger and more integrated scales, contributing to the formation of climate patterns (HOUGHTON, 2002).

The elements that compose and influence a meteorological system include:

Atmospheric: temperature, pressure, humidity, wind, clouds, and precipitation.

Oceanic: sea surface temperature, ocean currents, and air–sea interaction (heat and moisture transfer).

Trough: refers to an extended region of relatively low atmospheric pressure, characterized by a curvature or elongation in isotherms (temperature lines) or isobars (pressure lines) in upper-level pressure maps, particularly in the mid-troposphere. Unlike a closed low or a cyclone, which typically have a more circular shape, a trough is more elongated and can cover a wide geographic area (HOUGHTON, 2002).

During the summer, the BA contributes to the intensification of tropical convection over South America and plays a crucial role in transporting moisture from the Amazon to the Southeast, reaching much of the DRB (CUPOLILLO *et al.*, 2008; REBOITA *et al.*, 2010). When combined with the SACZ, its effects on precipitation events are amplified in the basin. The interaction between these systems gives rise to convective systems and increases the risk of extreme rainfall and flooding in the DRB (CUPOLILLO, 2008).

The displacement of the SASH, associated with the heat source over the Amazon and the extension of the NT, allows the entry of tropical convective systems, favoring intense rainfall in the DRB (CUPOLILLO, 2008; MATEUS, 2020). However, the prolonged presence of the SASH can also lead to short dry spells, during the rainy season in the basin. These short dry spells are often linked to the combined influence of the NT and the SASH.

Winter in the DRB is mainly influenced by the SASH. This system promotes atmospheric stability due to the cooling of the Amazon heat source, resulting in reduced precipitation throughout the basin (CUPOLILLO et al., 2008). Significant and prolonged deviations from normal winter precipitation patterns, intensified by the action of the SASH, can be particularly detrimental to agriculture and contribute to the temporary reduction of water availability, worsening the impacts of climate change in the region. This can lead to atypical and severe drought periods during winter, negatively affecting agricultural production and local water resources (LIMA, 2016). In addition to these atmospheric systems that influence the hydroclimatic dynamics in the basin, atmospheric blocking patterns also play an important role. These blocks occur mainly during the summer and disrupt the normal displacement of frontal systems and the SACZ (MARENGO et al., 2009). As a result, they can lead to prolonged drought periods in some parts of the basin and excessive rainfall in others, intensifying climate variability both spatially and temporally in the region (CRUZ et al., 2018; MATEUS et al., 2025).

Figure 2 - Schematic representation of atmospheric systems in the lower and upper troposphere over South America.

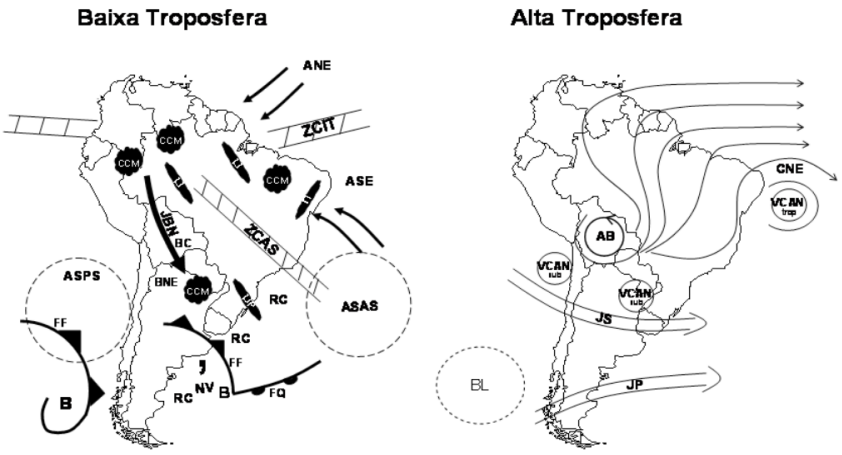

Source: REBOITA et al., 2010.

3.1.5 South Atlantic Convergence Zone (SACZ)

Characterized by a cloud band oriented in the Northwest–Southeast (NW–SE) direction over South America, the SACZ is identified in meteorological fields by low- and mid-level moisture convergence, a trough at 500 hPa over the eastern coast, the intrusion of frontal systems, the presence of the ULCV over northeastern Brazil, upper-level jets, and a strong potential temperature gradient. Regarding its occurrence, approximately 70% of SACZ episodes are classified as either intense or weak, with an average duration of about four days, while 30% persist for longer periods (CARVALHO *et al.*, 2004).

The SACZ is a crucial meteorological system in South America, with significant impacts on human activities such as agriculture, livestock, mining, energy, and transportation (Figure 3). The SACZ is known for triggering extreme precipitation events, which result in flooding and landslides (PEZZI *et al.*, 2023; REBOITA; VEIGA, 2017; SELUCHI; CHOU, 2009).

Recently, Antonio (2021) identified three geographical patterns of the SACZ: South (PS), Central (PC), and North (PN). Precipitation can vary depending on the pattern, resulting in a non-homogeneous spatial distribution (Figure 3). For example, most extreme rainfall episodes in Minas Gerais are associated with the presence of the SACZ, with precipitation totals exceeding 55 mm (SILVA *et al.*, 2020). Nascimento, 2012 addressed the impact of this system on extreme events in the municipality of Piranga, located within the DRB. The study concluded that there is an immediate response in peak streamflows associated with rainy days under the influence of the SACZ (Figure 3).

The existing literature highlights the significant influence of the SACZ on the hydrological and climatic aspects of the DRB. For instance, in the Rio Doce State Park (PERD) between 2015 and 2016, Lima et al. (2018) demonstrated a strong correlation between SACZ events and episodes of intense rainfall that significantly affected several municipalities within the basin. Additionally, on days of SACZ activity, regions near the lower course of the basin exhibited greater socio-environmental vulnerability (LIMA; CUPOLILLO, 2018; LIMA *et al.*, 2019). This pattern is intensified by the interaction between the SACZ and the circulation of systems such as the SASH, which transports moisture to southeastern Brazil, enhancing rainfall conditions in the basin. Despite its importance, the SACZ does not act uniformly across the entire basin. Conversely, the absence of this system leads to a strong water deficit throughout

the region. During the years 2014 and 2015, atypical severe drought events were recorded, associated with the absence or anomalous displacement of the SACZ—dynamics that had previously been unknown in the context of extreme events in the DRB. This displacement resulted in critical water deficits, impacting both water resources and economic activities dependent on rainfall (CRUZ *et al.*, 2015).

Furthermore, deforestation in the DRB also plays a crucial role in the interaction between the SACZ and local climate patterns. Areas with greater loss of forest cover show reduced moisture recycling capacity, which amplifies the negative impacts of climate extremes such as intense rainfall and prolonged droughts (CUPOLILLO et al., 2018). Pazini *et al.*, 2020 contributed to the understanding of the vulnerability of areas prone to landslides associated with the SACZ. The results indicated that regions with steeper slopes and urban occupation, as well as agricultural and pasture areas, show greater susceptibility to landslides when affected by this system. This susceptibility underscores the importance of considering the impacts of the SACZ in water resource management and land use planning, encompassing everything from the occurrence of extreme events to the variation in peak streamflows and energy generation.

The study by Kunzler (2018) reveals that precipitation resulting from SACZ events plays a crucial role in the energy potential of several regions in the Southeast (CUARTAS *et al.*, 2022). In particular, a decline in energy potential was observed during the summer of 2014, coinciding with the absence of SACZ formation—a phenomenon possibly associated with climate change, such as atmospheric blocking events (MARENGO et al., 2015; CUARTAS et al., 2022). Another study focused its analysis of extreme rainfall events in the municipality of Ubá, identifying the SACZ as the main system responsible for significant precipitation totals in six out of the seven cases examined (DOS SANTOS; FIALHO, 2016).

Figure 3 - Main meteorological systems operating in the Doce River basin.

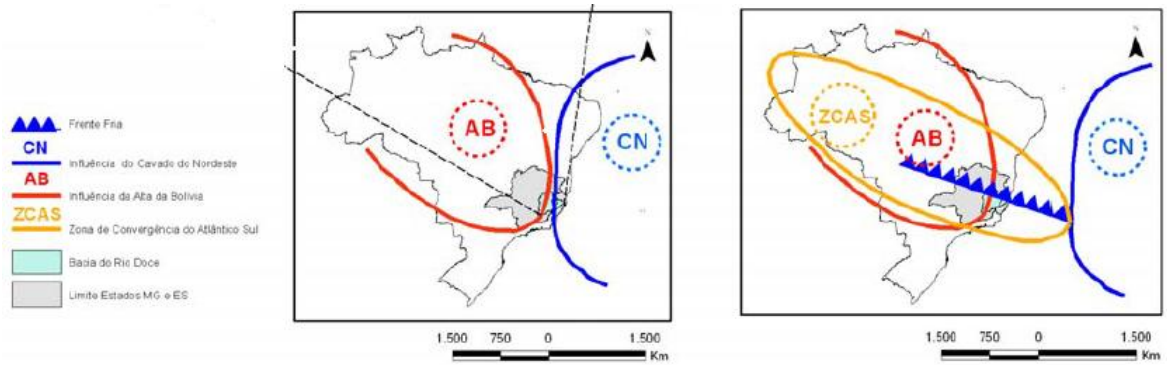

Source: Adapted of Copolillo (2008).

3.1.6 Extreme climate events in the DRB

The literature, as represented by studies such as Marengo et al. (2009) e Marengo et al. (2015), highlights the influence of extreme climate events in Brazil, characterizing them as deviations from the mean atmospheric state across different temporal scales: short, medium, and long duration. These events, predominantly hydrometeorological, trigger natural disasters with significant impacts, such as loss of life, agricultural damage, disruptions in public supply, and effects on energy generation (CUARTAS et al., 2022). Water resource management faces challenges due to the uncertainties and risks associated with hydrological events, such as intense rainfall and droughts, as discussed by Valverde e Marengo et al. (2009).

In the context of the DRB, the findings of Ferreira (2019) and Cavalcante et al. (2023), indicate a reduction in rainfall on wet days and an increase in dry days, associated with changes in precipitation patterns. Cavalcante et al., 2023, observed a clear trend of increasing consecutive dry days (CDD) and a reduction in consecutive wet days (CWD), particularly in the northern and southern regions of the basin. According to the authors, these effects can be explained by climate change, which alters the hydrological cycle, resulting in prolonged droughts and more intense and concentrated rainfall events within the basin (CAVALCANTI *et al.*, 2023). Furthermore, the reduction in total precipitation volume projected for the future aligns with the impacts of deforestation and land-use changes, which directly affect local evapotranspiration patterns and moisture recycling (BRÊDA *et al.*, 2020; DANTAS *et al.*, 2022). Camargo et al. (2014) investigated the relationship between floods, land use, and land cover, observing a 63% increase in peak streamflow during extreme rainfall events in the Piranga sub-basin (located within the DRB). In urban areas, however, there was a reduction in runoff depth and peak flow, ranging between 7% and 11%.

The impact of floods in the middle Doce River was analyzed by Cruz et al. (2015 highlighting patterns and recurrence, especially in long-term floods associated with the SACZ. In parallel, drought events have increased in frequency, with prolonged droughts in the middle Doce River region occurring more persistently and intensely over the years (CRUZ *et al.*, 2015). Lima (2019) evaluated the climatic conditions during the most critical drought years in the basin, identifying 2014–2015 as the most severe period, affecting the entire region.

The study by Cavalcante et al. (2023) evaluated the dynamics of extreme precipitation events using the Rx1day and Rx5day indices. These indices indicate greater variability in the future, with intense rainfall concentrated over fewer days and an increase in the standard deviation of these events. This behavior reflects a more irregular rainfall distribution, particularly in the northern sector of the basin, identified as the area most affected by reductions in precipitation and increased climate variability. Deforestation and land-use changes have also significantly impacted the basin's hydrology. In the Rio Piranga region, located at the headwaters of the DRB, the conversion of forests into pastures has led to increased surface runoff and reduced soil infiltration (NEVES, 2022). This process intensifies erosion, causes soil loss, and contributes to the siltation of watercourses, reducing water storage capacity and compromising water quality. Additionally, vegetation cover degradation on slopes worsens sediment transport, increasing the basin’s vulnerability to landslides and flooding (SALVADOR, 2014).

3.1.7 Land Use and Land Cover Changes and Climate of the DRB

In the dynamics of a watershed, various processes, including climate change, erosion, weathering, and socioeconomic factors related to political decisions, influence its hydrological characteristics (DUVEILLER *et al.*, 2020; FRICKO *et al.*, 2017; JANSEN; DI GREGORIO, 2002; MCCONNELL, 2002; PATEL *et al.*, 2023; WANG *et al.*, 2023). Coelho (2007) emphasizes that river flow velocities and precipitation patterns at daily, monthly, and annual scales are affected by such influences. The input of rainfall, especially intense events, plays a significant role in altering runoff velocity within the basin (COELHO, 2006; FRAGA *et al.*, 2020).

Box 4 - Land Use and Land Cover Change (LULC).

LULC

Land cover encompasses various types of biological or physical coatings present on the Earth's surface, highlighting the natural characteristics of the terrain, such as forests, pastures, agricultural lands, and urbanized areas (JANSEN; DI GREGORIO, 2002). On the other hand, land use refers to the ways in which humans make use of these land covers, taking into account the natural attributes that have been modified by the effects of human activities (FRESCO, 1994; MCCONNELL, 2002).

Thus, when we refer to LULC, we are referring to both aspects: that is, LULC refers to the land surface cover, including the spatial distribution and types of land use such as urban areas, forests, agricultural lands, and bodies of water. It encompasses both natural features (e.g., forests, deserts) and human-modified ones (e.g., urban areas, agricultural lands) (PATEL et al., 2023; WANG et al. 2023, DUVEILLER, 2020).

The importance of understanding the local effects of changes in precipitation patterns within a watershed is emphasized by Marengo et al. (2015) e Cuartas et al., 2022. These precipitation extremes, by altering local meteorological systems, can trigger more severe consequences. One example of such local variations is the DRB, which is characterized by significant climatic variability

According to the Köppen classification, the climate in the basin is generally tropical, covering most of the region. In the western portion, the rainy season is longer, while the dry season is shorter—this pattern is reversed in the eastern part (CUPOLILLO, 2008). The wettest period occurs from October to March, with peak rainfall in December and total precipitation ranging from 800 to 1.300 mm. In contrast, the driest period spans from April to September, with rainfall totals between 150 and 250 mm, and June and August being the driest months (CUPOLILLO, 2008; CUPOLILLO *et al.*, 2008). This climatic variability highlights the complexity of hydroclimatic conditions in the DRB.

The impact of climate change in the DRB was assessed by the IUCN (International Union for Conservation of Nature) using a regional climate model for each economic sub-region (Figure 4). Figure 4 presents maps showing variations in mean temperature (upper panels) and mean precipitation (lower panels) for the period from December to February (temperature) and June to August (precipitation) in 2080, under two emission scenarios (A2-

BR and B2-BR) (UICN, 2022). The results indicated a temperature increase of between 3°C and 3.6°C for the pessimistic scenario and between 2°C and 2.5°C for the more optimistic scenario. In the temperature variation maps, a color gradient illustrates the projected increase, with darker red tones concentrated in the western and southern regions of the basin in both scenarios.

Regarding precipitation, the study indicated a reduction in rainfall in some parts of the western sector, both during the dry and wet seasons. The precipitation variation maps show greater spatial heterogeneity. In the A2-BR scenario, the western portion of the basin exhibits a more pronounced decrease in precipitation, while in the B2-BR scenario, this reduction appears to be less intense and more spatially limited. It is important to note that other areas of the basin show smaller variations or even a slight increase in projected precipitation (Figure 4).

The comparison between the temperature and precipitation variation maps reveals a crucial aspect of the climate system's response in the DRB to the projected changes. While the temperature maps show a relatively uniform intensification of warming—with the western and southern regions exhibiting the highest increases—the precipitation maps display a more complex alteration in spatial patterns. This disparity in the response between temperature and precipitation underscores the complexity of climate projections and the need for variable- and region-specific analyses. Furthermore, projections indicate that future precipitation in the DRB will remain relatively high, resulting in maximum and average streamflows above the current mean. Significant changes in peak streamflows were also observed, with surpluses projected in these areas through 2041, particularly in the eastern region of the basin. (SANTANA *et al.*, 2021).

Climate change has impacted land use, as shown in recent studies (LEITE-FILHO et al., 2020; PATEL et al., 2023; WANG et al., 2023). In general, the conversion of forests into pasture has led to an increase in mean and maximum annual streamflows, along with a reduction in minimum flows. This dynamic is explained by the combined effects of converting native forests into pasture, which influence different components of the hydrological cycle (LYRA, 2018). For example, in the DRB, land use simulations indicated that replacing forests with pasture resulted in a reduction in mean and minimum annual streamflows, but with an increase in maximum flows in some sub-basins of the DRB, indicating the potential for flooding events (LYRA, 2018).

The deforestation of 25% of native vegetation for pasture conversion led to an increase in maximum streamflow and a decrease in minimum flow. These trends suggest concerning

impacts on soil loss and runoff rates over the next 90 years compared to the current period (LYRA, 2018). O estudo de Neves (2022) analyzed land use dynamics in the Doce River Basin between 2012 and 2019, relating them to the Samarco disaster. Using MapBiomas data and the driving force identification methodology, the author observed an almost complete shift in agropastoral expansion before (2012–2015) and after (2016–2019) the dam failure. Prior to the incident, precipitation and temperature had negative effects on agropastoral expansion, whereas after the disaster, slope had a positive effect and urban area a negative effect in the municipalities. In both periods, the extension of highways showed positive effects on the expansion of agropastoral activities.

Sposito (2021) addressed land use and land cover in the basin, identifying that approximately 50% of the area showed no changes in land use class. However, natural forest and pasture areas experienced reductions of -1.9% and -9.1%, respectively, between 1985 and 2018. Most of the natural forest conversions were to pasture, while there was an increase in agricultural land and planted forest, with distinct changes in each sub-basin. The study highlights the urgency of developing actions to reverse soil degradation. The work by Oliveira *et al.*, 2020 examined landscape changes over the past 30 years and projected future scenarios for the surroundings of the Rio Doce State Park (RDEP). The results indicated an increase in anthropogenic pressure, leading to a decrease in native vegetation areas and contributing to forest fragmentation and the loss of permanent ecological reserves.

Figure 4 - Variation in temperature and precipitation based on climate change.

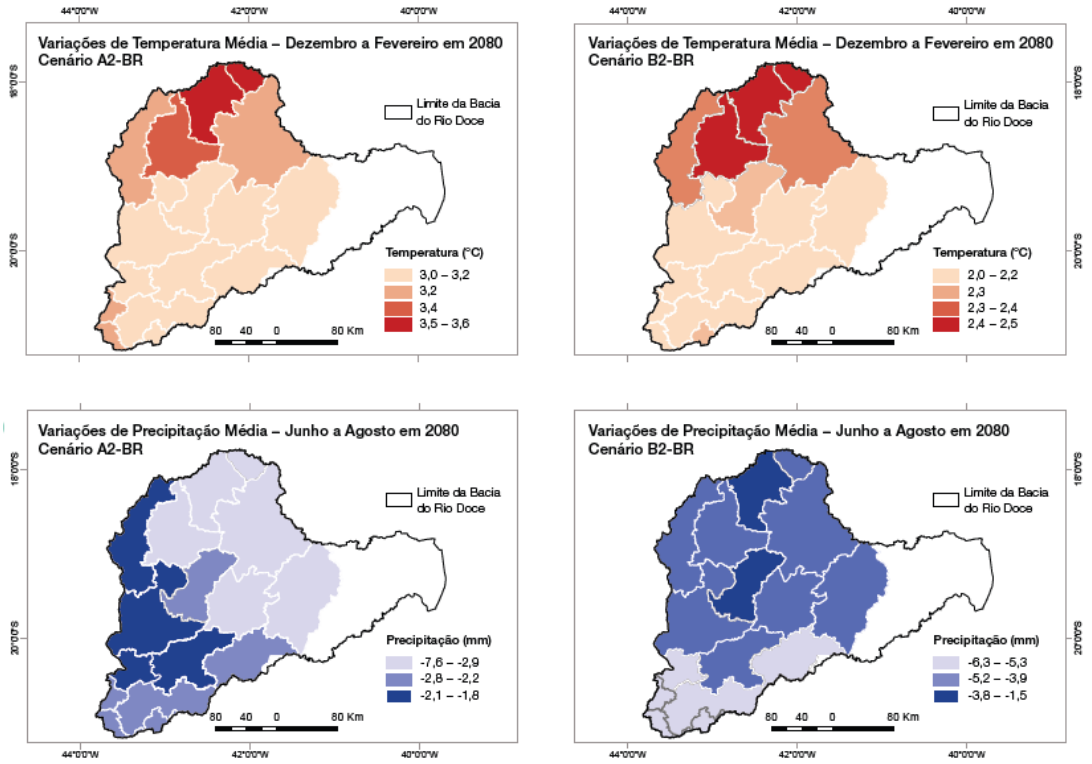

Source: UICN (2011).

3.1.8 Modeling with the Dinamica EGO Platform

Dinamica EGO is a free, non-commercial platform dedicated to environmental modeling, offering a wide range of possibilities—from simple static spatial models to complex dynamic models. The platform supports nested iterations, multiple transitions, dynamic feedbacks, regional and multi-scale approaches, as well as decision processes for bifurcation and merging of execution pipelines (Figure 5). It also includes a variety of advanced spatial algorithms for the analysis and simulation of spatiotemporal phenomena (SOARES-FILHO *et al.*, 2004; SOARES-FILHO *et al.*, 2002)

The variety of phenomena occurring across a landscape or surface is not static; it exhibits dynamics that play crucial roles in the climate. Processes such as urbanization, agricultural expansion, wildfires, desertification, and other factors exert direct or indirect influence on the climate. Spatial dynamic models perform numerical simulations of these processes in the real world by altering the state of a point on the surface through external variations (RODRIGUES *et al.*, 2007; SOARES-FILHO *et al.*, 2002).

In these models, various geographic elements that compose the landscape are incorporated and overlaid on a 2D raster, representing a mapped regular grid matrix. This approach enables a detailed representation and analysis of the spatiotemporal interactions among the different components of the landscape, providing a more comprehensive understanding of the dynamics that affect the climate.

Time is represented in a discrete manner, serving as the third dimension of the model. According to Soares-Filho et al., 2002, a spatial representation model of the landscape involves solving Equation [1].

$$X_{t+v} = f(X_t, Y_t) \quad (1)$$

Equation 1 describes the changes in the spatial pattern X_t, at time t, leading to a new spatial pattern X_{t+v} at time $t + v$, where Y_t represents the set of scalars that affect the model transition.

During the construction of the model, certain phases are fundamental and must be considered:

a) Define the conceptual model with the possible landscape transitions: this stage is represented by a transition matrix that contains all possible transitions. This matrix is obtained from known transitions, which are observed from one state to another in the landscape. Simple mathematical models, such as Markov chains, solve the transition function (Figure 5).

b) Through the Bayesian weights-of-evidence method, actual changes in the landscape are identified, and the functions that integrate Yt over time are defined using external variables (ALMEIDA *et al.*, 2005; KAWASHIMA *et al.*, 2016; SOARES-FILHO *et al.*, 2002). The Bayesian method is based on Bayes' theorem of conditional probability, which uses the prior probability of an event occurring as a function of spatial determinants (ALMEIDA et al., 2005).

c) The weights of evidence are obtained through cross-tabulation between the LULC change map and the maps of the variables considered in the conceptual model as spatial determinants. For example, those that can explain the transitions, based on the premise that these variables are spatially independent (SOREAS FILHO et al., 2002). Thus, when the goal is to test several variables in the model, the evidence from multiple maps

is combined, that is, the weights are first calculated independently and then incorporated into a single probability equation (Equation 2)

$$p(i \Rightarrow \frac{j(x,y)}{v}) = \frac{e^{\sum k W_{kn\ i=>j(V)^{xy}}}}{1+\sum ije^{\sum k W_{kn\ i=>j(V)^{xy}}}} \quad (2)$$

X, y are the spatial coordinates of the variables, *n* is the number of categories, and *W* is the weight of evidence, which represents the probability of an event occurring from one land use to another, for example, from forest to pasture.

In Brazil, many spatial modeling studies use the Dinamica EGO platform, which is based on cellular automata techniques. This platform employs an approach that uses two complementary transition functions, known as the "expander" (expansion function) and the "patcher" (patch formation function). The expander function acts on the expansion of existing patches, while the patcher function creates new patches (SOARES-FILHO et al., 2002). Both functions require user-defined specifications, usually through calibration tests, allowing direct adjustment of the Land Use and Land Cover (LULC) change patterns.

Figure 5 - Architecture of models that can be built through the EGO Dynamic platform.

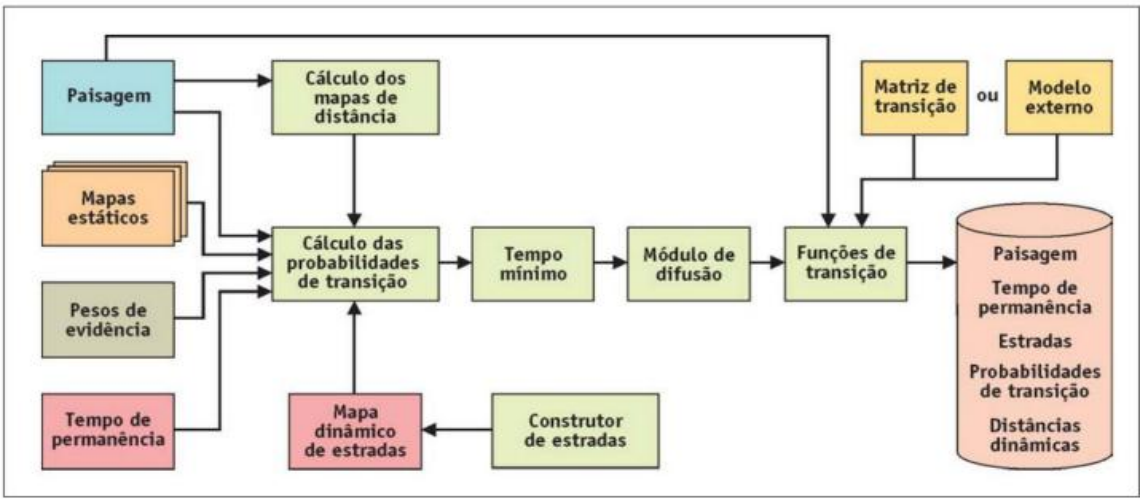

Source: Soares Filho et al. (2007).

3.1.9 Vegetation Response to Climatic Conditions and Extreme Events

Vegetation is one of the most important terrestrial components of ecosystems, playing a key role in biosphere–atmosphere interactions (DUVEILLER *et al.*, 2020; FORZIERI *et al.*,

2017; ZENG *et al.*, 2017). The structure and composition of vegetation are strongly influenced by several factors, including human activities, climate change, and high atmospheric CO_2 concentrations (DUVEILLER et al., 2018). Changes in forest cover cause a direct imbalance in the surface energy budget, affecting processes such as evapotranspiration and albedo, and consequently influencing temperatures at both local and regional levels (DE NOBLET-DUCOUDRÉ *et al.*, 2012; PITMAN *et al.*, 2009).

Evidence suggests that deforestation leads to an increase in temperature in low-latitude regions, although on smaller scales, it can also cause a cooling effect in high-latitude areas (D'ALMEIDA *et al.*, 2007; LAWRENCE *et al.*, 2016; LUO *et al.*, 2022; SPRACKLEN *et al.*, 2012). The loss of forest cover causes hydrological and thermal imbalances, affecting the displacement and intensity of heat sources, which in turn alters the dynamics of meteorological systems. In other words, some regions exhibit distinct patterns in the occurrence of extreme events, with some showing an increase in the frequency of such events, while others demonstrate a reduction in the incidence of droughts and heatwaves (MATEUS et al., 2020). Moreover, extreme climate events such as droughts, heavy rainfall, and heatwaves exacerbate the negative impacts on vegetation (REICHSTEIN *et al.*, 2014; VINCENT *et al.*, 2015). Droughts, for instance, increase water stress in plants and hinder forest regeneration, compromising essential functions such as photosynthesis and transpiration (REICHSTEIN et al., 2013; VINCENT et al., 2013). On the other hand, heavy rainfall contributes to soil saturation, reducing root oxygenation and promoting erosion, which further weakens ecosystems (ICHII *et al.*, 2002; LIU *et al.*, 2024).

Given these observed effects, satellite imagery has been used for the temporal and spatial monitoring of vegetation. Over the past 30 years, studies have shown that changes in vegetation, such as increased green cover in certain areas and deforestation in others, are linked to factors like higher CO_2 concentrations, nitrogen deposition, climate change, and land use changes (ANDERSON *et al.*, 2013; CHAPIN *et al.*, 2008; JACKSON *et al.*, 2008).

Changes in vegetation cover directly affect the exchange of energy and water between the land surface and the atmosphere, influencing climatic variables such as temperature and precipitation patterns (FORZIERI *et al.*, 2017). In tropical regions, for example, an increase in vegetation density tends to enhance local cooling, mainly due to greater transpiration and moisture recycling (FORZIERI et al., 2018). In higher-latitude areas, however, an increase in vegetation can lead to warming, as it reduces surface reflectivity (albedo) and increases solar radiation absorption. These biophysical effects can both amplify and offset the benefits of

carbon sequestration, highlighting the complex role of vegetation in climate regulation (FORZIERI *et al.*, 2017).

The loss of vegetation cover, especially due to deforestation, has significant impacts on precipitation patterns, temperature, and the frequency of droughts. Recent studies have provided strong evidence supporting these environmental effects (ASSUNÇÃO *et al.*, 2015; DOS REIS *et al.*, 2021; OLIVEIRA *et al.*, 2020, 2018). In the Amazon, for example, forest removal interferes with the hydrological cycle, resulting in reduced rainfall, increased drought risk, and a greater occurrence of forest fires (FEARNSIDE, 2006). Simulations using climate models show that deforestation directly affects precipitation by altering moisture availability and meteorological systems. This can lead to the reduction or displacement of heat sources, decreasing the intensity and frequency of heavy rainfall events and shortening the duration of rainy seasons in deforested areas (LUO *et al.*, 2022; MATEUS, 2020).

Several indices are used to monitor vegetation, with the NDVI (Normalized Difference Vegetation Index) standing out due to its simplicity and effectiveness. This index is calculated from the relationship between red (RED) and near-infrared (NIR) reflectance, providing a general view of vegetation density and vigor, and is commonly used to assess plant health ((BALLESTEROS *et al.*, 2015; FOLEY *et al.*, 1998; MULLA, 2013). However, NDVI has limitations, especially in areas with high biomass or under adverse atmospheric conditions, such as aerosol interference and shadows (HUETE *et al.*, 2002, 1997).

To overcome these limitations, the Enhanced Vegetation Index (EVI) was developed. It uses correction factors to minimize the effects of soil and atmosphere (HOFFMANN *et al.*, 2015; HONKAVAARA *et al.*, 2013; VANCINE *et al.*, 2024; XIA *et al.*, 2016). EVI is particularly useful in regions with high forest density, as it is more sensitive to subtle variations in vegetation cover. Additionally, its formula includes extra spectral bands, such as the blue (BLUE) band, which improves the accuracy in identifying different types of vegetation and eliminates noise that could compromise the analyses (HUETE et al., 1997).

4 CHAPTER 4: OVERCOMING THE IMPACTS OF THE SPATIAL VARIATION OF SOUTH ATLANTIC CONVERGENCE ZONE ON RAINFALL, FLOW AND WATER QUALITY IN DOCE RIVER BASIN, BRAZIL

4.1 Abstract

This study focuses on the Rio Doce basin in Minas Gerais, Brazil, analyzing the impact of geographic positions (patterns) of the South Atlantic Convergence Zone (SACZ) on the variability of precipitation, river flow, floods, and water quality. Despite its significance, the lack of studies considering different SACZ positions in defining precipitation thresholds for early warning in flood events and water quality parameters persists. The results highlight that distinct SACZ positions are associated with variations in the distribution of precipitation, river flow, and water quality. The Northern Pattern (NP) and Central Pattern (CP) contribute to higher accumulations of rainfall (≥18 mm/day) and river flow (80-800 m^3/s) in the basin. The Piracicaba and Santo António sub-basins record the highest number of extreme rainfall events, with 168 and 127, respectively. Most floods occur in the NP pattern, totaling 54 cases (28.63% causing substantial harm to the population). We identified that precipitation levels ≥43 mm/day are linked to floods in both NP and CP patterns, serving as a threshold for watershed committee decisions. Trend analysis indicates a decrease in rainfall and river flow across all patterns. Regarding water quality, the presence of SACZ primarily increases parameters such as turbidity and total suspended solids. This work contributes to integrating water-related criteria into policies and decisions, especially relevant in the Rio Doce basin following an environmental disaster caused by the rupture of a mining dam.

---

[1] ***Article published :*** https://doi.org/10.26848/rbgf.v18.1.p038-060.

1.Nelson Pedro António Mateus, 2.Diego Pujoni, 3. Ricardo Amorim, 4. Anacleto Diogo, 5.Ana Paula M A Cunha, 6.Sónia Carvalho Ribeiro

4.2 Introduction

In Brazil, extreme precipitation events severely impact water availability and can lead to floods, landslides, and natural disasters, affecting a large portion of the population (LAUREANTI *et al.*, 2024). Water resource management faces significant challenges due to the uncertainties and risks associated with extreme hydrological events, such as intense rainfall and droughts, as discussed by Valverde *et al.*, (2003) and Marengo et al., (2009). In this study, we investigate how the different geographical positions of the spatial variation of the South Atlantic Convergence Zone (SACZ) influence precipitation patterns, flow, and water quality. The central hypothesis of study suggests that these distinct patterns of SACZ result in varied amounts of precipitation in the region, with a predominant pattern that impacts rainfall and flow variability. Furthermore, the research aims to identify a precipitation threshold capable of triggering extreme events, such as floods, and investigate how the seasonal nature of the SACZ affects water quality parameters in the study area. In essence, this study not only enriches our comprehension of SACZ regional impacts but also establishes a robust foundation for effective flood event alerts associated with its performance, thereby contributing valuable insights to both scientific discourse and practical applications. Understanding these variabilities is essential for improving water resource management strategies and mitigating the impacts of extreme hydrological events.

The SACZ is a crucial meteorological element in Brazil, profoundly influencing the spatial distribution of rainfall and significantly impacting vital economic sectors, including agriculture, energy, and transportation (ANTÓNIO, 2020; QUADRO, 1999; WONG *et al.*, 2021, 2023). As a band of cloudiness extending from Northwest to Southeast South America the SACZ is intrinsically linked to meteorological events such as floods, landslides, and avalanches (QUADRO, 1999; REBOITA; VEIGA, 2017; SELUCHI; CHOU, 2009).

The mechanisms involving the formation of SACZ and the occurrence of associated extreme events have been explored in studies by Carvalho *et al.*, (2002), Zilli; Carvalho, (2021), Zhou; Lau, (2001). According to these authors, the formation of the SACZ incorporates several meteorological characteristics, including the convergence of moisture at low and mid-levels, the presence of a trough at 500 hPa over the eastern coast, incursions of frontal systems, the presence of an Upper-Level Cyclonic Vortex (ULCV) over Northeast Brazil, upper-level jets, and a strong potential temperature gradient. Given the significant socioeconomic impact of

SACZ events and the uncertainties in their predictions, previous studies have focused on better understanding their intensity, duration, and impacts. Approximately 70% of SACZ episodes last around four days, while the remaining 30% persist for more than four days (Carvalho et al., 2004; Ambrizzi e Ferraz, 2015; Escobar et al. 2020; Lauriante et al., 2024). The SACZ exhibits considerable spatial and temporal variability, playing a critical role in regulating the intensity and total precipitation that affects millions of people in South America (ANTÓNIO; ARAVÉQUIA, 2023; ESCOBAR; REBOITA, 2022).

The duration of SACZ events is closely related to the occurrence of extreme precipitation events. Through the analysis of circulation fields and longwave radiation, Da Silva Verdan, (2023) observed that longer SACZ events had a higher number of associated cyclones in their oceanic branch. However, it was not possible to determine the lifecycle duration of these associated cyclones. Another significant finding was that precipitation in the South-Central region of Brazil was higher when Low-Level Jets exhibited a northwest-southeast orientation during SACZ days.

The study conducted by Fialho *et al.*, 2023 and Viana *et al.*, 2021 investigated the mechanisms behind SACZ events lasting more than seven days and associated with extreme precipitation events, often leading to floods and landslides. The results indicated that these persistent SACZ events are typically preceded by a semi-stationary Rossby wave train of mid-latitude over the South Pacific. This phenomenon acquires a barotropic structure and moves towards the equator after crossing the subtropical latitudes of South America. These combined processes enhance low-level westerly winds on the equatorial edge of the SACZ, resulting in the expansion of the phenomenon over the continent and the formation of convective clouds that induce intense precipitation. These characteristics are supported by anomalous cyclonic circulation and an increased moisture transport towards the southeast in the region, as highlighted by Pezzi *et al.*, (2022). This pattern leads to heightened convection over the continent, keeping the SACZ active for prolonged periods and impacting the affected areas with high accumulations of rainfall over several consecutive days. Despite shorter SACZ events, lasting around four days, also being associated with a mid-latitude wave train, their transient nature results in distinct coupling effects. These observations play a crucial role in forecasting long-duration SACZ events, as emphasized by Escobar et al. (2022).

Braga *et al.*, (2022) investigated a spatial variation of precipitation associated with the SACZ. Utilizing data on zonal and horizontal wind components combined with longwave radiation, the study revealed that a strong westward tropical flow associated with SACZ allows

for the propagation of Rossby waves through the Equatorial Atlantic Ocean. These waves have the capacity to modify precipitation patterns, generating systems that either inhibit or trigger intense rainfall, leading to extreme rainfall events. Laureanti et al. (2024) further highlighted that wind circulation changes induce variations in Sea Surface Temperature (SST), ultimately impacting the dynamics of meteorological systems and influencing the duration of extreme precipitation events during SACZ occurrences. In essence, the Southwest Atlantic Ocean emerges as a potential influencer modulating the persistence of extreme precipitation events in the Central-Eastern region of Brazil.

Braga *et al.*, 2024 investigated a spatial variation of precipitation associated with the SACZ. Utilizing data on zonal and horizontal wind components combined with longwave radiation, the study revealed that a strong westward tropical flow associated with SACZ allows for the propagation of Rossby waves through the Equatorial Atlantic Ocean. These waves have the capacity to modify precipitation patterns, generating systems that either inhibit or trigger intense rainfall, leading to extreme rainfall events. Laureanti et al. (2024) further highlighted that wind circulation changes induce variations in Sea Surface Temperature (SST), ultimately impacting the dynamics of meteorological systems and influencing the duration of extreme precipitation events during SACZ occurrences. In essence, the Southwest Atlantic Ocean emerges as a potential influencer modulating the persistence of extreme precipitation events in the Central-Eastern region of Brazil.

Duarte, 2017, analyzing intense precipitation in southern Brazil (Santa Catarina state) during the periods of 1979-1999 and 2000-2015, made insightful discoveries. They found that the frequency and intensity of extreme precipitation events during the austral spring were reduced during El Niño years and increased in neutral years in the second period compared to the first. Their studies indicated a significant association between the historical series of extreme precipitation events and the SACZ, alongside a low-level anticyclone in the Southwest Subtropical Atlantic during the latter period. Moreover, Montini *et al.*, (2019) revealed that positive trends in precipitation and the occurrence of extreme precipitation events in southeastern South America between 1979 and 2016 were linked to increased moisture transport from the northwest Amazon region to the subtropics, a phenomenon influenced by the activity of the SACZ. The study by Jorgetti *et al.*, (2014) addressed precipitation variability due to the SACZ positioning. The researchers classified SACZ-North events when the precipitation band is over central Brazil and SACZ-South when it is over the southern region. SACZ-North occurs when waters of the Tropical Atlantic are cooler, and SACZ-South is associated with

warmer waters. During the SACZ-South period, the upper-level anticyclonic circulation shifts towards southeastern South America, with warmer waters in the Tropical Atlantic. Consequently, the modulation of SACZ activity is linked to Sea Surface Temperature (SST) anomalies through dynamic and thermodynamic mechanisms. However, in Antonio's study (2021) on SACZ dynamics, three geographical patterns of SACZ were observed: South (PS), Central (PC), and North (PN). According to the author, precipitation occurrence can vary depending on the pattern, resulting in non-uniform spatial distribution. This finding supports Jorgetti et al., (2014) study, which emphasized circulation dynamics.

The SACZ have been routinely studied from a regional perspective. For instance, in the state of Minas Gerais, Brazil, empirical evidence from 1995 to 2016 attributes 126 landslides, 546 inundations, 688 floods, and 41 overflows to the SACZ's presence (AGUIAR, 2018). The southeastern region of Brazil faces a substantial average probability of SACZ-induced disasters, reaching 24%. This risk amplifies differentially across Espírito Santo (60%), Minas Gerais (50%), Rio de Janeiro (40%), and São Paulo (31%), underscoring the region's susceptibility to heightened rainfall events and emphasizing the intricate interplay between territorial planning and risk management (ANTÓNIO; ARAVÉQUIA, 2023; CARVALHO *et al.*, 2002; DA FONSECA AGUIAR; CATALDI, 2021), unravels nuanced spatial dynamics, impacting Brazilian watersheds disparately(AGUIAR, 2018; FIALHO *et al.*, 2023; NETO *et al.*, 2010). Despite the acknowledgment of physical processes within hydrographic basins during extreme rainfall events such as erosion and weathering, comprehensive assessments of SACZ's influence on flow, flooding, and water quality remain conspicuous by their absence.

This study seeks to bridge this gap by categorizing SACZ patterns into three distinct types, scrutinizing their defining characteristics, and discerning their differential impacts on precipitation distribution, flow rates, flood occurrences and water quality. Focused on the Doce River Basin in the Southeast region of Brazil, a region distinguished by its rich biodiversity and the endangered Atlantic Forest biome, this research immerses itself in unraveling the intricate interrelationships between SACZ patterns and extreme weather events. The catastrophic rupture of the Fundão dam in 2015, releasing millions of cubic meters of mining tailings into the Rio Doce, serves as a poignant reminder of the region's vulnerability to environmental disasters exacerbated by SACZ-induced heavy rainfall. This event inflicted dire consequences on the entire ecosystem, including physical devastation by mud transport, 17 human casualties, 2 missing individuals, extensive fish mortality, and significant damage to local flora (Neves, 2022).

Moreover, the ongoing flow of mud, exacerbated by heavy rainfall, continues to compromise water quality and the well-being of communities in the Doce River basin (BOURGUIGNON *et al.*, 2021; HATJE *et al.*, 2017; PACHECO *et al.*, 2022). Furthermore, SACZ's impacts on the Piranga sub-basin are characterized by extreme rainfall events, leading to a substantial increase in peak flow rates, while urban areas experience a slight reduction in peak flow rates (CAMARGO *et al.*, 2011). These fluctuations in flow rates pose a threat to flood-prone areas, particularly those affected by long-term extreme rainfall events associated with the SACZ in the basin (CRUZ *et al.*, 2015). Notably, in Minas Gerais state, extreme precipitation events linked to SACZ are marked by accumulated precipitation exceeding 55 mm/day (SILVA *et al.*, 2020).

Ferreira (2019) found a decrease in rainfall on humid days and an increase in dry days in the Doce River basin, with varying effects on maximum and minimum flow in different regions. Moreover, high rainfall totals are linked to increased sediment transport, deteriorating water quality (JIA *et al.*, 2021; JIANG *et al.*, 2023; OLIVEIRA; DA SILVA QUARESMA, 2017; WANG *et al.*, 2022; YANG *et al.*, 2021). Studies have shown that meteorological and hydrological factors influence water quality parameters such as nitrogen, phosphorus, turbidity, pH, and biochemical oxygen demand (FAN; SHIBATA, 2015; XIA *et al.*, 2015). Despite advancements in understanding these factors, the relationship between SACZ and water quality parameters in the Doce basin remains largely unexplored.

The studies previously mentioned have identified SACZ events and characterized their formation, intensity, duration, and positioning. These studies have utilized methodologies that analyze not only the synoptic and dynamic characteristics of SACZ but also their impacts on precipitation extremes at both local and regional scales. This study aims to fill a gap in research by examining how different spatial patterns of the SACZ affect the distribution of precipitation, flow, and water quality in the Rio Doce basin.

4.3 Methodology

4.3.1 Data

The DRB (Figure 6) watershed covers an area of 86,715 km², primarily in the state of Minas Gerais (86% of the basin area) and partly in Espirito Santo (14%). This region includes 230 municipalities with around 2,341,206 urban residents and 833,437 rural inhabitants. In terms of water usage, 51% of the total water extracted directly from the Doce River basin is used for irrigation, 22% for urban supply, 17% for industries, 7% for animal watering and 3% for rural supply (Figure 6). The basin is divided into six Water Resources Planning and Management Units (UPGRHs), corresponding to six sub-basins and their respective Hydrographic Basin Committees (CBHs): Piranga River (DO1), Piracicaba (DO2), Santo Antônio (DO3), Suaçuí River (DO4), Caratinga (DO5), and Manhuaçu River (DO6). All data access links are duly detailed in the supplementary material (https://github.com/NelsonMateus/SM.git).

Precipitation data were obtained from the CHIRPS (Climate Hazards Group InfraRed Precipitation). This dataset combines satellite precipitation estimates with weather station observations to provide nearly global precipitation coverage from 1981 to the present (Funk, C. et al., 2015). CHIRPS is highly detailed, with a daily temporal resolution and a spatial resolution of 0.05 degrees (~5.5 km). Additional data were obtained from six weather stations managed by the National Water Agency (ANA).

Data from these stations used for the period from 1991 to 2020. The use of data from ANA stations aimed to complement and enrich the analysis conducted with CHIRPS data, providing validation and increasing the accuracy of the results. The CHIRPS precipitation data were integrated with the data from ANA stations to perform a detailed analysis of SACZ patterns. It was not necessary to apply any gap-filling techniques for the SACZ occurrence dates in each pattern, as the collected data were complete for the corresponding dates throughout the temporal series of the considered stations. For additional details on the source of each data point, refer to Table 1 in the supplementary material. The material can be accessed at the following repository: https://github.com/NelsonMateus/SM.git.

Figure 6 - Representation of the study area and the Sub-basins to be evaluated.

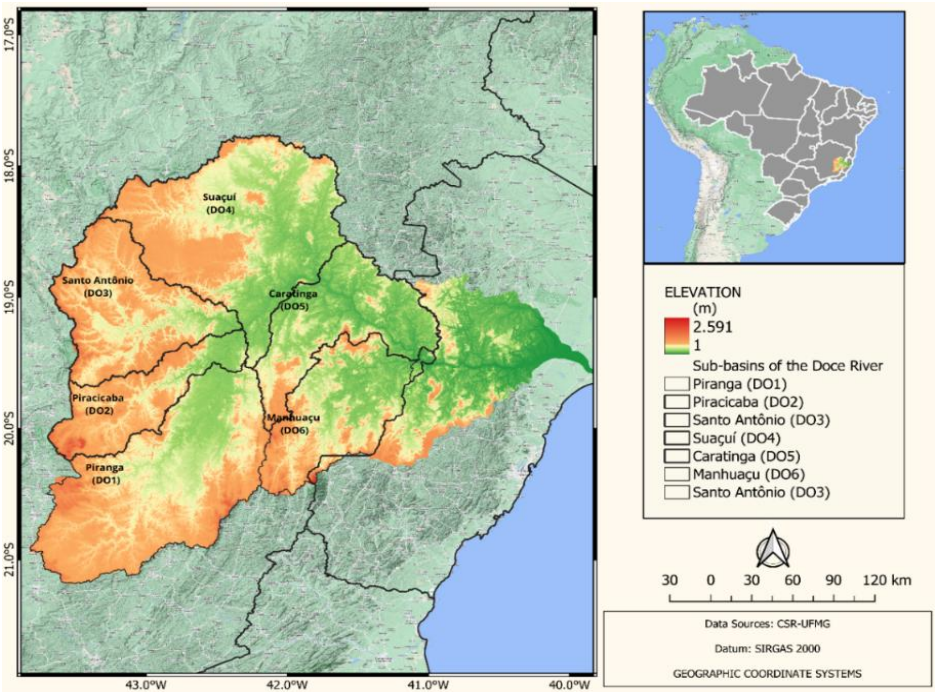

Source: elaborated by the author.

4.3.2 Spatial Segmentation and Classification of South Atlantic Convergence Zone (SACZ) Patterns

Our methodological approach begins with identifying the variation of SACZ over the basin, utilizing a time series from 1991 to 2020 (All data sources are provided in the supplementary material: https://github.com/NelsonMateus/SM.git). For this purpose, the spatial performance of the SACZ was segmented into three positions, referred to as patterns: North Pattern (NP), South Pattern (SP), and Central Pattern (CP), following the methodology adopted by António (2020). North Pattern (NP): Defined by the occurrence of negative Outgoing Longwave Radiation (OLR) anomalies located north of the climatological mean position of the SACZ. Central Pattern (CP): Serves as the baseline pattern, characterized by the climatological mean position of the SACZ with the most negative OLR anomalies centered around this mean. South Pattern (SP): Characterized by negative OLR anomalies situated south of the climatological mean position of the SACZ.

4.3.3 Selection of SACZ cases by default

To examine the extent to which different areas of the basin are affected by SACZ and how precipitation is distributed in the basin when the SACZ is in different geographical positions, we proceeded as follows:

a) The dates of occurrence of the SACZ were obtained from the study by António (2020) and from the bulletins of the National Institute for Space Research of Brazil (INPE), available at the link in Table 1 of the supplementary material (https://github.com/NelsonMateus/SM.git). The dates of occurrence of the SACZ were separated on a daily time scale, covering the summer season (from November to April). We used the software R (version 4.3.2,R (ANDREWS *et al.*, 2024)) and the Climate Data Operator (CDO) to build a filter capable of identifying each day of activity of the SACZ and the corresponding values of flow and precipitation for each pattern. All days with the occurrence of the SACZ were filtered, excluding the days without occurrence. We calculated the average of the selected values for each pattern: South Pattern (SP), North Pattern (NP) and Central Pattern (CP), obtaining the monthly average for the entire period evaluated.

b) After the separation dates of occurrence SACZ in the respective patterns, the average monthly precipitation of each pattern was elaborated. The purpose of this phase is to examine the extent to which the different areas of the basin are affected by SACZ and how the rain is distributed over the basin, when the SACZ is located in different geographical positions. Following, we evaluate the impact of each pattern on the monthly and annual flow of the six sub-basins of the Doce River.

4.3.4 Evaluation of extreme rainfall events and floods

We employed the percentile methodology to identify extreme precipitation events associated with flood events in the different positions of SACZ (CP, NP, SP). First, we calculated the 90th and 95th percentiles of the daily precipitation series for each of the six meteorological stations. We adopted the 95^{th} percentile to identify extreme precipitation events. Thus, the precipitation values corresponding to this percentile were considered as thresholds to define extreme events in each SACZ pattern. The number of extreme precipitation events

and flood events in the different SACZ pattern is presented in Table 3 of the supplementary material (https://github.com/NelsonMateus/SM.git). The percentile methodology is widely used to identify extreme events (BOMBARDI *et al.*, 2014; DERECZYNSKI *et al.*, 2009; FRAGA *et al.*, 2020; REBOITA; VEIGA, 2017).

After defining the extreme precipitation events for each SACZ pattern, as described above, we proceeded to separate all flood dates and alert quotas from the time series. For this purpose, we used the alert and flood quota data from the National Water Agency (ANA) in collaboration with the Geological Survey of Brazil (CPRM). We evaluated seven municipalities in the Doce River basin: Ponte Nova, Nova Era, Mário Carvalho, Belo Oriente, Vila Matias, and Governador Valadares. Each municipality has a quota level for the occurrence of floods, available on the CPRM website (see Table 1 of the supplementary material). Thus, we used the SACZ occurrence dates in the 95th percentile as a reference to filter the flood and flood warning events that occurred on those same dates. It is worth noting that the alert quota represents the river level that indicates a high possibility of flooding, while the flood quota represents the first damage observed in the municipality. The objective is to evaluate the number of cases of floods in SACZ events when it acts in different positions (CP, NP, SP).

4.3.5 Statistical analysis

The Modified Mann-Kendall test was employed to identify significant trends (increasing or decreasing) in precipitation and flow time series for each SACZ pattern. A significance level (α) of 0.05 was chosen, meaning we reject the null hypothesis (no trend) if the test statistic (Z) is greater than the critical value for a 5% significance level. Positive Z values indicate statistically significant upward trends, while negative Z values indicate statistically significant downward trends. For further details on the test statistic and critical values, refer to Yue; Wang, (2004). If a significant trend is identified, the linear trend component is removed from the time series to obtain a detrended (stationary) series. In MMK the trend part T_t of the new series X_t is linear then, trend part is removed to obtain the stationary series Y_t:

$$Y_t = X_t - T_t = X_t - B\ x\ T \quad (3)$$

The variance (S) an test statistic Z is calculated of the trend statistic S of autocorrelation series is obtained as follows:

$$z = \begin{cases} \frac{S-1}{\sqrt{V(S)}} & S > 0 \\ 0, & S = 0 \\ \frac{S-1}{\sqrt{V(s)}}, & S < 0 \end{cases} \quad (4)$$

Positive Z values indicate increasing trends, while negative Z shows decreasing trends. The trend test is done at a specific significance α level. In this study, the significance level α = 0.05, at the significance level of 5%, the null hypothesis of no trend is rejected. More details on the test in Yue & Wang, 2004.

4.3.6 Multiple Regression Model (MLR)

We employed multiple linear regression to assess the influence of rainfall on flow rates within each SACZ pattern (CP, NP, SP) across the Doce River sub-basins. This supervised learning technique identifies a linear relationship between a dependent variable (Y) and multiple independent variables (X) (MOORE *et al.*, 2007). In our case, the dependent variable (Y) is the monthly flow rate, and the independent variables (X) include monthly rainfall values for each SACZ pattern. This analysis aims to identify the SACZ pattern that has the strongest influence on flow rate variability in each sub-basin. The principle of linear regression is to model a quantitative dependent variable Y through a linear combination of p quantitative explanatory variables, X1, X2, ..., Xp. The deterministic model is written for observation i as follows:

$$y_i = \beta_0 + \sum_{j-1}^{p} \beta_j x_{ij} + \varepsilon_i \quad (5)$$

where yi is the observed value for the dependent variable for observation i, xij is the value assumed by variable j for observation i, and ε_i is the random error.

4.3.7 Principal Component Analysis (PCA)

To investigate the influence of SACZ on water quality in the Doce River basin, we meticulously collected and analyzed a comprehensive dataset. This dataset encompassed daily precipitation and flow data for each of the six sub-basins within the basin, along with water quality data for various indicators. We chose a six-day window for accumulated rainfall and average flow to correspond with the typical duration of SACZ events. The water quality indicators we selected included pH, total suspended solids, water temperature, turbidity, dissolved oxygen, conductivity, total chloride, nitrate, biochemical oxygen demand, total phosphorus, total nitrogen, and total coliforms. These classic indicators have been consistently monitored at least quarterly for over ten years, providing a robust dataset for analysis.

To unravel the complex interplay of factors influencing water quality variability, we employed a powerful statistical technique called Principal Component Analysis (PCA). PCA excels at identifying underlying patterns in large datasets by reducing them into a smaller number of components that explain most of the data's variance. We performed four sequential PCA analyses, each focusing on a specific dimension or scale of water quality variation.

a) Seasonal Contrasts: The initial PCA was performed on the entire dataset to identify seasonal contrasts between dry winters and wet summers. This analysis revealed the most significant water quality parameters that drive seasonal spatial variations, aligning with the SACZ's seasonal influence.

b) Sub-basin Differences: Subsequently, we focused on the months during which the SACZ occurs (October to April) and conducted a second PCA analysis to identify the differences between the Doce River sub-basins. This analysis highlighted the unique water quality characteristics of each sub-basin, providing insights into the spatial variability of water quality within the basin.

c) Spatial and Temporal Influences: To isolate the influence of the spatial component, we performed a third PCA after standardizing the data by the mean and standard deviation for each sub-basin. This analysis revealed how water quality varies across the months, providing insights into the temporal dynamics of water quality within each sub-basin.

d) SACZ Impact: Finally, we standardized the data using both spatial (sub-basin) and temporal (monthly) dimensions to isolate these respective influences. This last analysis aimed to identify how the SACZ specifically affects water quality. This multi-layered

statistical methodology highlights the complex interaction between climatic phenomena and river water quality, providing a unique understanding of environmental dynamics in the Doce River basin.

PCA reduces large sets of input variables into a reduced number of components. PCA can be used to indicate factors associated with water quality. At the seasonal level, the PCA obtains information on the most significant quality parameters of seasonal spatial variations, which is the time scale of the performance of the SACZ (OLSEN *et al.*, 2012). The PCA steps are shown below:

1. Normalize the X mxn data matrix to matrix Y = $(Y_1, \dots, Y_n)$

2. Calculation of the Z covariance matrix according to the following equation:

$$z = \frac{1}{m-1}\sum_{k=1}^{m}(Y_{ke\bar{u}}\bar{Y}_{eu})\,(Y_{ke\bar{u}} - \bar{Y}_{eu}) \qquad (6)$$

3. Calculate the eigenvalues and eigenvectors of the covariance matrix Z. Cumulative percentages of the eigenvalues indicate their contribution to the main components, and the eigenvectors present the loads. The eigenvectors are multiplied with the original matrix to obtain the scores of the main components.

4.4 Results

4.4. Evaluation of the spatial pattern of the SACZ in the rainfall regime

In our analysis, we examined the trends and durations of SACZ events over the years, considering all observed patterns in the event averages (Figure 7a, 7b). It was observed that the average duration of SACZ events during the time series (1991 to 2020) was approximately 6.2 days, a duration consistent with findings in previous (AMBRIZZI; FERRAZ, 2015; BRAGA *et al.*, 2022; DE OLIVEIRA VIEIRA *et al.*, 2013; PEZZI *et al.*, 2023). This finding solidifies the consistency of the observed duration of SACZ across different study periods. The maximum number of days with SACZ occurrence in a year varied between 6 and 70 days (Figure 7b), and this variability was attributed to the influence of large-scale atmospheric systems, such as Bolivia High, Cyclonic Vortices at high levels, and local weather conditions in the region (BRAGA *et al.*, 2022; PEZZI *et al.*, 2023).

These systems play a critical role in modulating the duration and intensity of SACZ events, contributing to the observed interannual variability. It is also noted that the years 2000 and 2012 stood out with prolonged durations of SACZ events, exceeding an average of 12 days (Figure 7a and 7b). Recent studies corroborate these observations, suggesting that large-scale anomalous events, possibly related to phenomena such as El Niño and the Pacific Decadal Oscillation, can prolong the duration of SACZ events (PEZZI et al., 2023). On the other hand, a decreasing trend in event duration was observed in the time series from 2013 to 2015. This decrease may be associated with changes in climatic variability and possible alterations in large-scale atmospheric circulation. Recent works discuss that climate change may be influencing the frequency and duration of the large-scale systems affecting SACZ, suggesting an urgent need for more studies to understand these trends and their implications (BRAGA *et al.*, 2022, 2024; PEZZI *et al.*, 2023).

Notably, the years 2000 and 2012 stood out with extended SACZ event durations, exceeding an average of 12 days (Figure 7a and 7b). Nevertheless, a decreasing trend in event duration was observed in the time series from 2013 to 2015. There was also a growing trend in the number of events, with peaks in 1999 and between 2004 and 2016, followed by a declining trend from 2017 to 2020. Recent studies, such as those by Da Fonseca Aguiar; Cataldi, 2021, affirm these trends and discuss the possible implications for regional hydrology and climate.

This upward trend suggests a higher prevalence of SACZ patterns in the basin, potentially leading to increased flood risks due to rising water levels in the basin (DA FONSECA AGUIAR; CATALDI, 2021; GUTJAHR; HEINEMANN, 2012; REBOITA; VEIGA, 2017).

Figure 7 - a) Duration of days of SACZ events, b) Number of events and trend of events

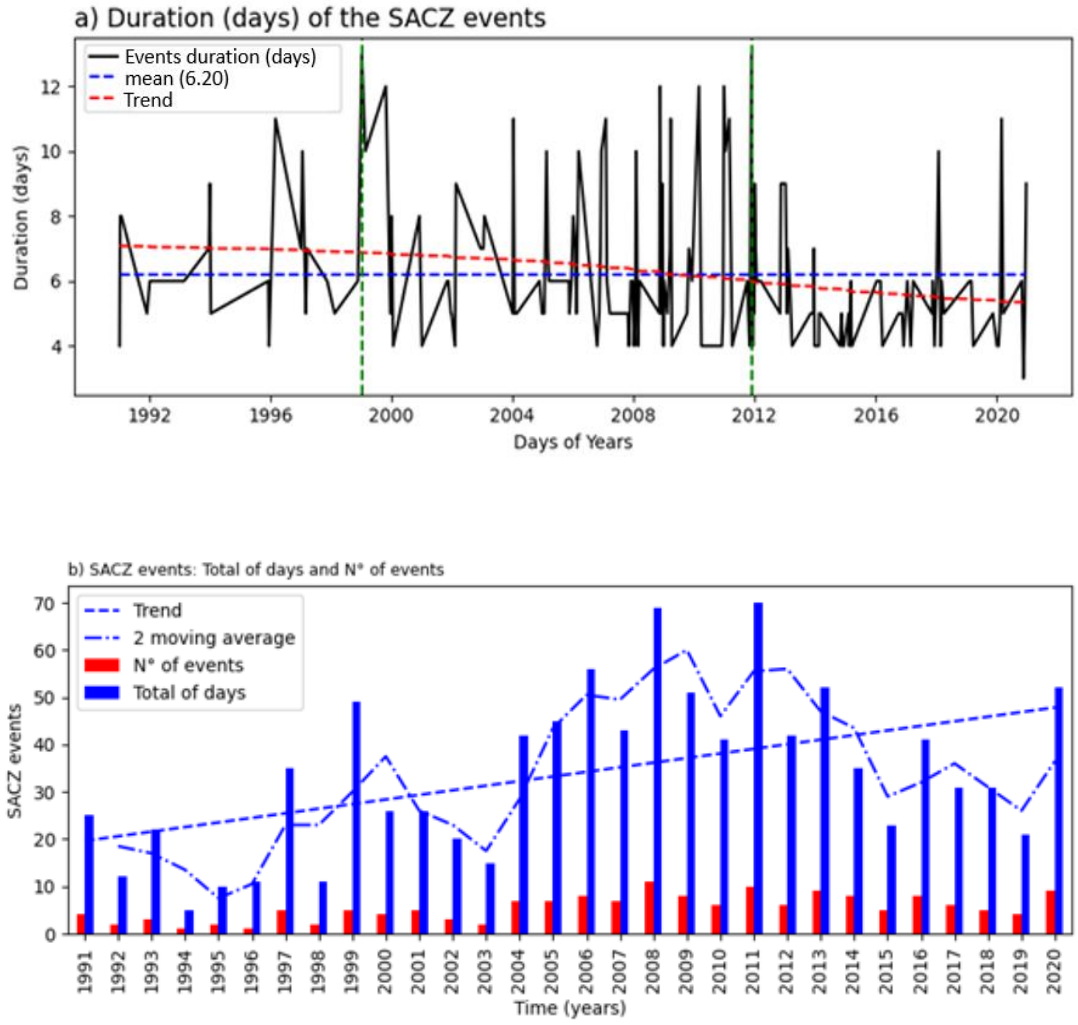

Source: elaborated by the author.

The spatial patterns SACZ are associated with different geographic regions, each impacting the Rio Doce basin differently. The North pattern (Figure 8) is characterized by higher accumulated rainfall in the northern and central areas of the basin, with an average of approximately 13 to 18.26 mm/day, in contrast to the southern sector with less than or equal to 9.4 mm/day. Recent studies, including Mayta *et al.*, 2020 and António et al., (2023), have illustrated similar spatial differentiation, highlighting the significance of precise regional climate assessments. Notably, the Suaçuí (DO4) and Santo António (DO3) sub-basins

experienced the highest levels of rainfall, averaging 18 mm/day with a monthly total of 547 mm. On the other hand, the Piranga and Piracicaba basins received lower rainfall in this pattern.

The observed rainfall concentration in the southern sub-basins (Suaçuí, Santo António, Piracicaba, and Piranga) under the Central Pattern (CP), with up to 14 mm/day, aligns with the findings of Silva et al. (2019) and Gomes et al. (2019), who highlighted the influence of local topography and land-use changes on precipitation distribution in these areas. The lower rainfall in the northern sub-basins (Suaçuí, Caratinga, and Manhuaçu) under CP, as low as 9 mm/day, could be attributed to the rain shadow effect caused by the Espinhaço mountain range, as suggested by Zilli; Carvalho (2021).

Similarly, the South Pattern (PS) reinforces this north-south rainfall gradient, with the Piracicaba, Piranga, and southern Santo António sub-basins receiving up to 14.90 mm/day, while the northern sub-basins experience less than 7 mm/day. This pattern is consistent with the findings by Escobar et al., (2022) and Zilli & Carvalho, 2021, who emphasized Synoptic patterns of SACZ enhancing convective activity and rainfall over the southern parts of southeastern Brazil during austral summer.

The North Position (NP), characterized by higher rainfall in the western and northern basin, is likely driven by the combined influence of the Bolivian High and Northeast trough, as documented by Barros et al. (2000) and Nogués-Paegle & Mo (1997). Recent work by Bombardi et al. (2023) has further elucidated the complex interactions between these systems and their modulation by the Madden-Julian Oscillation (MJO), leading to varying precipitation patterns across the basin. The uneven distribution of rainfall in the Doce River basin is intrinsically linked to the spatial variability of meteorological systems (DA SILVA *et al.*, 2019; GOMES *et al.*, 2019; ZILLI; CARVALHO, 2021). In the North Position (NP), the interaction of large-scale features like the Bolivian High and the Northeast trough plays a pivotal role (BARROS *et al.*, 2000; NOGUÉS-PAEGLE; MO, 1997). The work by Pezzi et al. (2023) has further elucidated how the Northeast trough, in conjunction with low-level moisture transport from the Amazon, fuels convective activity and concentrates rainfall in the western and northern parts of the basin. The CP and SP patterns, on the other hand, exhibit distinct atmospheric behaviors (Refer to Figures 1 and 2 in the supplementary material: https://github.com/NelsonMateus/SM.git). In CP, the SACZ becomes more pronounced, enhancing convective activity and promoting rainfall over the southern regions of the basin. This is consistent with the findings of António (2020), who highlighted the importance of SACZ-related moisture transport for precipitation in the central and southern parts of southeastern

Brazil. The SP pattern, although less frequent, is often associated with the southward displacement of SACZ, leading to increased rainfall in the southernmost region.

Figure 8 - Daily average precipitation for the patterns associated with SACZ (CP), (NP) and (SP).

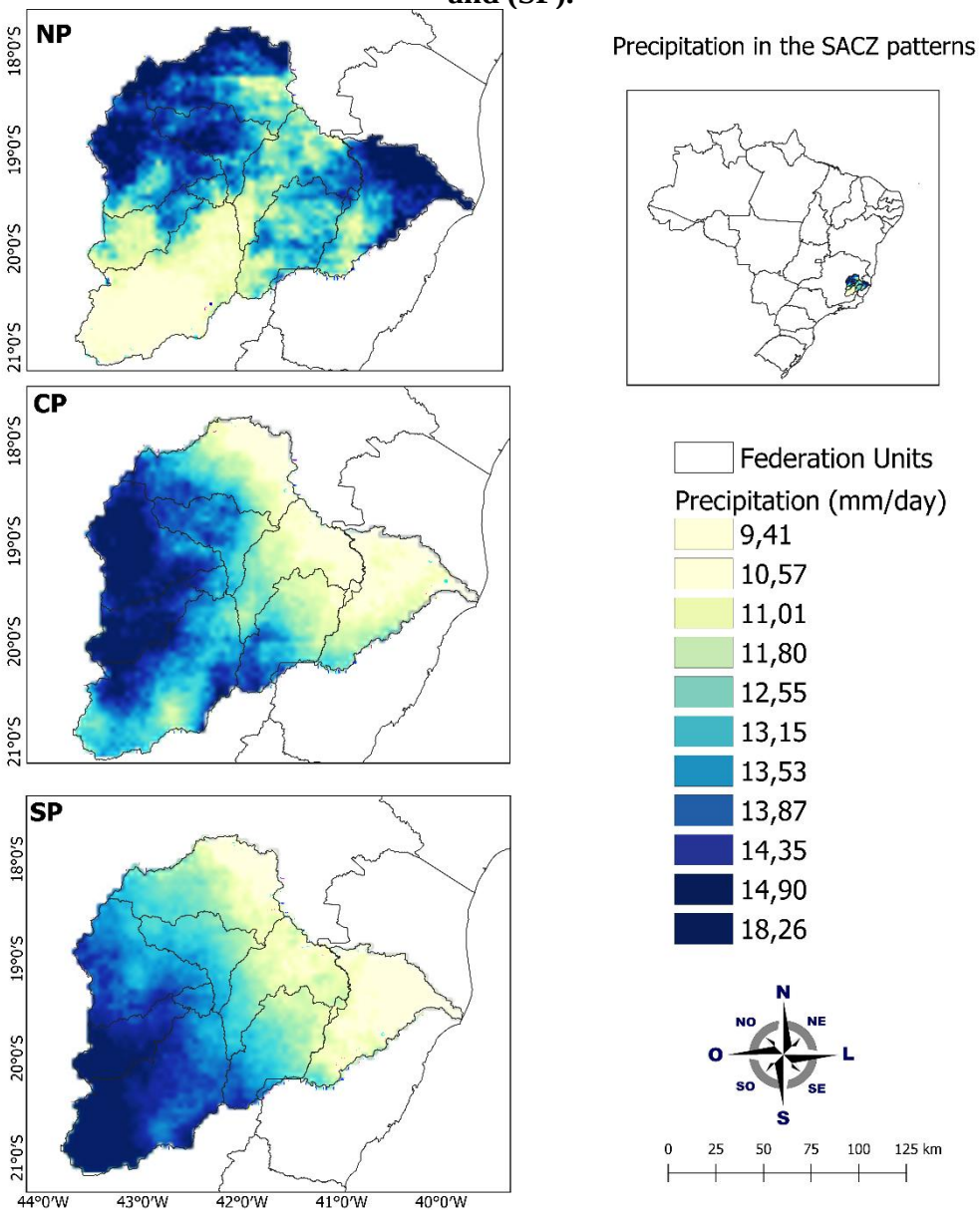

Source: elaborated by the author.

4.4.2 Monthly evaluation of SAZC patterns in precipitation and flow

In the Piranga, Piracicaba, Suaçuí, and Caratinga sub-basins, the highest monthly-accumulated rainfall is primarily associated with the NP and CP patterns, ranging from 10.5 to 24.5 mm/day, equivalent to approximately 304 to 730 mm/month. This region typically experiences the highest rainfall from December to February, which are the months with the highest accumulated rainfall (Figure 9) (COSTA, F. *et al.*, 2022), with March, April, and November being the drier months. In the Manhuaçu and Suaçuí sub-basins, significant accumulated rainfall is also observed in the SP, resulting in monthly rainfall amounts that usually exceed the climatological monthly average (represented by the cyan dashed line in Figure 9).

The CP demonstrates consistently above-average precipitation across all months in the six sub-basins, peaking in December (up to 16 mm/day) and January (up to 24 mm/day) (Figure 9). Notably, the uninterrupted action of the South Atlantic Convergence Zone (SACZ) for an average of 6.2 days can amplify these accumulations to approximately 43 to 155 mm/day. Such elevated rainfall totals significantly exacerbate water resource uncertainty and increase the risk of flood events, as highlighted by Marengo, 2004; Marengo *et al.*, 1998 and Zilli & Carvalho (2021).

The consequences of heightened rainfall during SACZ events are particularly evident in Minas Gerais, where landslides and flooding are prevalent. Aguiar (2018) and da Fonseca Aguiar & Cataldi (2021) reported that 58% of rainy days associated with SACZ coincide with landslides, while 49% trigger flooding, and 47% and 46% result in floods and overflow. These findings underscore the critical need for proactive disaster risk reduction strategies in regions prone to SACZ influence.

The NP and CP patterns dominate the rainfall regime across the sub-basins, coinciding with high flow values ranging from 19 to 890 m^3/s, predominantly between December and February (Figure 9). This period of elevated flows aligns with the increased precipitation observed under these patterns, particularly during the austral summer months. Importantly, from January to April, both NP and CP consistently generate flow rates exceeding the normal climatological across all sub-basins (Figure 10).

This finding strongly reinforces the association of these patterns with heightened flood risk and the occurrence of extreme hydrological events. In stark contrast, the SP demonstrates significantly lower accumulated flow values (Figure 10). This suggests that the SP, despite

potentially generating localized heavy rainfall events, does not contribute as substantially to the overall water balance and flood risk in the Doce River basin as the NP and CP patterns.

The heightened rainfall and subsequent peak flow rates associated with the North (NP) and Central (CP) patterns significantly elevate the likelihood of flooding in the Doce River basin. This finding underscores the critical role of these patterns in shaping the region's hydrological regime and flood risk. Notably, throughout the entire time series, there were no recorded instances of SACZ operating in either the NP or SP patterns during April across all analyzed sub-basins. This absence of SACZ activity in these patterns during April warrants further investigation to understand the underlying mechanisms and potential implications for water resource management.

Furthermore, the Suaçuí sub-basin exhibits a striking contrast in flow behavior under different patterns. The NP pattern generates exceptionally high flow values, reaching up to 800 m^3/s, while the accumulated flows under CP and SP remain below 200 m^3/s (Figure 10). This disparity highlights the unique vulnerability of the Suaçuí sub-basin to flooding under the NP pattern, emphasizing the need for tailored flood mitigation strategies in this specific area.

Figure 9 - Monthly precipitation on SACZ days on the six sub-basins of the Doce river. NP-North Pattern, CP- Center Pattern, SP-South Pattern (1991 to 2020).

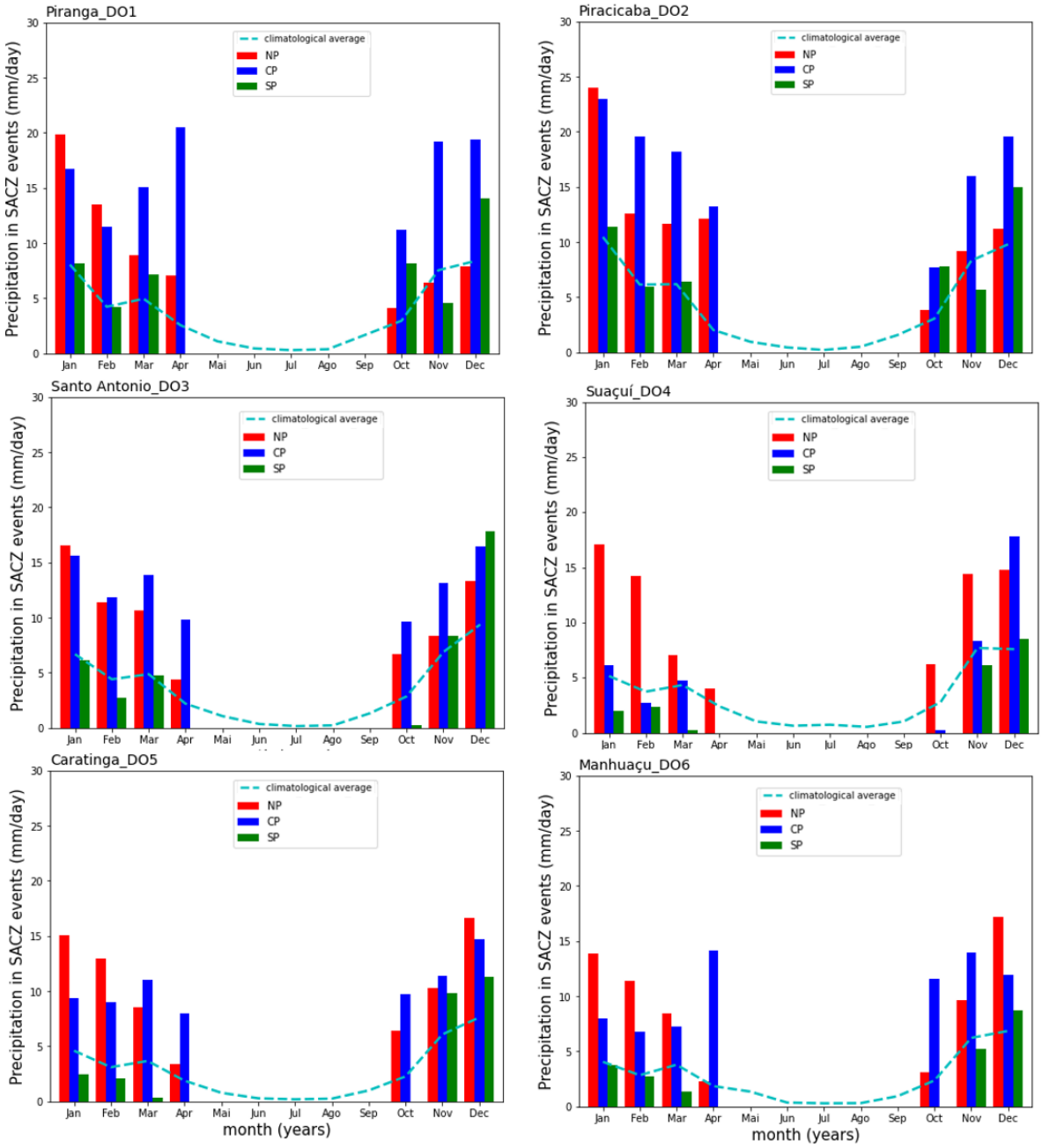

Source: elaborated by the author.

Figure 10 - Monthly Variation of rainfall and Flow rates in SACZ events, for the six sub-basins of the Doce River. NP-North Pattern, CP- Center Pattern, SP-South Pattern.

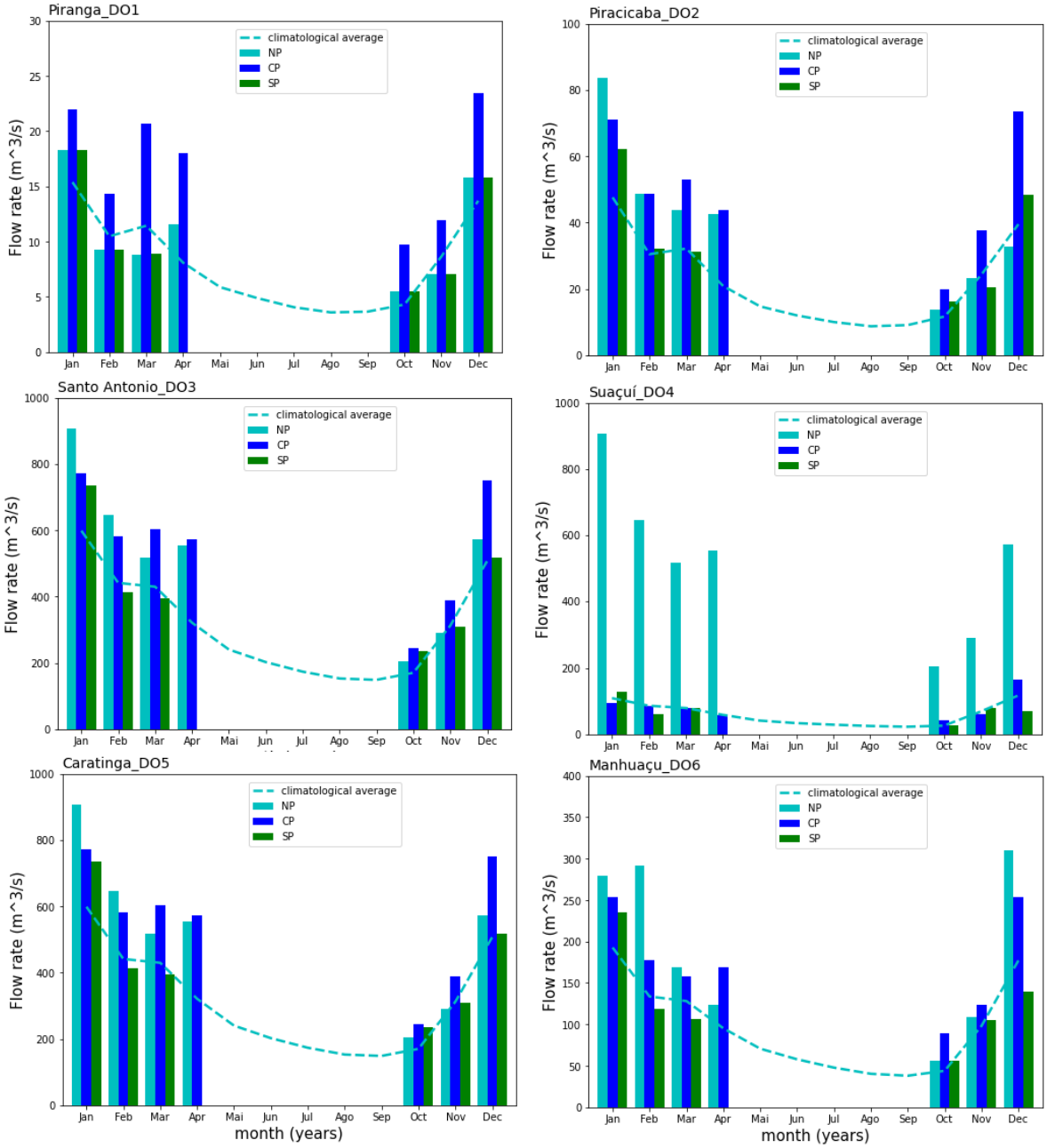

Source: elaborated by the author.

4.4.3 Trend analysis and statistics

The analysis utilizing the Modified Mann-Kendall Test (MMK) revealed a statistically significant ($p < 0.05$) decreasing trend in both precipitation and flow across all sub-basins (Table 3). This decline was particularly pronounced in the Northern and Central regions, aligning with recent studies that have documented a downward trend in precipitation and rising temperatures across Central and Northern Brazil (BARBOSA *et al.*, 2021; COSTA, F. *et al.*, 2022). For instance, Barbosa et al., (2021) attributed the declining precipitation in the Central region to shifts in atmospheric circulation patterns, while Costa et al., (2022) linked the Northern trend to deforestation and land use changes.

The observation of these decreasing trends has significant implications for water resource management, especially in the affected sub-basins. This analysis provides valuable insights for future decision-making, suggesting the need for adaptation strategies to address changes in hydrological conditions (COELHO, 2006; LIMA, 2016a). Furthermore, our findings echo the broader patterns observed in climate projections for the region (SHEKHAR *et al.*, 2020). These projections suggest that continued warming and altered atmospheric patterns will likely exacerbate the decreasing precipitation trends. The observed decrease in flow across all sub-basins underscores the direct hydrological consequences of these climatic shifts. Thus, while the influence of precipitation on flow variability is well-established (BARBOSA *et al.*, 2021; COSTA, F. *et al.*, 2022; KABIR *et al.*, 2024; MCCABE; WOLOCK, 2011), our analysis goes further by examining how precipitation within specific patterns impacts flow in each sub-basin.

Our multiple linear regression (MLR) model reveals that over 86% of flow variability across the six sub-basins can be explained by precipitation within the three SACZ patterns. Importantly, this analysis focuses on the relationship between monthly flow and monthly precipitation within each pattern. The statistical significance ($p < 0.05$) of the F statistic in our model confirms that these precipitation variables substantially improve our ability to predict flow variability compared to a simple average.

This finding reaffirms the substantial influence of precipitation within the SACZ patterns on the observed flow variability. Notably, our analysis reveals that precipitation within the NP pattern appears to be the most influential driver of flow variability across most sub-basins. This is evident in the MLR results (Table 3), where the NP pattern consistently demonstrates the strongest association with flow, except in the Santo Antônio sub-basin. In

Santo Antônio, both the NP and South Pacific (SP) patterns play significant roles in explaining flow variability.

Table 3 - Tau statistic values from the Mann−Kendall (MK) test values in the patterns of the SACZ. The highlighted in green lines indicate a significance level of 0.05. Results of the regression model, North Standard (NP), Center (CP), South (SP).

Basin	PN_Rainfall	PC_Rainfall	PS_Rainfall	R^2
Piranga	-0,019	-0,066	-0,049	0,88
Piracicaba	0,025	-0,058	0,006	0,91
Santo Antonio	0,011	-0,187	-0,049	0,86
Suaçuí	-0,04	-0,09	-0,02	0,87
Caratinga	-0,216	-0,263	0,001	0,97
Manhuaçu	-0,056	-0,141	-0,059	0,87
	PN_Flow	PS_Flow	PC_Flow	
Piranga	-0,233	-0,278	-0,114	
Piracicaba	-0,149	-0,190	-0,107	
Santo Antonio	0,001	-0,755	0,001	
Suaçuí	-0,196	-0,310	-0,273	
Caratinga	-0,155	-0,755	-0,241	
Manhuaçu	-0,111	-0,278	-0,114	

Source: elaborated by the author.

4.4.4 Extreme events and floods

The 95th percentile thresholds for daily rainfall vary across the SACZ patterns: 18.4 to 33.73 mm for the SP, 22.81 to 49.65 mm for the CP, and 32.57 to 56.30 mm/day for the NP Pattern. These thresholds, which define extreme rainfall events (Figure 11), represent the top 5% of daily rainfall values observed during each respective pattern.

Analysis of extreme events (Table V in SM) reveals distinct patterns across the sub-basins. The Piracicaba and Santo António sub-basins experienced a notably higher frequency of extreme precipitation events (168 and 127 events, respectively) primarily during the occurrence of the NP and CP patterns. Conversely, the Caratinga (58 events) and Manhuaçu

(88 events) sub-basins exhibited fewer extreme events, likely due to the infrequent influence of the NP and CP patterns in those areas throughout the time series (Figure 11).

These episodes of extreme rainfall are often associated with river overflow within the Doce River basin, leading to floods and damage to properties (NASCIMENTO, 2012; SILVA *et al.*, 2020). Therefore, considering the earlier average daily duration of SACZ episodes (6.2 days), extreme events linked to SACZ, occurring over this duration, can result in accumulated precipitation ranging from 114.08 to 394.32 mm.

While extreme rainfall events are a key factor, not all of them result in flooding. To gain a deeper understanding of the relationship between extreme rainfall and flooding during SACZ activity, we analyzed 54 flood events occurring during the northern SACZ position (NP), 13 during the central position (CP), and 33 during the southern position (SP).

Our analysis reveals that Governador Valadares, Ponte Nova, and Tumuritinga – municipalities previously identified as vulnerable to extreme hydrological events (SILVA *et al.*, 2020) were the most frequently impacted by floods during SACZ events, especially when was positioned further north. The average flood level during these events reached 432.98 cm, with a maximum of 552 cm (Figure 3 in Supplementary Material).

The NP pattern emerged as the most significant contributor to flood events, accounting for 28.63% of events with property damage and 23.91% without. The CP pattern followed, responsible for 6.32% of events with property damage and 11% without. The SP pattern contributed to approximately 6% of flood events (Figure 3 in SM). We also examined instances where flood warnings were issued but no damage occurred. Here, the NP pattern again dominated with 48 cases, followed by the CP pattern with 27 cases, and the SP pattern with 15 cases (Figure 11).

Figure 11 - Summary of the effects of SACZ patterns on flooding. (I) Position of weather systems in the definition of each standard. (II) Precipitation limit to evaluate extreme events through the 95% percentile. (III) Cases of flooding.

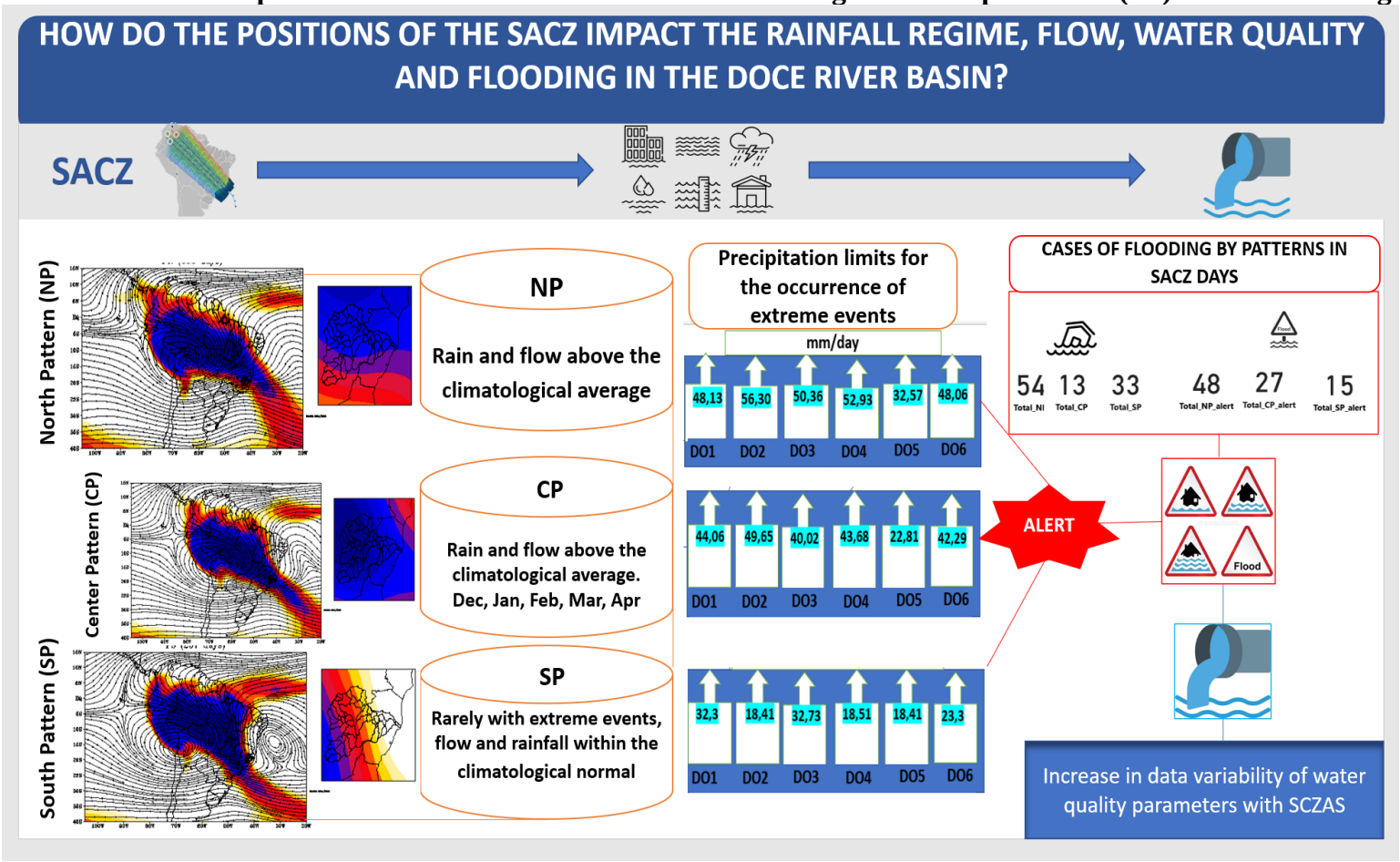

Source: elaborated by the author.

4.4.5 Impact of SACZ on water quality

Considering seasonal variation without filtering for SACZ events, our Principal Component Analysis (PCA) reveals that 45.30% of the variation in water quality parameters is explained by two primary components. The fact that neither set of principal components explains more than 50% of the variation suggests that other factors not considered in this analysis may be influencing water quality. Seasonal analysis indicates that the majority of variation occurs during the rainy season (summer) across all sub-basins. Monthly assessments further emphasize elevated levels of total solids and turbidity during months when SACZ is active.

Seasonality strongly influences water quality in the Doce River. The rainy season exhibits increased turbidity and total suspended solids, likely due to heightened erosion (BOURGUIGNON *et al.*, 2021; DA CUNHA RICHARD *et al.*, 2020; OLSEN *et al.*, 2012; VANELI *et al.*, 2022). Additionally, total coliforms, total phosphorus, and water temperature rise during this period, while dissolved oxygen increases during the dry winter months (Figure 7a).

Focusing on the months when SACZ is active, a second PCA highlights a stark contrast between the Caratinga sub-basin (DO5), with poorer water quality (higher conductivity, total chloride, ammonia, and biochemical oxygen demand), and the Santo Antônio sub-basin (DO3), which exhibits lower values for these variables and higher dissolved oxygen. The other four sub-basins fall between these extremes (Figures 12a-d). This disparity may be attributed to the impact of the dam rupture, which increased erosion and transport of contaminants during heavy rainfall, a phenomenon less pronounced in the Santo Antônio basin (DE MAGALHÃES *et al.*, 2022; OLIVEIRA; QUARESMA, 2017; ZORZAL-
ALMEIDA; DE OLIVEIRA FERNANDES, 2021).

Standardizing the data within each sub-basin and distinguishing points by month (Figure 12a) reveals that December and March exhibit the highest levels of total phosphorus, total coliforms, total suspended solids, and turbidity. These months coincide with peak SACZ rainfall and flow. Finally, a fourth PCA, controlling for sub-basin and month effects, demonstrates that SACZ presence is associated with elevated levels of turbidity, total suspended solids, total phosphorus, total coliforms, ammonia nitrogen, and biochemical oxygen demand.

Description of the figure: a) Graphical representation of the first two axes obtained from the first Principal Component Analysis (PCA) with all the available data. b) First two axes obtained from the second Principal Component Analysis (PCA) only with months of SACZ occurrence. C) First two axes obtained from the third Principal Component Analysis (PCA) only with months of SACZ occurrence and after applying standardization by sub-basin. d) First two axes obtained from the fourth Principal Component Analysis (PCA) only with months of SACZ occurrence and after standardization by sub-basin and by month of the year. The percentage of explanation of the total variance of each axis is specified in the title of the respective axis. Each point represents a sample from a site in a given campaign. The colors specify the dry and rainy seasons. The ellipses delimit the regions where approximately 68% of the group's values are concentrated (equivalent to 1 standard deviation of the bivariate normal distribution).

Figure 12 - Principal Component Analysis (PCA).

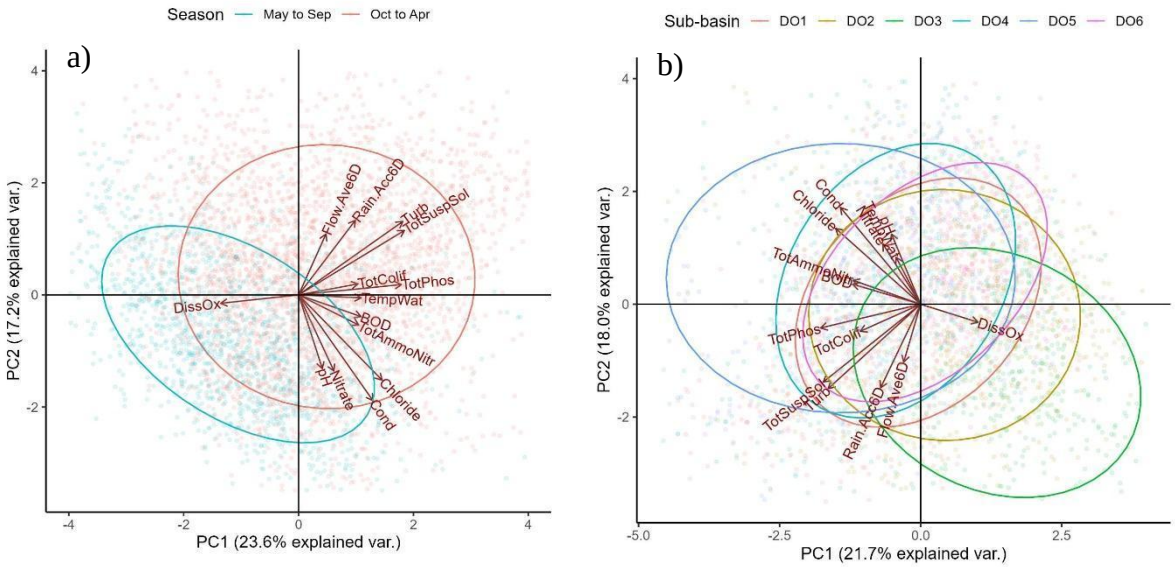

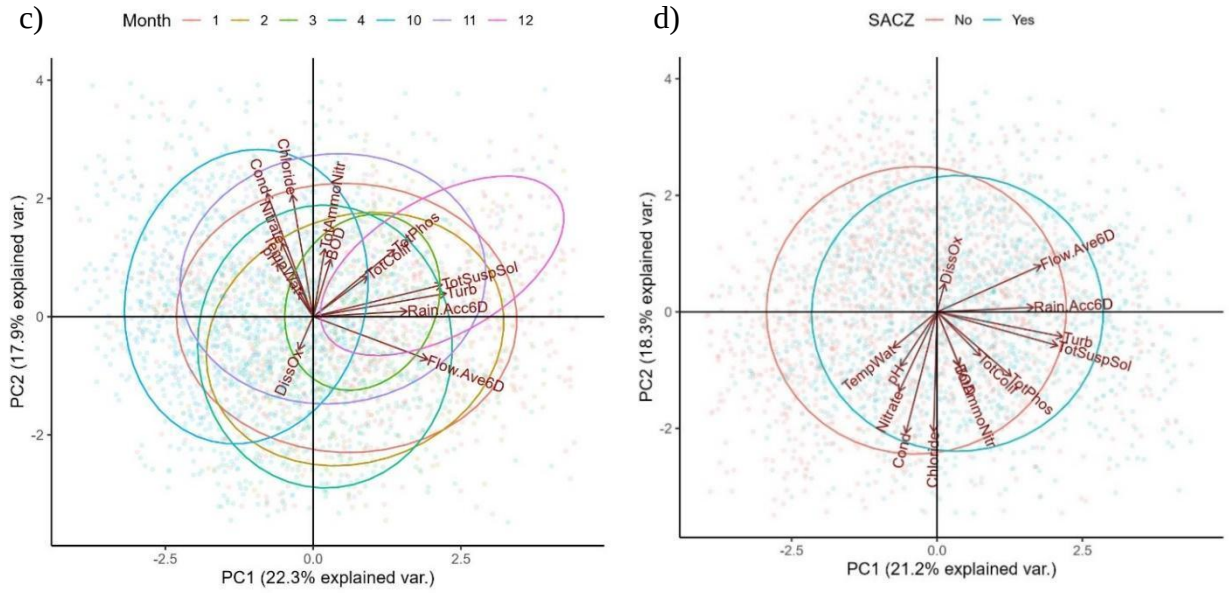

Source: elaborated by the author.

4.5 Final Considerations and Conclusion

This study reveals that the relationship between extreme weather events, floods, and flood warnings is complex and varies depending on the position of the South Atlantic Convergence Zone (SACZ) in the Doce river basin. To mitigate the impacts of flood, we established precipitation thresholds for extreme rainfall events: 43 mm for the northern (NP) and central (CP) positions, and 23 mm/day for the southern (SP) position. These thresholds are valuable information that can be utilized by weather centers to issue warnings of potential flooding in sub-basins.

Moreover, we identified that floods are more prevalent when the SACZ is in the northern position (NP), with 54 recorded cases, followed by 13 cases in the central position (CP) and 33 cases in the southern position (SP). The northern position (NP) of the SACZ is associated with the highest number of flood cases in the region, especially in the city of Governador Valadares. The central position (CP) also significantly contributes to flood cases, notably affecting the city of Ponte Nova.

With the identification of precipitation thresholds, we captured the positions of the main systems that define the SACZ patterns. This information is incomplete without knowing when each pattern occurs, as the SACZ patterns are defined by the meteorological systems that

compose them. The northern position (NP) occurs when the Bolivian High (BH) extends zonally up to 40°W, and the Northeast trough (CN) extends from 30° to 20°W. The central position (CP) occurs when the BH ranges from 80° to 60°W, and CN from 30° to 20°W. In the southern position (SP), the zonal extension of the BH ranges from 90° to 60°W, and the High-Level Cyclonic Vortex (HLCV) can extend up to 30°W, with characteristics predominantly observed at high altitudes (300hPa). At lower altitudes, there is an anomalous cyclone located between 20°-40°S in NP, 30°-35°S and 15°-20°S in CP, and 25°-30°W in SP. These findings offer valuable insights for meteorological forecasting.

Temporal analysis revealed that, on average, an SACZ event lasts 6.2 days, with annual occurrences varying from 6 to 70 days. We observed an increasing trend in SACZ events during the 1990s, peaking in 1999, and another period of higher activity between 2004 and 2016, followed by a decreasing trend from 2017 to 2020. From 2004 to 2020, the number of events per year increased from 5 to 11, in contrast to the decade from 1991 to 2003, when there were fewer than 6 events per year. The northern and central positions of the SACZ consistently experienced higher levels of precipitation (>=18 mm/day) in all sub-basins.

Our monthly analysis of precipitation and flow patterns identified the NP and CP positions as the most influential, with accumulations exceeding 18 mm/day for precipitation and flow ranging from 80 to 800 m^3/s. However, in April, the SP position was notably absent for both flow and precipitation, possibly due to its infrequent occurrence during this month. Using Multiple Linear Regression (MLR), we determined that all SACZ patterns significantly contribute to flow in all sub-basins, explaining more than 86% of the flow variability on SACZ days.

The analysis of water quality in the Doce River highlights seasonal influence, especially during the rainy season and events such as the SACZ. The monthly analysis highlights December and March, associated with higher values. The last PCA, by extracting the effects of both sub-basin and month, shows that the presence of SACZ is related to peaks, mainly in turbidity and total suspended solids, indicating the complexity in the dynamics of water quality in the Doce River. These findings have important implications for managing and preserving this crucial resource.

4.6 Future Research Proposals

Acknowledging the limitations of our study, we propose the following directions for future research: Influence of Climate Change on SACZ: Investigate how climate change affects the dynamics and frequency of SACZ events, using long-term climate models to project future changes and their implications for precipitation, flooding, flash floods, droughts, and other meteorological and climatic extremes in the Doce river basin. Modeling Flow and SACZ Positions: Develop hydrological models that correlate SACZ positions with flow cases in the Doce River sub-basins, using simulations based on historical data and climate forecasts. Temporal and Spatial Analysis of SACZ: Expand temporal analysis to include long-term data and utilize spatial analysis techniques to understand SACZ displacement patterns and regional impacts, exploring interannual and decadal variability. Integration of Satellite Data and Remote Sensing: Use satellite data and remote sensing techniques to monitor and model SACZ in real-time, aiding in the creation of early warning systems and rapid response plans.

5 CHAPTER 5: MODELING LAND USE AND COVER CHANGES: ASSOCIATIONS WITH EXTREME CLIMATE EVENTS IN CLIMATE CHANGE S2CENARIOS FOR THE DOCE RIVER BASIN.

5.1 Abstract

The Doce River Basin (DRB), located in southeastern Brazil, is crucial for biodiversity, water resources, and agriculture but faces growing environmental challenges due to climate change and land-use transformations. This study employs future land-use projections recommended by CMIP6 (Land-Use Harmonization 2, LUH2) within a land use and land cover model developed on the Dinamica EGO platform, aiming to assess how the frequency and intensity of extreme weather events in DRB impacts areas with major land-use changes. The model incorporates spatial factors such as slope, elevation, vegetation, and proximity to urban areas, roads, and conservation units. Climate projections were conducted using the regional models Eta-CanESM2 and Eta-MIROC5 were used under the RCP4.5 and RCP8.5 emission scenarios. The results indicate that, under the RCP4.5 scenario, native forest is expected to occupy 28.76% of the basin's area by 2030, with a projected reduction of -0.21% to -0.52% by 2080. Conversely, agricultural areas are expected to increase by 0.31% to 0.78%. In the RCP8.5 scenario, a reduction of -4.88% in native forest and an increase of 6.04% in agricultural areas are projected. For future climate conditions, the northwestern, southern, and southwestern areas of the basin were identified as having a high probability of land-use conversion, primarily due to the reduction of native forest, making them more susceptible to extreme climate events. These regions will experience an increase of 2°C to 3°C in mean temperature (TG) and extreme temperatures (TG90p). There will also be an increase in the number of dry days (CDD > 50 days), a higher frequency of intense rainfall (RX1day and RX5day), a reduction in total precipitation (PRCPTOT), and a rise in mean temperatures. Additionally, there will be a significant increase in cold days.

[2]**Article submitted to the journal for peer review**: Nelson Pedro António Mateus, Ana Paula M A Cunha, Ursula Ruchkys, Argemiro Filho, Anacleto Diogo, Ricardo Amorim.

GRAPHICAL ABSTRACT

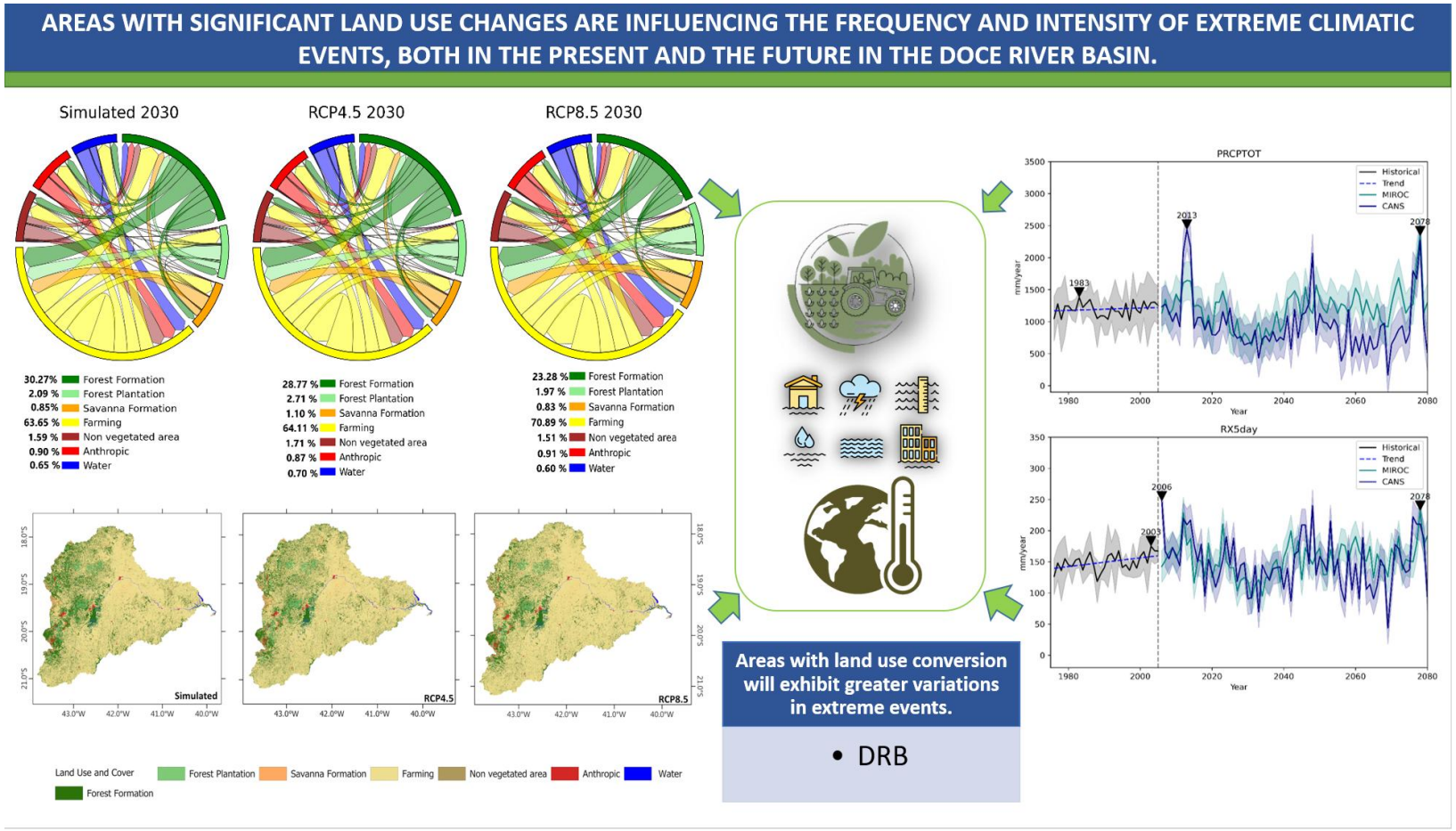

Source: elaborated by the author.

5.2 Introduction

Extreme weather events are widely recognized as one of the main environmental threats of the 21st century. They cause devastating disasters that impact ecosystems, economies, and communities globally. These events pose significant challenges to water resource management, which increasingly faces uncertainties and risks associated with climate change and land-use transformations, particularly in vulnerable watersheds (CAMPOS *et al.*, 2024; JIN *et al.*, 2024; MARENGO, 2004; NAQI *et al.*, 2021).

The Doce River Basin (DRB), located in the southeastern region of Brazil, faces significant environmental challenges due to climate change and land-use transformation (UICN, 2022). The DRB is crucial for Minas Gerais and Espírito Santo states, covering approximately 86,715 km² and serving about 3.5 million inhabitants across 228 municipalities (IUCN, 2022). In addition to supplying essential water resources for human consumption, agriculture, and industry, the basin boasts rich biodiversity, with 98% of its area within the Atlantic Forest biome, one of the world's most threatened.

However, the DRB has a significant history of disasters related to intense rainfall, highlighting its susceptibility to extreme climatic events. Since 1979, notable episodes include the major flood of that year, which left nearly 50.000 people homeless, affected approximately 4.400 residences, and resulted in 74 fatalities. In the summer of 1997, another large-scale flood impacted over 57.000 people, damaging 7.000 residences and causing two deaths. More recently, in the summer of 2013-2014, historic floods affected more than 54.000 people, reinforcing the need for effective mitigation and adaptation strategies (CEMADEN, 2018).

Beyond climate impacts, land-use transformations have exacerbated the basin's vulnerability. In the context of the DRB, studies such as Ferreira (2019) have identified a reduction in rainfall season on wet days and an increase in dry days, particularly in the southern and northern portions of the basin. Camargo et al., (2014) observed a 63% increase in peak discharge during extreme rainfall events in the Piranga sub-basin, while urban areas recorded a reduction in runoff depth and peak discharge by 7% and 11%, respectively. Cruz et al., (2015) analyzed the impact of floods in the middle river Doce, highlighting patterns and recurrences, particularly in long-term floods associated with extreme precipitation events linked to the South Atlantic Convergence Zone (SACZ). Additionally, drought events have increased in frequency,

duration, and intensity over the years in the DRB (Lima, 2016). Lima (2019) identified 2014/2015 as the most severe drought year, affecting the entire basin region.

The interaction between climate change and land-use changes is especially relevant t to the DRB. According to a report by UICN (2022), which used a regional climate model for each economic subregion of the basin, the results indicated a temperature increase of between 3°C and 3.6°C in the pessimistic scenario and between 2°C and 2.5°C in the more optimistic scenario. The analysis identified that the western and southern parts of the basin would be the most affected by the temperature increase. Regarding precipitation, the study indicated a reduction in rainfall in some parts of the western sector, both in the dry and rainy seasons. Land use and land cover (LULC) changes were associated with these variations in atmospheric variables (IUCN, 2020).

In the context of land use and change, significant changes in peak discharge were also observed, with projections of surpluses up to 2041, especially in the eastern region of the basin (COSTA *et al.*, 2022). The river flow velocity and precipitation patterns in the basin are affecting changes in hydrological characteristics, influenced by processes such as erosion, weathering, and socioeconomic factors. Intense rainfall events significantly alter runoff velocity in the DRB (COSTA *et al.*, 2022; LIMA; CUPOLILLO, 2018; NEVES, 2022; OLIVEIRA; QUARESMA, 2017).

The DRB has garnered significant attention in recent years, especially after the 2015 environmental disaster. The collapse of the Fundão tailing dam (located near Mariana, Minas Gerais, Brazil) resulted in one of the largest environmental disasters in Brazil's history. The dam collapse polluted more than 660 km of waterways and devastated 1.469 hectares of land, causing numerous severe environmental and socioeconomic impacts (CARMO *et al.*, 2017; IBAMA, 2023).

Recent studies suggest that, although some areas of the basin are beginning to recover their natural forests (FRAGA *et al.*, 2020; SALOMÃO *et al.*, 2020; SONDERMANN *et al.*, 2022), there is concerning evidence that rainfall has become more concentrated in some areas of the basin, even with a reduction in total annual precipitation (CAMPOS *et al.*, 2024; CUPOLILLO *et al.*, 2008; LIMA; CUPOLILLO, 2018). In other words, extreme precipitation events are becoming more frequent and intense in specific regions, raising questions about whether these areas overlap with critical land-use and land-cover zones (FERREIRA, 2019).

Projections indicate that by 2050, the average annual precipitation in the Doce River Basin (DRB) could decrease by more than 300 mm (a significant reduction considering the

current average annual precipitation, between 800 mm and 1.500 mm), while the average annual temperature may rise by up to 2°C, considering the RCP 4.5 and RCP 8.5(CAMPOS *et al.*, 2024). These results show a difference of at least 1°C compared to the 2020 IUCIN report, possibly due to differences in the periods analyzed between the studies. The land use and land cover analysis for 2050 shows that agriculture and livestock will account for 68.7% of the DRB area, while forests will occupy only 26.5%. However, if legal reserve areas are fully respected, native vegetation could reach 31.7%, reducing the pressure on agricultural and livestock activities to 63.8% of the basin (CAMPOS *et al.*, 2024).

These projections were developed considering the hypothetical inclusion of legal reserve areas as a conservative scenario in the land-use model. However, this approach does not assess the impact of land use under different climate scenarios, nor does it incorporate the guidelines established in the Intergovernmental Panel on Climate Change (IPCC) reports. Additionally, the inclusion of legal reserve areas does not account for the Integrated Assessment Models (IAMs) approach proposed by the IPCC. This research represents an advancement over previous studies as it integrates future land-use projections recommended by CMIP6 (LUH2) and incorporates legal reserve areas into the DRB model. The integration of IAMs enables a more comprehensive, interdisciplinary, and realistic analysis, providing a better understanding of the interactions between land use, climate change, and extreme events.

Integrated Assessment Models (IAMs) are a class of models that combine multiple disciplines, such as energy, economics, atmospheric chemistry, climate, and ecology, allowing for the construction of representative scenarios (CALVIN *et al.*, 2017; FRICKO *et al.*, 2017; FUJIMORI *et al.*, 2017).

In this context, this study aims to understand how land use and land cover changes are associated with the frequency and intensity of extreme weather events in DRB. To address this issue, we developed a land use simulation model using the Dinamica EGO platform, incorporating climate projections based on the RCP 4.5 and RCP 8.5 scenarios (which will be explained in detail in the following sections). This methodology enables the identification of future trends in extreme events and their relationships with land-use changes, contributing to a deeper understanding of the environmental challenges and the sustainable management of the basin.

This study addresses critical gaps in the literature by analyzing the interaction between climate change and land use changes, focusing on the context of the DRB. This integrated approach directly impacts the development of targeted mitigation and adaptation policies. By

investigating these relationships, we aim to provide well-founded evidence and scientific tools that strengthen community resilience and ensure sustainable water resource management in this vulnerable region.

5.3 Methodology

5.3.1 Study Area

The DRB extends between latitudes 17°45' and 21°15' S and longitudes 39°30' and 43°45' W (Figure 13), located in the southeastern region of Brazil, encompassing the Southeast Atlantic hydrographic region. With a drainage area of approximately 86,715 km², the majority lies within the state of Minas Gerais, accounting for about 86%, while 14% belongs to the state of Espírito Santo. The basin encompasses a total of 230 municipalities and is home to an urban population of approximately 2.341,206 inhabitants and 833,437 rural inhabitants (PIRH, 2010). The economic activity in the basin is highly diversified and plays a crucial role in water resource management. Among the key economic activities in the basin are mining, agriculture, forestry, and the food industry (PIRH, 2010). Water use is an important aspect of the DRB, with around 38.2% allocated for multiple uses, 19.3% for industrial purposes, 3.3% for mining activities, 30.1% for public water supply, and 1.6% for other uses.

Figure 13 - Representation of the study area.

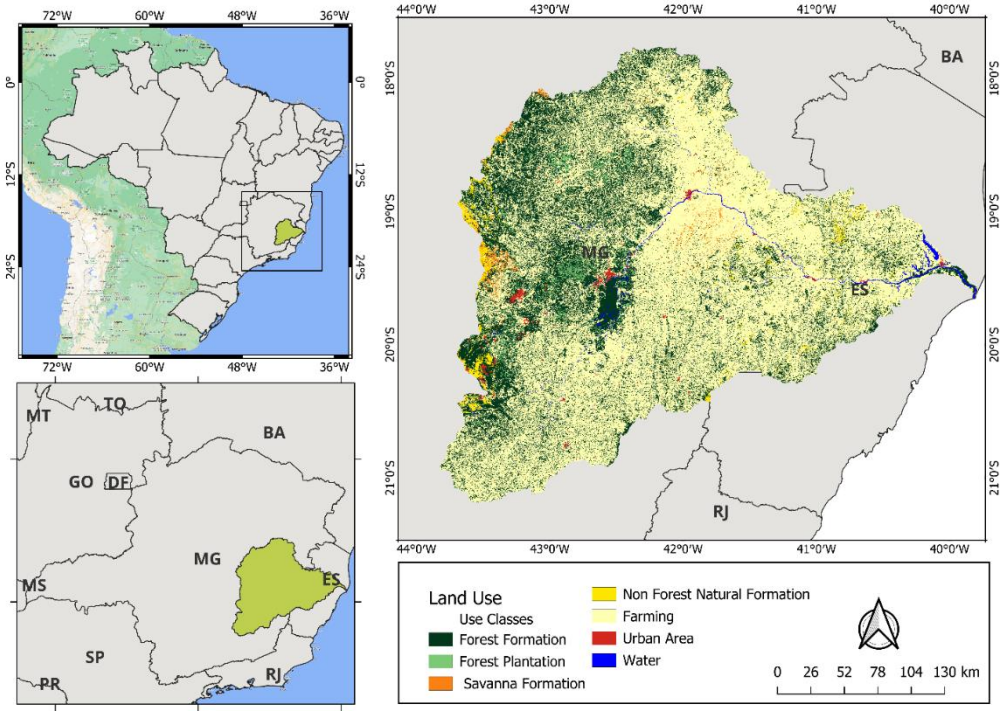

Source: elaborated by the author.

5.3.2 Materials and Methods

The data used in this study range from the modeling phase to the analysis of extreme rainfall and land use. Table 4 details the spatial determinants employed in the modeling stages, the analysis of climate extremes, and their respective sources (Table 4).

Table 4 - Key data, institutions, and resolutions used in the study.

Spatial Variables	Year	Resolution	Data Sources
Land use	1985 2015 2020	30 m	https://brasil.mapbiomas.org/colecoes-mapbiomas/
Precipitation/Temperature		--	CMIP6: https://www.worldclim.org/
Extreme Indices			Eta/INPE: https://lattesdata.cnpq.br/
Spatial Determinants used in the Modeling			
Conservation Units		--	https://maps.csr.ufmg.br/
Altimetry		--	https://maps.csr.ufmg.br/
Biomass		--	https://maps.csr.ufmg.br/
Pasture Quality		--	DinamicaEGO
Distance from Roads		--	DinamicaEGO
Distance from Railways		--	https://maps.csr.ufmg.br/
Forest Loss		--	NASA, Socioeconomic Data and Applications Center
Slope		--	Calculado pelo DinamicaEGO
Annual Temperature		--	https://www.worldclim.org/
Annual Precipitation		--	https://www.worldclim.org/
Vegetation Types		--	https://maps.csr.ufmg.br/
Tree Canopy Height		--	https://maps.csr.ufmg.br/

Source: elaborated by the author.

To develop the regionalized scenarios, we considered the following scale levels: (i) global, encompassing worldwide information, integrating factors such as GDP growth, population growth, per capita consumption of agricultural products, international and climate policies into the regional scenarios; (ii) regional, corresponding to the DRB, incorporating intra-

regional drivers such as national demand, institutions, and governance, economic and technological development; and (iii) local, which aggregates spatial factors at both local and regional scales, such as land use. It is important to note that several studies considered 1 km spatial resolutions (CHEN *et al.*, 2020; SILVA BEZERRA *et al.*, 2022), which do not capture significant details of land-use changes at the regional/local level. Our approach also aims to fill this gap, providing data with a more refined resolution (30x30m) for the study area.

Three stages were conducted in the modeling process, encompassing everything from land-use and change simulation to associations with extreme rainfall and temperature events, as illustrated in the flowchart of Figure 16. In the first stage, we acquired data from the Annual Mapping Project of Land Use and Cover in Brazil (MapBiomas) to identify the main land-use classes, prepare categorical and continuous variables, and use future datasets from the Land-Use Harmonization (LUH2) to provide different socioeconomic scenarios to the model.

5.3.3 Scenario Narratives

In this study, we analyzed the RCP4.5 (optimistic) and RCP8.5 (high emissions) scenarios. In the optimistic scenario, it is assumed that the positive trends of recent decades will be maintained. However, they do not fully realize the potential of an integrated socioeconomic, institutional, and environmental perspective. As a result, agricultural and extractive conversion policies and initiatives continue to be a source of tension and contradiction. Forest governance remains centralized, with the national government playing an important role in decision-making. Despite some improvements in addressing this issue, environmental system degradation persists (IPCC, 2022, 2023; SILVA BEZERRA *et al.*, 2022).

The pessimistic scenario (RCP8.5) is characterized by the continuous increase in greenhouse gas emissions. This scenario reflects projections from the literature that lead to elevated concentrations of these gases, indicating a worrying trajectory in environmental terms. It also suggests a decline in mitigation efforts, especially in recent years, with particularly negative impacts on the socio-environmental sphere (IPCC, 2022).

5.4 Modeling

Land-use changes were analyzed based on data from the Annual Mapping Project of Land Use and Cover in Brazil. Initially, we used the mapping from Collection 8, which covers

the years 1985 to 2020 and presents 23 LULC (Land Use and Land Cover) classes with a 30-meter resolution. These classes were simplified into seven main categories: Forest Formation, Planted Forest, Savannas, Farming, Non-Forest Natural Formation, Anthropogenic, and Water Bodies, to meet the study's objectives (NEVES, 2022; SPOSITO, 2021). Significant land cover transitions have been observed in the DRB, particularly from forested areas to pastures and agricultural lands. These changes are well-documented in studies utilizing MapBiomas data, which highlight the extensive deforestation and conversion of native vegetation to other land uses (ASSUNÇÃO *et al.*, 2015; NEVES, 2022; OLIVEIRA *et al.*, 2018; SILVA BEZERRA *et al.*, 2022).

Such transitions can directly impact climate dynamics by altering local temperature and precipitation patterns and increasing the frequency and intensity of extreme events like floods and droughts (NEVES, 2022). Therefore, focusing on these classes is crucial for understanding and mitigating climate-related impacts in the basin. In this study, we focused primarily on the classes that exhibit the most significant transitions in the basin and that can directly impact climate dynamics, particularly in the context of extreme events. The main transitions considered were: Natural Forest, Planted Forest, Savannas, non-vegetated regions, and water bodies to agriculture, as well as the conversion of natural forest to anthropogenic areas. We also took into account regeneration classes, considering the basin's context related to the environmental disaster, with a focus on the following transitions: Agriculture, non-vegetated areas, and planted forest to natural forest.

a) Dinâmica EGO is a free, non-commercial platform dedicated to environmental modeling, offering extensive design possibilities. It supports everything from simple static spatial models to complex dynamic models, including nested iterations, multi-transitions, dynamic feedbacks, and regional and multi-scale approaches. Additionally, the platform allows for decision-making processes for bifurcating and merging execution pipelines. It also stands out for including a variety of complex spatial algorithms, facilitating the analysis and simulation of spatio-temporal phenomena (RODRIGUES *et al.*, 2007; SOARES-FILHO *et al.*, 2002). In this study, the Dinamica-EGO platform was used to adapt the land use model, which is availa ble at the following link: https://www.csr.ufmg.br/dinamica/dokuwiki/doku.php?id=lesson_18 . The model involved the following steps:

i) The Weights of Evidence method (GOODACRE *et al.*, 1993) is applied in DINAMICA-EGO to generate a transition probability map, indicating areas more prone to changes (RODRIGUES *et al.*, 2007; SOARES-FILHO *et al.*, 2002). The Weights of Evidence

represent the influence of each variable on the spatial probability of a transition i-j. The weights of evidence can be calculated using the following formula:

$$P\{i \rightarrow j | \ B \ \cap C \ \cap D \ldots \cap N\} = \frac{e^{\sum w_n{}^-}}{1+ e^{\sum w_n{}^+}} \quad (6)$$

$$W^+ = \ln\left(\frac{y_{n=k} - y_{n=k-1}}{A_{n=k} - A_{n=k-1}}\right) \quad (7)$$

Where B, C, D e N, and N are the values of *k* spatial variables measured at the location *x,y* and represented by their weights $W+N$.

The spatial determinants used to calculate the weights of evidence are presented in Table 2. **ii)** A correlation analysis was conducted between the static variables to assess the presence or absence of autocorrelation among them. Following this, metric analyses and model adjustments were performed, followed by the development and validation of the model simulations (the entire procedure is succinctly detailed at: https://www.csr.ufmg.br/dinamica). **iii)** Validation: In this stage, we measured the model's ability to represent the cause-and-effect relationships in the selected transitions. The validation was based on two steps: a) The first step involved simulating using multiple windows and a constant decay function. Our model showed a similarity of 86% (Figure 14) in the 11x11 window (RODRIGUES *et al.*, 2007, 2007).

Figure 14 - Model Validation Using the Exponential Decay Technique

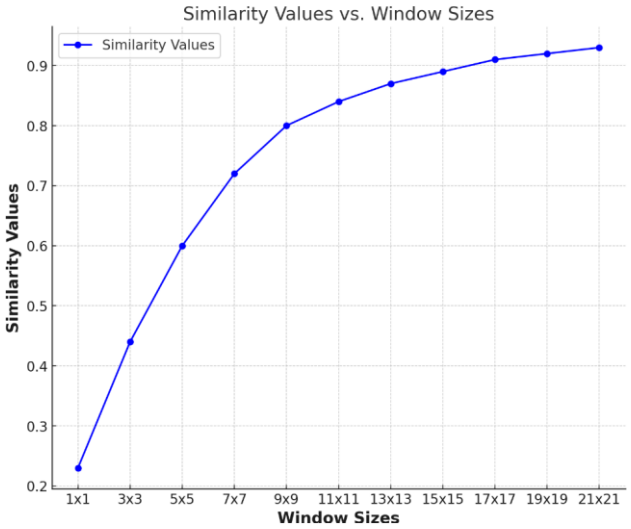

Source: elaborated by the author.

b) We validated the model's effectiveness by applying overall accuracy (OA) and the Kappa coefficient using a machine learning-based algorithm through the Geo-FLUS software (RAHNAMA, 2021; ZHU *et al.*, 2023. The OA and Kappa values typically range from 0 to 1, with higher values indicating greater accuracy in the model simulation. When the Kappa coefficient is greater than or equal to 0.8 (Table 5), it indicates that the model simulation has reached a satisfactory level of statistical significance. Figure 15 presents a comparison between the areas of simulated and actual land-use types. The observed differences are minimal, demonstrating the model's strong performance (Figure 14). Additionally, these small variations are common and can be attributed to minor changes during the validation time interval or the data source itself (ZHU *et al.*, 2023).

Figure 15 - Comparison of Reality and Land Use Simulation Details for 2020.

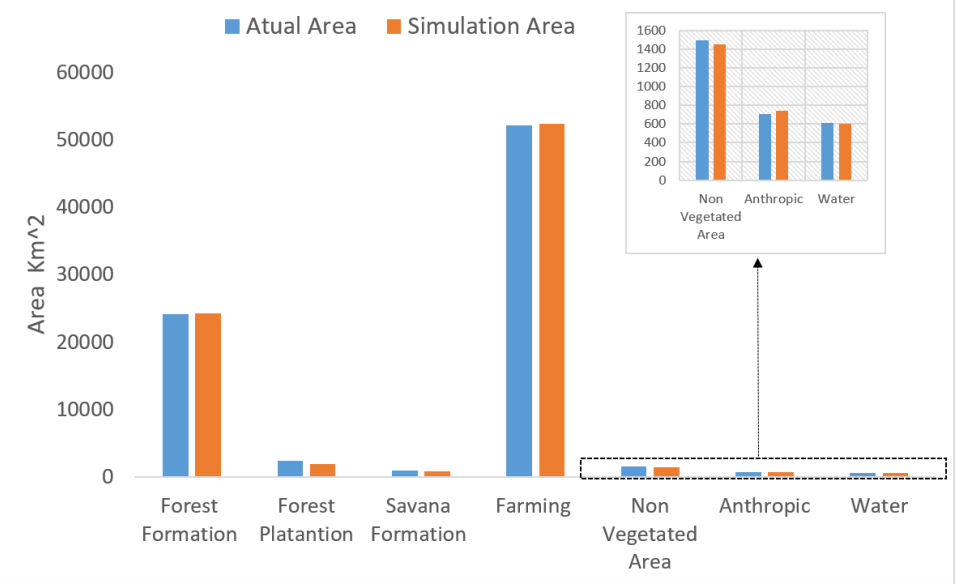

Source: elaborated by the author.

Table 5 - Model Validation through Kappa Coefficient and Overall Accuracy.

[Kappa Coefficient]	[Overall Accuracy]
0,812532	0, 880289

Source: elaborated by the author.

iii) The CMIP6 provides a dataset for future land use called LUH2 (Land-Use Harmonization), which can be accessed for free at http://luh.umd.edu/index.shtml. This dataset includes global projections of various land-use types from 2015 to 2100 under different Shared Socioeconomic Pathways (SSPs) and Representative Concentration Pathways (RCPs), with a resolution of approximately 0.25° (around 25 km). These data are generated through IAMs (Integrated Assessment Models), which integrate relevant models developed across multiple disciplines, such as energy, economics, atmospheric chemistry, climate, and ecology. This integration is achieved by constructing representative sectors (DOELMAN *et al.*, 2018; FUJIMORI *et al.*, 2017; KRIEGLER *et al.*, 2017). Recently, these data were upgraded to a resolution of 1 km, containing 17 land use types. This improvement was motivated by the fact that the LUH2 data did not match the classification scheme of the International Geosphere-Biosphere Programme. Additionally, the data were available in NetCDF, a complex data extension for manipulation (HOU *et al.*, 2022). In this context, to incorporate the Representative Concentration Pathway (RCPs) and Shared Socioeconomic Pathways (SSPs) scenarios from the sixth IPCC report (CMIP6) into the modeling process, we opted for the more refined (1 km) version of LUH2 (shown in Table 2). The average emission scenarios (RCP4.5-SSP2) and high emission scenarios (RCP8.5-SSP5) were mapped to the classification used in our simulation, using the MapBiomas land cover data as a reference (as). In other words, we performed a reclassification to align the LUH2 land use classes with those of MapBiomas (Table 6).

In DINAMICA-EGO, changes in geophysical characteristics, transportation costs, or social and political structures (such as bioclimatic variables, road projects, mining projects, etc.) are incorporated into a new raster cube. Additionally, changes in transition rates can be introduced by modifying the transition matrix. This is exemplified through public policy and socioeconomic scenarios related to Greenhouse Gas (GHG) emissions, as described by Soares-Filho et al. (2006). In the simulation of scenarios, we adopted the projected amount of change from LUH2 for the specific combinations of SSPs and RCPs (All data sources are available in the supplementary material (SM): https://github.com/NelsonMateus/SM/blob/main/Figuras_extras/Suplementar_Material_LUCL.pdf). This amount was adjusted to the land use and land cover classes provided by MapBiomas, considering SSP2/RCP4.5 and SSP5/RCP8.5 combinations, in order to generate the annual demand for each land use class in each scenario from 2025 to 2080.

To determine the amount of change in each scenario, we calculated the transitions for each land use type through a matrix, resulting in the percentage of annual changes. The

approach of incorporating the annual demand for the amount of change into LUH2 maps through class transitions was previously used in for integrating socioeconomic scenarios studies (CHEN *et al.*, 2020; HOU *et al.*, 2022; SILVA BEZERRA *et al.*, 2022). This methodology proved effective in incorporating different socioeconomic contexts into land use change simulations. Finally, we developed a matrix that quantifies the main annual changes for each socioeconomic scenario and incorporated it into the model. This process results in generating future land use patterns within the context of these specific scenarios (all procedures shown in the flowchart of Figure 16).

Figure 16 - Schematic diagram of the main steps of the work.

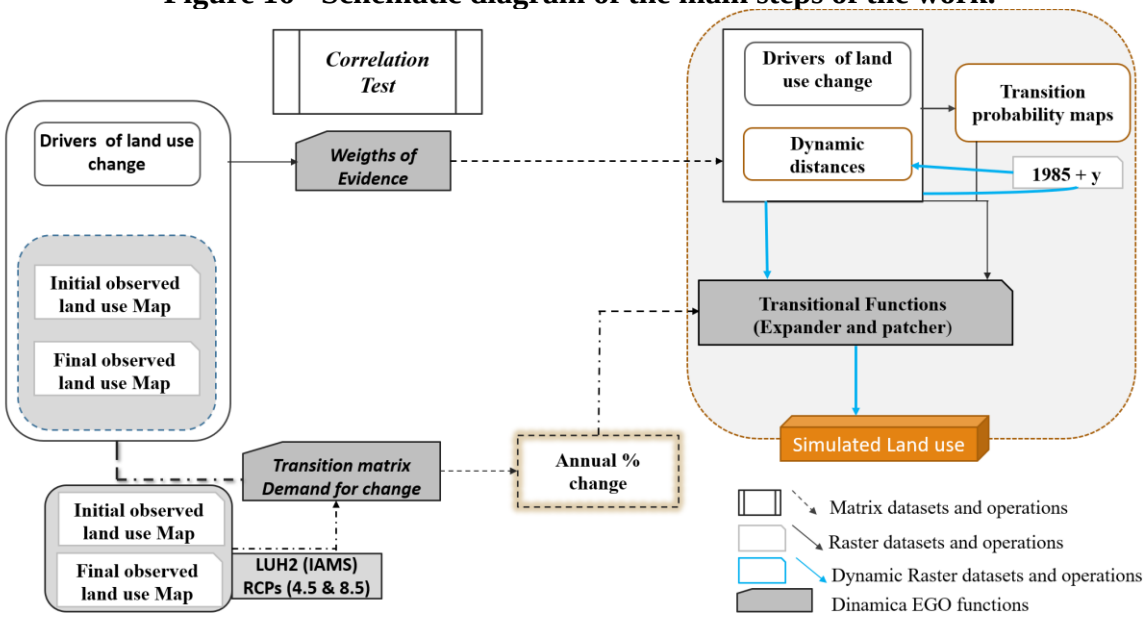

Source: elaborated by the author.

Although the adjusted LUH2 data classifies the Deciduous Broad-Leaf Forest category as forest, it is important to note that this category is considered planted forest in our study area. This is because these areas were established through tree planting for specific purposes, such as conservation or commercial production (Table 6). To more accurately reflect the conditions in our study area, we reclassified the Deciduous Broad-Leaf Forest as planted forest. This reclassification was validated through a comparison with the MapBiomas land use and cover map.

Table 6 - Land Use Classification in Our Simulation and LUH2.

Land Use Classification in Our Simulation	LUH2
Natural Forest	Evergreen broad-leaf forest
Planted Forest	Deciduous broad-leaf forest
Savannas	Woody savannas, Savannas
Farming	Cropland, mosaic
Non-Forest Natural Formation	Closed shrub lands
Urban Area	Urban and built-up
Water	Water

Source: elaborated by the author.

5.5 Extreme Climate Indices

Table 7 summarizes the extreme climate indices analyzed in this study, as defined by the European Climate Assessment & Dataset (ETCCDI). These indices, based on air temperature and precipitation, were calculated using the icclim Python library (CHERVENKOV; SLAVOV, 2021).

Precipitation and temperature data were obtained from the Eta model, nested within the global climate models CanESM2 and MIROC5, chosen for their ability to regionalize projections at a higher spatial resolution (0.2° x 0.2°) over South America. These models were chosen due to their good performance in representing the climatic conditions of the study basin, as demonstrated in previous studies (COSTA *et al.,* 2022; CAMPOS *et al.,* 2024). The dataset spans 1976–2005 for the historical reference and 2006–2099 for future projections under RCP4.5 and RCP8.5 scenarios. Bias correction was applied using empirical quantile mapping, comparing observed and simulated cumulative probability curves with datasets such as MSWEP, ERA5, and ERA5-Land (CHOU *et al.*, 2014; DE SOUZA FERREIRA *et al.*, 2024).

The study aims to assess the agreement between these models in representing climate extremes and trends in land use change areas within the DRB. Evaluating their performance is essential for understanding the robustness of climate projections and enhancing confidence in climate adaptation decisions. The climate indices (Table 5) were calculated on both monthly and annual scales, with monthly trends analyzed until 2030 and annual trends projected until

2080. This evaluation is crucial for understanding the robustness of climate projections and strengthening confidence in decision-making in the face of climate change in the DRB.

Table 7 - Summary of climate indices analyzed in this study.

Index	Description
PRCPTOT	Total annual precipitation (mm). Represents the sum of all daily precipitation throughout the year.
RX1day	Maximum daily precipitation (mm). Represents the highest amount of precipitation recorded on a single day during the year.
RX5day	Maximum precipitation over 5 consecutive days (mm). Represents the highest amount of precipitation accumulated over a period of five consecutive days throughout the year.
CDD	Maximum number of consecutive dry days. Represents the longest sequence of consecutive days without significant precipitation.
TG90p	TG90 (90th percentile of Mean Temperature). Used to identify exceptionally hot days, providing a measure of the highest temperatures experienced during the period.
TG10p	TG10 (10th percentile of Mean Temperature). Useful for identifying exceptionally cold days, providing a measure of the lowest temperatures experienced during the period.
TG	TG (Mean Temperature). Provides an overview of the average thermal conditions in a region.

Source: elaborated by the author.

5.6 Trend Analysis

Trend analysis is a technique used to determine the presence of significant or insignificant trends in a climate index and to quantify the magnitude of trends in a dataset. Trends in datasets can be monotonic, where a variable consistently increases or decreases over time, or step trends, where abrupt changes in the data may occur at specific points in time (DONG *et al.*, 2020; QUAN *et al.*, 2021).

In our study, trend analysis was conducted in two stages, in the form of temporal and spatial series, to evaluate how extreme climate indices are behaving in the regions of major

land-use changes. For the trend over months and years, the analysis was designed to show which months are experiencing worsening conditions and which years are showing higher intensity of extreme indices according to the models. This aims to estimate and propose alerts for the years and months that might be more critical or not due to the major land-use changes occurring in the basin.

Two non-parametric trend tests were used to detect significant trends in the DRB: the Mann-Kendall and Theil-Sen tests. Thus, we aim to achieve a detailed understanding of how extreme precipitation and temperature indices are behaving over time in the areas of land-use change. The results of this analysis are essential for formulating mitigation and adaptation policies to climate change, helping to identify critical periods, and guiding actions for the sustainable management of water resources in the DRB.

5.6.1 Trend-Free Pre-Whitening Method

Time series analysis with positive serial correlation can result in false detection of significance in regions where it does not exist, especially in the DRB, where climatic variability is quite heterogeneous (CUPOLILLO *et al.*, 2008; LIMA; CUPOLILLO, 2018). To avoid this issue, we checked for serial correlation before performing the trend analysis. This process ensures we correctly identify regions with significant trends in the DRB. We used the pre-whitening method to eliminate serial correlation ((AHMAD *et al.*, 2015; QUAN *et al.*, 2021; VON STORCH, 1999). This method ensures that the trend analysis appropriately considers positive serial correlation, resulting in a more accurate and reliable detection of significant trends. The procedure follows the steps below: a) Slope Estimation: We used the Theil-Sen method to estimate the slope of the time series, performed before removing the trend (WU *et al.*, 2008). b) Lag-1 Serial Correlation Calculation: We calculated the Lag-1 serial correlation coefficient in the detrended series and removed the AR(1) component, resulting in an independent residual time series. c) Combining Slope and Residual Series: We combined the estimated slope with the residual series to create a new time series that preserves the original trend without the influence of AR(1). d) Trend Testing: We applied the Mann-Kendall test to the combined series to detect trends, ensuring accuracy in identifying significant regions in the DRB (FELIX *et al.*, 2021).

5.6.2 Theil-Sen Slope Estimator (TS)

The Theil-Sen slope estimator is a non-parametric method used to calculate the median of all slopes between consecutive points in a time series that exhibits a linear trend. This method is particularly useful for time series with equal intervals and demonstrates robustness against outliers, ensuring reliable estimates even in the presence of atypical values (MACHIWAL; MADAN, 2012). The equation determines the magnitude of the trend:

$$\beta\ (inclinação) = median\left(\frac{y_j - y_i}{x_j - x_i}\right) \quad \text{where } i < j \qquad (8)$$

Where β is the median of all slopes, $y_i\ e\ y_j$ are the values of the time series at times j and i, respectively, and X_j , X_i are the corresponding time points. This estimator provides a robust measure of central tendency, minimizing the influence of extreme fluctuations in the data.

5.7 Results

5.7.1 Land Use in Climate Change Scenarios

Figures 17 and 18 show that, in the short term (2030), the regions with the most significant changes in the DRB are primarily concentrated in the northwest, south, and southwest of the basin. This trend is evident both in the simulation period without considering climate change scenarios and in the period incorporating these scenarios.

The identified regions with a high probability of changes in land use are also the most sensitive to extreme climate events, as shown in Figure 17. However, the changes are even more pronounced in the western and southern parts of the basin and some areas of the north and east. These findings align with previous studies that have highlighted the complex interplay between human activities and climate change impacts in these regions (COSTA *et al.*, 2022; OLIVEIRA; QUARESMA, 2017; SOUZA *et al.*, 2018).

This dual influence of anthropogenic and natural drivers underscores the need for targeted adaptation strategies that address both environmental and socioeconomic challenges. These considerations could be further explored in the final discussions, emphasizing the importance of integrative approaches to mitigate the compounded effects of climate change and human pressures on the basin (COSTA *et al.*, 2022; OLIVEIRA *et al.*, 2018; SOUZA *et al.*, 2018).

In the RCP4.5 scenario (Figure 17 and 18B), which assumes centralized forest governance with a significant role for the national government and basin committees in decision-making, a more controlled reduction in native forest areas is projected compared to the high emissions scenario (RCP8.5). By 2030, native forests are expected to cover approximately 29,339.38 km² (28.77%), decreasing to 29,123.91 km² (28.55%) in the medium term (2050) and to 28,803.29 km² (28.24%) in the long term (2080), representing a reduction about -0.52% by 2080 (Figure 17, Figure 18 and Figure 19).

Despite compliance with environmental laws in this scenario, an increase in the area allocated to farming is projected in the DRB compared to the simulated period. Agricultural land, which occupies the largest fraction of the basin and is responsible for much of the land-use changes (CAMPOS *et al.*, 2021; DE SOUZA FERREIRA *et al.*, 2024; LYRA, 2018), is expected to cover approximately 65,389.43 km² (64.11%) by 2030 (short term), increasing to

65,709.01 km² (64.42%) by 2050 (medium term). In the long term, by 2080, agricultural activity is projected to expand to 66,181.63 km² (64.89%), representing a 0.78% increase (Figure 14).

Figure 17 - Land Use and Cover (2030), Probability Map of Changes for the Simulated Period and Climate Change Scenarios. Representing the largest transition class in the basin (Forest to agriculture).

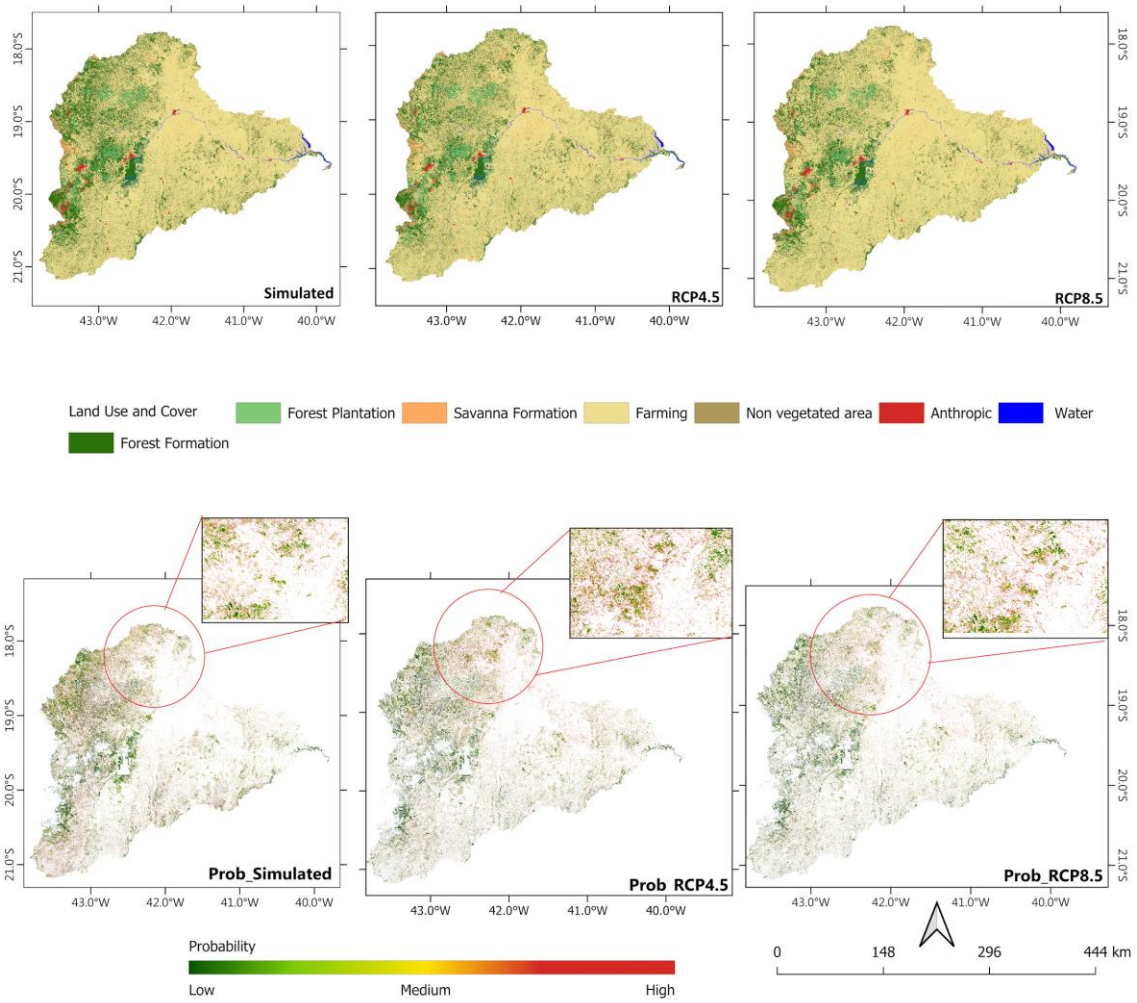

Source: elaborated by the author.

Our results corroborate the study by Campos et al., (2024), which estimated conservative and non-conservative scenarios using a model of hypothetical exclusion and inclusion of environmental conservation zones. This study predicts that, by 2050, if legal reserve areas are fully respected, pressure on agricultural and livestock activities will be reduced to 63.8%. This value is consistent with what our model predicts (64.42 %), which, in addition

to considering the effects of conservation areas, also incorporates the climatic effects projected by IAMs.

Furthermore, studies evaluating the basin's conditions before and after the 2015 disaster indicated that a significant portion of land use changes resulted from the conversion of native forest and other land uses to agriculture and livestock. Between 1985 and 2018, forest areas decreased by 1.9%. The largest conversions of natural forest were directed towards pastures, while areas occupied by agriculture increased (NEVES, 2022; OLIVEIRA *et al.*, 2018; SPOSITO, 2021).

In the RCP4.5 scenario, the areas of savanna formation showed minor variations in projections, both in the short and long term. By 2030, these areas will cover 1,124.56 km², slightly decreasing to 1,121.69 km² by 2050 and to 1,117.39 km² (a 1.10% reduction, Figure 13 and Figure 14) by 2080. Areas of planted forest also exhibit a small decrease of -0.10% over the same period, dropping from 2,765.47 km² (2.71%) in 2030 to 2,626.07 km² (2.57%) by 2080. Unvegetated areas and water bodies remain virtually constant, with insignificant variations over the years.

These small variations can be attributed to the fact that savanna formation, planted forests, unvegetated areas, and water bodies represent the smallest land cover classes in the basin. Due to their limited spatial extent, even minor absolute changes result in low percentage variations, making them less susceptible to major shifts compared to dominant classes, such as forest and agricultural land.

A significant decrease in forest areas is projected in the RCP8.5 scenario, which assumes weakened socio-environmental efforts. By 2030, forests will cover 23,748.49 km² (23.28%), and this will decrease to 18,771.67 km² (18.40%) by 2080, representing a reduction of approximately -4.88%. Meanwhile, the area designated for agriculture will increase considerably, rising from 72,301.18 km² (70.89%) in 2030 to 78,462.28 km² (76.93%) by 2080, an increase of 6.04% (Figure.13 and Figure.14).

In the RCP8.5 scenario, savanna areas also decrease over time, from 851.39 km² (0.83%) in 2030 to 736.97 km² (0.72%) in 2050, reaching 637.93 km² (0.63%) by 2080, resulting in a total reduction of -0.20%. Regarding other land classes, non-vegetated and anthropogenic areas show less pronounced changes, with a slight increase in anthropogenic areas and a small reduction in water bodies (Figure.12 and Figure 13).

Conversely, the simulation period without considering climate change scenarios shows a gradual increase of 0.74% in forest areas, reflecting reforestation initiatives, such as the

40,000-hectare forest restoration agreement established by the Transaction and Conduct Adjustment Agreement (TTAC) in 2016, which aims to improve forest cover in the basin (CAMPOS *et al.*, 2024).

Agricultural activities are also expected to continue expanding. In the short term, this activity is projected to cover an area of 64,920.11 km² (63.65%) by 2030, growing to 65,038.17 km² (63.77%) by 2050, and reaching 65,197.88 km² (63.92%) by 2080, which represents an increase of approximately 0.27% (Figure 13 and Figure 14).

Figure 18 - Land Use and Occupation for Short-Term (2030), Medium-Term (2050), and Long-Term (2080) for the Optimistic (RCP4.5), High Emissions (RCP8.5), and Simulated Scenarios.

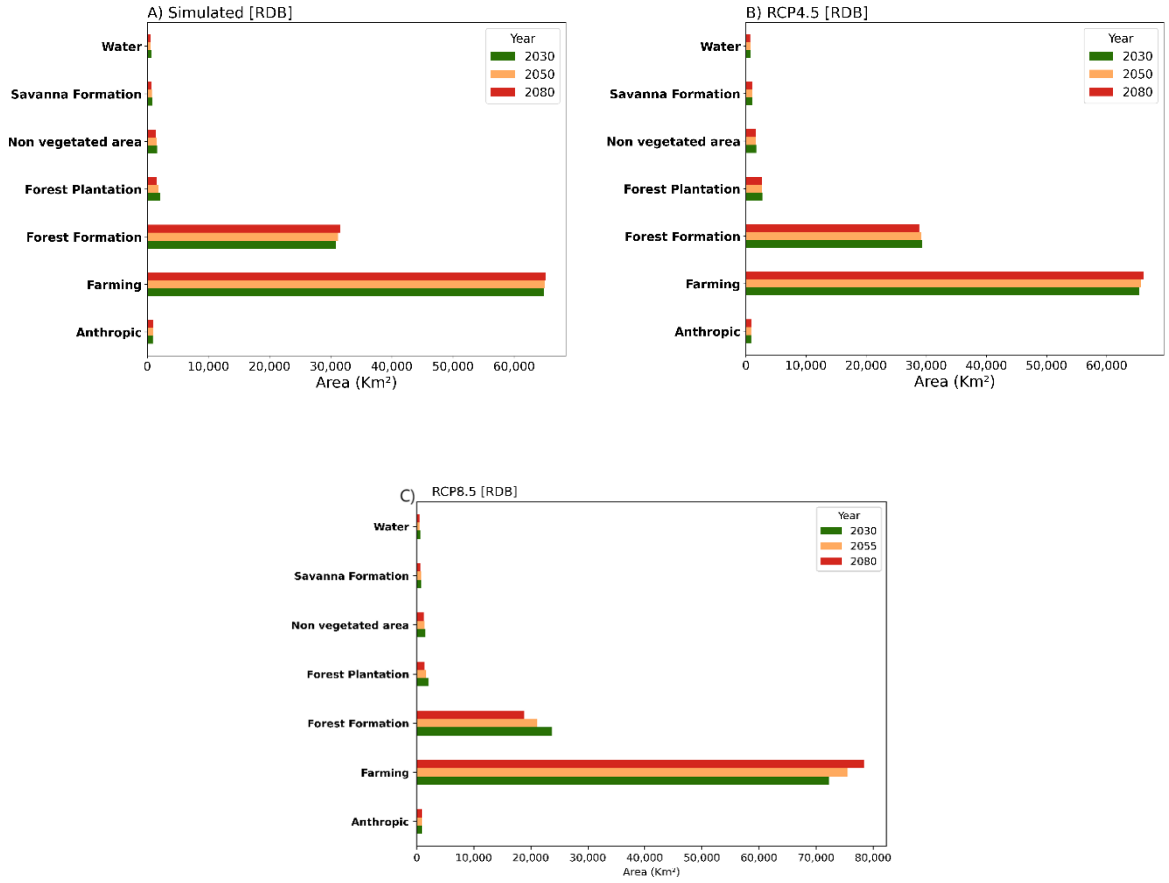

Source: elaborated by the author.

Figure 19 - Sankey diagram illustrating medium-term (2050) and long-term (2080) changes under the Optimistic (RCP4.5), High Emissions (RCP8.5), and Simulated Scenarios.

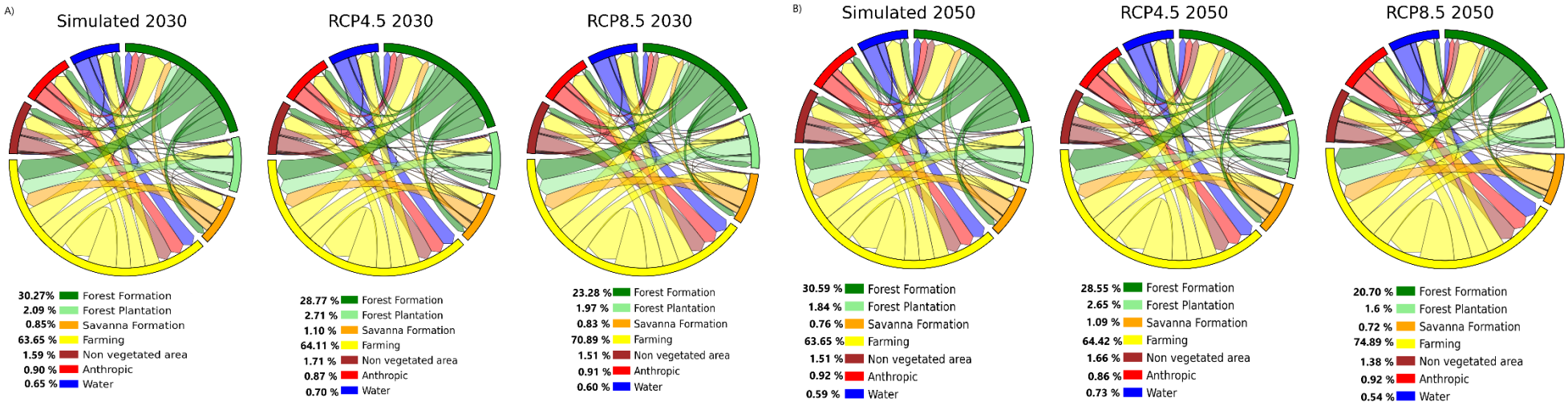

Source: elaborated by the author.

C)

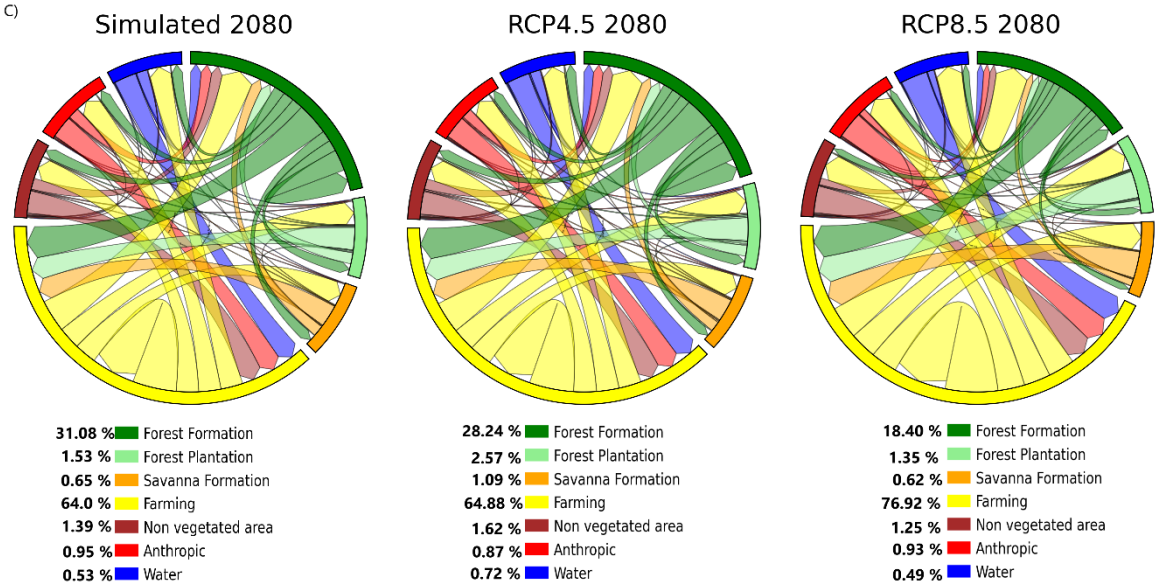

Source: elaborated by the author.

5.7.2 Extreme Rainfall Event Trends in the DRB

The projections from the CanESM2 and MIROC5 models provide consistent insights into trends in extreme precipitation in the DRB. Overall, both models show agreement in representing the trends of extreme climate indices. Under the RCP4.5 scenario, the RX1day and RX5day indices, which measure extreme rainfall over one and five consecutive days, respectively, exhibit a well-defined seasonal pattern, with a decreasing trend from January to March and October to December (Figure 20A, 20C). While both models agree on the direction of the trends, they differ in the intensity of the changes, particularly between January and March. This divergence may reflect differences in the physical processes governing extreme rainfall events as represented by each model (CHOU *et al.*, 2014).

Under the RCP8.5 scenario, the trends become more intense and consistent for both RX1day and RX5day indices (Figure 20B, 20D), especially showing a more pronounced decrease during the summer months. This suggests a possible reduction in the frequency and intensity of extreme precipitation events in the DRB. In high-emission scenarios, precipitation tends to occur on fewer days, which may result in lower monthly index values (FERREIRA, 2019b). The months of January, February, and December exhibit the strongest negative trends (up to -0.10 mm/month), with CanESM2 showing the most intense changes, particularly for the RX5day index. Model agreement is higher during the summer and early autumn, while seasonal

discrepancies under the RCP4.5 scenario suggest greater uncertainty in this intermediate scenario.

For the CDD index (Figure 20E, 20F), which represents the number of consecutive dry days, both models indicate an increase in the number of dry days in the DRB. Under RCP4.5, there is a trend of increasing CDD at the beginning and end of the year, coinciding with the rainy season, which may be linked to more irregular rainfall patterns. In the RCP8.5 scenario, trends for the CDD index are more intense, but the models generally agree on the direction of the trends. These results suggest a potential increase in the occurrence of flash droughts in the DRB, a phenomenon that could have significant impacts on water resources and local agriculture (FARIA *et al.*, 2023; SONDERMANN *et al.*, 2022).

The PRCPTOT index (Figure 20G, 20H), which represents the total annual precipitation, shows a generalized reduction throughout the year in both scenarios. Under RCP4.5, the largest reductions occur from January to April (approximately -2.5 mm/month). In the RCP8.5 scenario, these reductions are even more pronounced, reaching up to -3.5 mm/month, particularly in the early months of the year, corresponding to the rainy season. These projections align with observational studies that already indicate a decreasing trend in annual precipitation in the DRB (CAMPOS *et al.*, 2024; CUPOLILLO *et al.*, 2008; UICN, 2022).

Figure 20 - Extreme Precipitation Indices in the DRB. Number of Consecutive Dry Days (CDD), Annual Total Precipitation (PRCPTOT), Maximum Daily Precipitation (RX1day), and Maximum Five-Day Precipitation (RX5day).

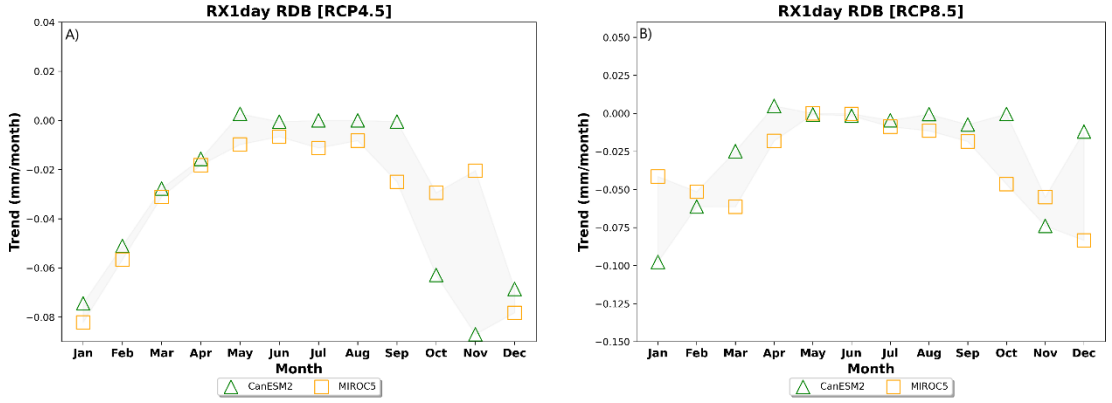

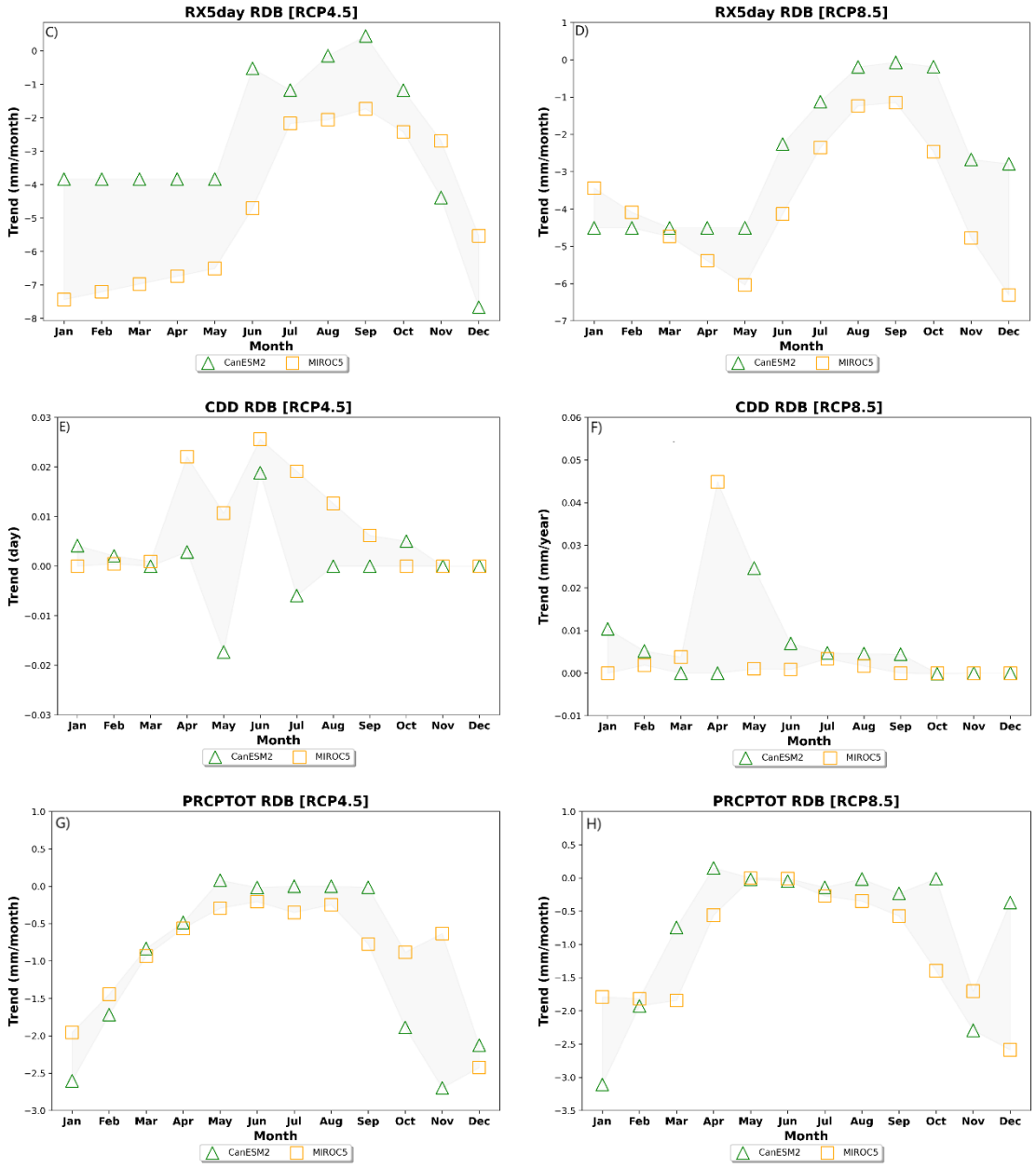

Source: elaborated by the author.

5.7.3 Annual Trends of Precipitation Extremes

Annual simulations from the regional Eta model, coupled with the global models MIROC5 and CanESM2 (Figure 21), project a future with increased frequency and intensity of extreme climate events and a reduction in annual precipitation totals. Historical data indicates an increase in consecutive dry days (CDD) from 30 to 50 days. In the optimistic scenario (RCP4.5), simulations from the two climate models for the future show an increase in the intensity of dry days as early as 2030, with the number of CDD days exceeding 50. The models

accurately represented the 2014/2015 drought, which severely affected the region, although with variations in intensity (MARENGO *et al.*, 2015). For the years 2025 and 2030, as well as long-term projections up to 2069, the models predict CDD peaks exceeding 50 days (Figure 21A).

These periods coincide with land use results, which show an increase in the area allocated to farming and a reduction in native forest areas in the DRB. These projections of increasing consecutive dry days (CDD) align with a notable reduction in native forest cover observed in the same period. Between 2030 and 2050, the native forest area is expected to decline from 28.77% under the conservation scenario (RCP4.5) to 23.28% in the pessimistic scenario (RCP8.5). This substantial forest loss suggests a possible feedback mechanism in which land cover changes exacerbate drought conditions, further intensifying the frequency and duration of dry spells. The reduction in forest cover, particularly in critical ecological zones, may weaken the land-atmosphere moisture balance, diminishing regional evapotranspiration and contributing to longer and more intense dry periods (RAHNAMA, 2021; SHEKHAR *et al.*, 2020).

The conversion of forests into pastures and croplands can affect the moisture balance and alter local precipitation patterns, intensifying dry periods (BEUCHLE *et al.*, 2022; GAO *et al.*, 2020; LEITE-FILHO *et al.*, 2021; SHEKHAR *et al.*, 2020; ZEMP *et al.*, 2017). Among the models, CanESM2 shows the highest CDD peaks (Figure 21A and Figure 21E). However, both models captured the increase in dry days in the basin. In the high-emissions scenario (RCP8.5), both historically and in future simulations, a significant increase in consecutive dry days is observed. In the short term (2021-2040), medium term (2041-2060), and long term (2061-2080), the models project maximum CDD peaks between 2026 and 2030 and again between 2060 and 2070. These consecutive dry periods could exceed 70 days, with much greater intensity compared to the RCP4.5 scenario. The CanESM2 model shows the greatest intensity in these peaks, possibly due to its slight tendency to overestimate precipitation in the southeastern region (CHOU *et al.*, 2014; LYRA, 2018).

For extreme rainfall frequency indices, RX1day and RX5day (Figure 21C, 21D), annual variations show an increasing trend in the historical scenario, with values ranging between 40 and 250 mm/year. This trend will become more pronounced in future scenarios, with the greatest magnitude observed under high-emission conditions. The most intense peaks are projected between 2030 and 2077, with all models indicating a significant increase in extreme

rainfall. While the RCP4.5 scenario also shows an upward trend, it is more pronounced under RCP8.5 (Figure 21G and 21H), with higher intensities expected in the years 2048 and 2077.

The PRCPTOT index (Figure 21B), which reflects annual total precipitation, shows a clear reduction trend both in the historical period and in future simulations. This reduction is more pronounced in the RCP8.5 scenario (Figure 21F), with projected values falling below the climatological annual average (~1700 mm/year) in the DRB. The significant reduction in precipitation may exacerbate the pressures already observed in land use, particularly with the expansion of agriculture and the reduction of forested areas in the basin.

The conversion of large areas of native forest into agricultural and pastureland, as discussed in the land use results, can amplify the impacts of these climate extremes (LIU *et al.*, 2024; PIELKE *et al.*, 2002; SAMBIENI *et al.*, 2024). The increase in agriculture in critical regions of the DRB, combined with the reduction in forest cover, affects the hydrological cycle by reducing soil water retention capacity and intensifying the effects of prolonged droughts and precipitation variability. This cycle can heighten the basin's vulnerability to extreme rainfall and drought events, underscoring the need for integrated climate adaptation policies and sustainable land use management (CUPOLILLO *et al.*, 2008)

Figure 21 - Annual Trends of Extreme Rainfall.

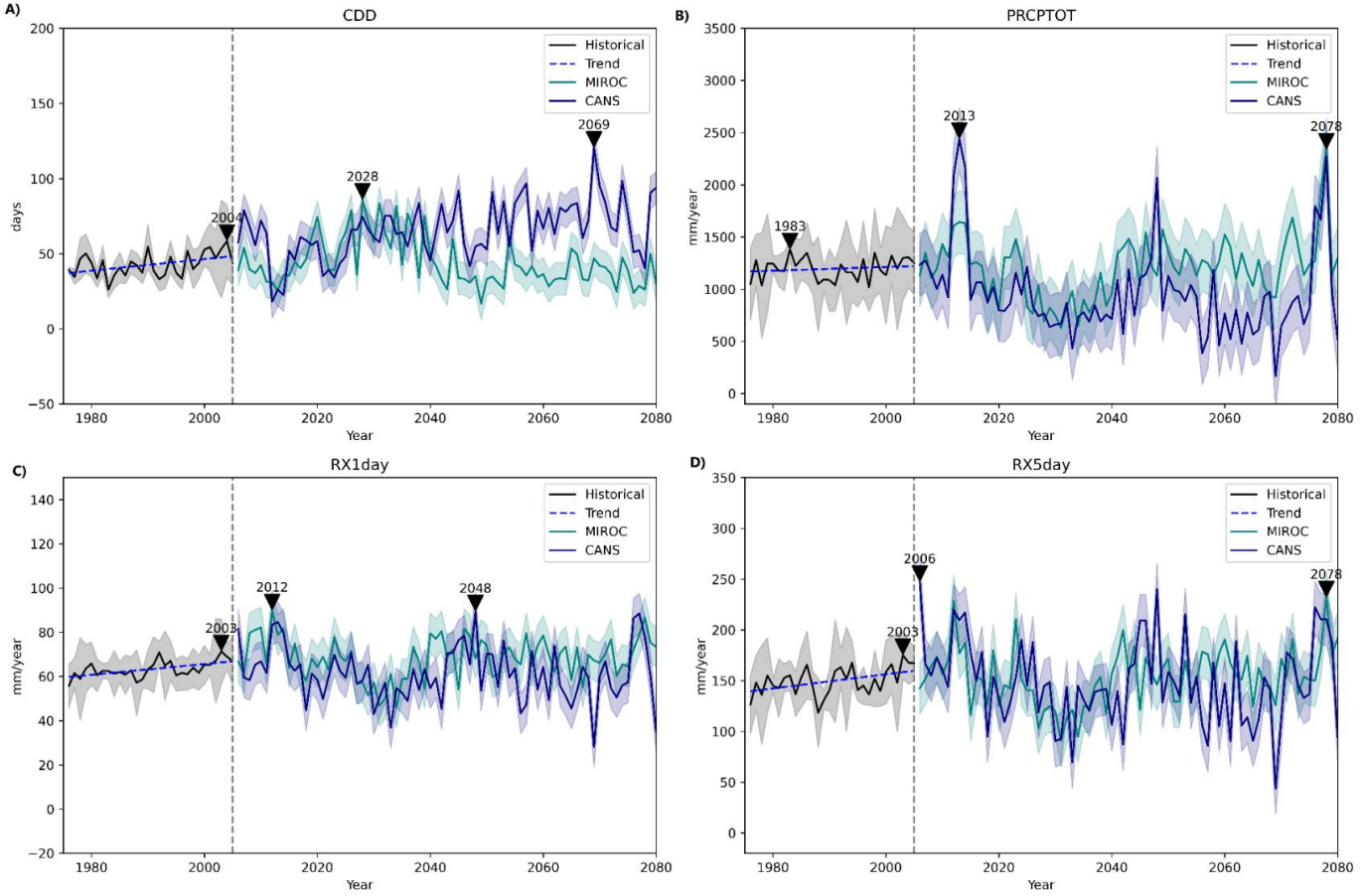

Source: elaborated by the author.

Figure 21 (continued).

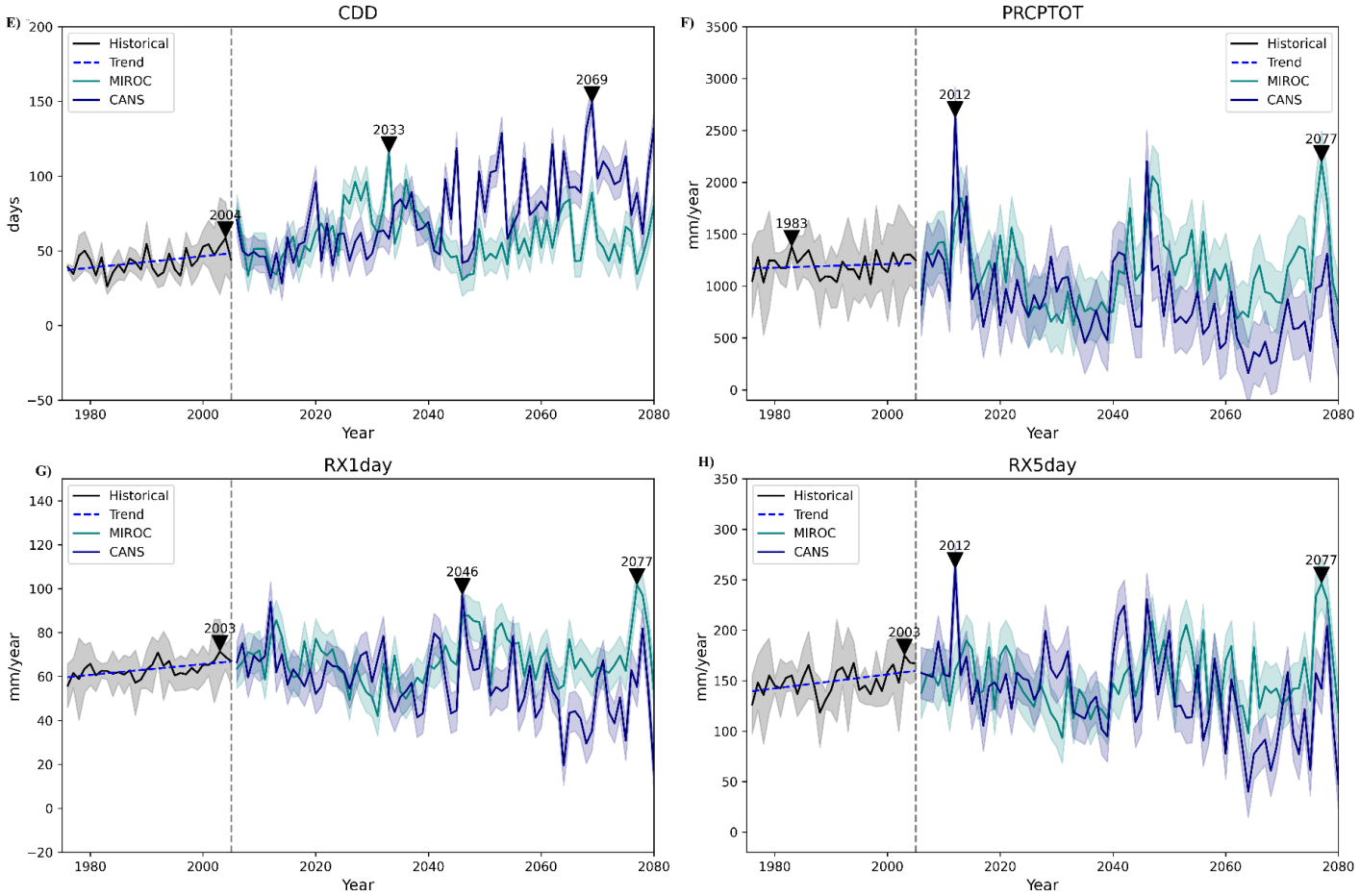

Source: elaborated by the author.

5.7.4 Spatial Trends of Extreme Rainfall Events

The presented maps illustrate trends in extreme rainfall events in the DRB for different evaluated scenarios (Figure 22) and the climate models used. Projections for the CDD index indicate an increase of up to 2 days in the number of consecutive dry days, especially in the northern, western, and parts of the eastern regions of the basin. This increase is more pronounced in the RCP8.5 scenario, suggesting greater duration and severity of dry periods under high-emission scenarios. Regions with significant trends, represented by points on the maps, coincide with areas affected by deforestation and agricultural expansion (Figure 12).
For the PRCPTOT index, which measures annual total precipitation, trends indicate a significant reduction across the entire basin for both climate models, with greater intensity in the southern and eastern regions. This reduction becomes even more pronounced in the RCP8.5 scenario, suggesting a sharp decline in annual precipitation totals under high-emission scenarios (DE OLIVEIRA *et al.*, 2023; DE SOUZA FERREIRA *et al.*, 2024; VEIGA *et al.*, 2023).

Notably, areas that have undergone the most significant land use conversion—primarily due to agricultural expansion and deforestation—coincide spatially with regions experiencing the greatest reductions in mean precipitation (Figure 17 and Figure 18). Additionally, in some of these regions, there is a concurrent increase in extreme rainfall events (RX1day and RX5day). This pattern suggests a complex relationship between land cover changes and hydroclimatic extremes, where a reduction in forested areas and expansion of agricultural lands may be linked to both a decrease in mean precipitation and heightened variability in extreme rainfall.

The RX1day and RX5day indices, which represent intense precipitation over one and five consecutive days, exhibit notable spatial variability in extreme precipitation trends across the DRB. While some regions—particularly in the eastern basin—show an increase in extreme precipitation, others, notably in the south and west, display a reduction in both emission scenarios. The western and northern regions present the most pronounced trends, particularly under the RCP8.5 scenario, suggesting an intensification of hydroclimatic extremes in a high-emission future. Statistically significant areas encompass the northern, western, southern, and parts of the eastern DRB (Figure 17).

Among the models analyzed, CanESM2 emerges as the most consistent in capturing the increasing trend of CDD and the decreasing trend of PRCPTOT. However, CanESM2 exhibits

a systematic overestimation of extreme precipitation changes (RX1day and RX5day) compared to MIROC5, which, in turn, demonstrates greater variability in CDD and PRCPTOT trends (Figure 22). This divergence between models underscores the uncertainties associated with climate projections while reinforcing the robustness of certain regional patterns in the DRB.

Thus, the two climate models highlight the northern, western, southern, and parts of the eastern DRB as statistically significant areas for changes in extreme precipitation events. These areas coincide with regions undergoing major land use changes, including agricultural expansion and forest reduction (CAMPOS *et al.*, 2024; DE OLIVEIRA *et al.*, 2023).

Figure 22 - Spatial trend of extreme rainfall events with BESM and CanESM2 models.

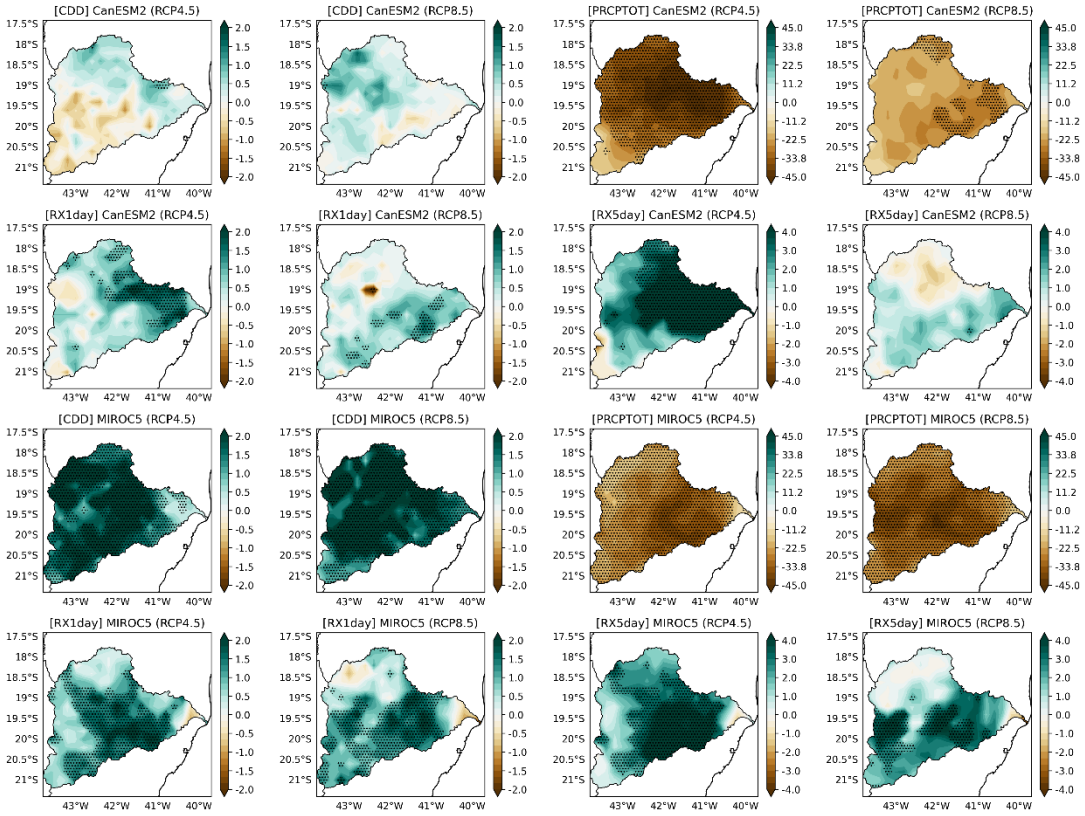

Source: elaborated by the author.

5.7.5 Monthly Trends in Temperature Extremes

Figure 23(A, B, C, D, E, F) represents the trends in extreme temperature indices in the DRB under the RCP4.5 and RCP8.5 scenarios. For both scenarios, average temperatures generally increase in all months, with this increase being more pronounced under the high-

emissions scenario. However, there are some variations between the models. In the summer months, all models indicate increases, although with small variations in magnitude.

The trends in extreme temperature indices, represented by the percentiles TG10p (coldest temperatures) and TG90p (hottest temperatures), particularly between October and April, show an upward trend in both scenarios. CanESM2 frequently presents the highest elevation trends for all indices, suggesting a more extreme forecast of climate changes in the DRB. All models agree on a trend of increasing extreme temperature indices, with elevations ranging between 0.05°C and 0.10°C, particularly in the RCP8.5 scenario (Figure 23B, 23D,23F). This aligns with expectations of greater warming in the DRB found in previous studies (IUCN, 2022; SONDERMANN *et al.*, 2022).

Figure 23 - Trend of Extreme Temperature Indices.

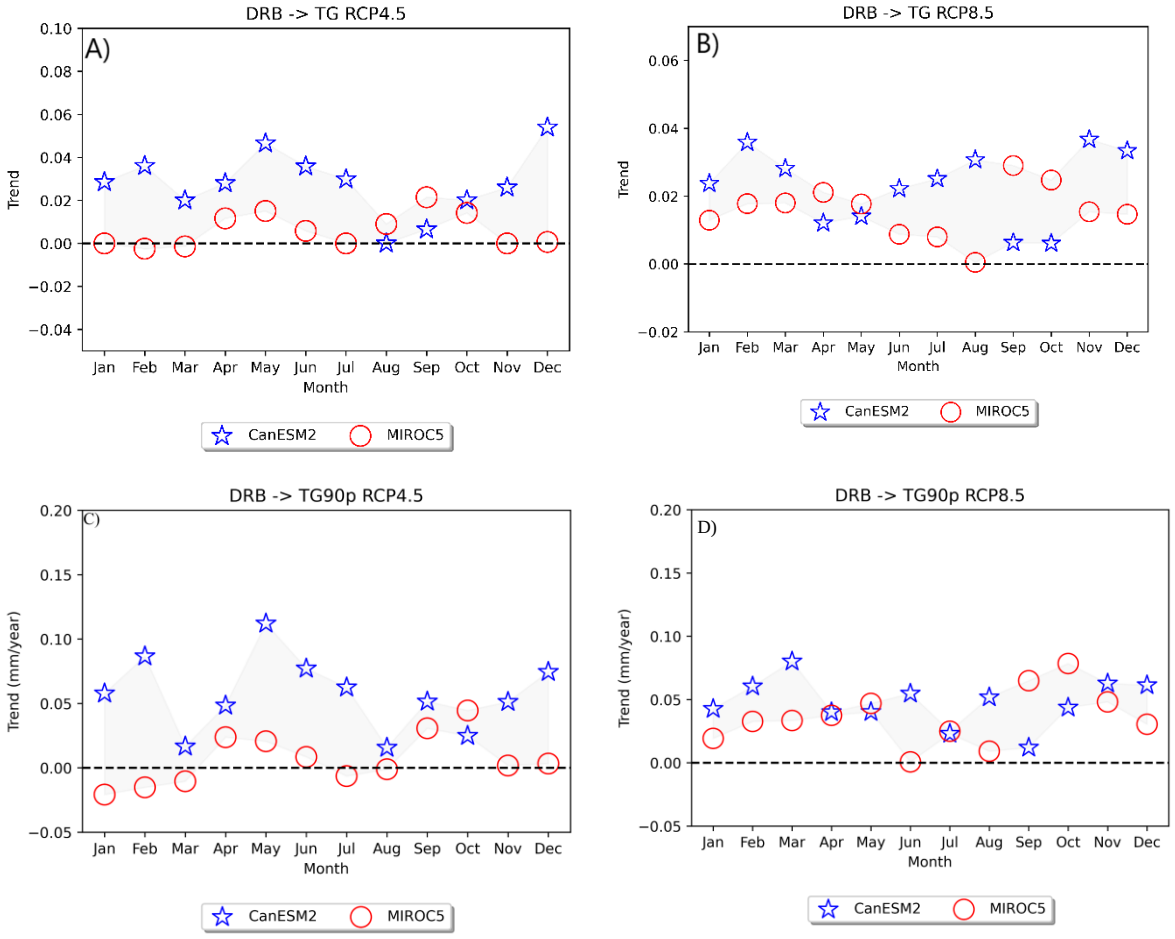

Source: elaborated by the author.

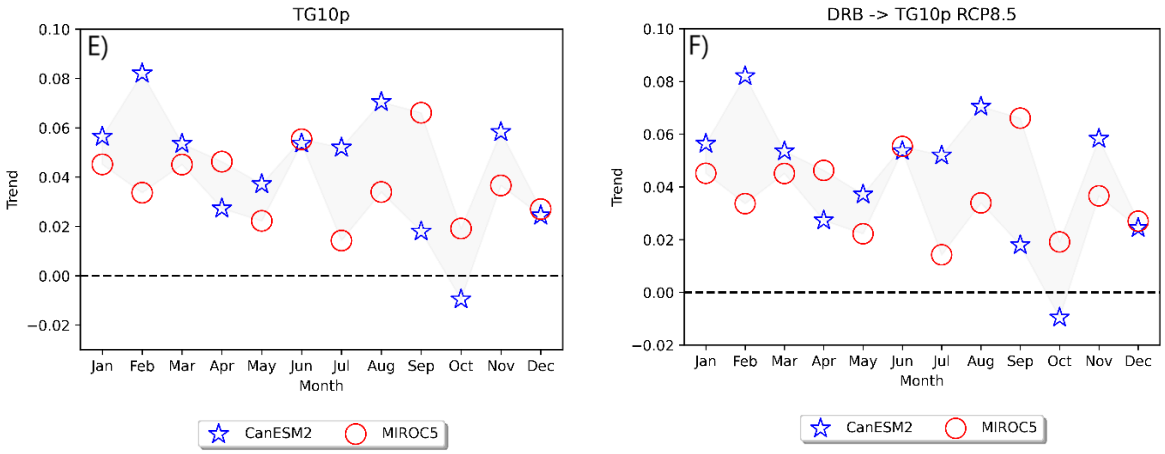

Source: elaborated by the author.

5.7.6 Annual Trend of Extreme Temperature

The analysis of the RCP2-4.5 and RCP5-8.5 scenarios reveals significant differences in the projections of temperature indices for the DRB (Figure 24 and 25). The results indicate that the high-emissions scenario (RCP5-8.5) projects a more pronounced increase in all analyzed temperature indices, aligning with expectations for a scenario without significant mitigation of greenhouse gas emissions (CHOU *et al.*, 2014).

In the RCP4.5 scenario, a more controlled increase in mean temperature (TG) is observed over time. Projected temperatures range between 22°C and 24°C, with a significant rise between 2050 and 2080, reaching approximately 26°C to 26.5°C. In contrast, the RCP5-8.5 scenario shows a more pronounced increase, with mean temperatures reaching between 28°C and 30°C in the medium term (2050-2060) and the long term (2080). This increment of about 2°C in the high-emissions scenario aligns with projections observed in previous studies, such as those reported by UICN (2022).

Minimum temperatures (TG10p), which historically range between 17°C and 21°C in the DRB, also show a significant increase. In the RCP2-4.5 scenario, projected minimum temperatures rise to around 22°C to 24°C in the short and medium term. However, in the RCP5-8.5 scenario, this increase is even more pronounced, with minimum temperatures projected to reach up to 26°C, which could strongly affect nighttime cooling patterns and influence thermal comfort.

The hottest days (TG90p) follow a concerning trend. In the RCP2-4.5 scenario, maximum temperatures projected for the basin reach approximately 28°C, with a significant increase to around 30°C in the RCP5-8.5 scenario (Figure 20).

This 2°C difference reflects the rise in the frequency and intensity of extreme temperatures, which are known to cause thermal stress in human populations, increase energy consumption for cooling, and negatively impact agriculture (JIN *et al.*, 2010). Additionally, the higher temperatures and prolonged dry conditions can significantly increase the risk of wildfire spread in the region. Changes in maximum and minimum temperatures directly influence the availability of soil moisture and vegetation dryness, creating favorable conditions for fire ignition and propagation (ULLAH *et al.*, 2024; YOUNESZADEH *et al.*, 2015).

Expanding agricultural areas and reducing native forests, driven by more severe climatic conditions, can increase the risk of wildfires and contribute to changes in the basin's surface runoff. The conversion of forests to agricultural crops or pastures often reduces the landscape's resilience to fires, as these areas tend to have lower biodiversity and fewer natural firebreaks (FUJIMORI *et al.*, 2017). Additionally, land use alteration can modify surface runoff patterns, affecting the basin's hydrology and potentially increasing the incidence of floods or erosion. The increased risk of wildfires poses a severe threat to biodiversity, water resources, and human safety in the DRB, highlighting the urgent need for integrated fire management strategies and sustainable land use planning to mitigate these cascading impacts (BEUCHLE *et al.*, 2022).

Figure 24 - Spatial trend of temperature extremes.

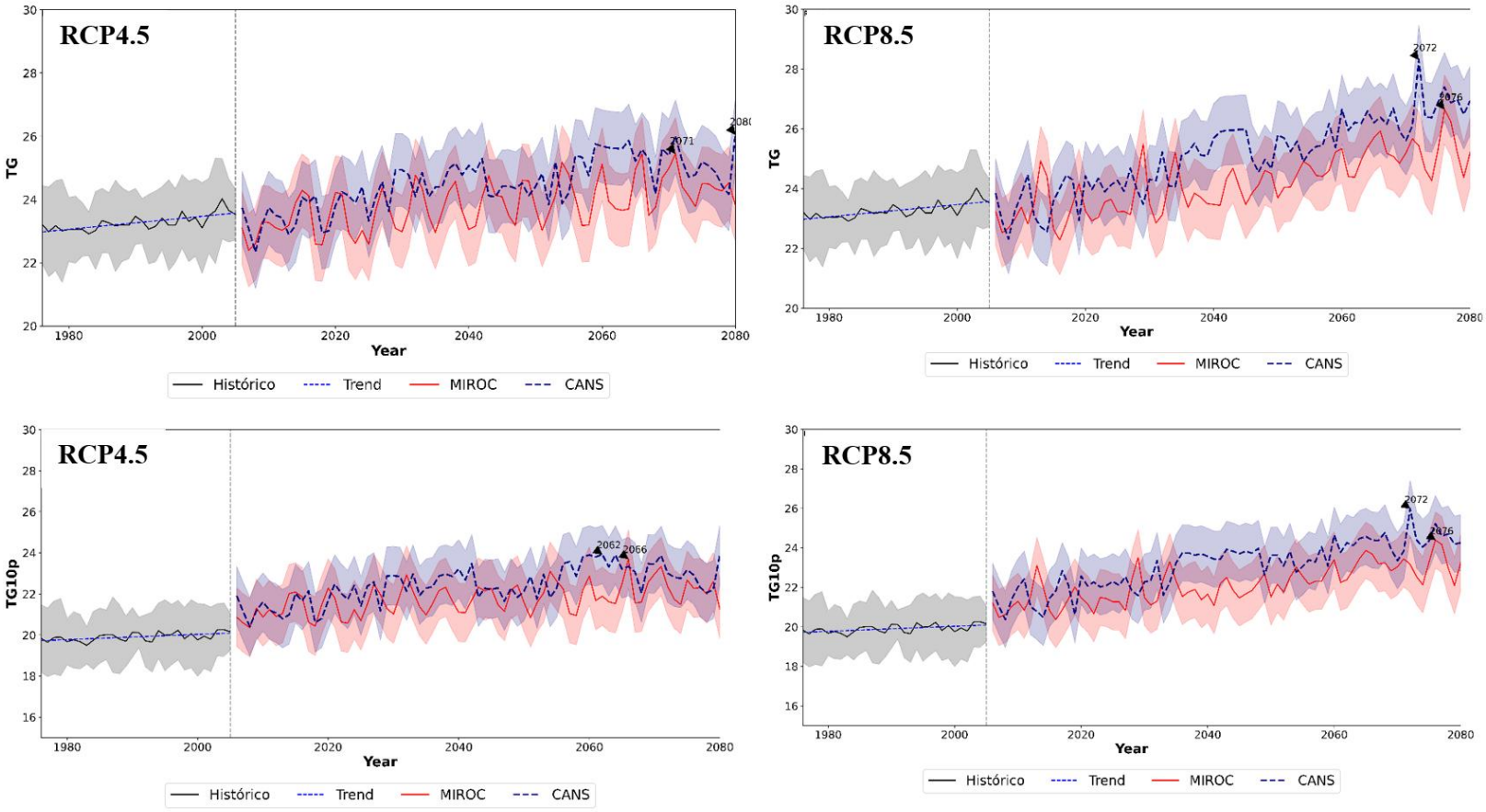

Source: elaborated by the author.

Figure 25 - Continuation Figure 24.

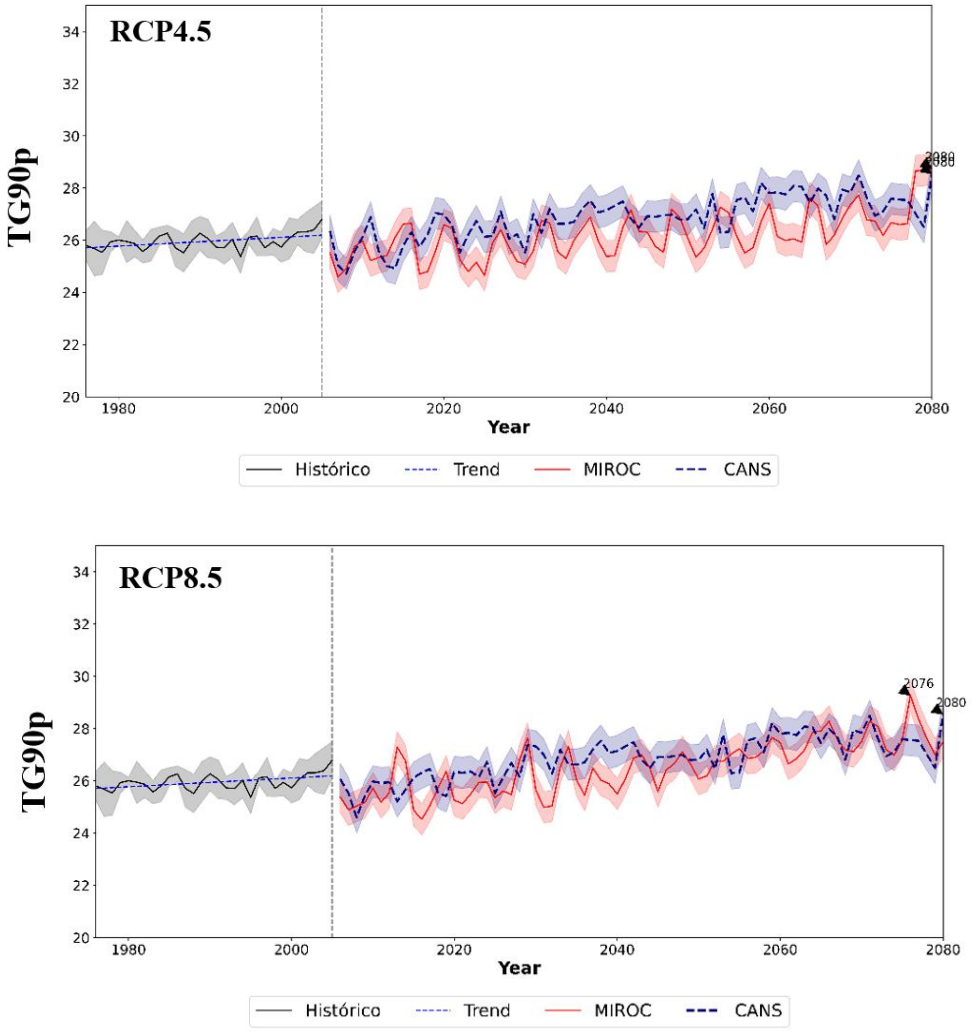

Source: elaborated by the author.

5.7.7 Spatial Trends of Temperature Extremes

The spatial analysis of temperature indices (TG, TG10p, TG90p) in the DRB under the RCP4.5 and RCP8.5 scenarios highlights significant variations across different regions of the basin and among climate models. Figure 26, illustrates the spatial distribution of temperature within the basin, emphasizing areas with statistically significant changes and the models that show the greatest agreement in their projections.

In the emission stabilization scenario (RCP4.5), a moderate increase in average temperature (TG) is observed, with statistical significance across much of the basin, ranging from 0.5°C to 0.9°C. In contrast, under the high-emission scenario (RCP8.5), the increase in average temperature is more pronounced and spatially uniform, with much of the basin experiencing variations up to 0.9°C, particularly in the central, northwestern, and western regions. These areas coincide with regions undergoing significant land-use changes related to agricultural expansion and loss of native vegetation, as shown in Figure 12, 13 and 14. The conversion of forests to agricultural land reduces the natural cooling capacity of the region, increasing soil temperatures and, consequently, local averages (HU *et al.*, 2021). This scenario makes these areas particularly vulnerable to extreme heat events, exacerbating water stress and challenges for sustainable agriculture (GROSSMAN-CLARKE *et al.*, 2010; RUSTICUCCI, 2012; XU *et al.*, 2023).

The analyzed climate models indicate that the TG10p index, which measures the lowest temperatures, shows an increasing trend across much of the basin, with values ranging from 0.4°C to 0.9°C. Meanwhile, maximum temperatures (TG90p), which reflect the hottest days, exhibit more pronounced upward trends in the central and northwestern regions of the basin, with projected increases of up to 0.9°C. In the RCP8.5 scenario (Figure 26), these increases become even more significant, particularly in the central and western regions, where values may reach up to 1.3°C. The northern, northwestern, and southwestern regions, which show the largest increases in maximum temperatures, also have high probabilities of native vegetation loss due to agricultural expansion.

While the models show differences in projected intensities, they consistently capture the trends, emphasizing the relevance of these results for future scenarios (BAZZANELA *et al.*, 2024; FIRPO *et al.*, 2022; VEIGA *et al.*, 2023).

Figure 26 - Spatial trend of extreme temperature events with the CanESM2 and MIRC5 models. Regions with significant trends (dotted).

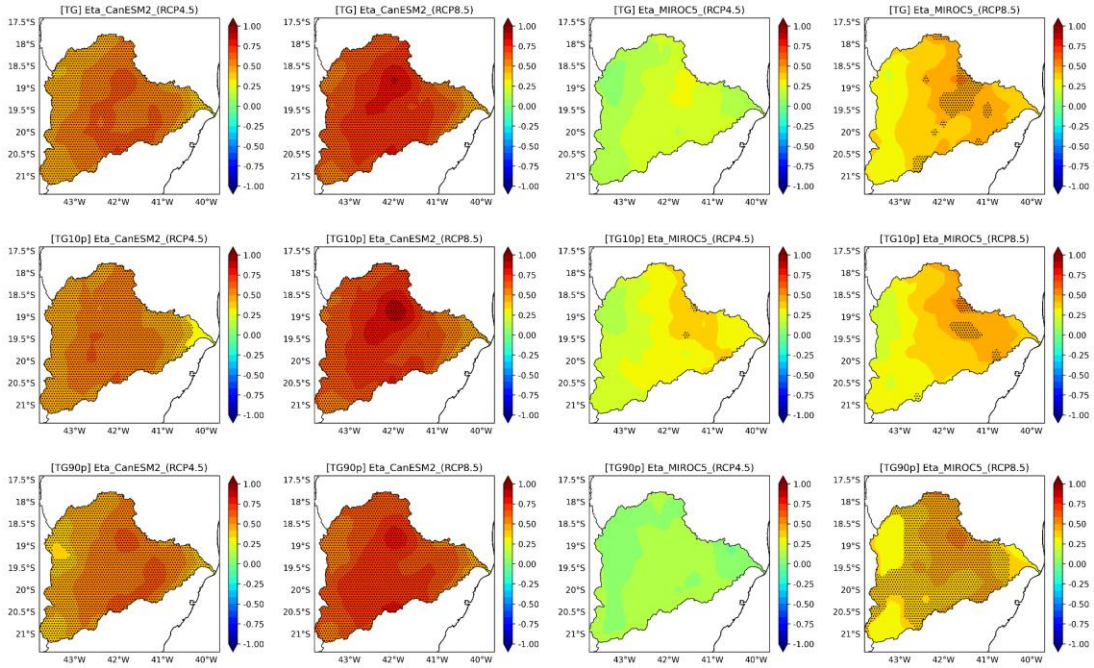

Source: elaborated by the author.

5.8 Conclusions

This study primarily aims to identify the regions within the Doce River Basin (DRB) undergoing significant land-use and land-cover changes, and to assess the intensity and frequency of extreme climate events occurring in these same areas. The spatial analysis revealed that the southern, southwestern, northern, and northeastern regions of the basin are the most affected by land-use transitions, such as the replacement of native forests with agricultural land and pastures. These regions therefore concentrate the highest risks associated with the intensification of climate extremes and are priority zones for mitigation and adaptation strategies.

Land-use projections were derived from future scenarios provided by CMIP6 (Land-Use Harmonization 2 – LUH2) and a dynamic land-use model developed on the Dinamica EGO platform, enabling an integrated and realistic assessment of the expected transformations by the end of the century. By integrating these data with high-resolution regional climate projections under RCP4.5 and RCP8.5 scenarios, it was observed that areas undergoing the greatest forest cover conversion also experience a significant increase in the frequency and intensity of extreme events, such as CDD exceeding 70 days in the northern and western regions, and extreme precipitation events (RX1day and RX5day) surpassing 170 mm/year in the eastern and central parts of the basin.

Moreover, the loss of native forest cover in the western, northwestern, and parts of the northern DRB is associated with a decline in total precipitation (PRCPTOT), coupled with a rise in rainfall variability and intensity. This shift suggests a more irregular precipitation regime, characterized by prolonged dry spells interrupted by intense rainfall episodes. In addition, the rise in extreme temperatures (TG90p), reaching up to 1.3°C in these regions, further exacerbates the challenges to agricultural sustainability and water resource management, revealing strong feedback mechanisms between deforestation, climate change, and hydroclimatic extremes.

These findings underscore the urgent need for integrated public policies that align land-use planning with climate adaptation. Preserving legal reserves, promoting forest restoration in the most critical regions, and implementing sustainable agroecological practices are essential actions to balance production and conservation, ultimately reducing the socio-environmental vulnerability of the DRB in the face of future climate scenarios.

Summary of Findings and Practical Implications

The projected scenarios reveal worrying trends of native forest loss and a significant increase in agricultural areas, particularly in the northern, north-western, and western regions of the DRB. This dynamic underscores the urgent need to integrate resilient agricultural practices and forest restoration policies to mitigate impacts on soil, water resources, and biodiversity while avoiding environmental degradation cycles that exacerbate socio-economic vulnerabilities.

Examples of Inspiring Practical Solutions

National and international experiences suggest that mechanisms such as Payments for Ecosystem Services (PES) and incentives for adopting regenerative agricultural practices can be effective strategies to balance environmental conservation with agricultural production. These programs, combined with rigorous enforcement of the Forest Code and the restoration of degraded areas, could enhance the resilience of the basin and its local communities to climate change impacts.

Linking to Biodiversity and Local Communities

Beyond land-use changes, the projected transformations threaten local biodiversity and the well-being of populations dependent on the ecosystem services provided by the basin, such as water supply, agricultural pollination, and erosion control. Mitigation strategies must not only focus on recovering native vegetation but also actively involve local communities, which play a key role in sustainably managing these resources.

Emphasizing the Urgency of Action

Given the rapid pace of the projected changes, it is imperative to implement mitigation and adaptation measures without delay. Inaction could lead to irreparable losses, including soil degradation, compromised water security, and a dramatic reduction in the basin's agricultural capacity. Integrated environmental management policies must be treated as a priority to safeguard natural resources and the quality of life for future generations.

Specific Proposals for Future Research

Future research should explore the impacts of climate change on biodiversity and ecological connectivity within the basin, investigating how ecological corridors could be implemented to minimize habitat fragmentation. Furthermore, studies evaluating adaptation scenarios that incorporate innovative technologies, such as remote sensing and predictive modeling, could provide more robust support for sustainable territorial planning.

6 CHAPTER 6: VEGETATION RESPONSE TO EXTREME RAINFALL AND DROUGHT EVENTS IN DEFORESTED AREAS OF THE DOCE RIVER BASIN.

6.1 Abstract

Climate change has increased the frequency and intensity of extreme events, affecting ecosystems globally. In the Doce River Basin (DRB), a region historically impacted by deforestation and the Mariana disaster (2015), the interaction between droughts, extreme rainfall, and vegetation response remains insufficiently understood. This study investigates the relationships between extreme climate events and vegetation dynamics through wavelet coherence analysis, exploring multi-scale patterns of vegetation response—an approach not previously applied in this context. Time series of the Enhanced Vegetation Index (EVI) and climate indices SPI (1, 3, and 6 months), RX1day, RX5day, PRCPTOT, and CDD from 2000 to 2023 were analyzed to identify spatial and temporal trends across the basin. The results show that vegetation responds to extreme precipitation events—RX1day, RX5day, PRCPTOT, and CDD—predominantly on time scales of 8 to 16 months, reflecting a seasonal recovery pattern. In contrast, vegetation responds to drought events (SPI_1, SPI_3, and SPI_6) more quickly, within 2 to 4 months and at most up to 8 months, with increased sensitivity observed in the post-disaster period. This asymmetry suggests that, under climate change, the impacts of degradation (drought-induced stress) are manifesting more rapidly than the processes of vegetation recovery, indicating a delayed regeneration dynamic. These transformations are particularly evident in the northwestern, southwestern, southern, and northern regions of the basin, where significant native forest loss and agricultural expansion have occurred. In these areas, SPI_3 and SPI_6 exhibit negative trends, pointing to an increased frequency of prolonged droughts, while RX1day and RX5day show strong spatial variability associated with remaining forest cover. The findings highlight the urgent need for public policies that integrate environmental conservation, forest restoration, and sustainable agricultural practices to reduce the socio-environmental vulnerability of the DRB under future climate change scenarios.

[3] ***Article Submitted*** to the journal for peer review.

6.2 Introduction

Over the past four decades, we have witnessed a continuous rise in temperatures, making this period the hottest since 1850. Between 2011 and 2020, a 1.59°C increase in land temperatures was observed, surpassing the 0.88°C increase recorded in the oceans. Global warming has significantly accelerated since 1970, exceeding any other 50-year period in the last two millennia, as indicated in the latest report from the Intergovernmental Panel on Climate Change (IPCC, 2022, 2023). Additionally, the Copernicus Climate Change Service (C3S) of the European Union confirmed that, global average temperature reached 15.10 °C, which is 0.72 °C above the 1991-2020 average and 0.12 °C above the previous record set in 2023. Notably, 2024 was the first year in which the average temperature exceeded the pre-industrial level by 1.5 °C. The report highlighted that the amount of water vapor in the atmosphere reached a record high, approximately 5 % above the 1991–2020 average. The increase in temperature and humidity contributed to the development of significant storms, including tropical cyclones. Furthermore, prolonged periods of drought in various regions created favorable conditions for wildfires (COPERNICUS, 2024).

IPCC projections for the period between 2081 and 2100 point to an additional global temperature increase ranging from 1°C to 1.8°C under the optimistic emissions scenario (RCP2-45) and from 3.3°C to 5.7°C under the pessimistic scenario (RCP5-85), compared to the decades of 1850 to 1900. Such changes foretell a future scenario with more frequent and intense climate extremes, ranging from heatwaves to extreme rainfall and drought events across various regions of the world.

Despite the clear influence of these changes on climatic conditions, studies addressing the impact of extreme events on vegetation response remain scarce in the context of the DRB. The increasing incidence of extreme rainfall events and rising temperatures are triggering alterations in the distribution and displacement of plant ecosystems, highlighting the urgency of understanding the implications of these transformations. Understanding these phenomena is crucial to anticipating future challenges and developing effective adaptation and mitigation strategies. Despite the alarming projections, uncertainty persists, particularly at smaller temporal and spatial scales, underscoring the need for further investigations to better comprehend the local impacts of these extreme events (DE ALMEIDA *et al.*, 2019).

From the perspective of vegetation cover, climate change exerts a broad impact, manifesting on both global and regional scales. In the DRB context, various studies have contributed to understanding vegetation dynamics, employing diverse approaches. One example is the work of Silva; Siqueira (2017), which utilized the NDVI (Normalized Difference Vegetation Index) and SAVI (Soil Adjusted Vegetation Index) indices derived from Landsat images captured by the TM and OLI sensors. These indices were used to assess changes in dense vegetation, grassland, and exposed soil. The results revealed significant losses in grassland and increased soil exposure, with 2016 highlighted as a critical year, during which almost 100% of vegetation was lost. This data underscores severe degradation in areas surrounding the DRB. Another relevant approach was conducted by Almeida et al., (2020), who employed a multi-criteria analysis to establish priorities for recovering degraded areas within the basin. Using images from the RapidEye satellite, the study identified that approximately 60% of the analyzed area, corresponding to about 24% of the DRB, demonstrates a need for vegetation recovery classified as medium to very high. These findings provide essential insights for developing restoration strategies and sustainable management in the region (ALMEIDA *et al.*, 2020).

The transformations in vegetation cover before and after the disaster were analyzed in the study by Silva et al. (2020), which highlighted the potential of the NDVI in identifying changes in soil cover. Recently, a study on land cover changes resulting from the Mariana disaster in Minas Gerais, Brazil, using a time series of vegetation indices, indicated the degradation of over 300 hectares due to the collapse of the Fundão dam (CARMO *et al.*, 2017; NEVES *et al.*, 2024). The temporal analysis associated with precipitation estimation was investigated employing linear trend techniques and correlations (FORMIGONI, 2018).

Formigoni (2018) observed that significant trends are mainly concentrated in areas of vegetation and forest remnants, while areas used for agricultural activities, pasture, and farming show non-significant trends. However, the DRB is sensitive to climate extremes, with an uneven distribution of rainfall, as the western part is more susceptible to extreme events due to higher rainfall accumulation compared to the eastern part of the basin (LIMA; CUPOLILLO, 2018). For instance, climatological droughts in the middle Doce River region have manifested as events of greater duration and intensity (LIMA, 2016). In this context, there is a likelihood of a more critical and challenging future regarding water resource management in the basin, although there is no defined or probabilistic timeline for such occurrences (JESUS *et al.*, 2020; LIMA, 2016).

The Renova Foundation (an organization dedicated to environmental conservation and sustainable development) recently completed the implementation of forest restoration in preservation areas affected by tailings (MAY *et al.*, 2020). However, a gap is evident in the climate-focused approach regarding extreme events in the DRB. Despite advances in the study of extreme climate events, critical gaps remain in understanding how vegetation responds to these events on broader temporal and spatial scales, particularly in areas of high deforestation. Unlike previous studies, which have analyzed climate trends and vegetation changes separately, this study adopts an integrated approach to assess vegetation response to extreme climate events in the Doce River Basin.

The interaction between extreme climate indices—such as SPI (1, 3, and 6 months), RX1day, and RX5day, PRCPTOT, and CDD— and vegetation response in areas of intense degradation is still partially unknown. Moreover, there are no records of studies that have applied wavelet coherence analysis to investigate these interactions in the basin, specifically concerning drought and extreme precipitation events. This methodology will allow us to identify how vegetation responses occur at different temporal scales and whether there is a lag or coupling with extreme climate events, particularly in deforested areas.

Another key aspect of this research is the investigation of how trends in extreme events have changed since the Mariana disaster (2015) and whether there has been a shift in vegetation response over time, especially in the year of the disaster and in the subsequent years. This is particularly important, as the environmental impacts of this event altered water availability and soil structure, possibly amplifying or modifying vegetation resilience to climate variations.
Understanding these dynamics is crucial not only for advancing ecological research but also for providing insights for forest restoration strategies and environmental management. Identifying critical areas where extreme climate events accelerate vegetation degradation can help guide reforestation efforts and policies for sustainable water resource management in the Doce River Basin. Given the urgency to understand these impacts, this study aims to address these knowledge gaps by investigating the complex relationship between extreme climate events and vegetation dynamics in the DRB. The main objectives of the study are: (a) to identify spatial and temporal trends in EVI and extreme rainfall and drought events, mapping critical areas of ecological vulnerability; (b) to examine trends in extreme climate indices in regions of high deforestation, assessing their cumulative impacts on vegetation; and (c) to explore vegetation responses to extreme climate events through wavelet coherence analyses across multiple

temporal scales, unraveling the processes that connect abrupt environmental changes to ecological resilience in the basin.

6.3 Materials and Methods

6.3.1 Study Area

Our main focus is the DRB, with considerations for a possible expansion of the study area to achieve a broader understanding of the spatial patterns of extreme events. It is important to emphasize that the expansion of the analysis area aims solely to identify and contextualize external pressures that may influence the DRB. This study does not seek to discuss in detail the environmental dynamics of other regions included in the maps. This methodological choice was made to enhance understanding of how human activities in nearby areas can compromise the environmental resilience of the DRB, offering an integrated and strategic perspective for the management of its natural resources.

Scientific studies demonstrate that deforestation in one region can trigger effects in neighboring areas, influencing the migration of vegetation ecosystems and catalyzing anthropogenic pressures in adjacent river basins. For instance, in the São Francisco River Basin, the intensification of anthropogenic activities, such as agricultural expansion and the conversion of native areas into pastures, has generated impacts that are not confined to the basin itself. These pressures can migrate to neighboring regions, including the western portion of the Doce River Basin, exacerbating existing environmental and climatic challenges (NEVES *et al.*, 2024; SVENNING; SANDEL, 2013). Therefore, although the central focus of this study remains on the DRB, the analysis was strategically expanded to include some areas of Minas Gerais state outside the basin's boundaries.

Located in southeastern Brazil, the basin lies between the parallels 17°45' and 21°15' S and the meridians 39°30' and 43°45' W (Figure 27), encompassing part of the Southeast Atlantic Hydrographic Region. With a drainage area of 86,715 km², approximately 86% of the basin is located in Minas Gerais, while the remaining 14% is in Espírito Santo. The basin includes 230 municipalities and is home to approximately 2.34 million urban inhabitants and 833,000 rural inhabitants (PIRH, 2010). The basin’s economy is diverse and plays a crucial role in the management of its water resources. Key economic activities include mining, agriculture, pig farming, and the food industry (PIRH, 2010). Water use in the basin reflects this economic diversity: 38.2% is allocated to multiple uses, 30.1% to public supply, 19.3% to the industrial sector, 3.3% to mining activities, and 1.6% to other uses (PIRH, 2010).

In 2015, the basin was the site of one of Brazil's largest environmental disasters: the collapse of the Fundão dam in Mariana (MG). This event released millions of cubic meters of mining tailings into the Doce River, devastating aquatic ecosystems, biodiversity, and water quality and causing severe social and economic consequences for local populations (G1, 2021; PORTAL GOV, 2015).

These characteristics, combined with the challenges posed by extreme climate events, underscore the Doce River Basin's strategic importance from environmental and economic perspectives. Thus, it is a critical region for studies assessing the impacts of climate change and promoting sustainable water resource management.

Figure 27 - Study area Doce River Basin.

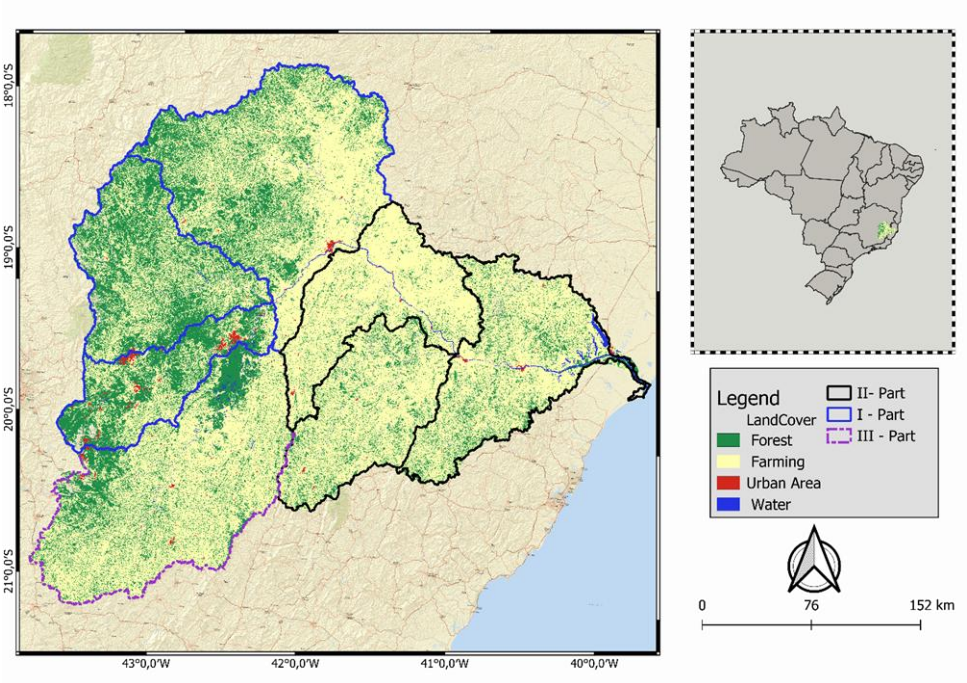

Source: elaborated by the author.

6.4 Data

6.4.1 Rainfall Data

Precipitation data from the Climate Hazards Group InfraRed Precipitation (CHIRPS, Funk et al., 2015), available at https://www.chc.ucsb.edu/data/chirps, were used for the calculation of SPI and other extreme rainfall indices. According to Funk et al. (2014), CHIRPS integrates three main sources: (1) monthly precipitation climatology (CHPClim); (2) thermal infrared (IR) geostationary satellite data provided by NOAA and CPC; and (3) in-situ precipitation data from sources such as the Global Historical Climate Network (GHCN), Global Summary of the Day (GSOD), and the Global Telecommunication System of the WMO. Additionally, since 2020, precipitation measurements from approximately 3000 rain gages in the Brazilian National Center for Monitoring and Alerts for Natural Disasters (CEMADEN/MCTI) observational network have been included in the CHIRPS dataset.

Monthly precipitation data were used for the period from January 2000 to December 2023, with a spatial resolution of 0.05°. These data provide a robust foundation for analyzing precipitation variability and its regional impacts.

6.4.2 Vegetation Index Data

EVI (Enhanced Vegetation Index), similar to the NDVI (Normalized Difference Vegetation Index), is an index used in remote sensing to monitor and evaluate the health and density of vegetation on the Earth's surface. However, the EVI was developed to overcome some limitations of the NDVI, offering greater sensitivity in areas of dense vegetation and reducing the influence of atmospheric and soil factors (ZHENGXING *et al.*, 2003). EVI data with a spatial resolution of 250 meters were obtained through AppEARS/Earthdata (https://appeears.earthdatacloud.nasa.gov/). These data are available on a monthly/daily scale and provided in GeoTIFF or NetCDF format.

6.4.3 Deforestation Data

The deforestation data, used to assess how areas with trends in extreme indices are changing in deforested regions between 2000 and 2023 in the DRB, were obtained from the

PRODES system (Monitoring Program of Deforestation in the Legal Amazon by Satellite), accessible via the TerraBrasilis portal. Developed by the National Institute for Space Research (INPE). PRODES conducts systematic annual monitoring of clear-cut deforestation in native vegetation areas, employing high-resolution satellite imagery to ensure accuracy in identifying land-use changes.

The system defines deforestation as the complete removal of native vegetation, regardless of the future use of these areas. This definition encompasses conversion to agricultural use as well as other forms of land use, such as pasture, mining, or urbanization. The data provided by PRODES offer a robust and reliable basis for investigating the relationship between extreme climatic indices and deforestation dynamics in different regions, contring to the undeanding of interactions between environmental and anthropogenic changes.

6.5 Methods

6.5.1 Extreme Indices

The extreme climatic indices analyzed in this study are described in Table 8. These indices, widely recognized and utilized by the scientific community, were developed by the European Climate Assessment & Dataset (ETCCDI) and are based on fundamental climatic variables such as air temperature and precipitation. The indices were calculated using the Python library icclim (Index Calculation for CLIMate), which strictly adheres to the methodological standards established by the ETCCDI, ensuring the standardization and comparability of results (CHERVENKOV; SLAVOV, 2021).

The indices were generated using daily precipitation data from the CHIRPS dataset. To ensure accuracy and methodological compliance, a custom algorithm was developed to implement the procedures of icclim, tailoring them to the specific characteristics of the study region and the analysis requirements. This customized approach enabled tighter control over the calculation process, ensuring consistency, quality, and reliability in the results obtained.

The climatic indices were calculated monthly and annually, providing a detailed and comprehensive analysis of climatic variations in the region. The monthly evaluation covers the period from 2000 to 2023, allowing the observation of seasonal fluctuations and specific climatic events, while the annual-scale analysis enables the identification of long-term climatic trends and patterns over the same time span. This combined approach contributes to a deeper understanding of climatic dynamics and their impacts on the study area.

Table 8 - Summary of climate indices analyzed in this study.

Index	Description
PRCPTOT	Total annual precipitation (mm). Represents the sum of all daily precipitation throughout the year.
RX1day	Maximum daily precipitation (mm). Represents the highest amount of precipitation recorded on a single day during the year.
RX5day	Maximum precipitation over 5 consecutive days (mm). Represents the highest amount of precipitation accumulated over a period of five consecutive days throughout the year.
CDD	Maximum number of consecutive dry days. Represents the longest sequence of consecutive days without significant precipitation.

Source: elaborated by the author.

6.5.2 SPI Calculation

The SPI (Standardized Precipitation Index) is widely used to characterize droughts, assessing the spatial and temporal variation in their severity (MCKEE, 1995; MCKEE *et al.*, 1993). In this study, the SPI-1, SPI-3, and SPI-6 scales were employed to analyze the spatiotemporal characteristics of droughts. These scales were selected because they effectively capture short-term vegetation responses to drought events, providing a dynamic view of the relationship between precipitation and vegetation indices such as EVI (LI *et al.*, 2021).

The SPI is calculated over different temporal scales, considering accumulated precipitation periods (Barker et al., 2016). In this study, monthly precipitation time series from 2000 to 2023 were used to evaluate climatic variability across various temporal scales.

The SPI calculation is based on fitting monthly precipitation time series to a gamma probability density function, as defined by Equation (1). In this equation, $\alpha>0$ represents the shape parameter, $B>0$ represents the scale parameter, x represents monthly precipitation, and g is the incomplete gamma function. Using these parameters, the cumulative probability of an observed event for each month is calculated. This probability is obtained by solving the integral of the gamma cumulative distribution function, as outlined in Equation (10).

This method robustly identifies precipitation anomalies, which is essential for understanding the impacts of droughts on vegetation and ecosystems. The approach used in this

study ensures methodological consistency and accuracy in analyzing vegetation responses to short-term precipitation variations.

$$G(X) = \int_0^x g(x) = \int_0^x \frac{x^{\propto-1} e^{-x/B}}{B^{\propto} T(\propto)} \quad (10)$$

The values resulting from this function are adjusted to the inverse normal distribution with a mean of zero and a standard deviation of one. This distribution produces SPI values that can be represented by Equation 11.

$$SPI = \Psi^{-1}[G(x)] \quad (11)$$

Where Ψ^{-1} It is the inverse of the normal probability function with a mean of zero and a standard deviation of one. Further details about the calculation are thoroughly addressed in the work of McKee et al. (1993). Drought events are considered when the SPI reaches values less than or equal to -1, as shown in Table 9.

Table 9 - Classification of SPI.

Drought Grade	SPI Value
Extreme drought	SPI ≤ −2.00
Severe drought	−2 < SP I ≤ −1.5
Moderate drought	−1.5 < SPI ≤ −1
Mild drought	−1 < SPI ≤ −0.5
Normal	SPI ≥ −0.5

Source: elaborated by the author.

6.5.3 Trend Analysis

To evaluate trends in precipitation and drought indices, we applied a non-parametric method that identifies the magnitude and direction of trends in the study area. The analysis was based on the Kendall Tau statistic and Theil-Sen slope (GILBERT, 1987; SEN, 1968; SIEGEL, 1982; THEIL, 1950), applied to gridded time series of SPI_1, SPI_3, and SPI_6, as well as extreme precipitation indices (RX1day, RX5day, PRCPTOT, and CDD).

The Kendall Tau statistic measures monotonic trends in time series, expressing the proportion between the observed rank correlation score and the maximum possible score. For this, the data are ranked in ascending order of time, and the score is calculated for each time series. Tau values range from -1 to +1, where negative values indicate a downward trend (more negative "steps") and positive values indicate an upward trend (more positive "steps").

The Theil-Sen slope provides a robust estimate of trend magnitude by calculating the median of the slopes between all possible pairs of points in the time series. This approach is less sensitive to outliers, making it suitable for climatic time series. We used a significance level of $\alpha = 0.05$ to determine statistically significant trends. This analysis helps distinguish between natural variability and significant changes in the time series. Further details on the structure and application of these methods can be found in (EL-NESR *et al.*, 2010).

6.5.4 Coherence analysis

The Wavelet Coherence Transform (WTC) is a powerful tool for investigating the relationship between extreme events, drought conditions, and vegetation in the Doce River Basin (DRB). Combining WTC with cross-spectral analysis offers an innovative methodology for signal analysis, enabling the exploration of complex patterns and multiscale dynamics (IRANNEZHAD *et al.*, 2020). The WTC computes a coherence coefficient that is localized in both time and frequency, allowing for a detailed analysis of the linear connection between two non-stationary time series across different temporal and spectral scales (DONG *et al.*, 2020; KIRBY; SWAIN, 2004). This capability makes WTC an essential tool for identifying dynamic temporal and spectral relationships, providing deeper insights into the interactions between extreme climatic events and environmental variables.

To ensure statistical robustness, the significance level of WTC was estimated through Monte Carlo simulations, with 1000 iterations, ensuring the reliability of the results. The cone of influence was employed to delineate regions where the analysis remains statistically valid, adopting a significance level of 5% (corresponding to a confidence level of 95%) (GRINSTED *et al.*, 2004). Mathematically, WTC is computed as the squared cross-spectrum of the two time series, normalized by their individual power spectra. This normalization provides a measure of cross-correlation as a function of frequency, allowing for the identification of consistent patterns between the series (TORRENCE; COMPO, 1998).

In this study, WTC was applied to assess the relationship between the Enhanced Vegetation Index (EVI) and extreme climatic events, including precipitation and drought indices. Before conducting the wavelet analysis between EVI and the climatic indices (SPI-1, SPI-3, and SPI-6) as well as extreme precipitation indices (RX1day, RX5day, PRCPTOT, and CDD), the EVI accumulated score was calculated. This score was computed for each grid point, summing EVI variations over time to account for seasonal trends and interannual variability. This step ensures the adjustment of the data and facilitates the identification of significant changes in vegetation response to extreme climatic conditions, thereby improving the sensitivity of the analysis. Additionally, WTC was used to analyze the relationship between EVI and extreme climatic indices, focusing on temporal and spectral coherence (HU; SI, 2016).

To assess the temporal phase relationship, WTC phase angles were analyzed to determine whether EVI variations lead or lag behind extreme climatic indices. Arrows pointing to the bottom-right or top-left indicate that EVI leads the climatic variable. Arrows pointing to the top-right or bottom-left indicate that climatic indices lead EVI in the identified scales. This methodology enables the precise identification of temporal and spectral relationships between EVI and extreme climatic events, providing a better understanding of vegetation responses to environmental changes.

Equation 12 describes the entire process employed in the analysis, where $w^{\leftrightarrow Y,X}$ represents the cross-wavelet power spectra, referring to the smoothed matrix of auto- and cross-wavelet power spectra between the various predictor variables X and the response variable Y.

$$\rho_m^2(s,\tau)\ \frac{w^{\leftrightarrow Y,X}(s,\tau)w^{\leftrightarrow X,X}(s,\tau)^{-1}w^{\leftrightarrow Y,X}(s,\tau)^*}{w^{\leftrightarrow Y,Y}(s,\tau)} \qquad (12)$$

Thus, an arrow in the wavelet coherence plots represents the phase lead/lag relationships between the examined series. A zero-phase difference indicates that the two-time series move together on a specific scale. Arrows pointing to the right (left) signify that the time series are in phase (antiphase). When the series are in phase, it means they move in the same direction, while antiphase indicates they move in opposite directions (Figure 2).

Arrows pointing to the bottom-right or top-left indicate that the first variable is leading, whereas arrows pointing to the top-right or bottom-left indicate that the second variable is leading (Figure 28).

Figure 28 - Phase differences of time series X(t) against time series Y(t) in cross-wavelet analysis.

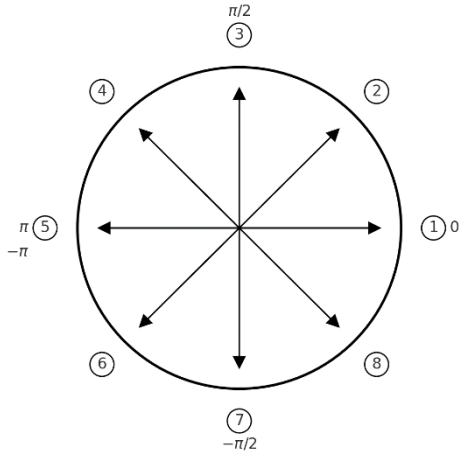

Phase	Interpretation
P1	In phase | Positive correlation
P2	In phase | Leading X(t), lagging Y(t)
P3	Transition π/2
P4	Out of phase | Leading Y(t), lagging X(t)
P5	Out of phase | Negative correlation
P6	Out of phase | Leading X(t), lagging Y(t)
P7	Transition -π/2
P8	In phase | Leading Y(t), lagging X(t)

Source: elaborated by the author.

6.5.5 Limitations of Wavelet Coherence Transform

The Wavelet Coherence Transform (WTC) is a powerful tool for analyzing the relationship between vegetation and extreme climatic events, offering unique insights into temporal and spectral dynamics. However, like any analytical method, it has certain limitations that should be acknowledged without undermining its value. One key consideration is its sensitivity to strong seasonality and long-term trends in vegetation indices, which can mask more subtle responses to climatic extremes. Proper preprocessing, such as detrending and seasonal adjustment, is crucial to enhance the accuracy of the analysis (GRINSTED *et al.*, 2004).

Another limitation is related to the cone of influence, which reduces the reliability of results near the edges of the time series. While this can impact the analysis of abrupt changes

in vegetation, the use of sufficiently long time series minimizes this constraint. The WTC's reliance on linear associations is another factor to consider, as vegetation often responds to climatic events in nonlinear ways. However, this can be mitigated by complementing wavelet analysis with other statistical approaches to capture more complex interactions (IRANNEZHAD *et al.*, 2020).

6.6 Results

6.6.1 Spatial Trends (Rainfall Extremes) and Deforestation

The analysis of climate trends in the indices CDD, PRCPTOT, RX1day, and RX5day reveals a strong interaction between environmental characteristics and the observed impacts in the Doce River Basin (Figure 29). The basin shows distinct responses to precipitation extremes in areas with high deforestation, reflected in hydrological patterns and local ecological dynamics. Below, we discuss these interactions in detail.

The CDD index showed significant positive trends ($\tau > 0.62$) during the summer (DJF) in the DRB, indicating an increase in the duration of consecutive dry periods (Figure.24). This trend is particularly concerning as it suggests an intensification of prolonged drought conditions. With approximately 60% of the municipalities in the northern part of the basin located in Brazil's semi-arid region, this area already faces natural water deficits, further exacerbated by annual precipitation often below 800 mm (CUNHA *et al.*, 2015, 2019; MATEUS *et al.*, 2025; NATIVIDADE *et al.*, 2017; SONDERMANN *et al.*, 2022b).

The increase in CDD may further compromise the availability of surface and groundwater, increasing risks to agriculture and urban water supply in the region (NATIVIDADE *et al.*, 2017). Additionally, deforestation, concentrated in strategic areas of the basin, may be exacerbating the positive trends in CDD (Figure 29 and Figure 30). The removal of native vegetation reduces the soil's capacity for water infiltration and retention, exacerbating surface runoff and accelerating moisture loss during drought periods (FERREIRA, 2019; TIAN *et al.*, 2018).

It is observed that significant trends in the increase of dry days are concentrated in the northern and eastern sectors of the basin (Figure 29 and Figure 30). These areas have consequently experienced an expansion in agricultural activity and a corresponding decrease in water deficits. Additionally, there has been a less frequent positioning of the South Atlantic Convergence Zone (SACZ) over this part of the basin (Pires et al., 2017; Mateus et al., 2025). Thus, in Figure 30, it is possible to observe that areas with the highest deforestation coincide with statistically significant areas for consecutive dry days.

The PRCPTOT index showed negative trends, although not significant ($\tau < -1.5$), in some areas of the DRB, indicating a reduction in accumulated precipitation (Figure 29). This

pattern aligns with the observed increase in CDD, reinforcing the scenario of water deficit in the region. The relationship with deforestation is evident, as areas with high forest cover loss, as shown in Figures 29 and 30, exhibit greater susceptibility to changes in the microclimate and moisture recycling, exacerbating the effects of climate change (CORDEIRO *et al.*, 2022; DE SOUZA FERREIRA *et al.*, 2024; NEVES *et al.*, 2024).

The extreme precipitation indices, RX1day (maximum rainfall in 1 day) and RX5day (maximum rainfall over 5 consecutive days), reveal similar patterns in the DRB, particularly in the southern sector. RX1day shows a significant negative trend, indicating a reduction in the maximum rainfall volumes recorded in a single day. This region of the basin relies heavily on the South Atlantic Convergence Zone (SACZ), which, when positioned further south, plays a crucial role in local water supply. However, studies such as that by Mateus et al. (2025) highlight the decreasing frequency of SACZ occurrences in southern positions within the basin and the intensification of extreme events, which further exacerbate the water deficit in the region. This shift in climate patterns directly affects water availability and aquifer recharge, making the southern areas of the basin more vulnerable to water scarcity (MATEUS *et al.*, 2025).

Moreover, the areas in the southern sector of the basin that exhibit negative trends in RX1day coincide with regions of high deforestation rates (Figures 29 and 30). The loss of forest cover intensifies the impacts of climate change by reducing moisture recycling and the soil's water retention capacity. This creates a vicious cycle in which deforestation not only worsens drought conditions but also amplifies the effects of decreasing maximum rainfall events(LIMA; CUPOLILLO, 2018; VALVERDE *et al.*, 2003).

Regarding the RX5day index, negative trends ($\tau > -1.5$) are also observed in the southern sector of the basin, although they are less pronounced compared to RX1day. This pattern suggests that accumulated rainfall events over five consecutive days are becoming less frequent or less intense in this region of the basin, with some areas showing growth trends that are not statistically significant (MATEUS et al., 2025). Similar to RX1day, the areas with negative RX5day trends coincide with regions of high deforestation (Figure 30).

Figure 29 - Spatial distribution of the Mann-Kendall tau values (DJF) for time series (2000–2023) across the river basins of Minas Gerais. The analysis includes key climate indices: CDD (Consecutive Dry Days); PRCPTOT (Total Precipitation); RX1day (Maximum 1-day.

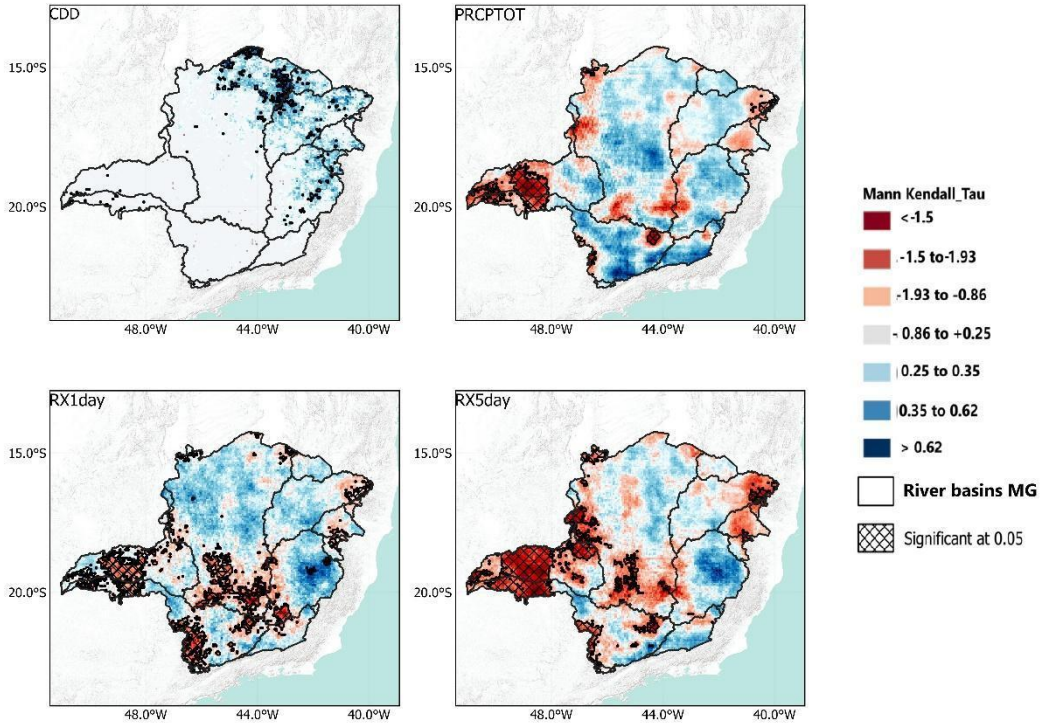

Source: elaborated by the author.

Figure 30 - Spatial distribution of Mann-Kendall tau values (2000–2023) for Minas Gerais River basins (DJF). Indices include CDD (Consecutive Dry Days), PRCPTOT (Total Precipitation), RX1day (Maximum 1-day Precipitation), and RX5day (Maximum 5-day Precipitation).

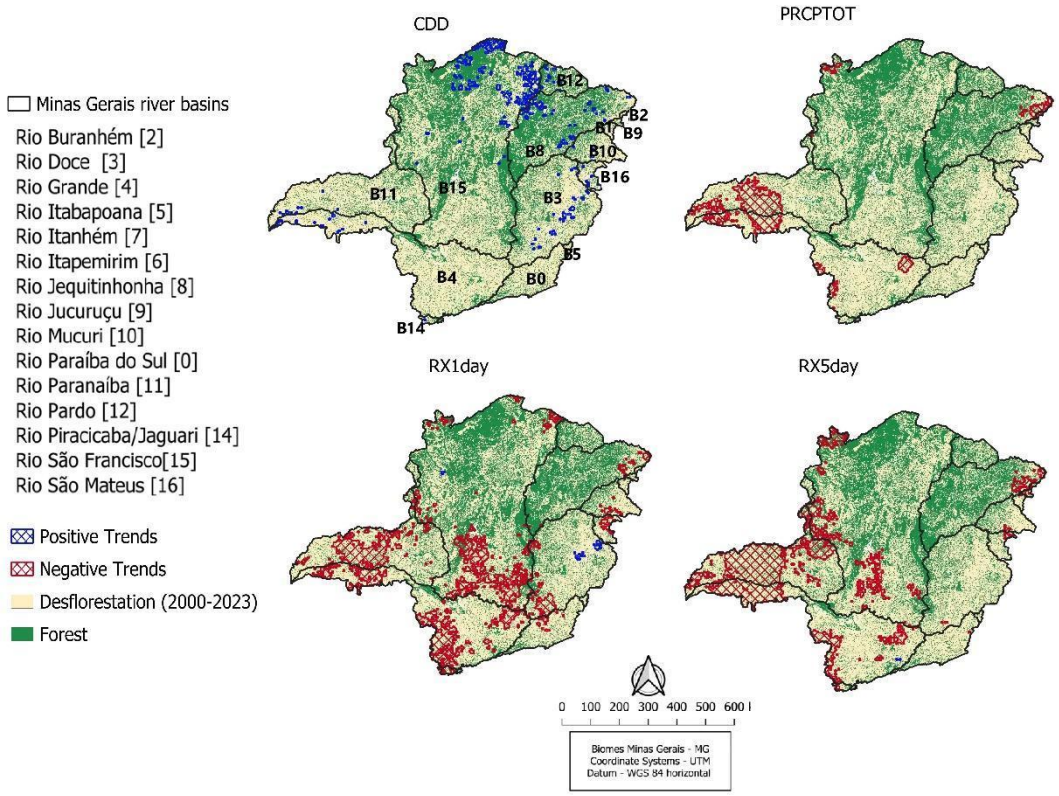

Source: elaborated by the author.

During the winter (JJA), the Doce River Basin shows positive trends in CDD ($0.35 < \tau < 0.62$), particularly in its western sector, indicating an increase in the duration of dry periods (Figure 31 and Figure 32). This pattern reflects the characteristic challenges of the dry season in maintaining water availability, which are aggravated by the vulnerability of northern regions of the basin near deforested areas and less protected by vegetation, where prolonged drought periods are more intense (ALMEIDA *et al.*, 2020; MAY *et al.*, 2020).

The PRCPTOT index exhibits significant negative trends ($\tau < -1.5$) in the far north of the basin, indicating a reduction in accumulated precipitation, which may compromise water recharge and the water security of local communities. This region of the basin was highlighted in the study by Campos et al., (2024) for future climate change scenarios. In contrast, areas in the central and western parts of the basin, where greater remnants of forest cover remain (Figure

31), show positive trends in PRCPTOT, emphasizing the essential role of forests in regulating the hydrological cycle, stabilizing rainfall, and mitigating water deficits.

The extreme precipitation indices, RX1day and RX5day, display similar patterns, with significant negative trends ($\tau < -1.5$) in the southern and western sectors of the basin. These reductions in the intensity of extreme rainfall coincide with areas of high deforestation rates and water deficits, as evidenced by Mateus et al., (2025). Continuous deforestation in these regions reduces the soil's water retention capacity and moisture recycling, intensifying the basin's vulnerability to prolonged droughts and the reduction of intense rainfall events. In summary, the results reinforce the strong connection between vegetation loss and the intensification of climate impacts in the Doce River Basin (HOYOS *et al.*, 2013; MA *et al.*, 2024; SMITH *et al.*, 2023; WEI *et al.*, 2024).

Figure 31 - Same as figure 3, but for JJA.

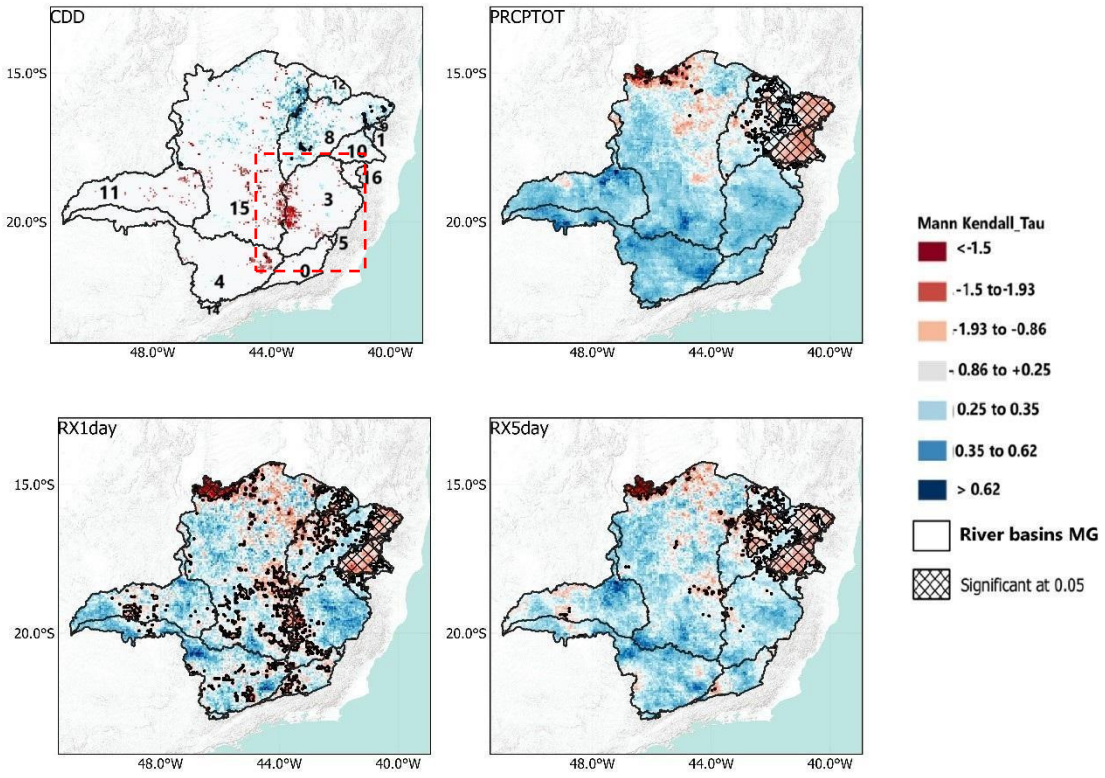

Source: elaborated by the author.

Figure 32 - Same as figure 4, but for JJA.

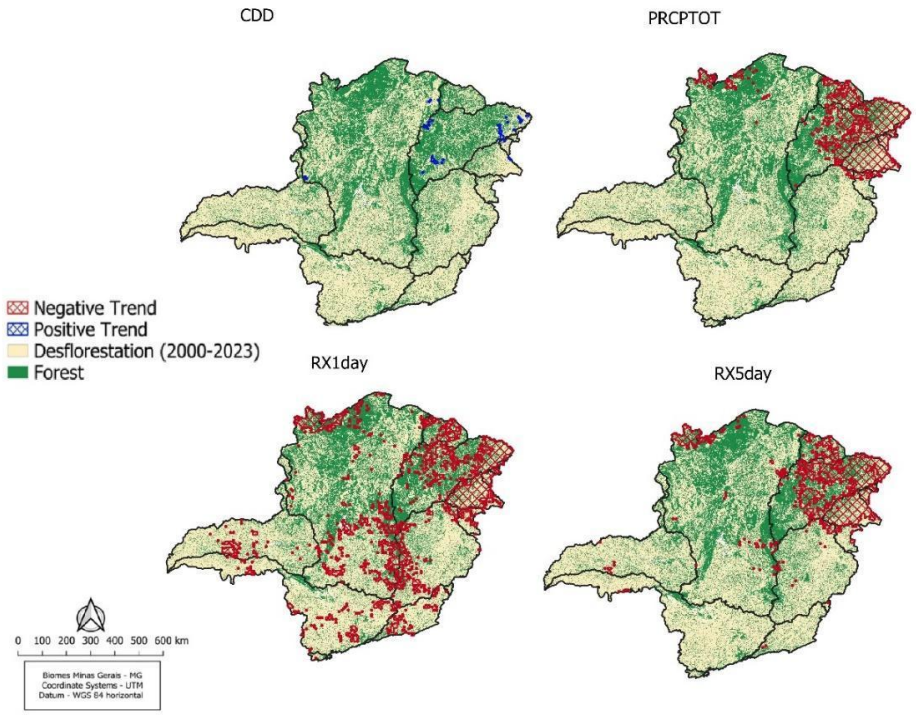

Source: elaborated by the author.

6.6.2 Connection between Extreme Events and EVI

The cross-wavelet coherence graphs provide a detailed insight into how vegetation (EVI) in the Doce River Basin (DRB) responds to different climatic indices, such as CDD, PRCPTOT, RX1day, and RX5day, across various temporal scales. This analysis is crucial for understanding the complex interactions between climate extremes, hydrological cycles, and ecosystems in the DRB—a region significantly vulnerable due to environmental degradation and climate change (CAMPOS *et al.*, 2024; CUPOLILLO *et al.*, 2008; MATEUS *et al.*, 2025).

Overall, vegetation response to extreme events showed strong coherence at the 8–16 month scales across the basin (Figure 33). The predominance of high coherence at this scale is

common, as vegetation does not immediately respond to drought or rainfall events—there is a lag time before changes in vegetation can be observed. This pattern has been documented in studies analyzing vegetation response to extreme events in various regions (KULESZA; HOŚCIŁO, 2024; REN *et al.*, 2022; WANG *et al.*, 2023; ZHANG *et al.*, 2017).

For the CDD index, vegetation response predominantly occurs out of phase, indicating that an increase in dry days is associated with a reduction in EVI values. In other words, vegetation shows signs of water stress. However, this response exhibits a delay, suggesting that vegetation takes time to manifest the impacts of consecutive dry periods and to recover after the end of such events in the DRB (Figure 31A).

This dynamic is consistent with studies such as Marengo et al. (2008) and Brito et al. (2022), which highlight that vegetation sensitivity to drought periods depends on factors such as soil water retention capacity, vegetation cover, and seasonal precipitation patterns. In the Doce River Basin (DRB), regions that have experienced deforestation or the replacement of native forests with pastures are particularly vulnerable, as exposed or compacted soil reduces water infiltration and amplifies the impacts of droughts (CUPOLILLO *et al.*, 2008; OLIVEIRA *et al.*, 2020; PIRES *et al.*, 2017).

Between 2014 and 2016, the wavelet coherence graph between EVI and CDD reveals a significant relationship on the 4 to 8-month scale (Figure 33A). During this period, the two variables are in phase, meaning there is synchronization between variations in consecutive dry days and EVI values. This implies that vegetation responded proactively to changes in drought conditions. The coherence between EVI and CDD on the 4 to 8-month scale may have been directly influenced by the 2015 environmental disaster in the Doce River Basin (NEVES *et al.*, 2024).

The environmental disaster may have intensified local variability in the relationship between EVI and CDD, reflecting the heterogeneity of the affected areas. While some regions may have experienced initial recovery due to vegetation resilience, others, more severely impacted, may have shown a sharp decline in EVI values(DE CARVALHO *et al.*, 2024; NEVES *et al.*, 2024).

The 2014–2016 period also coincides with adverse climatic conditions, including severe droughts in Brazil, potentially exacerbated by the El Niño event active in 2015 (ALMEIDA *et al.*, 2024; ANYAMBA *et al.*, 2019; KOGAN; AND GUO, 2017; MARENGO *et al.*, 2015).

The strong coherence between EVI and PRCPTOT on the 8 to 16-month scale shows that the indices are in phase, but PRCPTOT leads the relationship with a slight lag (Figure 33B). This

pattern suggests that vegetation directly depends on accumulated precipitation over longer seasonal cycles in the basin(ALMEIDA *et al.*, 2020; NEVES *et al.*, 2024). The lead of PRCPTOT over EVI may reflect the impact of rainfall events that provide sufficient water for vegetation to regenerate after periods of water stress. This is particularly evident in 2015–2016, when rainfall following the disaster may have contributed to partial recovery in less affected areas, as observed in the years 2018 to 2020.

For scales greater than 32 months, the arrows fall outside the cone of influence during the 2000–2007 period, reducing the statistical reliability of the relationship between PRCPTOT and EVI in this interval (Figure 33B). This means that the patterns observed at this scale may be less relevant for robust interpretations. However, it may also indicate that long-term climate events, such as ENSO cycles, do not have a directly measurable relationship with vegetation at large temporal scales in the DRB, likely due to the interference of other factors such as local soil variations and land use changes (CUPOLILLO, 2008; CUPOLILLO *et al.*, 2008).

Between 2013 and 2016, significant coherence on the 2 to 4-month scale indicates that extreme precipitation events (RX1day and RX5day) are out of phase with EVI, with EVI leading the relationship (Figure 33C and 33D). The environmental degradation resulting from the collapse of the Fundão dam in 2015 may have reduced vegetation's response capacity, exacerbating the impacts of extreme rainfall by limiting water infiltration and amplifying surface runoff (NEVES et al., 2022). The disaster acted as a "watershed moment," altering the factors influencing land use. Previously, climatic conditions such as precipitation and temperature limited the expansion of agro-pastoral activities. After the event, anthropogenic factors gained greater relevance: slope began to favor these activities, while urbanized areas limited their expansion. This transition reflects a socioeconomic and environmental adaptation to the new conditions imposed by the disaster (NEVES, 2022).

On the 8 to 16-month scale, the RX1day and RX5day indices lead the relationship with EVI, reflecting vegetation’s direct dependence on accumulated precipitation events for recovery over longer seasonal periods. This in-phase relationship suggests that intense rainfall provides the water resources needed for vegetation recovery, especially in less degraded areas of the basin.

On the other hand, at larger scales (32 to 64 months), the arrows fall outside the cone of influence for both indices, indicating that the relationships between extreme precipitation events and vegetation over the long term were not statistically reliable for the evaluated period. This may reflect the influence of other factors, such as land-use changes, shifts in forest cover, and

global climate cycles such as El Niño and La Niña, which strongly influence rainfall variability in the basin (LIMA; CUPOLILLO, 2018; NEVES *et al.*, 2024).

Figure 33 - Wavelet Coherence Analysis between EVI and the CDD and PRCPTOT Indices for the DRB (2000-2023).

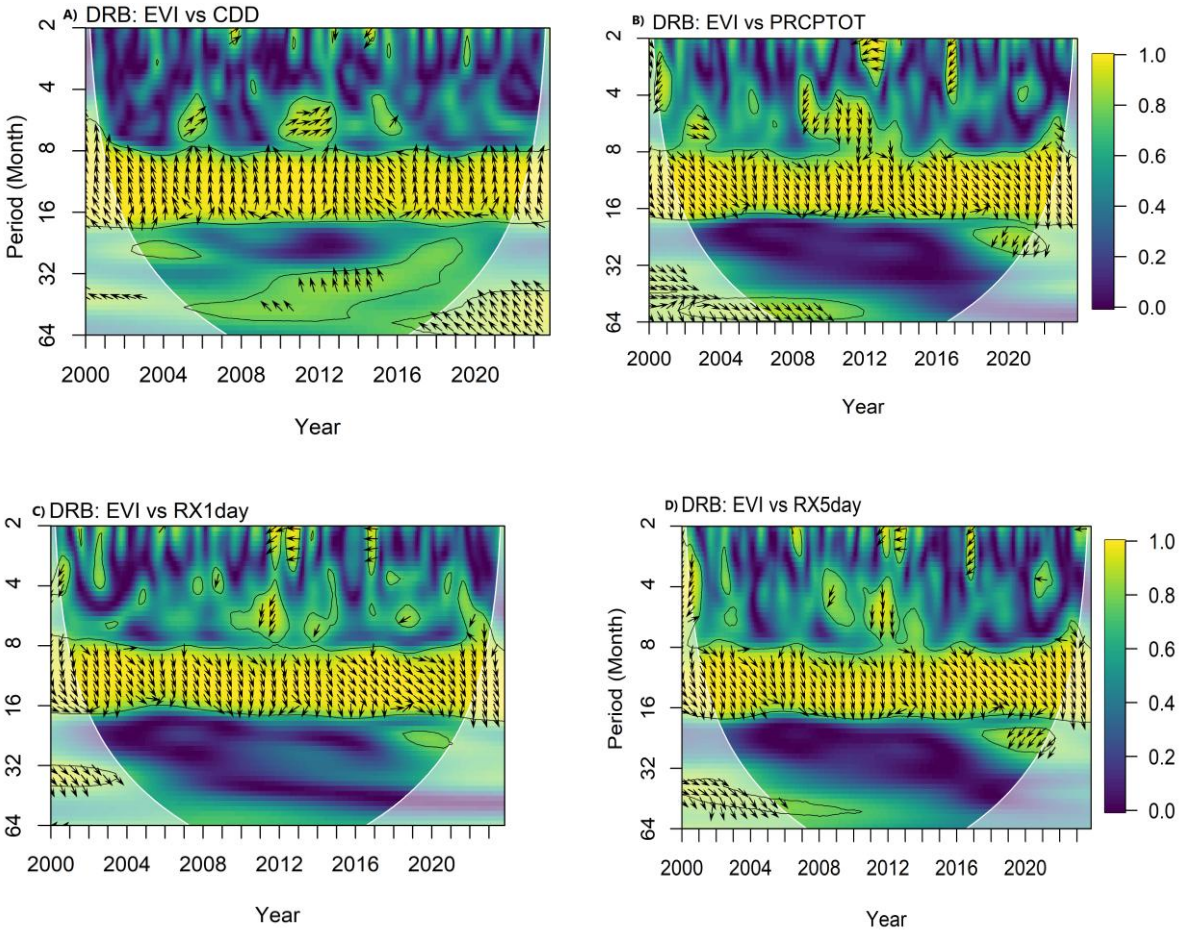

Source: elaborated by the author.

6.6.3 Spatial Trends (SPI) and Deforestation

The analysis of SPI trends for the SPI_1, SPI_3 and SPI_6 (Figure 34) scales during the DJF period (December, January, February) in the Doce River Basin reveals significant variations in drought and wetness regimes, reflecting the combined impacts of climate change and deforestation in the region.

Significant negative trends ($\tau < -1.5$), predominantly observed in the southern and western portions of the basin, indicate an increase in water deficits across various temporal scales. At the SPI_1 scale, these trends reveal the intensification of rapid and severe droughts, particularly in deforested areas (Figure 34A), where the loss of forest cover reduces the soil's water retention capacity. At the SPI_3 scale, water deficits extend over an entire season, affecting water availability for vegetation and human activities. At the SPI_6 scale (Figure 34), the cumulative effects of prolonged droughts make water recovery even more challenging, with drought impacts extending across the northwestern and eastern sectors of the basin, showing a stronger signal. These regions exhibit high deforestation potential and declines in water regimes(Figure 35), threatening sensitive ecosystems and ecosystem services (CAMPOS *et al.*, 2024; MATEUS *et al.*, 2025).

On the other hand, non-significant positive SPI trends ($\tau > 0.35$) were identified in some areas in the central portion of the basin, which still maintain greater densities of native vegetation (Figure 33). These regions exhibit increases in moisture or a reduction in the frequency of drought events. However, these positive trends are localized and insufficient to offset the impacts of prolonged droughts in degraded areas, particularly at the basin's edges.
Moreover, the negative trends in SPI_3 and SPI_6 suggest that the reduction in forest cover is compromising essential ecosystem services, such as hydrological cycle regulation and carbon sequestration, amplifying the effects of droughts and climate change (CAMPOS *et al.*, 2024; CRUZ *et al.*, 2015; LIMA *et al.*, 2019). In the western and southern portions of the basin, the intensification of anthropogenic pressures and the loss of native vegetation have exacerbated water deficits and hindered ecosystem recovery (MATEUS *et al.*, 2025).

Figure 34 - Spatial distribution of Mann-Kendall tau values (2000–2023) for Minas Gerais basins (DJF) using SPI indices at different time scales: SPI_1, SPI_3, and SPI_6. Positive trends (blue) and negative trends (red) highlight areas with significant increases

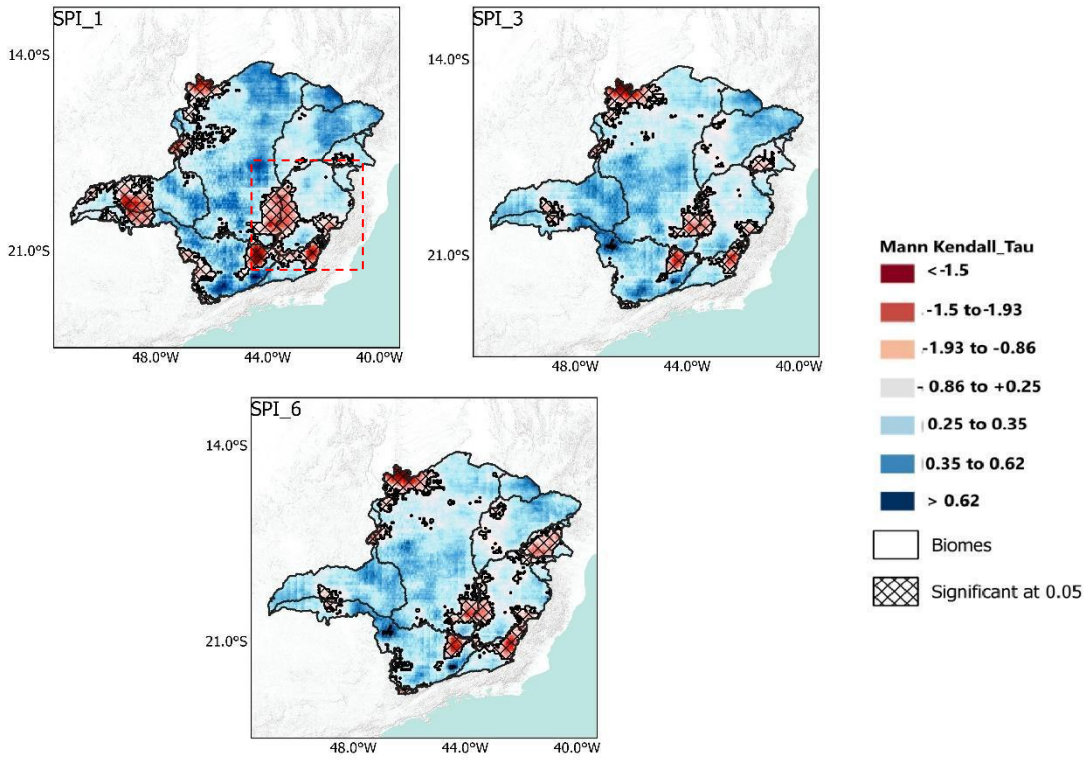

Source: elaborated by the author.

Figure 35 - Spatial distribution of Mann-Kendall tau values (2000–2023) for Minas Gerais River basins (DJF). Indices include SPI_1, SPI_3, and SPI_6. Positive trends (blue) and negative trends (red) are overlaid with forest cover and deforestation (2000–2023). Ba

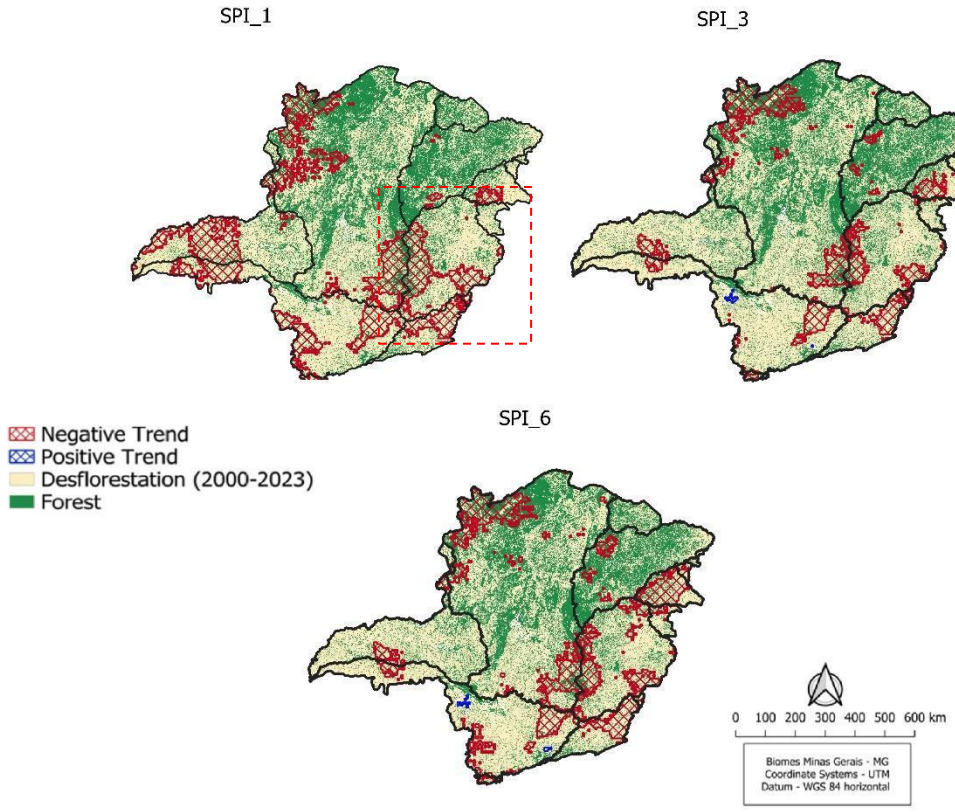

Source: elaborated by the author.

The analysis of SPI trends for the JJA period (June, July, August), which coincides with the dry season, highlights significant impacts on vegetation in the DRB, reflecting the worsening climatic and anthropogenic conditions in the region. The most pronounced negative trends ($\tau < -1.5$), particularly in the northern part of the basin, indicate an increase in the frequency and intensity of droughts in areas already weakened by environmental pressures, such as deforestation (Figures 36 and 37). These patterns directly affect vegetation, intensifying water deficits and reducing the ability of ecosystems to recover over time (CUARTAS *et al.*, 2022; CUNHA *et al.*, 2019; SALOMÃO *et al.*, 2020).

In the context of prolonged water deficits observed at the SPI_3 and SPI_6 scales, there is a significant increase in the magnitude of trends, although the affected area decreases. Reduced water availability compromises the regeneration of native species and favors the proliferation of drought-resistant species, which are less effective in water retention and the

maintenance of ecosystem services. This process can lead to significant functional changes in the basin's ecosystems, harming biodiversity and resilience (CUARTAS *et al.*, 2022; DE MORAES *et al.*, 2016).

The overlap of these trends with deforested areas in the Doce River Basin is particularly concerning. Studies indicate that forest cover loss reduces water infiltration, increases surface runoff, and hinders aquifer recharge, exacerbating drought conditions (MA *et al.*, 2024). Regions in the southern and western parts of the basin, where deforestation is most intense, exhibit the highest water deficits, suggesting that anthropogenic activities are amplifying the impacts of climate change. These regions are also expected to face further precipitation deficits due to the low frequency of South Atlantic Convergence Zone (SACZ) activity in the southern pattern (MATEUS *et al.*, 2025).

On the other hand, areas in the central and northern parts of the basin with greater forest cover show positive SPI trends, indicating greater water resilience. These fragments of native vegetation play a crucial role in regulating the hydrological cycle, helping to mitigate the impacts of the dry season (ALBUQUERQUE *et al.*, 2018; CORREIA FILHO *et al.*, 2019; KLINK; MACHADO, 2005; TRIGUEIRO *et al.*, 2020).

Figure 36 - Same as figure 34, but for JJA.

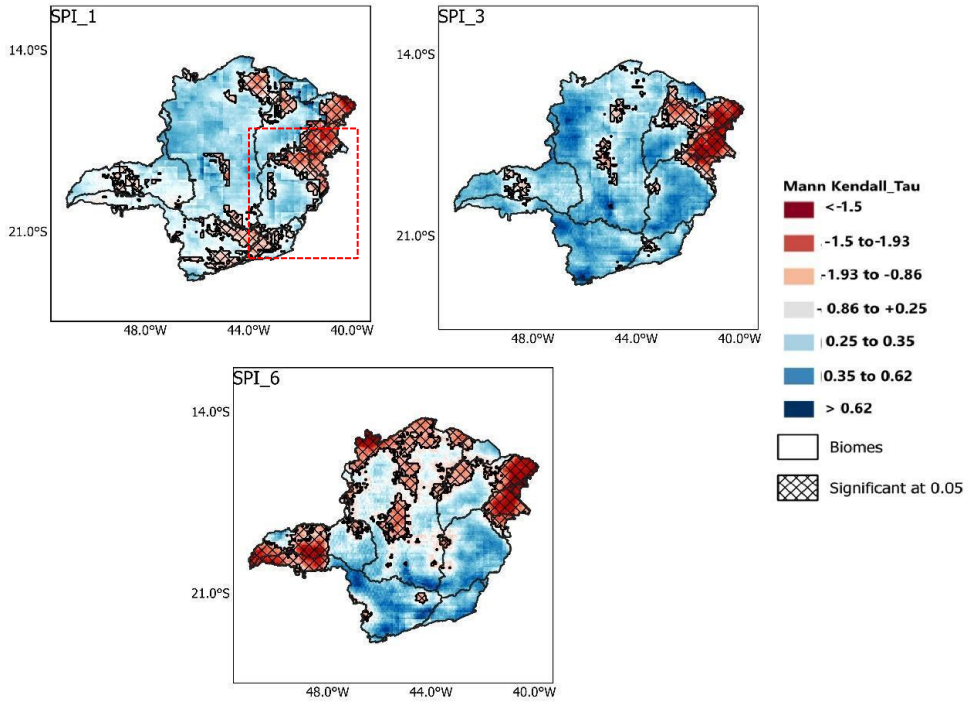

Source: elaborated by the author.

Figure 37 - Same as figure 34 , but for JJA.

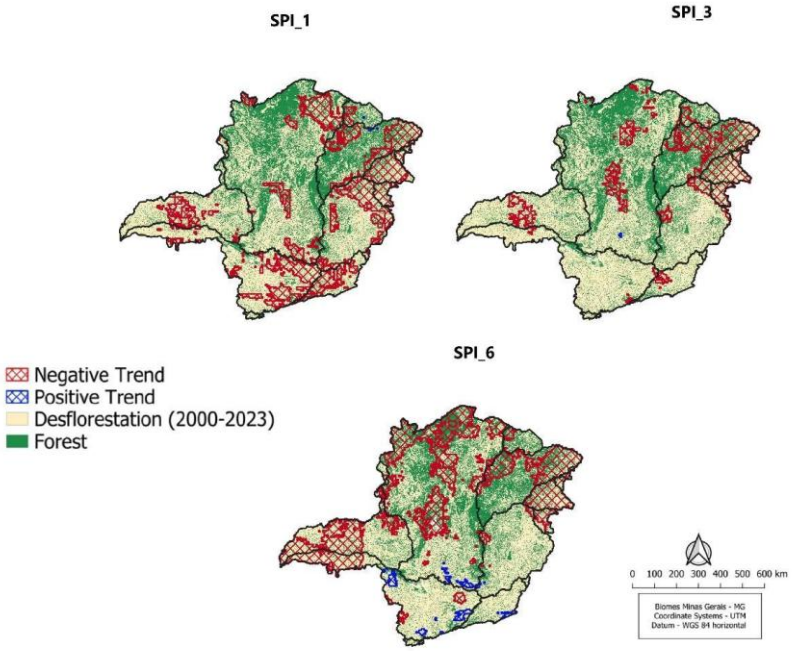

Source: elaborated by the author.

6.6.4 Connection Between SPI and EVI

For SPI_1, which assesses short-term droughts (monthly scale), the significant coherence on the 8 to 16-month scale during the periods 2000–2004 and 2014–2016 highlights that vegetation response to drought events is out of phase, with EVI leading (arrows inclined to the left and downward). This suggests that the prior condition of vegetation is a key factor in modulating the impacts of drought, particularly during short periods of water deficit in the basin (PEIXOTO *et al.*, 2008; PIRES *et al.*, 2017; SALOMÃO *et al.*, 2020). From 2014 to 2016, marked by the Fundão dam disaster (2015) and a strong El Niño, environmental degradation and changes in water flows amplified the effects of droughts, making vegetation recovery difficult even after subsequent rainfall events (CUPOLILLO *et al.*, 2008, 2008; DUTRA *et al.*, 2018; LIMA; ASSIS, 2025).

On the 2 to 4-month scale, significant coherence observed in 2008, 2014, and 2016 reinforces the sensitivity of vegetation to short-term droughts, although the response is delayed and modulated by factors such as degraded soils and forest fragmentation in the basin (Figure 38). The drought induced by the 2015–2016 El Niño, for example, had immediate effects on vegetation, while the environmental disaster exacerbated water deficit conditions by limiting water infiltration and intensifying surface runoff (NEVES *et al.*, 2024; OLIVEIRA *et al.*, 2020; PIRES *et al.*, 2017). These conditions prevented vegetation from quickly reflecting the benefits of subsequent rainfall.

For SPI_3, significant coherence on the 8 to 16-month scale between 2000 and 2004 indicates that EVI leads drought events. This leadership can be explained by vegetation's dependence on cumulative conditions from previous periods, particularly during seasonal drought events (DE OLIVEIRA *et al.*, 2021). In 2012, 2015, and 2016, the coherence on the 2 to 4-month scale reinforces the impact of moderate drought events on vegetation.

For SPI_6, which captures long-term droughts (6 months), the most pronounced coherence occurs in 2019 and 2022, particularly on the 2 to 8-month scale. This suggests that even during prolonged periods of accumulated drought, vegetation in the Doce River Basin still demonstrates an out-of-phase relationship, with EVI leading. However, the signal is less intense compared to SPI_1 and SPI_3, reflecting that vegetation responds more steadily to prolonged drought events. On larger scales (32 to 64 months), the signals fall outside the cone of influence, indicating that extremely prolonged drought events have a less statistically reliable relationship with vegetation dynamics.

Comparing the three indices, SPI_1 highlights the most immediate response of vegetation to short-term drought events, demonstrating a dynamic relationship where EVI leads over periods of 2 to 4 months. SPI_3 shows that seasonal droughts have a significant impact on vegetation, particularly over 8 to 16-month periods, while SPI_6 reflects that prolonged, accumulated drought events have a more diffuse impact, with a less pronounced vegetative response.

Figure 38 - Wavelet Coherence Analysis between EVI and SPI_1, SPI_3, and SPI_6 Indices for the DRB (2000–2023).

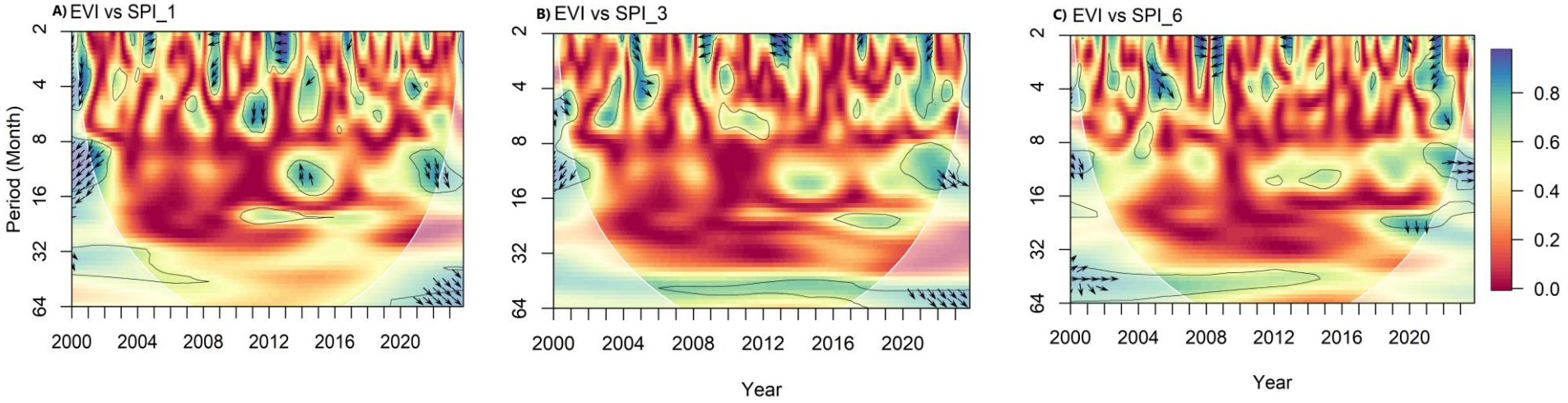

Source: elaborated by the author.

6.7 Conclusion

The analysis of interactions between extreme climate events and vegetation response in the Doce River Basin revealed distinct vegetation response patterns to variations in climate indices (SPI, RX1day, RX5day, CDD, and PRCPTOT). The results highlight the combined influence of climate change and deforestation, with more severe impacts observed in the northern, northwestern, western, southern, and southwestern portions of the basin—regions experiencing the most intense drought events and the most pronounced precipitation deficits, overlapping with areas of significant forest loss. Forest fragmentation in these regions increases vegetation vulnerability, reducing its ability to adapt and regenerate under prolonged water deficits.

The cross-wavelet coherence analysis identified three predominant temporal scales of vegetation response to extreme events:

8 to 16-month scale: This emerged as the primary window of vegetation response, with strong coherence between EVI and precipitation indices (PRCPTOT, RX1day, and RX5day). This pattern underscores the role of hydrological and biological processes in vegetation resilience, indicating that biomass recovery occurs with a time lag relative to extreme precipitation events. In deforested areas, this delay is intensified due to reduced soil moisture retention, making vegetation more sensitive to seasonal water stress.

2 to 8-month scale: At this temporal scale, vegetation responded more rapidly and intensely to drought events—especially those indicated by SPI_1, SPI_3, and SPI_6—particularly in the post-Mariana disaster period (2015), when additional disturbances such as soil degradation and abrupt hydrological changes amplified the effects of prolonged droughts. In more degraded areas, the coherence between SPI indices and EVI became phase-shifted, revealing a decline in vegetation resilience after critical disturbances.

Scales greater than 34 months: At longer time scales, coherence between climate indices and EVI was weak or absent, suggesting that local factors—such as soil type, forest fragmentation, and land-use change—modulate vegetation dynamics more than climate patterns alone. The absence of strong climatic signals at these scales reinforces the dominant role of anthropogenic pressures in shaping ecological trajectories in the basin.

In addition, the extreme precipitation indices (RX1day and RX5day) also showed coherence with vegetation at short time scales (≤4 months), reflecting vegetation's punctual

response to intense rainfall events. Conversely, the CDD index showed weaker responses in these short time frames (2 to 8 months), indicating that the effects of prolonged drought accumulate over time and take longer to significantly impact vegetation. The contrast between the faster vegetation response to droughts (2 to 4 months, up to a maximum of 8 months) and the slower response to precipitation events (8 to 16 months) reveals a critical imbalance in the degradation–recovery cycle. This mismatch suggests that environmental degradation is progressing more rapidly than vegetation regeneration, exacerbating ecological vulnerability in the basin.

The spatial overlap between negative trends in SPI_3 and SPI_6 and the most deforested areas reinforces that vegetation loss compromises hydrological regulation and amplifies the impacts of prolonged drought. In contrast, regions with higher forest preservation showed localized positive trends, emphasizing vegetation's role as a stabilizing factor in the hydrological cycle and a buffer against climate extremes.

Given these findings, urgent conservation and ecological restoration strategies are needed to strengthen vegetation resilience and mitigate the impacts of extreme climate events. Implementing public policies focused on sustainable vegetation management and the recovery of degraded areas can significantly contribute to hydrological regulation and reduce the basin's overall vulnerability.

Finally, this study reinforces the importance of a multi-scale approach to understanding vegetation response to climate extremes, demonstrating that different temporal scales reveal distinct dynamics of impact and recovery. Future research should further investigate the factors that modulate this response, considering large-scale atmospheric drivers, land-use changes, and ecological adaptation processes to climate change. Advancing this knowledge will be essential to inform effective policies for natural resource management and environmental impact mitigation in the Doce River Basin.

7 CHAPTER 7: GENERAL CONCLUSIONS OF THE THESIS

This study synthesized the results of three interrelated investigations, providing a comprehensive overview of the most vulnerable areas of the Doce River Basin (DRB) in the face of climate extremes and land-use changes. The approach adopted integrates hydroclimatic and land-use dynamics, with emphasis on identifying the regions most vulnerable to extreme rainfall and temperature events, contributing valuable input for territorial planning in the basin.

The results showed that the South Atlantic Convergence Zone (SACZ) is the main modulator of hydroclimatic variability in the DRB. The analysis revealed that using spatial averages of the SACZ tends to mask relevant variations in rainfall distribution. Therefore, the thesis proposed an evaluation based on distinct geographic patterns of the SACZ (North, Central, and South), allowing the identification of areas with greater exposure to extreme events. The Northern and Central patterns are associated with the highest precipitation totals in the northern, northwestern, and part of the western regions of the basin, especially affecting the Suaçuí, Santo Antônio, Caratinga, and Piracicaba sub-basins. The Southern pattern, on the other hand, concentrated the highest rainfall amounts in the southern sector, with emphasis on the Piranga sub-basin.

Furthermore, it was found that the Northern and Central patterns showed a higher occurrence of floods during extreme events associated with the SACZ, with precipitation thresholds defined as ≥43 mm/day in the Northern and Central regions, and ≥23 mm/day in the South — a relevant contribution to the improvement of early warning systems. The Central pattern was observed to be the main contributor to water input in the central part of the basin, while the Northern pattern has a broader influence, affecting both northern and southern regions. In contrast, the Central and Southern patterns showed a tendency toward reduced precipitation, which may worsen water deficits and intensify drought periods.

The modeling of land use and land cover (LULC) changes reinforced the findings from the SACZ analysis by indicating that the areas previously identified as vulnerable — located in the northern, northwestern, southwestern, and southern regions of the Doce River Basin (DRB) — are likely to undergo significant transformations in the short (2030), medium (2050), and long term (2080). The main changes were observed in the classes with the largest territorial coverage. For instance, a reduction in native vegetation is projected at -0.15% by 2050 (from 28.7% to 28.5%) and up to -0.52% by 2080 (28.2%) under the RCP4.5 scenario, which assumes reasonable compliance with environmental laws. In the RCP8.5 scenario, which assumes non-compliance with such laws, the reduction could reach -4.8% (from 23.28% to 18.40%).

Conversely, the farming class shows a tendency for expansion, particularly under the RCP8.5 scenario, with an increase ranging from +3.9% to +6.0% (from 70.9% to 76.9%) by 2080.

Projections from the Eta-MIROC and Eta-CanESM2 models supported these trends, indicating a reduction in mean annual precipitation (PRCPTOT) in regions under higher anthropogenic pressure. Additionally, an increase was observed in the number of consecutive dry days (CDD > 70 days) and in extreme rainfall events (RX1day and RX5day > 170 mm/year), which heightens the risks of erosion, flooding, and soil degradation. The lower frequency of occurrence of the Central and Southern SACZ patterns in these areas reinforces the existence of a structural water deficit, compromising the environmental resilience of the DRB.

The analysis of vegetation response in these same vulnerable areas revealed a differentiated behavior in relation to the types of extreme events. Vegetation responded more quickly to drought events, with reactions occurring within 2 to 4 months (SPI_1, SPI_3, and SPI_6), compared to extreme rainfall events, which elicited responses between 8 and 16 months. This suggests that, in a context of climate change, the impacts of degradation may manifest more rapidly than the processes of vegetation recovery. The southern, southwestern, northern, and northwestern regions of the basin — including the sub-basins of the Suaçuí, Santo Antônio, Piracicaba, and Piranga rivers — showed a significant trend of increasing consecutive dry days, as well as intense precipitation events over 1 day (RX1day) and 5 days (RX5day). Moreover, during both the wet and dry seasons, there was an increase in the frequency of drought events (negative values of SPI_1 to SPI_6) in the western, northern, and southern portions of the basin.

Thus, the results of this thesis provide essential support for the incorporation of climate change into territorial planning and landscape management of the Doce River Basin. The identification of the most vulnerable regions and the understanding of the impacts resulting from vegetation degradation contribute to the improvement of public policies focused on environmental conservation and restoration, as well as to the definition of adaptive strategies aimed at mitigating future impacts on the basin’s water resources and ecosystems.

7.1 Main contributions

- *Understanding Hydroclimatic and Ecological Dynamics*

This thesis established an integrated approach that enables the incorporation of climate change and land use projections into the identification of environmentally vulnerable areas in the Doce River Basin. By combining observational data and future scenarios with spatial modeling, the results provide valuable support for the formulation of adaptation strategies and land-use planning actions that are more responsive to ongoing environmental changes. The northern, northwestern, southwestern, and southern regions of the basin—covering the sub-basins of the Suaçuí, Santo Antônio, Piracicaba, and Piranga rivers—were identified as the most susceptible to extreme events due to land use and land cover changes.

The proposal to assess the South Atlantic Convergence Zone (SACZ) through distinct geographic patterns (North, Central, and South) represents a methodological advancement in characterizing extreme events. This approach made it possible to identify areas more susceptible to floods and droughts, as well as to establish critical precipitation thresholds, contributing to the improvement of early warning systems and climate risk management in the basin.

The analysis of the RCP4.5 and RCP8.5 scenarios revealed a trend of agricultural expansion, especially under the RCP8.5 scenario, with an increase between +3.9% and +6.0% by 2080. To mitigate the impacts of this expansion, the adoption of agroforestry systems and other practices that reconcile agricultural production with environmental conservation is recommended, particularly in areas identified as vulnerable.

- *Prioritization of Mitigation Actions in Regions with Higher Climate Risk and Vegetation Degradation*

The analysis of vegetation response revealed that the vegetation of the Doce River Basin (DRB) responds more rapidly to drought events (2 to 4 months) than to intense rainfall events (8 to 16 months), suggesting that degradation processes may occur faster than recovery processes. Given this, it becomes essential that ecological restoration strategies in the basin — already underway through initiatives such as those by Fundação Renova — go beyond the mere planting of native species and instead incorporate climatic feedbacks and the actual ecological resilience observed over time. Adaptive measures such as ecological restoration and sustainable soil management should be implemented in areas identified as more susceptible to prolonged

droughts and floods, as indicated by the spatial patterns of the SACZ and the analyzed climatic indicators.

The continued accelerated response to drought may compromise the success of restoration efforts if not adjusted to emerging climatic conditions. Therefore, it is recommended that restoration programs consider: the selection of species adapted to drier or more variable regimes; management practices that enhance water infiltration and retention in the soil; the use of climate and vegetation monitoring databases to adapt restoration strategies in near-real time; and the prioritization of ecological mosaics that combine assisted natural regeneration with climate refuge areas. These measures make restoration efforts more adaptive and effective under the new climatic regime of the DRB, ensuring ecosystem functionality and the continuity of essential environmental services for the basin's resilience.

7.2 Future research directions

Analysis of SACZ patterns and their long-term impacts:
investigate how climate change influences the frequency and intensity of extreme events associated with the SACZ, enabling the prediction of future impacts on water availability and hydrological risks. relationship between land-use change and global climate phenomena: deepen the analysis of the interactions between land-use changes and global climate patterns, such as El Niño and La Niña, to better understand the impacts on ecosystem functions and environmental services. development of integrated models for adaptive management: develop models that combine ecological, hydrological, and socioeconomic variables, enabling the formulation of more effective management strategies for the most vulnerable areas of DRB and other biomes under climate risk.

REFERENCES

AGUIAR, L. da F. **Vulnerabilidade socioambiental na região sudeste do Brasil associada à configuração da ZCAS**. 2018. 80 f. - Escola de Engenharia, Nitrói 2018. Disponível em: https://app.uff.br/riuff/handle/1/12220. Acesso em: 31 mar. 2025.

AHMAD, I.; TANG, D.; WANG, T.; WANG, M.; WAGAN, B. Precipitation Trends over Time Using Mann-Kendall and Spearman's rho Tests in Swat River Basin, Pakistan. **Advances in Meteorology**, v. 2015, p. 1–15, 2015.

AIRES, U. R. V.; SANTOS, B. S. M.; COELHO, C. D.; DA SILVA, D. D.; CALIJURI, M. L. Changes in land use and land cover as a result of the failure of a mining tailings dam in Mariana, MG, Brazil. **Land use policy**, v. 70, p. 63–70, 2018.

ALBUQUERQUE, R. L.; DOS SANTOS PROTÁZIO, A.; BARBOSA DE QUEIROGA CAVALCANTI, L.; LOPEZ, L. C. S.; MESQUITA, D. O. Geographical ecology of Tropidurus hispidus (Squamata: Tropiduridae) and Cnemidophorus ocellifer (Squamata: Teiidae) in a Neotropical region: a comparison among Atlantic Forest, Caatinga, and coastal populations. **Journal of Herpetology**, v. 52, n. 2, p. 145–155, 2018.

ALMEIDA, L. P. de; FORMIGA-JOHNSSON, R. M.; FILHO, F. de A. de S.; ESTÁCIO, Á. B. S.; PORTO, V. C.; NAUDITT, A.; RIBBE, L. Development of DRIP - drought representation index for CMIP climate model performance, application to Southeast Brazil. **Science of The Total Environment**, v. 954, p. 176443, 2024.

ALMEIDA, C. M. D.; MONTEIRO, A. M. V.; CÂMARA, G.; SOARES-FILHO, B. S.; CERQUEIRA, G. C.; PENNACHIN, C. L.; BATTY, M. GIS and remote sensing as tools for the simulation of urban land-use change. **International Journal of Remote Sensing**, v. 26, n. 4, p. 759–774, 2005.

ALMEIDA, F. de; SILVEIRA, E. de O.; ACERBÍJUNIOR, F. W.; FRANÇA, L. D. J.; BUENO, I. T.; TERRA, B. J. O. Multicriteria analysis to define priority areas for forest recovery in the Rio Doce Basin, Minas Gerais. , 2020. Disponível em: https://www.cabidigitallibrary.org/doi/full/10.5555/20203112592. Acesso em: 31 mar. 2025.

AMBRIZZI, T.; FERRAZ, S. E. An objective criterion for determining the South Atlantic Convergence Zone. **Frontiers in Environmental Science**, v. 3, p. 23, 2015.

ANDERSON, T. A.; SALICE, C. J.; ERICKSON, R. A.; MCMURRY, S. T.; COX, S. B.; SMITH, L. M. Effects of landuse and precipitation on pesticides and water quality in playa lakes of the southern high plains. **Chemosphere**, v. 92, n. 1, p. 84–90, 2013.

ANDREWS, J. L.; MAINDONALD, J. H.; BRAUN, W. J. (org.). References to R Packages. *Em*: **A Practical Guide to Data Analysis Using R: An Example-Based Approach**. Cambridge: Cambridge University Press, 2024. p. 508–513. Disponível em: https://www.cambridge.org/core/books/practical-guide-to-data-analysis-using-r/references-to-r-packages/05877A8EB1065902F87D4AD72834D7EB. Acesso em: 3 abr. 2025.

ANTÓNIO, J. F. **Energética da zona de convergência do Atlântico Sul (ZCAS)**. 2020. 181 f. - INPE, 2020. Disponível em:

https://bdtd.ibict.br/vufind/Record/INPE_7e7f163a6dd0a81065ac494f742d3f28. Acesso em: 31 mar. 2025.

ANTÓNIO, J. F.; ARAVÉQUIA, J. A. Diabatic Heat Effects on the Generation of Energy for Evolution of a SACZ Event: A Perspective from the Lorenz Energy Cycle. **Journal of the Atmospheric Sciences**, v. 80, n. 9, p. 2287–2304, 2023.

ANYAMBA, A.; CHRETIEN, J.-P.; BRITCH, S. C.; SOEBIYANTO, R. P.; SMALL, J. L.; JEPSEN, R.; FORSHEY, B. M.; SANCHEZ, J. L.; SMITH, R. D.; HARRIS, R.; TUCKER, C. J.; KARESH, W. B.; LINTHICUM, K. J. Global Disease Outbreaks Associated with the 2015–2016 El Niño Event. **Scientific Reports**, v. 9, n. 1, p. 1930, 2019.

ASSUNÇÃO, J.; GANDOUR, C.; ROCHA, R. Deforestation slowdown in the Brazilian Amazon: prices or policies? **Environment and Development Economics**, v. 20, n. 6, p. 697–722, 2015.

BALLESTEROS, R.; ORTEGA, J. F.; HERNÁNDEZ, D.; MORENO, M. Á. Characterization of Vitis vinifera L. canopy using unmanned aerial vehicle-based remote sensing and photogrammetry techniques. **American Journal of Enology and Viticulture**, v. 66, n. 2, p. 120–129, 2015.

BARBOSA, R. A.; DA SILVEIRA, L. J.; SPLETOZER, A. G.; TONELLO, K. C.; CORRÊA, J. B. L.; BRAMORSKI, J.; DIAS, H. C. T. Temporal variation of precipitation and flow in 16 mountainous sub-basins of the Manhuaçu River. **Revista Brasileira de Ciências Agrárias**, v. 16, n. 2, p. 1–9, 2021.

BARROS, A. P.; JOSHI, M.; PUTKONEN, J.; BURBANK, D. W. A study of the 1999 monsoon rainfall in a mountainous region in central Nepal using TRMM products and rain gauge observations. **Geophysical Research Letters**, v. 27, n. 22, p. 3683–3686, 2000.

BAUDENA, M.; TUINENBURG, O. A.; FERDINAND, P. A.; STAAL, A. Effects of land-use change in the Amazon on precipitation are likely underestimated. **Global Change Biology**, v. 27, n. 21, p. 5580–5587, 2021.

BAZZANELA, A. C.; DERECZYNSKI, C.; LUIZ-SILVA, W.; REGOTO, P. Performance of CMIP6 models over South America. **Climate Dynamics**, v. 62, n. 2, p. 1501–1516, 2024.

BEILLOUIN, D.; CARDINAEL, R.; BERRE, D.; BOYER, A.; CORBEELS, M.; FALLOT, A.; FEDER, F.; DEMENOIS, J. A global overview of studies about land management, land-use change, and climate change effects on soil organic carbon. **Global Change Biology**, v. 28, n. 4, p. 1690–1702, 2022.

BEUCHLE, R.; ACHARD, F.; BOURGOIN, C.; VANCUTSEM, C.; EVA, H. D.; FOLLADOR, M. **Desflorestação e degradação florestal na Amazónia**. , 2022. Disponível em:https://publications.jrc.ec.europa.eu/repository/bitstream/JRC124955/jrc124955_eur30727pt_2022_amazon_deforestation_forest_degradation_%282%29.pdf. Acesso em: 31 mar. 2025.

BOMBARDI, R. J.; CARVALHO, L. M. V.; JONES, C.; REBOITA, M. S. Precipitation over eastern South America and the South Atlantic Sea surface temperature during neutral ENSO periods. **Climate Dynamics**, v. 42, n. 5–6, p. 1553–1568, 2014.

BOURGUIGNON, D. A. da S.; FRAGA, M. de S.; LYRA, G. B.; CECÍLIO, R. A.; ABREU, M. C. Effect of rainfall seasonality and land use on the water quality of the paraíba do sul river. **Revista Engenharia na Agricultura - REVENG**, v. 29, n. Contínua, p. 211–228, 2021.

BRAGA, H. A.; AMBRIZZI, T.; HALL, N. M. J. Relationship between interhemispheric Rossby wave propagation and South Atlantic convergence zone during La Niña years. **International Journal of Climatology**, v. 42, n. 16, p. 8652–8664, 2022.

BRAGA, H. A.; AMBRIZZI, T.; HALL, N. M. J. South Atlantic Convergence Zone as Rossby wave source. **Theoretical and Applied Climatology**, v. 155, n. 5, p. 4231–4247, 2024.

BRÊDA, J. P. L. F.; DE PAIVA, R. C. D.; COLLISCHON, W.; BRAVO, J. M.; SIQUEIRA, V. A.; STEINKE, E. B. Climate change impacts on South American water balance from a continental-scale hydrological model driven by CMIP5 projections. **Climatic Change**, v. 159, n. 4, p. 503–522, 2020.

CALVIN, K.; BOND-LAMBERTY, B.; CLARKE, L.; EDMONDS, J.; EOM, J.; HARTIN, C.; KIM, S.; KYLE, P.; LINK, R.; MOSS, R. The SSP4: A world of deepening inequality. **Global Environmental Change**, v. 42, p. 284–296, 2017.

CAMARGO, R.; COMINI, U.; CALIJURI, M. L.; ASSIS, L. SIMULAÇÃO HIDROLÓGICA DE EVENTOS EXTREMOS UTILIZANDO O HEC-HMS: A relação uso e cobertura do solo com a ocorrência de cheias. , 2011.

CAMPOS, J. A.; DA SILVA, D. D.; MOREIRA, M. C.; DE MENEZES FILHO, F. C. M. Environmental fragility and land use capacity as instruments of environmental planning, Caratinga River basin, Brazil. **Environmental Earth Sciences**, v. 80, n. 7, p. 264, 2021.

CAMPOS, J. A.; DA SILVA, D. D.; PIRES, G. F.; AMORIM, R. S. S.; DE MENEZES FILHO, F. C. M.; DE MELO RIBEIRO, C. B.; LORENTZ, J. F.; AIRES, U. R. V. Modeling Environmental Vulnerability for 2050 Considering Different Scenarios in the Doce River Basin, Brazil. **Water**, v. 16, n. 10, p. 1459, 2024.

CARMO, Flávio Fonseca do; KAMINO, L. H. Y.; JUNIOR, R. T.; CAMPOS, I. C. de; CARMO, Felipe Fonseca do; SILVINO, G.; CASTRO, K. J. da S. X. de; MAURO, M. L.; RODRIGUES, N. U. A.; MIRANDA, M. P. de S.; PINTO, C. E. F. Fundão tailings dam failures: the environment tragedy of the largest technological disaster of Brazilian mining in global context. **Perspectives in Ecology and Conservation**, v. 15, n. 3, p. 145–151, 2017.

CARVALHO, L. M.; JONES, C.; LIEBMANN, B. Extreme precipitation events in southeastern South America and large-scale convective patterns in the South Atlantic convergence zone. **Journal of Climate**, v. 15, n. 17, p. 2377–2394, 2002.

CARVALHO, L. M.; JONES, C.; LIEBMANN, B. The South Atlantic convergence zone: Intensity, form, persistence, and relationships with intraseasonal to interannual activity and extreme rainfall. **Journal of climate**, v. 17, n. 1, p. 88–108, 2004.

CAVALCANTI, J. R.; PONTES, P. R. M.; CAVALCANTE, R. B. L.; DE OLIVEIRA SERRÃO, E. A.; FERREIRA, D. M.; XAVIER, A. C. F. Índices hidrológicos e projeções climáticas na bacia do rio Doce. , 2023. Disponível em:

https://files.abrhidro.org.br/Eventos/Trabalhos/191/XXV-SBRH1047-1-0-20230730-143728.pdf. Acesso em: 31 mar. 2025.

CEMADEN. **Pesquisa do Cemaden contribui para aumentar antecedência de emissão de alerta de cheias na Bacia do Rio Doce – Cemaden**. , 2018. Disponível em: http://www2.cemaden.gov.br/antecipacao-do-alerta-de-cheias-na-bacia-do-rio-doce-e-demonstrada-por-pesquisa-do-cemaden/. Acesso em: 5 abr. 2025.

CHAPIN, T. S.; DEYLE, R. E.; BAKER, E. J. A Parcel-Based GIS Method for Evaluating Conformance of Local Land-Use Planning with a State Mandate to Reduce Exposure to Hurricane Flooding. **Environment and Planning B: Planning and Design**, v. 35, n. 2, p. 261–279, 2008.

CHEN, M.; VERNON, C. R.; GRAHAM, N. T.; HEJAZI, M.; HUANG, M.; CHENG, Y.; CALVIN, K. Global land use for 2015–2100 at 0.05 resolution under diverse socioeconomic and climate scenarios. **Scientific Data**, v. 7, n. 1, p. 320, 2020.

CHERVENKOV, H.; SLAVOV, K. ETCCDI Climate Indices for Assessment of the Recent Climate over Southeast Europe. *Em*: ADVANCES IN HIGH PERFORMANCE COMPUTING, 2021, Cham. **Anais**. Cham: Springer International Publishing, 2021. p. 398–412.

CHOKKAVARAPU, N.; MANDLA, V. R. Comparative study of GCMs, RCMs, downscaling and hydrological models: a review toward future climate change impact estimation. **SN Applied Sciences**, v. 1, n. 12, p. 1698, 2019.

CHOU, S. C.; LYRA, A.; MOURÃO, C.; DERECZYNSKI, C.; PILOTTO, I.; GOMES, J.; BUSTAMANTE, J.; TAVARES, P.; SILVA, A.; RODRIGUES, D.; CAMPOS, D.; CHAGAS, D.; SUEIRO, G.; SIQUEIRA, G.; MARENGO, J. Assessment of Climate Change over South America under RCP 4.5 and 8.5 Downscaling Scenarios. **American Journal of Climate Change**, v. 03, n. 05, p. 512–527, 2014.

COELHO, A. L. N. Hotspots de erosão marginal no médio-baixo rio doce: identificação e análise. **REVISTA EQUADOR**, v. 9, n. 1, p. 266–281, 2020.

COELHO, A. L. N. Situação hídrico-geomorfológica da bacia do rio doce com base nos dados da série histórica de vazões da estação de colatina-es1. , 2006. Disponível em: https://seer.ufu.br/index.php/caminhosdegeografia/article/download/15489/8768. Acesso em: 31 mar. 2025.

COPERNICUS. **Copernicus: 2024 is the first year to exceed 1.5°C above pre-industrial level | Copernicus**. , 2024. Disponível em: https://climate.copernicus.eu/copernicus-2024-first-year-exceed-15degc-above-pre-industrial-level. Acesso em: 31 mar. 2025.

CORDEIRO, J.; GOMES, A. R.; SANTOS, C. H. B.; RIGOBELO, E. C.; BAPTISTA, M. B.; MOURA, P. M.; SCOTTI, M. R. Rehabilitation of the Doce River Basin after the FUNDÃO dam collapse: What has been done, what can be done and what should be done? **River Research and Applications**, v. 38, n. 2, p. 194–208, 2022.

CORREIA FILHO, W. L. F.; DE OLIVEIRA-JÚNIOR, J. F.; DE BARROS SANTIAGO, D.; DE BODAS TERASSI, P. M.; TEODORO, P. E.; DE GOIS, G.; BLANCO, C. J. C.; DE ALMEIDA SOUZA, P. H.; DA SILVA COSTA, M.; GOMES, H. B.; DOS SANTOS, P. J.

Rainfall variability in the Brazilian northeast biomes and their interactions with meteorological systems and ENSO via CHELSA product. **Big Earth Data**, v. 3, n. 4, p. 315–337, 2019.

COSTA, F.; BUARQUE, D. C.; BRÊDA, J. P. L. F.; FÖEGER, L. B. Impact of climate change on the flow of the Doce River basin. **RBRH**, v. 27, p. e34, 2022.

COSTA; BUARQUE, D. C.; BRÊDA, J. P. L. F.; FÖEGER, L. B. Impact of climate change on the flow of the Doce River basin. **RBRH**, v. 27, p. e34, 2022.

COSTA, F. de P. D.; BUARQUE, D. C.; BRÊDA, J. P. L. F.; FÖEGER, L. B. Impacto das mudanças climáticas na vazão na bacia do Rio Doce. **RBRH**, v. 27, p. e34, 2022.

CRESPO, A.; VELÁZQUEZ, J.; HERRÁEZ, F.; GÜLÇIN, D.; ÖZCAN, A. U.; HERNANDO, A.; CASTANHO, R. A. Territorial planning of rustic land constructions and their adaptation to climate change in the province of Málaga, Spain. **Land Use Policy**, v. 129, p. 106644, 2023.

CRUZ, F. M.; ROCHA, L. O.; CUNHA, D. M.; PANQUESTOR, E. K.; SENA, I. Ondas de cheia no médio rio Doce: uma abordagem conceitual e estatística. *Em*: VI CONGRESSO BRASILEIRO DE GESTÃO AMBIENTAL. PORTO ALEGRE: IBEAS, 2015, . **Anais**, 2015. p. 1–6. Disponível em: https://www.ibeas.org.br/congresso/Trabalhos2015/VIII-028.pdf. Acesso em: 31 mar. 2025.

CUARTAS, L. A.; CUNHA, A. P. M. do A.; ALVES, J. A.; PARRA, L. M. P.; DEUSDARÁ-LEAL, K.; COSTA, L. C. O.; MOLINA, R. D.; AMORE, D.; BROEDEL, E.; SELUCHI, M. E. Recent hydrological droughts in Brazil and their impact on hydropower generation. **Water**, v. 14, n. 4, p. 601, 2022.

CUNHA, A. P. M.; ALVALÁ, R. C.; NOBRE, C. A.; CARVALHO, M. A. Monitoring vegetative drought dynamics in the Brazilian semiarid region. **Agricultural and Forest Meteorology**, v. 214–215, p. 494–505, 2015.

CUNHA, A. P. M.; ZERI, M.; DEUSDARÁ LEAL, K.; COSTA, L.; CUARTAS, L. A.; MARENGO, J. A.; TOMASELLA, J.; VIEIRA, R. M.; BARBOSA, A. A.; CUNNINGHAM, C. Extreme drought events over Brazil from 2011 to 2019. **Atmosphere**, v. 10, n. 11, p. 642, 2019.

CUPOLILLO, F. **Diagnóstico hidroclimatológico da bacia do rio Doce**. 2008. 156 f. - UFMG, Belo Horizonte, MG 2008. Disponível em: https://repositorio.ufmg.br/handle/1843/MPBB-7F8NTB. Acesso em: 31 mar. 2025.

CUPOLILLO, F.; DE ABREU, M. L.; VIANELLO, R. L. Climatologia da bacia do rio Doce e sua relação com a topografia local. **Revista Geografias**, v. 4, n. 2, p. 45–60, 2008.

CUSTÓDIO, V. A crise hídrica na região metropolitana de São Paulo (2014-2015). **GEOUSP Espaço e Tempo (Online)**, v. 19, n. 3, p. 445–463, 2015.

DA CUNHA RICHARD, E.; DE AGUIAR DUARTE JR, H.; CALDERUCIO DUQUE ESTRADA, G.; BECHTOLD, J.-P.; GUSSO MAIOLI, B.; ARAUJO DE FREITAS, A. H.; ELIZABETH WARNER, K.; MELGES FIGUEIREDO, L. H. Influence of Fundão tailings

dam breach on water quality in the Doce River watershed. **Integrated Environmental Assessment and Management**, v. 16, n. 5, p. 583–595, 2020.

DA FONSECA AGUIAR, L.; CATALDI, M. Social and environmental vulnerability in Southeast Brazil associated with the South Atlantic Convergence Zone. **Natural Hazards**, v. 109, n. 3, p. 2423–2437, 2021.

DA SILVA, F. P.; JUSTI DA SILVA, M. G. A.; ROTUNNO FILHO, O. C.; PIRES, G. D.; SAMPAIO, R. J.; DE ARAÚJO, A. A. M. Synoptic thermodynamic and dynamic patterns associated with Quitandinha River flooding events in Petropolis, Rio de Janeiro (Brazil). **Meteorology and Atmospheric Physics**, v. 131, n. 4, p. 845–862, 2019.

DA SILVA VERDAN, I. Variabilidade interanual da Zona de Convergência do Atlântico Sul e sua associação com o El Niño-Oscilação Sul entre 2000 e 2021. , 2023. Disponível em: https://bdtd.ibict.br/vufind/Record/USP_082d3f831945fe30011fbdd5d6983bd8. Acesso em: 3 abr. 2025.

D'ALMEIDA, C.; VÖRÖSMARTY, C. J.; HURTT, G. C.; MARENGO, J. A.; DINGMAN, S. L.; KEIM, B. D. The effects of deforestation on the hydrological cycle in Amazonia: a review on scale and resolution. **International Journal of Climatology**, v. 27, n. 5, p. 633–647, 2007.

DANTAS, L. G.; DOS SANTOS, C. A.; SANTOS, C. A.; MARTINS, E. S.; ALVES, L. M. Future changes in temperature and precipitation over northeastern Brazil by CMIP6 model. **Water**, v. 14, n. 24, p. 4118, 2022.

DE ALMEIDA, F. C.; DE OLIVEIRA SILVEIRA, E. M.; DE PAIVA, L. L.; JUNIOR, F. W. A. Mapping of priority areas for forest recovery using multicriteria analysis in the brazilian atlantic forest mapeamento de áreas prioritárias para recuperação utilizando análise multicritério na floresta atlântica brasileira. **R. Ra'e Ga**, v. 46, n. 3, p. 113–124, 2019.

DE CARVALHO, D. R.; FERREIRA, F. F.; DERGAM, J. A.; MOREIRA, M. Z.; POMPEU, P. S. Food web structure of fish communities of Doce River, 5 years after the Fundão dam failure. **Environmental Monitoring and Assessment**, v. 196, n. 3, p. 300, 2024.

DE CASTRO SENA, I. B. D.; CRUZ, F. M.; CUNHA, D. M.; CUPOLILLO, F.; DO NASCIMENTO CAMPOS, K. B. E. Determinação de regiões pluviometricamente homogêneas na bacia do rio Doce/MG. **Revista Mineira de Recursos Hídricos**, v. 1, n. 1, 2020. Disponível em: https://periodicos.meioambiente.mg.gov.br/NM/article/view/193. Acesso em: 1 abr. 2025.

DE MAGALHÃES, S. F. C.; DE MOURA BARBOZA, C. A.; MAIA, M. B.; MOLISANI, M. M. Influence of land cover, catchment morphometry and rainfall on water quality and material transport of headwaters and low-order streams of a tropical mountainous watershed. **Catena**, v. 213, p. 106137, 2022.

DE MORAES, M. G.; DE CARVALHO, M. A. M.; FRANCO, A. C.; POLLOCK, C. J.; FIGUEIREDO-RIBEIRO, R. de C. L. Fire and drought: soluble carbohydrate storage and survival mechanisms in herbaceous plants from the Cerrado. **BioScience**, v. 66, n. 2, p. 107–117, 2016.

DE NOBLET-DUCOUDRÉ, N.; BOISIER, J.-P.; PITMAN, A.; BONAN, G. B.; BROVKIN, V.; CRUZ, F.; DELIRE, C.; GAYLER, V.; VAN DEN HURK, B.; LAWRENCE, P. J. Determining robust impacts of land-use-induced land cover changes on surface climate over North America and Eurasia: results from the first set of LUCID experiments. **Journal of Climate**, v. 25, n. 9, p. 3261–3281, 2012.

DE OLIVEIRA, B. R.; CARVALHO-RIBEIRO, S. M.; MAIA-BARBOSA, P. M. Rio Doce State Park buffer zone: forest fragmentation and land use dynamics. **Environment, Development and Sustainability**, v. 23, n. 6, p. 8365–8376, 2021.

DE OLIVEIRA, D. M.; RIBEIRO, J. G. M.; DE FARIA, L. F.; REBOITA, M. S. Performance dos modelos climáticos do CMIP6 em simular a precipitação em subdomínios da América do Sul no período histórico. **Revista Brasileira de Geografia Física**, v. 16, n. 01, p. 116–133, 2023.

DE OLIVEIRA VIEIRA, S.; SATYAMURTY, P.; ANDREOLI, R. V. On the South Atlantic Convergence Zone affecting southern Amazonia in austral summer. **Atmospheric Science Letters**, v. 14, n. 1, p. 1–6, 2013.

DE SOUZA FERREIRA, G. W.; REBOITA, M. S.; RIBEIRO, J. G. M.; CARVALHO, V. S. B.; SANTIAGO, M. E. V.; SILVA, P. L. L. S.; BALDONI, T. C.; DE SOUZA, C. A. Assessment of the wind power density over South America simulated by CMIP6 models in the present and future climate. **Climate Dynamics**, v. 62, n. 3, p. 1729–1763, 2024.

DERECZYNSKI, C. P.; OLIVEIRA, J. S. de; MACHADO, C. O. Climatologia da precipitação no município do Rio de Janeiro. **Revista Brasileira de Meteorologia**, v. 24, p. 24–38, 2009.

DIRMEYER, PAUL A.; SHUKLA, J. Albedo as a modulator of climate response to tropical deforestation. **Journal of Geophysical Research: Atmospheres**, v. 99, n. D10, p. 20863–20877, 1994.

DOELMAN, J. C.; STEHFEST, E.; TABEAU, A.; VAN MEIJL, H.; LASSALETTA, L.; GERNAAT, D. E.; HERMANS, K.; HARMSEN, M.; DAIOGLOU, V.; BIEMANS, H. Exploring SSP land-use dynamics using the IMAGE model: Regional and gridded scenarios of land-use change and land-based climate change mitigation. **Global Environmental Change**, v. 48, p. 119–135, 2018.

DONG, Y.; ZHAI, J.; ZHAO, Y.; LI, H.; WANG, Q.; JIANG, S.; CHANG, H.; DING, Z. Teleconnection patterns of precipitation in the Three-River Headwaters region, China. **Environmental Research Letters**, v. 15, n. 10, p. 104050, 2020.

DOS REIS, M.; DE ALENCASTRO GRAÇA, P. M. L.; YANAI, A. M.; RAMOS, C. J. P.; FEARNSIDE, P. M. Forest fires and deforestation in the central Amazon: Effects of landscape and climate on spatial and temporal dynamics. **Journal of Environmental Management**, v. 288, p. 112310, 2021.

DOS SANTOS, V. J.; FIALHO, E. S. Zona de convergência do atlântico sul (zcas) e impactos pluviais intensos: o caso da cidade de Ubá/MG. **Revista Brasileira de Climatologia**, v. 19, 2016. Disponível em: https://ojs.ufgd.edu.br/rbclima/article/view/13909. Acesso em: 2 abr. 2025.

DUARTE, L. G. F. **O FENÔMENO EL NIÑO-OSCILAÇÃO SUL E OS EVENTOS EXTREMOS DE PRECIPITAÇÃO EM SANTA CATARINA**. 2017. 86 f. Dissertação - Universidade Federal de Santa Catarina, SC 2017.

DUTRA, S. F. R. L.; LEAL DE QUADRO, M. F.; MÜLLER, G. V.; VALADÃO, R. C. ASSOCIAÇÕES ENTRE A ZONA DE CONVERGÊNCIA DO ATLÂNTICO SUL E O EL NIÃ‘O E SUA INFLUÊNCIA SOBRE A DISTRIBUIÇÃO ESPAÇOTEMPORAL DA LEPTOSPIROSE EM MINAS GERAIS. **Hygeia - Revista Brasileira de Geografia Médica e da Saúde**, v. 14, n. 27, p. 1–13, 2018.

DUVEILLER, G.; CAPORASO, L.; ABAD-VIÑAS, R.; PERUGINI, L.; GRASSI, G.; ARNETH, A.; CESCATTI, A. Local biophysical effects of land use and land cover change: towards an assessment tool for policy makers. **Land Use Policy**, v. 91, p. 104382, 2020.

EL-NESR, M. N.; ABU-ZREIG, M. M.; ALAZBA, A. A. Temperature trends and distribution in the Arabian Peninsula. , 2010. Disponível em: https://www.cabidigitallibrary.org/doi/full/10.5555/20103203556. Acesso em: 5 abr. 2025.

ESCOBAR, G. C. J.; REBOITA, M. S. Relationship between daily atmospheric circulation patterns and South Atlantic Convergence Zone (SACZ) events. **Atmósfera**, v. 35, n. 1, p. 1–25, 2022.

FAN, M.; SHIBATA, H. Simulation of watershed hydrology and stream water quality under land use and climate change scenarios in Teshio River watershed, northern Japan. **Ecological Indicators**, v. 50, p. 79–89, 2015.

FARIA, B. N.; MENDONÇA, A. S. F.; REIS, J. A. T. Regional Flood Frequency Analysis in the Doce River Basin and Coastal Regions in Espírito Santo State, Brazil – Evaluation of the Performance of L-Moments Approach. **Revista de Gestão Social e Ambiental**, v. 18, n. 3, p. e04367, 2023.

FEARNSIDE, P. M. Desmatamento na Amazônia: dinâmica, impactos e controle. **Acta amazônica**, v. 36, p. 395–400, 2006.

FELIX, M. L.; KIM, Y.; CHOI, M.; KIM, J.-C.; DO, X. K.; NGUYEN, T. H.; JUNG, K. Detailed Trend Analysis of Extreme Climate Indices in the Upper Geum River Basin. **Water**, v. 13, n. 22, 2021. Disponível em: https://www.mdpi.com/2073-4441/13/22/3171.

FERREIRA, G. R. **Eventos extremos de precipitação nas bacias hidrográficas dos rios Doce e Paraíba do Sul**. 2019a. 47 f. Dissertação - Universidade Federal de Viçosa, Viçosa 2019. Disponível em: https://locus.ufv.br/items/9c1df119-3970-4f42-899a-a9d11bbddda3. Acesso em: 31 mar. 2025.

FERREIRA, G. R. Eventos extremos de precipitação nas bacias hidrográficas dos rios Doce e Paraíba do Sul. , 2019b. Disponível em: https://agris.fao.org/search/en/providers/125323/records/67484b6d7625988a3719f868. Acesso em: 31 mar. 2025.

FERREIRA, M. L.; KNIESS, C. T.; SILVA, W. M.; FERREIRA, A. T. da S. Urban forests, territorial planning and political stability: key factors to face climate change in a megacity. **Sustainability**, v. 15, n. 13, p. 10092, 2023.

FIALHO, W. M. B.; CARVALHO, L. M. V.; GAN, M. A.; VEIGA, S. F. Mechanisms controlling persistent South Atlantic Convergence Zone events on intraseasonal timescales. **Theoretical and Applied Climatology**, v. 152, n. 1–2, p. 75–96, 2023.

FINDELL, K. L.; SUTTON, R.; CALTABIANO, N.; BROOKSHAW, A.; HEIMBACH, P.; KIMOTO, M.; OSPREY, S.; SMITH, D.; RISBEY, J. S.; WANG, Z. Explaining and predicting earth system change: a world climate research programme call to action. **Bulletin of the American Meteorological Society**, v. 104, n. 1, p. E325–E339, 2023.

FIRPO, M. Â. F.; GUIMARÃES, B. D. S.; DANTAS, L. G.; SILVA, M. G. B. D.; ALVES, L. M.; CHADWICK, R.; LLOPART, M. P.; OLIVEIRA, G. S. D. Assessment of CMIP6 models' performance in simulating present-day climate in Brazil. **Frontiers in Climate**, v. 4, p. 948499, 2022.

FOLEY, J. A.; DEFRIES, R.; ASNER, G. P.; BARFORD, C.; BONAN, G.; CARPENTER, S. R.; CHAPIN, F. S.; COE, M. T.; DAILY, G. C.; GIBBS, H. K.; HELKOWSKI, J. H.; HOLLOWAY, T.; HOWARD, E. A.; KUCHARIK, C. J.; MONFREDA, C.; PATZ, J. A.; PRENTICE, I. C.; RAMANKUTTY, N.; SNYDER, P. K. Global Consequences of Land Use. **Science**, v. 309, n. 5734, p. 570–574, 2005.

FOLEY, W. J.; MCILWEE, A.; LAWLER, I.; ARAGONES, L.; WOOLNOUGH, A. P.; BERDING, N. Ecological applications of near infrared reflectance spectroscopy - a tool for rapid, cost-effective prediction of the composition of plant and animal tissues and aspects of animal performance. **Oecologia**, v. 116, n. 3, p. 293–305, 1998.

FORMIGONI, M. D. H. **Análise temporal da vegetação associada à estimativa de precipitação pluvial por sensoriamento remoto na bacia hidrográfica do rio Doce.**

. 2018. Tese - Universidade Federal do Espírito Santo, 2018. Disponível em: https://repositorio.ufes.br/items/c8cebabd-7db5-4042-8b2b-9aa7fcbd4e83.

FORZIERI, G.; ALKAMA, R.; MIRALLES, D. G.; CESCATTI, A. Satellites reveal contrasting responses of regional climate to the widespread greening of Earth. **Science**, v. 356, n. 6343, p. 1180–1184, 2017.

FRAGA, M. D. S.; REIS, G. B.; DA SILVA, D. D.; GUEDES, H. A. S.; ELESBON, A. A. A. Use of multivariate statistical methods to analyze the monitoring of surface water quality in the Doce River basin, Minas Gerais, Brazil. **Environmental Science and Pollution Research**, v. 27, n. 28, p. 35303–35318, 2020.

FRICKO, O.; HAVLIK, P.; ROGELJ, J.; KLIMONT, Z.; GUSTI, M.; JOHNSON, N.; KOLP, P.; STRUBEGGER, M.; VALIN, H.; AMANN, M. The marker quantification of the Shared Socioeconomic Pathway 2: A middle-of-the-road scenario for the 21st century. **Global Environmental Change**, v. 42, p. 251–267, 2017.

FUJIMORI, S.; HASEGAWA, T.; MASUI, T.; TAKAHASHI, K.; HERRAN, D. S.; DAI, H.; HIJIOKA, Y.; KAINUMA, M. SSP3: AIM implementation of shared socioeconomic pathways. **Global Environmental Change**, v. 42, p. 268–283, 2017.

G1. **Desastre ambiental: 6 anos após rompimento de barragem, pesca continua proibida na foz do Rio Doce** Desastre ambiental. , 2021. Disponível em: https://g1.globo.com/es/espirito-santo/noticia/2021/11/05/desastre-ambiental-6-anos-apos-

rompimento-de-barragem-pesca-continua-proibida-na-foz-do-rio-doce.ghtml. Acesso em: 5 abr. 2025.

GAO, X.; ZHANG, A.; SUN, Z. How regional economic integration influence on urban land use efficiency? A case study of Wuhan metropolitan area, China. **Land Use Policy**, v. 90, p. 104329, 2020.

GILBERT, R. O. **Statistical methods for environmental pollution monitoring**. : John Wiley & Sons, 1987. 1987. Disponível em: https://books.google.com/books?hl=pt-BR&lr=&id=lEo1rvDGUEkC&oi=fnd&pg=PA1&dq=GILBERT,+R.+O.+Statistical+methods+for+environmental+pollution+monitoring.+New+York:+John+Wiley+%26+Sons,+1987.&ots=Fc1dTQ3Dp2&sig=iWMAon7Qur_npKpDjES21zExagE. Acesso em: 31 mar. 2025.

GOMES, Helber B.; AMBRIZZI, T.; PONTES DA SILVA, B. F.; HODGES, K.; SILVA DIAS, P. L.; HERDIES, D. L.; SILVA, M. C. L.; GOMES, Heliofábio B. Climatology of easterly wave disturbances over the tropical South Atlantic. **Climate Dynamics**, v. 53, n. 3–4, p. 1393–1411, 2019.

GOODACRE, R.; KELL, D. B.; BIANCHI, G. Rapid assessment of the adulteration of virgin olive oils by other seed oils using pyrolysis mass spectrometry and artificial neural networks. **Journal of the Science of Food and Agriculture**, v. 63, n. 3, p. 297–307, 1993.

GRINSTED, A.; MOORE, J. C.; JEVREJEVA, S. Application of the cross wavelet transform and wavelet coherence to geophysical time series. **Nonlinear processes in geophysics**, v. 11, n. 5/6, p. 561–566, 2004.

GROSSMAN-CLARKE, S.; ZEHNDER, J. A.; LORIDAN, T.; GRIMMOND, C. S. B. Contribution of land use changes to near-surface air temperatures during recent summer extreme heat events in the Phoenix metropolitan area. **Journal of Applied Meteorology and Climatology**, v. 49, n. 8, p. 1649–1664, 2010.

GUTJAHR, O.; HEINEMANN, G. Comparing bias correction methods for high-resolution COSMO-CLM daily precipitation fields. *Em*: EGU GENERAL ASSEMBLY CONFERENCE ABSTRACTS, 2012, . **Anais** [...]. , 2012. p. 4773. Disponível em: https://ui.adsabs.harvard.edu/abs/2012EGUGA..14.4773G/abstract. Acesso em: 31 mar. 2025.

HATJE, V.; PEDREIRA, R. M.; DE REZENDE, C. E.; SCHETTINI, C. A. F.; DE SOUZA, G. C.; MARIN, D. C.; HACKSPACHER, P. C. The environmental impacts of one of the largest tailing dam failures worldwide. **Scientific reports**, v. 7, n. 1, p. 10706, 2017.

HOFFMANN, H.; NIETO, H.; JENSEN, R.; GUZINSKI, R.; ZARCO-TEJADA, P. J.; FRIBORG, T. Estimating evapotranspiration with thermal UAV data and two source energy balance models. **Hydrology and Earth System Sciences Discussions**, v. 12, n. 8, p. 7469–7502, 2015.

HONKAVAARA, E.; SAARI, H.; KAIVOSOJA, J.; PÖLÖNEN, I.; HAKALA, T.; LITKEY, P.; MÄKYNEN, J.; PESONEN, L. Processing and assessment of spectrometric, stereoscopic imagery collected using a lightweight UAV spectral camera for precision agriculture. **Remote sensing**, v. 5, n. 10, p. 5006–5039, 2013.

HOU, H.; ZHOU, B.-B.; PEI, F.; HU, G.; SU, Z.; ZENG, Y.; ZHANG, H.; GAO, Y.; LUO, M.; LI, X. Future Land Use/Land Cover Change Has Nontrivial and Potentially Dominant

Impact on Global Gross Primary Productivity. **Earth's Future**, v. 10, n. 9, p. e2021EF002628, 2022.

HOYOS, L. E.; CINGOLANI, A. M.; ZAK, M. R.; VAIERETTI, M. V.; GORLA, D. E.; CABIDO, M. R. Deforestation and precipitation patterns in the arid C haco forests of central A rgentina. **Applied Vegetation Science**, v. 16, n. 2, p. 260–271, 2013.

HU, W.; SI, B. C. Technical note: Multiple wavelet coherence for untangling scale-specific and localized multivariate relationships in geosciences. **Hydrology and Earth System Sciences**, v. 20, n. 8, p. 3183–3191, 2016.

HU, J.; WU, Y.; WANG, L.; SUN, P.; ZHAO, F.; JIN, Z.; WANG, Y.; QIU, L.; LIAN, Y. Impacts of land-use conversions on the water cycle in a typical watershed in the southern Chinese Loess Plateau. **Journal of Hydrology**, v. 593, p. 125741, 2021.

HUETE, A.; DIDAN, K.; MIURA, T.; RODRIGUEZ, E. P.; GAO, X.; FERREIRA, L. G. Overview of the radiometric and biophysical performance of the MODIS vegetation indices. **Remote sensing of environment**, v. 83, n. 1–2, p. 195–213, 2002.

HUETE, A. R.; LIU, H. Q.; BATCHILY, K. V.; VAN LEEUWEN, W. A comparison of vegetation indices over a global set of TM images for EOS-MODIS. **Remote sensing of environment**, v. 59, n. 3, p. 440–451, 1997.

IBAMA. **Rompimento da Barragem de Fundão: Documentos relacionados ao desastre da Samarco em Mariana/MG** Rompimento da Barragem de Fundão. , 2023. Disponível em: https://www.gov.br/ibama/pt-br/assuntos/notas/2020/rompimento-da-barragem-de-fundao-documentos-relacionados-ao-desastre-da-samarco-em-mariana-mg. Acesso em: 5 abr. 2025.

ICHII, K.; KAWABATA, A.; YAMAGUCHI, Y. Global correlation analysis for NDVI and climatic variables and NDVI trends: 1982-1990. **International Journal of Remote Sensing**, v. 23, n. 18, p. 3873–3878, 2002.

IPCC. **AR6 Climate Change 2022: Impacts, Adaptation and Vulnerability — IPCC**. , 2022. Disponível em: https://www.ipcc.ch/report/sixth-assessment-report-working-group-ii/. Acesso em: 31 mar. 2025.

IPCC. **Climate change 2007: the physical science basis**. , 2007. Disponível em: https://www.slvwd.com/sites/g/files/vyhlif1176/f/uploads/item_10b_4.pdf. Acesso em: 31 mar. 2025.

IPCC. **IPCC, 2023: Climate Change 2023: Synthesis Report. Contribution of Working Groups I, II and III to the Sixth Assessment Report of the Intergovernmental Panel on Climate Change [Core Writing Team, H. Lee and J. Romero (eds.)]. IPCC, Geneva, Switzerland.** : Intergovernmental Panel on Climate Change (IPCC), 2023. Disponível em: https://www.ipcc.ch/report/ar6/syr/. Acesso em: 31 mar. 2025.

IRANNEZHAD, M.; LIU, J.; CHEN, D. Influential Climate Teleconnections for Spatiotemporal Precipitation Variability in the Lancang-Mekong River Basin From 1952 to 2015. **Journal of Geophysical Research: Atmospheres**, v. 125, n. 21, p. e2020JD033331, 2020.

JACKSON, R. B.; RANDERSON, J. T.; CANADELL, J. G.; ANDERSON, R. G.; AVISSAR, R.; BALDOCCHI, D. D.; BONAN, G. B.; CALDEIRA, K.; DIFFENBAUGH, N. S.; FIELD, C. B. Protecting climate with forests. **Environmental research letters**, v. 3, n. 4, p. 044006, 2008.

JALLIFFIER-VERNE, I.; LECONTE, R.; HUARINGA-ALVAREZ, U.; MADOUX-HUMERY, A.-S.; GALARNEAU, M.; SERVAIS, P.; PRÉVOST, M.; DORNER, S. Impacts of global change on the concentrations and dilution of combined sewer overflows in a drinking water source. **Science of the Total Environment**, v. 508, p. 462–476, 2015.

JANSEN, L. J.; DI GREGORIO, A. Parametric land cover and land-use classifications as tools for environmental change detection. **Agriculture, ecosystems & environment**, v. 91, n. 1–3, p. 89–100, 2002.

JESUS, E.; AMORIM, J.; VIOLA, M.; MELLO, C. R. Meteorological and hydrological drought from 1987 to 2017 in Doce River Basin, Southeastern Brazil. , 2020.

JIA, Z.; CHANG, X.; DUAN, T.; WANG, X.; WEI, T.; LI, Y. Water quality responses to rainfall and surrounding land uses in urban lakes. **Journal of environmental management**, v. 298, p. 113514, 2021.

JIANG, M.; PENG, H.; LIANG, S.; WANG, S.; KALIN, L.; BALTACI, E.; LIU, Y. Impact of extreme rainfall on non-point source nitrogen loss in coastal basins of Laizhou Bay, China. **Science of The Total Environment**, v. 881, p. 163427, 2023.

JIN, J.; MILLER, N. L.; SCHLEGEL, N. Sensitivity Study of Four Land Surface Schemes in the WRF Model. **Advances in Meteorology**, v. 2010, n. 1, p. 167436, 2010.

JIN, H.; WILLEMS, P.; CHEN, X.; LIU, M. Comprehensive evaluation of extreme hydrometeorological events coincidence and their interrelationships in the Hanjiang River Basin, China. **Journal of Hydrology**, v. 638, p. 131506, 2024.

JORGETTI, T.; DA SILVA DIAS, P. L.; DE FREITAS, E. D. The relationship between South Atlantic SST and SACZ intensity and positioning. **Climate Dynamics**, v. 42, n. 11–12, p. 3077–3086, 2014.

KABIR, S. M. A.; BHUIYAN, M. A.; ZHANG, G.; PRAMANIK, B. K. Microplastic distribution and ecological risks: investigating road dust and stormwater runoff across land uses. **Environmental Science: Advances**, v. 3, n. 1, p. 62–75, 2024.

KASTNER, T.; MATEJ, S.; FORREST, M.; GINGRICH, S.; HABERL, H.; HICKLER, T.; KRAUSMANN, F.; LASSLOP, G.; NIEDERTSCHEIDER, M.; PLUTZAR, C.; SCHWARZMÜLLER, F.; STEINKAMP, J.; ERB, K. Land use intensification increasingly drives the spatiotemporal patterns of the global human appropriation of net primary production in the last century. **Global Change Biology**, v. 28, n. 1, p. 307–322, 2022.

KAWASHIMA, R. S.; GIANNOTTI, M. A.; ALMEIDA, C. M. de; QUINTANILHA, J. A. Modelagem Dinâmica Espacial como ferramenta para simulação de cenários da paisagem na região portuária da Baixada Santista. **Boletim de Ciências Geodésicas**, v. 22, p. 703–718, 2016.

KIRBY, J. F.; SWAIN, C. J. Global and local isostatic coherence from the wavelet transform. **Geophysical Research Letters**, v. 31, n. 24, 2004. Disponível em: https://agupubs.onlinelibrary.wiley.com/doi/abs/10.1029/2004GL021569.

KLAAS, D. K.; IMTEAZ, M. A.; SUDIAYEM, I.; KLAAS, E. M.; KLAAS, E. C. Assessing climate changes impacts on tropical karst catchment: Implications on groundwater resource sustainability and management strategies. **Journal of Hydrology**, v. 582, p. 124426, 2020.

KLINK, C. A.; MACHADO, R. B. Conservation of the Brazilian Cerrado. **Conservation Biology**, v. 19, n. 3, p. 707–713, 2005.

KOGAN, F.; AND GUO, W. Strong 2015–2016 El Niño and implication to global ecosystems from space data. **International Journal of Remote Sensing**, v. 38, n. 1, p. 161–178, 2017.

KRIEGLER, E.; BAUER, N.; POPP, A.; HUMPENÖDER, F.; LEIMBACH, M.; STREFLER, J.; BAUMSTARK, L.; BODIRSKY, B. L.; HILAIRE, J.; KLEIN, D.; MOURATIADOU, I.; WEINDL, I.; BERTRAM, C.; DIETRICH, J.-P.; LUDERER, G.; PEHL, M.; PIETZCKER, R.; PIONTEK, F.; LOTZE-CAMPEN, H.; BIEWALD, A.; BONSCH, M.; GIANNOUSAKIS, A.; KREIDENWEIS, U.; MÜLLER, C.; ROLINSKI, S.; SCHULTES, A.; SCHWANITZ, J.; STEVANOVIC, M.; CALVIN, K.; EMMERLING, J.; FUJIMORI, S.; EDENHOFER, O. Fossil-fueled development (SSP5): An energy and resource intensive scenario for the 21st century. **Global Environmental Change**, v. 42, p. 297–315, 2017.

KULESZA, K.; HOŚCIŁO, A. Coherency and time lag analyses between MODIS vegetation indices and climate across forests and grasslands in the European temperate zone. **Biogeosciences**, v. 21, n. 10, p. 2509–2527, 2024.

KUNZLER, S. S. Análise interanual da influência da SACZ na Energia Natural Afluente dos Subsistemas em bacias hidrográficas da região Sudeste do Brasil. , 2018.

LAL, P.; DUBEY, A. K.; KUMAR, A.; KUMAR, P.; DWIVEDI, C. S. SAR–optical Remote Sensing Based Forest Cover And greenness esti-mation over India. **ISPRS Annals of the Photogrammetry, Remote Sensing and Spatial Information Sciences**, v. 4, p. 49–56, 2019.

LAL, P.; SHEKHAR, A.; KUMAR, A. Quantifying temperature and precipitation change caused by land cover change: a case study of India using the WRF model. **Frontiers in Environmental Science**, v. 9, p. 766328, 2021.

LAUREANTI, N. C.; CHOU, S. C.; NOBRE, P.; CURCHITSER, E. On the relationship between the South Atlantic Convergence Zone and sea surface temperature during Central-East Brazil extreme precipitation events. **Dynamics of Atmospheres and Oceans**, v. 105, p. 101422, 2024.

LAWRENCE, D. M.; HURTT, G. C.; ARNETH, A.; BROVKIN, V.; CALVIN, K. V.; JONES, A. D.; JONES, C. D.; LAWRENCE, P. J.; DE NOBLET-DUCOUDRÉ, N.; PONGRATZ, J. The Land Use Model Intercomparison Project (LUMIP) contribution to CMIP6: rationale and experimental design. **Geoscientific Model Development**, v. 9, n. 9, p. 2973–2998, 2016.

LEITE-FILHO, A. T.; SOARES-FILHO, B. S.; DAVIS, J. L.; ABRAHÃO, G. M.; BÖRNER, J. Deforestation reduces rainfall and agricultural revenues in the Brazilian Amazon. **Nature Communications**, v. 12, n. 1, p. 2591, 2021.

LI, P.; WANG, J.; LIU, Mengmeng; XUE, Z.; BAGHERZADEH, A.; LIU, Mengyun. Spatio-temporal variation characteristics of NDVI and its response to climate on the Loess Plateau from 1985 to 2015. **CATENA**, v. 203, p. 105331, 2021.

LIMA, R. P. C. **Avaliação de índices de severidade de seca na bacia do rio Doce visando ao desenvolvimento de sistema de classificação de secas**. 2016a. Dissertação - Universidade Federal de Viçosa, Viçosa 2016. Disponível em: https://bdtd.ibict.br/vufind/Record/UFV_888c3d8d2f2a178a55c3264a11092f6e. Acesso em: 1 abr. 2025.

LIMA, R. P. C. **Avaliação de índices de severidade de seca na bacia do rio Doce visando ao desenvolvimento de sistema de classificação de secas**. 2016b. Dissertação, 2016. Disponível em: https://bdtd.ibict.br/vufind/Record/UFV_888c3d8d2f2a178a55c3264a11092f6e. Acesso em: 31 mar. 2025.

LIMA, J. M.; ASSIS, W. L. O papel dos veranicos na variabilidade climática: bacia hidrográfica do Rio Doce-MG/ES e seu entorno. **Revista Brasileira de Climatologia**, v. 36, p. 100–128, 2025.

LIMA, J. M.; CUPOLILLO, F. Análise espaço-temporal das chuvas persistentes na região do Parque Estadual do Rio Doce–PERD, sob influências das ZCAS e ZCOU (OUT/2015 A DEZ/2016). **Revista Brasileira de Climatologia**, 2018. Disponível em: https://ojs.ufgd.edu.br/rbclima/article/view/14059. Acesso em: 2 abr. 2025.

LIMA, R. P.; SILVA, D. D.; MOREIRA, M. C.; PASSOS, J. B.; COELHO, C. D.; ELESBON, A. A. Development of an annual drought classification system based on drought severity indexes. **Anais da Academia Brasileira de Ciências**, v. 91, p. e20180188, 2019.

LIU, Y.; HUANG, T.; QIU, Z.; GUAN, Z.; MA, X. Effects of precipitation changes on fractional vegetation cover in the Jinghe River basin from 1998 to 2019. **Ecological Informatics**, v. 80, p. 102505, 2024.

LOVEJOY, S.; SCHERTZER, D.; VARON, D. Do GCMs predict the climate... or macroweather?. **Earth System Dynamics**, v. 4, n. 2, p. 439–454, 2013.

LUO, X.; GE, J.; GUO, W.; FAN, L.; CHEN, C.; LIU, Y.; YANG, L. The biophysical impacts of deforestation on precipitation: results from the CMIP6 model intercomparison. **Journal of Climate**, v. 35, n. 11, p. 3293–3311, 2022.

LYRA, B. U. **Efeitos das alterações no uso da terra sobre o regime hidrológico da bacia hidrográfica do rio Doce**. 2018. - Universidade Federal do Espirito Santo, 2018. Disponível em: https://repositorio.ufes.br/items/c38b9add-21dc-425e-a59b-cb5add144887. Acesso em: 31 mar. 2025.

MA, S.; ZHOU, S.; YU, B.; SONG, J. Deforestation-induced runoff changes dominated by forest-climate feedbacks. **Science Advances**, v. 10, n. 33, p. eadp3964, 2024.

MACHIWAL, D.; MADAN, K. **Hydrologic time series analysis: theory and practice**. , 2012. 2012. Disponível em: https://books.google.com.br/books?hl=pt-BR&lr=&id=GCCp1HuVb_EC&oi=fnd&pg=PR3&ots=sVgoezMX4A&sig=xd5mQLVRKVIklnyn6d9rZs3uchI&redir_esc=y#v=onepage&q&f=false. Acesso em: 5 abr. 2025.

MAHOWALD, N. M.; RANDERSON, J. T.; LINDSAY, K.; MUNOZ, E.; DONEY, S. C.; LAWRENCE, P.; SCHLUNEGGER, S.; WARD, D. S.; LAWRENCE, D.; HOFFMAN, F. M. Interactions between land use change and carbon cycle feedbacks. **Global Biogeochemical Cycles**, v. 31, n. 1, p. 96–113, 2017.

MARENGO, J. A. Interdecadal variability and trends of rainfall across the Amazon basin. **Theoretical and Applied Climatology**, v. 78, n. 1–3, 2004. Disponível em: http://link.springer.com/10.1007/s00704-004-0045-8. Acesso em: 31 mar. 2025.

MARENGO, J. A.; JONES, R.; ALVES, L. M.; VALVERDE, M. C. Future change of temperature and precipitation extremes in South America as derived from the PRECIS regional climate modeling system. **International Journal of Climatology: A Journal of the Royal Meteorological Society**, v. 29, n. 15, p. 2241–2255, 2009a.

MARENGO, J. A.; JONES, R.; ALVES, L. M.; VALVERDE, M. C. Future change of temperature and precipitation extremes in South America as derived from the PRECIS regional climate modeling system. **International Journal of Climatology: A Journal of the Royal Meteorological Society**, v. 29, n. 15, p. 2241–2255, 2009b.

MARENGO, J. A.; NOBRE, C. A.; SELUCHI, M. E.; CUARTAS, A.; ALVES, L. M.; MENDIONDO, E. M.; OBREGÓN, G.; SAMPAIO, G. A seca e a crise hídrica de 2014-2015 em São Paulo. **Revista Usp**, n. 106, p. 31–44, 2015.

MARENGO, J. A.; TOMASELLA, J.; UVO, C. R. Trends in streamflow and rainfall in tropical South America: Amazonia, eastern Brazil, and northwestern Peru. **Journal of Geophysical Research: Atmospheres**, v. 103, n. D2, p. 1775–1783, 1998.

MARENGO, J. A.; VALVERDE, M. C.; OBREGON, G. O. Observed and projected changes in rainfall extremes in the Metropolitan Area of São Paulo. **Climate research**, v. 57, n. 1, p. 61–72, 2013.

MATEUS, N. P. A. **Conexões entre fontes de calor, oscilação Madden Julian e vórtices ciclônicos de altos níveis na vizinhança do Nordeste do Brasil**. 2020. 141 f. - INPE, CPTEC/Cachoeira Paulista 2020. Disponível em: http://mtc-m21c.sid.inpe.br/col/sid.inpe.br/mtc-m21c/2020/03.16.12.40/doc/publicacao_FA%20provisoria.pdf. Acesso em: 31 mar. 2025.

MATEUS, N. P. A.; PUJONI, D. G. F.; CUNHA, M. A.; RIBEIRO, S. C. The impacts of the spatial variation of south atlantic convergence zone on rainfall, flow and water quality in river doce, Brazil. **S. C.**, 2025.

MATSON, P. A.; PARTON, W. J.; POWER, A. G.; SWIFT, M. J. Agricultural Intensification and Ecosystem Properties. **Science**, v. 277, n. 5325, p. 504–509, 1997.

MAY, P. H.; ALONSO, L. B. N.; BARBOSA, F. A. R.; BRITO, M. C. W. de; LAUREANO, F. V.; MAROUN, C.; SÁNCHEZ, L. E.; KAKABADSE, Y. Mainstreaming climate change in the Rio Doce watershed restoration. , 2020. Disponível em:

https://repositorio.usp.br/directbitstream/e30cb381-eb5e-491a-885b-c6b6b7e390cb/Sanchez-2020-Mainstreaming+climate+change+in+the+Rio+Doce+watershed+restoration.pdf. Acesso em: 31 mar. 2025.

MAYTA, V. C.; TERUYA, A. S.; RAPHALDINI, B.; DA SILVA DIAS, P. L.; SAPUCCI, C. **South America Intraseasonal Precipitation: A Normal-Mode Approach** : Atmospheric Sciences, 2020. Disponível em: https://essopenarchive.org/doi/full/10.1002/essoar.10505130.1. Acesso em: 3 abr. 2025.

MCCABE, G. J.; WOLOCK, D. M. Independent effects of temperature and precipitation on modeled runoff in the conterminous United States. **Water Resources Research**, v. 47, n. 11, p. 2011WR010630, 2011.

MCCONNELL, W. J. Misconstrued land use in Vohibazaha: participatory planning in the periphery of Madagascar's Mantadia National Park. **Land Use Policy**, v. 19, n. 3, p. 217–230, 2002.

MCKEE, B. T. Drought monitoring with multiple time scales. , 1995. Disponível em: t: https://ci.nii.ac.jp/naid/ 10028178079.

MCKEE, T. B.; DOESKEN, N. J.; KLEIST, J. The relationship of drought frequency and duration to time scales. , 1993.

MONTINI, T. L.; JONES, C.; CARVALHO, L. M. V. The South American Low-Level Jet: A New Climatology, Variability, and Changes. **Journal of Geophysical Research: Atmospheres**, v. 124, n. 3, p. 1200–1218, 2019.

MOORE, A. W.; ANDERSON, B.; DAS, K.; WONG, W.-K. Combining multiple signals for biosurveillance. **Handbook of biosurveillance**, p. 235, 2007.

MULLA, D. J. Twenty five years of remote sensing in precision agriculture: Key advances and remaining knowledge gaps. **Biosystems engineering**, v. 114, n. 4, p. 358–371, 2013.

NAQI, N. M.; AL-JIBOORI, M. H.; AL-MADHHACHI, A.-S. T. Statistical analysis of extreme weather events in the Diyala River basin, Iraq. **Journal of Water and Climate Change**, v. 12, n. 8, p. 3770–3785, 2021.

NASCIMENTO, R. A. A Zona de Convergência do Atlântico Sul-ZCAS e os eventos pluviais intensos no município de Piranga-MG. **Revista Acta Geográfica, Roraima-RR**, v. 6, p. 101–113, 2012.

NATIVIDADE, U. A.; GARCIA, S. R.; TORRES, R. R. Tendência dos índices de extremos climáticos observados e projetados no estado de Minas Gerais. **Revista Brasileira de Meteorologia**, v. 32, p. 600–614, 2017.

NETO, O. B.; ESCOBAR, G. C.; SILVA, PHILIPE. Método objetivo para identificar episódios de Zonas de Convergência de Umidade (ZCOU) no ambiente operacional do Centro de Previsão de Tempo e Estados Climáticos - CPTEC. , 2010.

NEVES, D. de S. **Uso do solo na bacia do rio Doce: relações com o clima e com o desastre da SAMARCO/BHP Billiton/VALE**. 2022. 72 f. Dissertação - Universidade Federal de Viçosa, Viçosa 2022. Disponível em:

https://bdtd.ibict.br/vufind/Record/UFV_f9eb04c5ab4bc7f13f333fdead9653cc. Acesso em: 31 mar. 2025.

NEVES, D. de S.; SILVÉRIO, D. V.; ROTHE-NEVES, M.; FERREIRA, F. F.; IORIO, G. S.; SPERBER, C. F. Changes in land use dynamics following the Fundão dam collapse in the Doce River Basin, Brazil. **Total Environment Advances**, v. 12, p. 200112, 2024.

NOGUÉS-PAEGLE, J.; MO, K. C. Alternating wet and dry conditions over South America during summer. **Monthly Weather Review**, v. 125, n. 2, p. 279–291, 1997.

OLIVEIRA, B. R. D.; CARVALHO-RIBEIRO, S. M.; MAIA-BARBOSA, P. M. A multiscale analysis of land use dynamics in the buffer zone of Rio Doce State Park, Minas Gerais, Brazil. **Journal of Environmental Planning and Management**, v. 63, n. 5, p. 935–957, 2020.

OLIVEIRA, K. S. S.; DA SILVA QUARESMA, V. Temporal variability in the suspended sediment load and streamflow of the Doce River. **Journal of South American Earth Sciences**, v. 78, p. 101–115, 2017.

OLIVEIRA, V. A. de; MELLO, C. R. de; VIOLA, M. R.; SRINIVASAN, R. Land-use change impacts on the hydrology of the upper Grande river basin, Brazil. **Cerne**, v. 24, n. 4, p. 334–343, 2018.

OLIVEIRA, K. S. S.; QUARESMA, V. D. S. Temporal variability in the suspended sediment load and streamflow of the Doce River. **Journal of South American Earth Sciences**, v. 78, p. 101–115, 2017.

OLSEN, R. L.; CHAPPELL, R. W.; LOFTIS, J. C. Water quality sample collection, data treatment and results presentation for principal components analysis–literature review and Illinois River watershed case study. **Water research**, v. 46, n. 9, p. 3110–3122, 2012.

PACHECO, F. A. L.; DE OLIVEIRA, M. D.; OLIVEIRA, M. S.; LIBÂNIO, M.; DO VALLE JUNIOR, R. F.; DE MELO SILVA, M. M. A. P.; PISSARRA, T. C. T.; DE MELO, M. C.; VALERA, C. A.; FERNANDES, L. F. S. Water security threats and challenges following the rupture of large tailings dams. **Science of The Total Environment**, v. 834, p. 155285, 2022.

PAIVA, C. M. **Determinação das datas inicial e final da estação chuvosa e da ocorrência de veranico na Bacia do Rio Doce**. 1996. Tese - Universidade Federal de Viçosa, Viçosa 1996. Disponível em: http://www.locus.ufv.br/handle/123456789/11418. Acesso em: 1 abr. 2025.

PATEL, L.; SINGH, R.; THOTTATHIL, S. D. Land use drivers of riverine methane dynamics in a tropical river basin, India. **Water Research**, v. 228, p. 119380, 2023.

PAZINI, D. F.; FREITAS, A. C. V.; BELOTTI, F. M. A influência da Zona de Convergência do Atlântico Sul (ZCAS) na ocorrência de deslizamentos de massa em Belo Horizonte e cidades vizinhas. **Revista Brasileira de Climatologia**, v. 27, p. 635–659, 2020.

PBMC. **Mudanças Climáticas e Cidades: Relatório Especial do Painel Brasileiro de Mudanças Climáticas**. , 2014. Disponível em: http://adaptaclima.mma.gov.br/conteudos/56. Acesso em: 2 abr. 2025.

PEIXOTO, A. L.; SILVA, I. M.; JOSÉ, O.; SIMONELLI, M.; DE JESUS, R. M.; ROLIM, S. G. Tabuleiro Forests North of the Rio Doce: Their Representation in the Vale do Rio Doce Natural Reserve, Espírito Santo, Brazil. , 2008.

PEZZI, L. P.; QUADRO, M. F. L.; LORENZZETTI, J. A.; MILLER, A. J.; ROSA, E. B.; LIMA, L. N.; SUTIL, U. A. The effect of Oceanic South Atlantic Convergence Zone episodes on regional SST anomalies: the roles of heat fluxes and upper-ocean dynamics. **Climate Dynamics**, v. 59, n. 7–8, p. 2041–2065, 2022.

PEZZI, L. P.; QUADRO, M. F.; SOUZA, E. B.; MILLER, A. J.; RAO, V. B.; ROSA, E. B.; SANTINI, M. F.; BENDER, A.; SOUZA, R. B.; CABRERA, M. J. Oceanic SACZ produces an abnormally wet 2021/2022 rainy season in South America. **Scientific Reports**, v. 13, n. 1, p. 1455, 2023.

PIELKE, R. A.; MARLAND, G.; BETTS, R. A.; CHASE, T. N.; EASTMAN, J. L.; NILES, J. O.; NIYOGI, D. D. S.; RUNNING, S. W. The influence of land-use change and landscape dynamics on the climate system: relevance to climate-change policy beyond the radiative effect of greenhouse gases. **Philosophical Transactions of the Royal Society of London. Series A: Mathematical, Physical and Engineering Sciences**, v. 360, n. 1797, p. 1705–1719, 2002.

PIRES, A. P.; REZENDE, C. L.; ASSAD, E. D.; LOYOLA, R.; SCARANO, F. R. Forest restoration can increase the Rio Doce watershed resilience. **Perspectives in ecology and conservation**, v. 15, n. 3, p. 187–193, 2017.

PIRH. Plano Integrado de Recursos Hídricos da Bacia Hidrográfica do Rio Doce-PIRH Bacia do Rio Doce-Volume I. **Consórcio Ecoplan-Lume**, 2010.

PITMAN, A. J.; DE NOBLET-DUCOUDRÉ, N.; CRUZ, F. T.; DAVIN, E. L.; BONAN, G. B.; BROVKIN, V.; CLAUSSEN, M.; DELIRE, C.; GANZEVELD, L.; GAYLER, V.; VAN DEN HURK, B. J. J. M.; LAWRENCE, P. J.; VAN DER MOLEN, M. K.; MÜLLER, C.; REICK, C. H.; SENEVIRATNE, S. I.; STRENGERS, B. J.; VOLDOIRE, A. Uncertainties in climate responses to past land cover change: First results from the LUCID intercomparison study. **Geophysical Research Letters**, v. 36, n. 14, p. 2009GL039076, 2009.

PONGRATZ, J.; REICK, C. H.; RADDATZ, T.; CLAUSSEN, M. Biogeophysical versus biogeochemical climate response to historical anthropogenic land cover change. **Geophysical Research Letters**, v. 37, n. 8, p. 2010GL043010, 2010.

PORTAL GOV. **Conheça a linha do tempo da tragédia de Mariana (MG)**. , 2015. Disponível em: https://www.gov.br/planalto/pt-br/repactuacao-do-acordo-do-rio-doce/conheca-a-linha-do-tempo-da-tragedia-de-mariana-mg. Acesso em: 5 abr. 2025.

POTAPOV, P.; TURUBANOVA, S.; HANSEN, M. C.; TYUKAVINA, A.; ZALLES, V.; KHAN, A.; SONG, X.-P.; PICKENS, A.; SHEN, Q.; CORTEZ, J. Global maps of cropland extent and change show accelerated cropland expansion in the twenty-first century. **Nature Food**, v. 3, n. 1, p. 19–28, 2022.

QUADRO, M. F. L. de. Estudo de episódios de zonas de convergência do Atlântico Sul (ZCAS) sobre a América do Sul. **Revista Brasileira de Geofísica**, v. 17, p. 210–210, 1999.

QUAN, N. T.; KHOI, D. N.; HOAN, N. X.; PHUNG, N. K.; DANG, T. D. Spatiotemporal Trend Analysis of Precipitation Extremes in Ho Chi Minh City, Vietnam During 1980–2017. **International Journal of Disaster Risk Science**, v. 12, n. 1, p. 131–146, 2021.

RAHNAMA, M. R. Forecasting land-use changes in Mashhad Metropolitan area using Cellular Automata and Markov chain model for 2016-2030. **Sustainable Cities and Society**, v. 64, p. 102548, 2021.

REBOITA, M. S.; GAN, M. A.; ROCHA, R. P. da; AMBRIZZI, T. Regimes de precipitação na América do Sul: uma revisão bibliográfica. **Revista brasileira de meteorologia**, v. 25, p. 185–204, 2010.

REBOITA, M. S.; VEIGA, J. A. P. Análise Sinótica e Energética de um VCAN que Causou Chuva no Deserto do Atacama em Março de 2015. **Revista Brasileira de Meteorologia**, v. 32, n. 1, p. 123–139, 2017.

REICHSTEIN, M.; BAHN, M.; MAHECHA, M. D.; KATTGE, J.; BALDOCCHI, D. D. Linking plant and ecosystem functional biogeography. **Proceedings of the National Academy of Sciences**, v. 111, n. 38, p. 13697–13702, 2014.

REN, Y.; ZHANG, J.; FU, J.; PENG, S.; LI, Z. Spatiotemporally varied extreme precipitation events simultaneously controlled by multiple circulation factors in China's Loess Plateau. **International Journal of Climatology**, v. 42, n. 12, p. 6351–6372, 2022.

RODRIGUES, H. O.; SOARES-FILHO, B. S.; COSTA, W. de S. Dinamica EGO, uma plataforma para modelagem de sistemas ambientais. **Simpósio Brasileiro de Sensoriamento Remoto**, v. 13, p. 3089–3096, 2007.

RODRIGUES, R. R.; TASCHETTO, A. S.; SEN GUPTA, A.; FOLTZ, G. R. Common cause for severe droughts in South America and marine heatwaves in the South Atlantic. **Nature Geoscience**, v. 12, n. 8, p. 620–626, 2019.

RUSTICUCCI, M. Observed and simulated variability of extreme temperature events over South America. **Atmospheric Research**, v. 106, p. 1–17, 2012.

SALOMÃO, C. C. de S.; DE SOUZA PAULA, L. G.; TIMBÓ ELMIRO, M. A. Use of multicriteria analysis to define priority areas for reforestation in the Piranga River Basin, MG, Brazil. **Sustainability in Debate/Sustentabilidade em Debate**, v. 11, n. 2, 2020. Disponível em: https://pdfs.semanticscholar.org/aa47/ad7aaa72f8d263028cf00bfcbe60b9c7ef3b.pdf. Acesso em: 31 mar. 2025.

SALVADOR, M. da M. **Identificação e avaliação de eventos extremos na bacia hidrográfica do Rio Piranga**. 2014. 49 f. Dissertação - Universidade Federal de Viçosa, Viçosa 2014. Disponível em: https://www.locus.ufv.br/bitstream/123456789/3823/1/texto%20completo.pdf. Acesso em: 31 mar. 2025.

SAMBIENI, K. S.; HOUNTONDJI, F. C.; SINTONDJI, L. O.; FOHRER, N.; BIAOU, S.; SOSSA, C. L. G. Climate and Land Use/Land Cover Changes within the Sota Catchment (Benin, West Africa). **Hydrology**, v. 11, n. 3, p. 30, 2024.

SANTANA, F. C.; FRANCELINO, M. R.; SCHAEFER, C. E. G. R.; VELOSO, G. V.; FERNANDES-FILHO, E. I.; SANTANA, A. D. J. P.; TIMO, L. B.; ROSA, A. P. Water Quality of the Gualaxo do Norte and Carmo Rivers After the Fundão Dam Collapse, Mariana, MG. **Water, Air, & Soil Pollution**, v. 232, n. 4, p. 155, 2021.

SELUCHI, M. E.; CHOU, S. C. Synoptic patterns associated with landslide events in the Serra do Mar, Brazil. **Theoretical and Applied Climatology**, v. 98, n. 1–2, p. 67–77, 2009.

SEN, P. K. Estimates of the Regression Coefficient Based on Kendall's Tau. **Journal of the American Statistical Association**, v. 63, n. 324, p. 1379–1389, 1968.

SHEKHAR, A.; CHEN, J.; PAETZOLD, J. C.; DIETRICH, F.; ZHAO, X.; BHATTACHARJEE, S.; RUISINGER, V.; WOFSY, S. C. Anthropogenic CO2 emissions assessment of Nile Delta using XCO2 and SIF data from OCO-2 satellite. **Environmental Research Letters**, v. 15, n. 9, p. 095010, 2020.

SIEGEL, A. F. Robust regression using repeated medians. **Biometrika**, v. 69, n. 1, p. 242–244, 1982.

SILVA BEZERRA, F. G.; VON RANDOW, C.; ASSIS, T. O.; BEZERRA, K. R. A.; TEJADA, G.; CASTRO, A. A.; GOMES, D. M. de P.; AVANCINI, R.; AGUIAR, A. P. New land-use change scenarios for Brazil: Refining global SSPs with a regional spatially-explicit allocation model. **PLoS One**, v. 17, n. 4, p. e0256052, 2022.

SILVA, P. do N.; ESCOBAR, G. C. J.; REBOITA, M. S. Eventos extremos de precipitação no Estado de Minas Gerais associados com a ocorrência de episódios de Zona de Convergência do Atlântico Sul. **Revista Brasileira de Geografia Física**, v. 13, n. 3, p. 1013–1023, 2020.

SILVA, J. R.; SIQUEIRA, L. AVALIAÇÃO TEMPORAL DA VARIAÇÃO DE COBERTURA DE SOLO ATRAVÉS DA UTILIZAÇÃO DE ÍNDICES DE VEGETAÇÃO NORMALIZADO (NDVI) E AJUSTADO AO SOLO (SAVI): CASO DE ESTUDO PARA O RIO DOCE E O DESASTRE AMBIENTAL DE MARIANA. , 2017. Disponível em: https://www.cartografia.org.br/cbc/2017/trabalhos/4/fullpaper/CT04-92_1506820306.pdf.

SMITH, C.; BAKER, J. C. A.; SPRACKLEN, D. V. Tropical deforestation causes large reductions in observed precipitation. **Nature**, v. 615, n. 7951, p. 270–275, 2023.

SOARES-FILHO, B.; ALENCAR, A.; NEPSTAD, D.; CERQUEIRA, G.; VERA DIAZ, M. D. C.; RIVERO, S.; SOLÓRZANO, L.; VOLL, E. Simulating the response of land-cover changes to road paving and governance along a major Amazon highway: the Santarém–Cuiabá corridor. **Global Change Biology**, v. 10, n. 5, p. 745–764, 2004.

SOARES-FILHO, B. S.; CERQUEIRA, G. C.; PENNACHIN, C. L. DINAMICA—a stochastic cellular automata model designed to simulate the landscape dynamics in an Amazonian colonization frontier. **Ecological modelling**, v. 154, n. 3, p. 217–235, 2002.

SONDERMANN, M.; CHOU, S. C.; LYRA, A.; LATINOVIC, D.; SIQUEIRA, G. C.; JUNIOR, W. C.; GIORNES, E.; LEITE, F. P. Climate change projections and impacts on the eucalyptus plantation around the Doce River basin, in Minas Gerais, Brazil. **Climate Services**, v. 28, p. 100327, 2022a.

SONDERMANN, M.; CHOU, S. C.; LYRA, A.; LATINOVIC, D.; SIQUEIRA, G. C.; JUNIOR, W. C.; GIORNES, E.; LEITE, F. P. Climate change projections and impacts on the eucalyptus plantation around the Doce River basin, in Minas Gerais, Brazil. **Climate Services**, v. 28, p. 100327, 2022b.

SOUZA JR, C. M.; Z. SHIMBO, J.; ROSA, M. R.; PARENTE, L. L.; A. ALENCAR, A.; RUDORFF, B. F.; HASENACK, H.; MATSUMOTO, M.; G. FERREIRA, L.; SOUZA-FILHO, P. W. Reconstructing three decades of land use and land cover changes in brazilian biomes with landsat archive and earth engine. **Remote Sensing**, v. 12, n. 17, p. 2735, 2020.

SOUZA, E. de; PONTES, L. M.; FERNANDES FILHO, E. I.; SCHAEFER, C. E. G. R.; SANTOS, E. E. dos. Spatial and temporal potential groundwater recharge: The case of the doce river basin, Brazil. **Revista Brasileira de Ciência do Solo**, v. 43, p. e0180010, 2018.

SPOSITO, E. C. **Uso e cobertura do solo na bacia hidrográfica do rio Doce (MG/ES): inter-relações para a governança**. 2021. 203 f. Dissertação - Universidade Federal de Viçosa, 2021. Disponível em: https://bdtd.ibict.br/vufind/Record/UFV_81c90eee0d59beac33025fcea5dde2b2. Acesso em: 31 mar. 2025.

SPRACKLEN, D. V.; ARNOLD, S. R.; TAYLOR, C. M. Observations of increased tropical rainfall preceded by air passage over forests. **Nature**, v. 489, n. 7415, p. 282–285, 2012.

SVENNING, J.-C.; SANDEL, B. Disequilibrium vegetation dynamics under future climate change. **American Journal of Botany**, v. 100, n. 7, p. 1266–1286, 2013.

TEIXEIRA, R. L. P.; PESSOA, Z. S. Planejamento urbano e adaptação climática: entre possibilidades e desafios em duas grandes cidades brasileiras. **Revista Brasileira de Estudos de População**, v. 38, p. e0165, 2021.

THEIL, hENRI. A rank-invariant method of linear and polynomial regression analysis}. , 1950. Disponível em: https://ir.cwi.nl/pub/18446/18446A.pdf.

TIAN, W.; LIU, X.; LIU, C.; BAI, P. Investigation and simulations of changes in the relationship of precipitation-runoff in drought years. **Journal of Hydrology**, v. 565, p. 95–105, 2018.

TORRENCE, C.; COMPO, G. P. A Practical Guide to Wavelet Analysis. **Bulletin of the American Meteorological Society**, Boston MA, USAv. 79, n. 1, p. 61–78, 1998.

TRIGUEIRO, W. R.; NABOUT, J. C.; TESSAROLO, G. Uncovering the spatial variability of recent deforestation drivers in the Brazilian Cerrado. **Journal of Environmental Management**, v. 275, p. 111243, 2020.

TUNDISI, J. G. Recursos hídricos no futuro: problemas e soluções. **Estudos avançados**, v. 22, p. 7–16, 2008.

UICN. **Integração da perspectiva da mudança climática na restauração da Bacia do Rio Doce**. : IUCN, International Union for Conservation of Nature, 2022. Disponível em: https://portals.iucn.org/library/node/49067. Acesso em: 2 abr. 2025.

ULLAH, S.; QIAO, X.; ABBAS, M. Addressing the impact of land use land cover changes on land surface temperature using machine learning algorithms. **Scientific Reports**, v. 14, n. 1, p. 18746, 2024.

VALVERDE, A. E. L.; SILVA, D. da; PRUSKI, F. F.; LEITE, H. G.; BRANDÃO, V. dos S. Análise regional de chuvas intensas para a bacia do rio Doce. **Revista Brasileira de Recursos Hídricos**, v. 8, n. 4, p. 157–168, 2003.

VANCINE, M. H.; MUYLAERT, R. L.; NIEBUHR, B. B.; DE FARIA OSHIMA, J. E.; TONETTI, V.; BERNARDO, R.; DE ANGELO, C.; ROSA, M. R.; GROHMANN, C. H.; RIBEIRO, M. C. The Atlantic Forest of South America: spatiotemporal dynamics of the vegetation and implications for conservation. **Biological Conservation**, v. 291, p. 110499, 2024.

VANELI, B. P.; ARAÚJO, E. M. de S.; OLIVEIRA, D. B.-H. S. de; SPAGNOL, I. T.; TEIXEIRA, E. C. Conceptual model to analyze the effects caused by technological disaster on the physical-chemical state of the lower Doce River waters, Brazil. **Science of The Total Environment**, v. 809, p. 152168, 2022.

VEIGA, S. F.; NOBRE, P.; GIAROLLA, E.; CAPISTRANO, V. B.; DA SILVA JR, M. B.; CASAGRANDE, F.; SOARES, H. C.; KUBOTA, P. Y.; FIGUEROA, S. N.; BOTTINO, M. J. Climate change over South America simulated by the Brazilian Earth system model under RCP4. 5 and RCP8. 5 scenarios. **Journal of South American Earth Sciences**, v. 131, p. 104598, 2023.

VIANA, L. P.; MANCO, J. A.; HERDIES, D. L. Dynamic Characteristics of the Circulation and Diurnal Spatial Cycle of Outgoing Longwave Radiation in the Different Phases of the Madden–Julian Oscillation during the Formation of the South Atlantic Convergence Zone. **Atmosphere**, v. 12, n. 11, p. 1399, 2021.

VINCENT, J. B.; HENNING, B.; SAULEI, S.; SOSANIKA, G.; WEIBLEN, G. D. Forest carbon in lowland P apua N ew G uinea: Local variation and the importance of small trees. **Austral Ecology**, v. 40, n. 2, p. 151–159, 2015.

VON STORCH, H. Misuses of Statistical Analysis in Climate Research. *Em*: VON STORCH, Hans; NAVARRA, Antonio (org.). **Analysis of Climate Variability**. Berlin, Heidelberg: Springer Berlin Heidelberg, 1999. p. 11–26. Disponível em: http://link.springer.com/10.1007/978-3-662-03744-7_2. Acesso em: 31 mar. 2025.

VON STORCH, H.; ZORITA, E.; CUBASCH, U. Downscaling of global climate change estimates to regional scales: an application to Iberian rainfall in wintertime. **Journal of Climate**, v. 6, n. 6, p. 1161–1171, 1993.

WAMSLER, C.; BRINK, E.; RIVERA, C. Planning for climate change in urban areas: from theory to practice. **Journal of Cleaner Production**, v. 50, p. 68–81, 2013.

WANG, Yanzhao; SUN, Y.; CAO, X.; WANG, Yihan; ZHANG, W.; CHENG, X. A review of regional and Global scale Land Use/Land Cover (LULC) mapping products generated from satellite remote sensing. **ISPRS Journal of Photogrammetry and Remote Sensing**, v. 206, p. 311–334, 2023.

WANG, Z.-J.; YUE, F.-J.; WANG, Y.-C.; QIN, C.-Q.; DING, H.; XUE, L.-L.; LI, S.-L. The effect of heavy rainfall events on nitrogen patterns in agricultural surface and underground streams and the implications for karst water quality protection. **Agricultural Water Management**, v. 266, p. 107600, 2022.

WEI, S.; WANG, X.; WANG, C.; XIE, Q. El Niño phase transition by deforestation in the Maritime Continent. **npj Climate and Atmospheric Science**, v. 7, n. 1, p. 3, 2024.

WILLIAMS, K. D.; INGRAM, W. J.; GREGORY, J. M. Time variation of effective climate sensitivity in GCMs. **Journal of Climate**, v. 21, n. 19, p. 5076–5090, 2008.

WONG, M. L.; BATTISTI, D. S.; LIU, X.; DING, Q.; WANG, X. A North–South Dipole Response of the South Atlantic Convergence Zone During the Mid-Holocene. **Geophysical Research Letters**, v. 50, n. 23, p. e2023GL105130, 2023.

WONG, M. L.; WANG, X.; LATRUBESSE, E. M.; HE, S.; BAYER, M. Variations in the South Atlantic Convergence Zone over the mid-to-late Holocene inferred from speleothem δ18O in central Brazil. **Quaternary Science Reviews**, v. 270, p. 107178, 2021.

WU, H.; SOH, L.-K.; SAMAL, A.; CHEN, X.-H. Trend Analysis of Streamflow Drought Events in Nebraska. **Water Resources Management**, v. 22, n. 2, p. 145–164, 2008.

XIA, T.; KUSTAS, W. P.; ANDERSON, M. C.; ALFIERI, J. G.; GAO, F.; MCKEE, L.; PRUEGER, J. H.; GELI, H. M.; NEALE, C. M.; SANCHEZ, L. Mapping evapotranspiration with high-resolution aircraft imagery over vineyards using one-and two-source modeling schemes. **Hydrology and Earth System Sciences**, v. 20, n. 4, p. 1523–1545, 2016.

XIA, X. H.; WU, Q.; MOU, X. L.; LAI, Y. J. Potential impacts of climate change on the water quality of different water bodies. **J. Environ. Inform**, v. 25, n. 2, p. 85–98, 2015.

XU, W.; LIN, T.; LEI, X.; CHEN, Y.; GAO, L. Anthropogenic emissions and land use/cover change contributions to extreme temperature changes over China. **Atmospheric Research**, v. 292, p. 106845, 2023.

YANG, L.; LI, J.; ZHOU, K.; FENG, P.; DONG, L. The effects of surface pollution on urban river water quality under rainfall events in Wuqing district, Tianjin, China. **Journal of Cleaner Production**, v. 293, p. 126136, 2021.

YOUNESZADEH, S.; AMIRI, N.; PILESJO, P. The effect of land use change on land surface temperature in the Netherlands. **The International Archives of the Photogrammetry, Remote Sensing and Spatial Information Sciences**, v. 40, p. 745–748, 2015.

YUE, S.; WANG, C. The Mann-Kendall Test Modified by Effective Sample Size to Detect Trend in Serially Correlated Hydrological Series. **Water Resources Management**, v. 18, n. 3, p. 201–218, 2004.

ZEMP, D. C.; SCHLEUSSNER, C. -F.; BARBOSA, H. M. J.; RAMMIG, A. Deforestation effects on Amazon forest resilience. **Geophysical Research Letters**, v. 44, n. 12, p. 6182–6190, 2017.

ZENG, Z.; PIAO, S.; LI, L. Z.; ZHOU, L.; CIAIS, P.; WANG, T.; LI, Y.; LIAN, X. U.; WOOD, E. F.; FRIEDLINGSTEIN, P. Climate mitigation from vegetation biophysical

feedbacks during the past three decades. **Nature Climate Change**, v. 7, n. 6, p. 432–436, 2017.

ZHANG, J.; HAO, Y.; HU, B. X.; HUO, X.; HAO, P.; LIU, Z. The effects of monsoons and climate teleconnections on the Niangziguan Karst Spring discharge in North China. **Climate Dynamics**, v. 48, n. 1–2, p. 53–70, 2017.

ZHENGXING, W.; CHUANG, L.; ALFREDO, H. From AVHRR-NDVI to MODIS-EVI: Advances in vegetation index research. **Acta Ecologica Sinica**, v. 23, n. 5, p. 979—987, 2003.

ZHOU, J.; LAU, K. -M. Principal modes of interannual and decadal variability of summer rainfall over South America. **International Journal of Climatology**, v. 21, n. 13, p. 1623–1644, 2001.

ZHU, K.; CHENG, Y.; ZANG, W.; ZHOU, Q.; EL ARCHI, Y.; MOUSAZADEH, H.; KABIL, M.; CSOBÁN, K.; DÁVID, L. D. Multiscenario simulation of land-use change in Hubei Province, China based on the Markov-FLUS Model. **Land**, v. 12, n. 4, p. 744, 2023.

ZILLI, M. T.; CARVALHO, L. M. V. Detection and attribution of precipitation trends associated with the poleward shift of the South Atlantic Convergence Zone using CMIP5 simulations. **International Journal of Climatology**, v. 41, n. 5, p. 3085–3106, 2021.

ZORZAL-ALMEIDA, S.; DE OLIVEIRA FERNANDES, V. Ecological thresholds of periphytic communities and ecosystems integrity in lower Doce River basin. **Science of the Total Environment**, v. 796, p. 148965, 2021.

APPENDIX A - CHAPTER 4 SUPPLEMENTAL INFORMATION

The shading refers to longwave radiation, the lines represent the streamlines at the 300 hPa level. On the left is a zoom of the Doce River Basin.

Figure 39 - Analysis of SACZ Patterns Using OLR

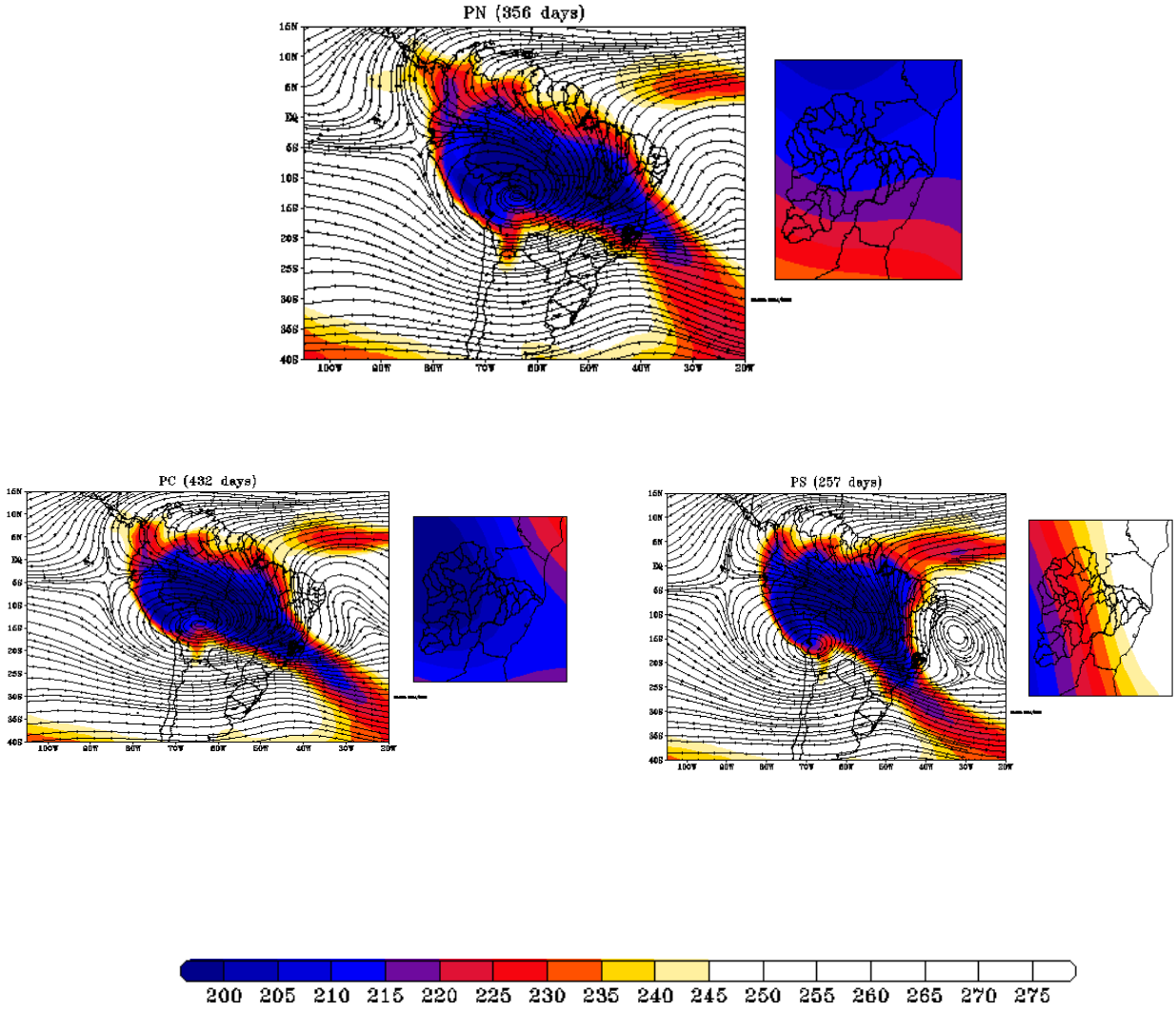

Source: elaborated by the author.

Figure 40 - Moisture transport at the 925 hPa level.

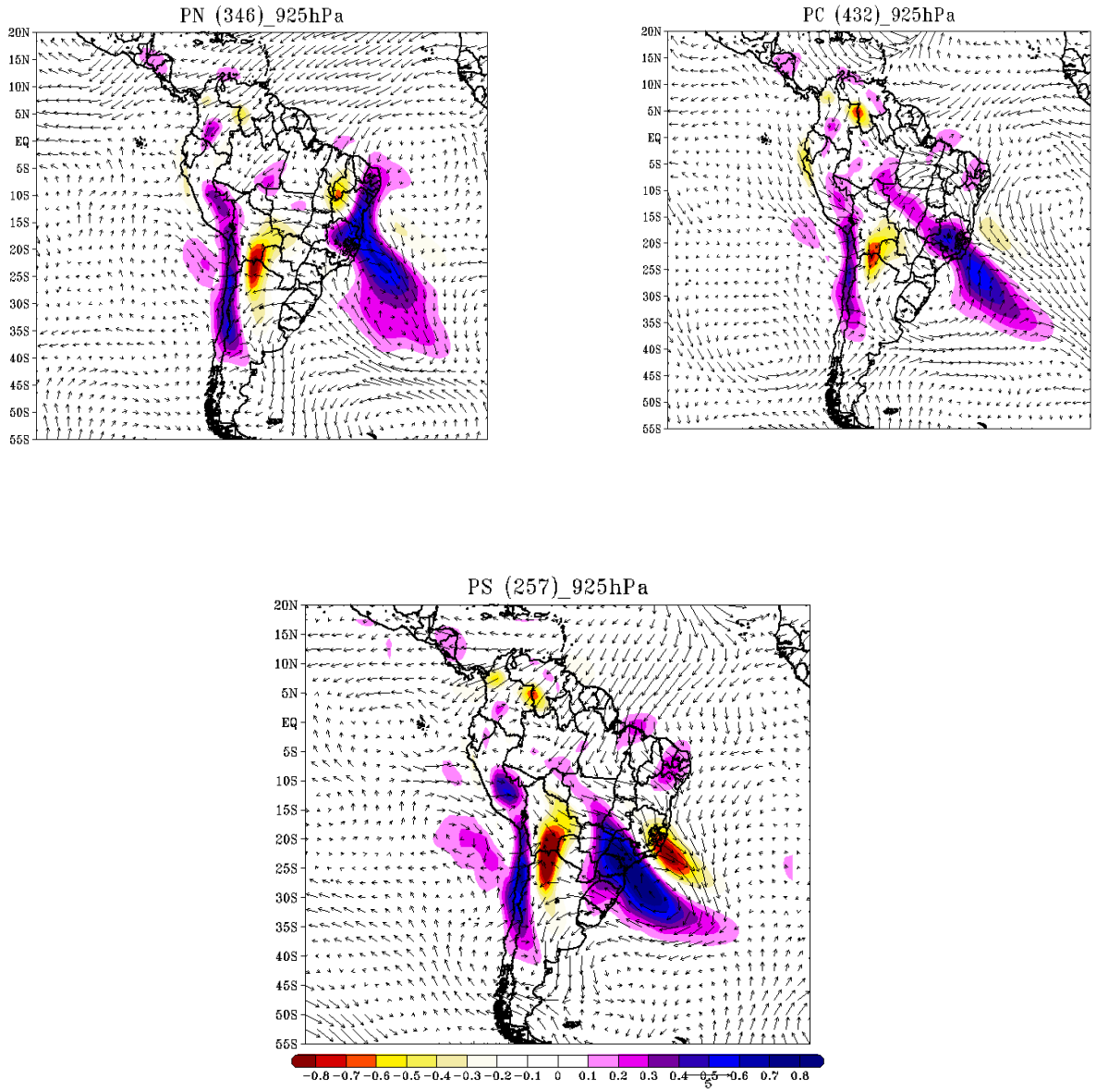

Source: elaborated by the author.